ICTP *Lecture Notes*

WORKSHOP ON NUCLEAR REACTION DATA AND NUCLEAR REACTORS: PHYSICS, DESIGN AND SAFETY

25 February - 28 March 2002

Editors

M. Herman
National Nuclear Data Center, New York, USA
N. Paver
University of Trieste and INFN, Trieste, Italy

NUCLEAR REACTION DATA AND NUCLEAR REACTORS
– First edition

ISBN 92-95003-30-6

Printed in Trieste by the ICTP Publications & Printing Section

PREFACE

One of the main missions of the Abdus Salam International Centre for Theoretical Physics in Trieste, Italy, founded in 1964, is to foster the growth of advanced studies and scientific research in developing countries. To this end, the Centre organizes a number of schools and workshops in a variety of physical and mathematical disciplines.

Since unpublished material presented at the meetings might prove to be of interest also to scientists who did not take part in the schools and workshops, the Centre has decided to make it available through a new publication series entitled ICTP Lecture Notes. It is hoped that this formally structured pedagogical material on advanced topics will be helpful to young students and seasoned researchers alike.

The Centre is grateful to all lecturers and editors who kindly authorize the ICTP to publish their notes in this series.

Since the initiative is new, comments and suggestions are most welcome and greatly appreciated. Information regarding this series can be obtained from the Publications Section or by e-mail to "`pub_off@ictp.it`". The series is published in-house and is also made available on-line via the ICTP web site: "`http://www.ictp.it/~pub_off/lectures/`".

Katepalli R. Sreenivasan, Director
Abdus Salam Honorary Professor

Contents

Introduction

This volume contains a partial collection of lectures delivered at the workshop on "Nuclear Reaction Data and Nuclear Reactors: Physics, Design and Safety", held at the Abdus Salam International Centre for Theoretical Physics in February-March 2002.

The aim of the Workshop was to present extensive, and up-to-date information on the whole scientific field underlying nuclear reactor calculations, from the theory of nuclear reactions and nuclear data production and validation down to the applications to nuclear reactor physics, design and safety.

In particular, the collection of lecture notes included in this volume presents techniques for modelling microscopic calculations of light nuclei reactions, the use of a database of parameters for calculations of nuclear reactions and the nuclear data requirements for the calculation of the decay heat in nuclear reactors. As far as the nuclear reactors themselves are concerned, the fields of advanced nuclear technology developments for power production, of non-electric applications of nuclear energy and of the safety procedures for decommissioning old nuclear power plants are covered. We hope that, although limited to these few topics, the volume will nevertheless represent a useful reference for researchers interested in the field of nuclear data and nuclear reactors. For the benefit of potential readers who could not participate in the Workshop, these lecture notes are also available on-line at: `http://www.ictp.it/ pub_off/lectures/` for free access and consultation.

The Workshop was organized by ICTP and IAEA. The editors are grateful to these Institutions for their support and sponsorship. They thank the authors for their excellent presentations of the lecture notes, and the ICTP staff for their invaluable help in successfully running the Workshop and for the professional preparation of this volume.

M. Herman
N. Paver
Trieste, April 2005

Refined Resonating Group Model and Standard Neutron Cross Sections

Hartmut M. Hofmann*

Institute for Theoretical Physics, University of Erlangen-Nürnberg, Erlangen, Germany

Lectures given at the
Workshop on Nuclear Reaction Data and
Nuclear Reactors: Physics, Design and Safety
Trieste, 25 February - 28 March 2002

LNS0520001

*hmh@theorie3.physik.uni-erlangen.de

Abstract

We describe in some detail the refined resonating group model and its application to light nuclei. Microscopic calculations employing realistic nuclear forces are given for the reaction ^{3}He(n,p). The extension to heavier nuclei is briefly discussed.

1 Introduction

The neutron standard cross sections cover a wide range of target masses from hydrogen to uranium. The high mass range is characterized by many overlapping resonances, which cannot be understood individually. In contrast, the few-nucleon regime is dominated by well-developed, in general, broad resonances. The interpolation and to less extend extrapolation of data relies heavily on R-matrix analysis. This analysis has to fit a large number of parameters related to position and decay properties of resonances. Due to the limited number of data and their experimental errors, any additional input is highly welcome. Except for neutron scattering on the proton any of the standard cross sections involve few to many nucleon bound states. These many body systems can no more be treated exactly. The best model to treat scattering reactions of such systems proved the resonating group model (RGM) in its various modifications. Therefore we begin with a discussion of the RGM.

The solution of the many-body problem is a long standing problem. The few-body community developed methods, which allow an exact solution of few-body problems, via sets of integral equations. In this way the 3-body problem is well under control, whereas the 4-body problem is still in its infancy. Hence, for systems containing four or more particles one has to rely on approximations or purely numerical methods. One of the most successful methods is the resonating group model (RGM), invented by Wheeler [1] more than 50 years ago in molecular physics. The basic idea was a resonant jump of a group of electrons from one (group of) atom(s) to another one.

This seminal idea sets already the framework for present day calculations: Starting from the known wave function of the fragments, the relative wave function between the fragments has to be determined e.g. via a variational principle. The basic idea, however, also sets the minimal scale for the calculation: a jump of a group of electrons needs at least two different states per fragment leading to coupled channels. Hence, an RGM calculation is basically a multi-channel calculation, which renders immediately the technicality problem. This essential point of any RGM calculation is the key to an understanding of the various realisations of the basic idea. Besides the most simple cases, for which even exact solutions are possible, the RGM is always plagued with necessary, huge numerical efforts. Therefore, a discussion about the various approaches has to be given. In most applications

of the RGM till now, the evaluation of the many-body r-space integrals is the largest obstacle. It can only be overcome by using special functions, essentially Gaussians, for the internal wave functions of the fragments. Two basically different methods are well developed: One uses shell model techniques to perform the integration over the coordinates of the known internal wave functions leading to systems of integro-differential equations, whose kernels have to be calculated analytically. The other expands essentially all wave functions in terms of Gaussian functions and integrates over all Jacobian coordinates leading to systems of linear equations, whose matrices can be calculated via Fortran-programs. Since the latter is more suited for few-body systems and I'm more familiar with it, I will concentrate on this so-called refined resonanting group model (RRGM) introduced by Hackenbroich [2]. As detailed descriptions of the first method exist [3], I will not discuss it. I will, however, compare the advantages and disadvantages of both methods at various stages.

In order to allow the reader to find further applications of the RRGM, I will try to generalize the formal part from the nuclear physics examples I will give later on. Therefore I will first discuss the variational principle for the determination of the relative motion wave function. I will then demonstrate how the r-space integrals are calculated in the RRGM. The next two chapters deal with the treatment of the antisymmetriser and the evaluation of spin-isospin matrix elements. The last chapter, dealing with formal developments, demonstrates how the wave function itself is used by the evaluation of matrix elements of electric transition operators.

A chapter on various results from nuclear physics illustrates various points of the formal part and helps to understand the final part on possible extensions and also on the limitations of the model. Part of the work is already described previously [4]. Some repetition cannot be avoided in order to keep this article self-contained, so I will refer sometimes to ref. [4] for details.

2 Variational principle for scattering functions

Whereas the Ritz variational principle for bound states is a standard textbook example, variational principles for scattering wave functions are still under discussion, especially for composite systems, see the review by Gerjuoy [5]. I will therefore repeat the essential points and refer to [4] for some details. With respect to bound state wave functions of fragments, the

RRGM is nothing but a standard Ritz variation with an ansatz for the wave functions in terms of Gaussian functions, see eqs. (2.33 - 2.36) below. That this expansion converges pretty fast was shown in [4] and is also discussed in chapter 5.1.

2.1 Potential scattering

In this section I briefly review potential scattering following along the lines of ref. [4]. Let us consider for simplicity first the scattering of a spinless particle off a fixed potential. The wave function ψ can then be expanded in partial waves

$$\psi(\mathbf{r}) = \sum_{lm} \frac{u_l(r)}{r} Y_{lm}(\hat{\mathbf{r}}) \tag{2.1}$$

Here, as everywhere vectors are bold faced and unit vectors carry additionally a hat. We use for the asymptotic scattering wave function $u_l(r)$ a linear combination of regular $f_l(r)$ and irregular $g_l(r)$ solutions of the free Hamiltonian, so that all wave functions are real, thus simplifying the numerical calculations. The wavefunction u_l is normalized to a δ-function in the energy by using the ansatz

$$u_l(r) = \sqrt{\frac{M}{\hbar^2 k}} \left(f_l(r) + a_l \, \tilde{g}_l \, (r) + \sum_\nu b_{\nu l} \, \chi_{\nu l} \, (r) \right) \tag{2.2}$$

Here M denotes the mass of the particle. The momentum k is related to the energy by $E = \hbar^2 k^2 / 2M$. For the variational principle $u_l(r)$ has to be regular at the origin, therefore $\tilde{g}_l(r)$ is the irregular solution g_l regularized via

$$\tilde{g}_l(r) = T_l(r) g_l(r) \quad \text{with} \quad T_l(r) \underset{r \to 0}{\longrightarrow} r^{2l+1} \quad \text{and} \quad T_l(r) \underset{r \to \infty}{\longrightarrow} 1 \tag{2.3}$$

The regularisation factor T_l should approach 1 just outside the interaction region. A convenient choice is

$$T_l(r) = \sum_{n=2l+1}^{\infty} \frac{(\beta_0 r)^n}{n!} e^{-\beta_0 r} = 1 - \sum_{n=0}^{2l} \frac{(\beta_0 r)^n}{n!} e^{-\beta_0 r} \tag{2.4}$$

where the limiting values are apparent in the different representations. A typical value for β_0 is $1.1 fm^{-1}$. The calculation is rather insensitive to this parameter, see, however, the discussion below eq. (4.6).

The last term in eq. (2.2) accounts for the difference of the true solution of the scattering problem and the asymptotic form. Furthermore, in the region where T_l differs from this term one has to compensate the difference between $\tilde{g}_l(r)$ and $g_l(r)$. Since this term is different from zero only in a finite region, just somewhat larger than the interaction region, it can be well approximated by a finite number of square integrable terms. We will choose the terms in the form

$$\chi_{\nu l}(r) = r^{l+1} e^{-\beta_\nu r^2} \tag{2.5}$$

where β_ν is an appropriately chosen set of parameters (see discussions in chapters 4.2 and 4.3).

Since f_l and $\tilde{g}_l$ are not square integrable, we have to use Kohn's variational principle [6] to determine the variational parameters a_l and $b_{\nu l}$ via

$$\delta \left[\int d\, r\; u_l(r)(H_l - E)u_l(r) - \frac{1}{2}a_l \right] = 0 \tag{2.6}$$

where H_l denotes the Hamiltonian for the partial wave of angular momentum l. It is easy to show [2], that all integrals in eq. (2.6) are well behaved if and only if the functions f_l and g_l are solutions of the free Hamiltonian to the energy E. See also the discussion in [5].

2.2 Scattering of composite fragments

The RGM, however, usually deals with the much more complex case of the scattering of composite particles on each other. We will assume in the following, that the constituents interact via two-body forces, e.g. a short ranged nuclear force and the Coulomb force. An extension to three-body forces is straightforward and effects essentially only the treatment of the spin-isospin matrix elements. As alluded to in ref. [5], three body break-up channels pose a serious formal problem. Since for break-up channels the asymptotic wave function is not of the form of eq. (2.2), we have to neglect such channels. How they can be approximated is discussed in chapter 5.1.

With two-body forces alone, the Hamiltonian of an N-particle system can be split into

$$H(1,\ldots,N) = \sum_{i=1}^{N} T_i + \frac{1}{2}\sum_{i\neq j} V_{ij} \tag{2.7}$$

where the centre of mass kinetic energy can be separated off by

$$\sum_{n=1}^{N} T_i = T_{CM} + \frac{1}{2mN} \sum_{i<j}^{N} (\mathbf{p_i} - \mathbf{p_j})^{\mathbf{2}} \tag{2.8}$$

Here we assumed equal masses m for all the constituents, a restriction which can be removed, see ref. [7].

Due to our restriction we can decompose the translationally invariant part H' of the Hamiltonian into the internal Hamiltonians of the two fragments, the relative motion one, and the interaction between nucleons being in different fragments

$$H'(1,\ldots,N) = H_1(1,\ldots,N_1) + H_2(N_1+1,\ldots,N) + T_{rel} + \sum_{\substack{i\in\{1,\ldots,N_1\}\\ j\in\{N_1+1,\ldots,N\}}} V_{ij} \tag{2.9}$$

By adding and subtracting the point Coulomb interaction between the two fragments $Z_1 Z_2 e^2/R_{rel}$ the potential term becomes short ranged.

$$\begin{aligned} H'(1,\ldots,N) &= H_1(1,\ldots,N_1) + H_2(N_1+1,\ldots N) + T_{rel} + Z_1 Z_2 e^2/R_{rel} \\ &+ \sum_{\substack{i\in\{1,\ldots,N_1\}\\ j\in\{N_1+1,\ldots,N\}}} V_{ij} - Z_1 Z_2 e^2/R_{rel} \end{aligned} \tag{2.10}$$

Here R_{rel} denotes the relative coordinate between the centres of mass of the two fragments. This decomposition of the Hamiltonian directs to an ansatz for the wave function in terms of an internal function of H_1 and one of H_2 and a relative motion function of type eq. (2.2). The total wave function is then a sum over channels formed out of the above functions properly antisymmetrised.

$$\psi_m = \mathcal{A} \sum_{n=1}^{N_k} \psi_{ch}^n \psi_{rel}^{mn} \tag{2.11}$$

where $\mathcal{A}$ denotes the antisymmetriser, N_k the number of channels with channel wave functions ψ_{ch} described below and the relative motion wave function

$$\psi_{rel}^{mn}(R_{rel}) = \delta_{mn} f_m(R_{rel}) + a_{mn} \tilde{g}_n(R_{rel}) + \sum_{\nu} b_{mn\nu} \chi_{n\nu}(R_{rel}) \tag{2.12}$$

The subscript m on ψ_m indicates the boundary condition that only in channel m regular waves exist. The functions f and $\tilde{g}$ are now regular and regularised

irregular Coulomb wavefunctions. How to use in- and outgoing waves and calculate the S-matrix directly is described in [8]. The sum n runs over physical channels, open or closed, and "distortion channels" without the standing wave terms. Such "distortion channels" allow to take the distortion of the fragments in the interaction region into account, see the discussion in chapter 5.1. Sometimes they are called "pseudo-inelastic" channels [3]. The coefficients a_{mn} and $b_{mn\nu}$ are variational parameters to be determined from

$$\delta(< \psi_m|H' - E|\psi_m > -\frac{1}{2}a_{mm}) = 0 \tag{2.13}$$

To simplify the notation we combine the channel functions and the relative motion part into one symbol and write in the obvious notation

$$\psi_m = \mathcal{A}\left\{\sum_n \left(\delta_{mn}F_n + a_{mn}\tilde{G}_n + \sum_\nu b_{mn\nu}\chi_{n\nu}\right)\right\} \tag{2.14}$$

The Hamiltonian H' can be diagonalised in the space spanned by all the $\chi_{n\nu}$. Let us assume this diagonalisation to be done, then we can switch to new square integrable functions Γ_ν with

$$< \Gamma_\nu|\mathcal{A}\Gamma_\mu >= \delta_{\nu\mu} \qquad \text{and} \tag{2.15}$$

$$< \Gamma_\nu|H'|\mathcal{A}\Gamma_\mu >= \epsilon_\nu\ \delta_{\nu\mu} \tag{2.16}$$

Since H' commutes with the antisymmetrizer $\mathcal{A}$ it suffices to apply $\mathcal{A}$ on one side, see also chapter 3.2.

In eq. (2.14) the eigenfunctions Γ of the Hamiltonian can be used as

$$\psi_m = \mathcal{A}\left\{\sum_n \left(\delta_{mn}F_n + a_{mn}\tilde{G}\right) + \sum_\nu d_{m\nu}\Gamma_\nu\right\} \tag{2.17}$$

where now the variational parameters a_{mn} and $d_{m\nu}$ have to be determined from the set of variational equations

$$\begin{aligned} < \tilde{G}_n|\hat{H}|\mathcal{A}F_m > \ &+ \ \sum_{n'} < \tilde{G}_n|\hat{H}|\mathcal{A}\tilde{G}_{n'} > a_{mn'} \\ &+ \ \sum_\nu < \tilde{G}_n|\hat{H}|\mathcal{A}\Gamma_\nu > d_{m\nu} = 0 \end{aligned} \tag{2.18}$$

$$< \Gamma_\nu|\hat{H}|\mathcal{A}F_m > \quad + \quad \sum_{n'} < \Gamma_\nu|\hat{H}|\mathcal{A}\tilde{G}_{n'} > a_{mn'}$$
$$+ \quad \sum_{\nu'} < \Gamma_\nu|\hat{H}|\mathcal{A}\Gamma_{\nu'} > d_{m\nu'} = 0 \tag{2.19}$$

with $\hat{H} = H' - E$. Since we prediagonalised the Hamiltonian only one term survives in the sum in eq. (2.19). Solving for $d_{m\nu}$ and taking eqs. (2.15, 2.16) into account we find

$$d_{m\nu} = \frac{1}{E - \epsilon_\nu} \left(< \Gamma_\nu|\hat{H}|\mathcal{A}F_m > + \sum_{n'} < \Gamma_\nu|\hat{H}|\mathcal{A}\tilde{G}_{n'} > a_{mn'} \right) \tag{2.20}$$

Defining the operator $\tilde{H}$ as

$$\tilde{H} = \hat{H} - \sum_\nu \frac{\hat{H}|\mathcal{A}\Gamma_\nu >< \Gamma_\nu|\hat{H}}{\epsilon_\nu - E} \tag{2.21}$$

and inserting eq. (2.20) into eq. (2.18) yields

$$\sum_{n'} < \tilde{G}_n|\tilde{H}|\mathcal{A}\tilde{G}_{n'} > a_{mn'} = - < \tilde{G}_n|\tilde{H}|\mathcal{A}F_m > \tag{2.22}$$

or in the obvious matrix notation

$$< \tilde{G}|\tilde{H}|\tilde{G} > a^T = - < \tilde{G}|\tilde{H}|F > \tag{2.23}$$

where a^T denotes the transposed matrix a. This equation can easily be solved for a

$$a = - < \tilde{G}|\tilde{H}|F >^T < \tilde{G}|\tilde{H}|\tilde{G} >^{-1} \tag{2.24}$$

For known matrix elements of $\tilde{H}$, a_{mn} is known and via eq. (2.20) also $d_{m\nu}$ and hence the total wave function. Note that for a complete knowledge of the matrix a and the coefficients $d_{m\nu}$ the boundary condition of the total wavefunction ψ_m has to run over all channels N_k. The expression for $\tilde{H}$ (eq. (2.21)) indicates the close relationship of this approach to the quasiparticle method of Weinberg [9].

In general the reactance matrix a_{mn} in eq. (2.24) is not symmetric, therefore also the S-matrix given by the Caley transform

$$S = (\mathbf{1} + ia)(\mathbf{1} - ia)^{-1} \tag{2.25}$$

is not symmetric thus violating time-reversal invariance, even unitarity is not guaranteed. To enforce unitarity we have to have a symmetric reactance matrix a, which can be achieved by the so-called Kato correction [10]. In potential scattering the condition of stationarity leads to the same results [5]. For the scattering of composite systems, however, some integrals might diverge, see the discussion below, so the more rigorous derivation [5] cannot be applied.

If we choose instead of eq. (2.17) another boundary condition as

$$\psi'_m = \mathcal{A}\left\{\sum_n (b_{mn}F_n + \delta_{mn}\tilde{G}_n) + \sum_\nu d'_{m\nu}\Gamma_\nu\right\} \tag{2.26}$$

then following along the lines of eqs. (2.17 - 2.24) we find

$$b = - < F|\tilde{H}|\tilde{G} >^T < F|\tilde{H}|F >^{-1} \tag{2.27}$$

again with an obviously unsymmetric matrix b. Since the boundary condition should not affect observables, we should have

$$a = b^{-1} \tag{2.28}$$

Therefore we can judge the quality of the calculation, by comparing the results of the two calculations. On the other hand we can follow the ideas of John [11] and insert the relation

$$< F|\tilde{H}|\tilde{G} >=< \tilde{G}|\tilde{H}|F >^T + \frac{1}{2}\,\mathbf{1} \tag{2.29}$$

into eq. (2.28)

$$- < \tilde{G}|\tilde{H}|F >^T < \tilde{G}|\tilde{H}|\tilde{G} >^{-1} = - < F|\tilde{H}|F > \left(< \tilde{G}|\tilde{H}|F > + \frac{1}{2}\,\mathbf{1}\right)^{-1} \tag{2.30}$$

Multiplying by the transpose of the r.h.s of eq. (2.29) leads to [4]

$$a = -2(< F|\tilde{H}|F > - < \tilde{G}|\tilde{H}|F >^T < \tilde{G}|\tilde{H}|\tilde{G} >^{-1} < \tilde{G}|\tilde{H}|F >) \tag{2.31}$$

which is obviously symmetric. This expression has been derived as a second order correction in [2] and also in [5]. Analogously we find

$$b = -2(< \tilde{G}|\tilde{H}|\tilde{G} > - < F|\tilde{H}|\tilde{G} >^T < F|H|F >^{-1} < F|\tilde{H}|\tilde{G} >) \tag{2.32}$$

Again from the comparison of the results for a and b we can judge the quality of the calculation. The most direct criterion of $a \cdot b$ being the unit matrix can easily fail near poles of a (resonances) or b without affecting physical observables. What remains to be done is the calculation of the matrix elements of $\tilde{H}$ between F and $\tilde{G}$. For this purpose we need the channel wave function in eq. (2.11).

The ansatz for the internal wave functions is the most critical input. Because of the antisymmetrizer only two cases are realised in complicated systems: expansion in terms of harmonic oscillator wave functions or Gaussian functions and powers of r^2, which can again be combined to harmonic oscillator functions. The difference of both expansions lies in the choice of parameters, a single oscillator frequency in one case, which allows to use the orthogonality of different functions, and a set of Gaussian width parameters, which allows to adjust the wave functions to different sizes of the fragments more easily. Therefore the harmonic oscillator expansion is well suited for the description of scattering of identical particles, or of the scattering of large nuclei on each other. In this case even algebraic methods can be used [12], [13]. Whereas the expansion in terms of Gaussians and powers of r^2 can, in principle, be converted to harmonic oscillator functions, it becomes technically glumpy in more complicated cases, see the discussion in chapter 3. Since the sizes of light nuclei are quite different, we consider it, however, an advantage that different width parameters can be used.

To clarify our ansatz we consider just one term in eq. (2.11). Here the channel function has the structure

$$\psi_{ch} = \left[\frac{Y_l(\hat{\mathbf{R}}_{rel})}{R_{rel}} \left[\phi_1^{J_1} \phi_2^{J_2} \right]^{Sc} \right]^J \tag{2.33}$$

where the square brackets indicate angular momentum coupling of the translationally invariant wave functions ϕ_i^{Ji} of the two fragments to channel spin S_c and the coupling of the orbital angular momentum l and the channel spin S_c to the total angular momentum J. In case of a bound state calculation the coupling to good channel spin is usually omitted. Since all the latter examples are nuclear physics ones, I will consider in the sequel wave functions of light nuclei for the fragment wave functions, but we could also use the technique described below for describing electron scattering off atomic or molecular systems [14].
The individual fragment wave function consists of a spatial part and a spin

(-isospin)-part, which may contain an arbitrary number of clusters. We use the expression "cluster" only for groups of particles without internal orbital angular momenta, that means that in nuclear physics a cluster can, at most, contain 4 nucleons, two protons and two neutrons with opposite spin projections. In hadron physics, a typical cluster would be a baryon containing 3 quarks or a meson containing a quark-antiquark pair.

The spatial wave function of a cluster h consists of a single Gaussian function

$$\chi_{h,int} = exp\left(-\frac{\beta_h}{n_h}\sum_{i<j}^{n_h}(\mathbf{r}_i-\mathbf{r}_j)^2\right) \tag{2.34}$$

with n_h the number of particles inside the cluster h and the width parameter β_h. Clusters containing only one particle are described by $\chi_h \equiv 1$. In hadron physics the spin-isospin function is coupled to good total spin and isospin, in nuclear physics this coupling is not necessary in most cases, because the antisymmetriser projects onto total singlet states anyhow. The cluster relative functions $\chi^{l_k}_{k,rel}$ contain, in addition to the Gaussian function, a solid spherical harmonic $\mathcal{Y}_{l_k}$ of angular momentum l_k

$$\chi^{l_k}_{k,rel} = \exp(-\gamma_k\rho_k^2)\mathcal{Y}_{l_k}(\boldsymbol{\rho}_k) \tag{2.35}$$

where $\boldsymbol{\rho}_k$ denotes the Jacobi coordinate between the center-of-mass of cluster $k+1$ and the center-of-mass of the clusters 1 to k, see fig. 1. The total wave function of a fragment is now a superposition of various combinations of internal and relative functions, e.g.

$$\phi^J = \sum_{l_I,S,\alpha} C_\alpha^{l_I S}\left(\prod_{h=1}^{n_c}\chi_{\alpha,h,int}\right)\left[\left(\prod_{n=1}^{n_c-1}\chi^{l_k}_{\alpha,k,rel}\right)\Xi^{S,(T)}\right]^J \tag{2.36}$$

The spin-(-isospin) function $\Xi^{S,(T)}$ is, in general, coupled to good spin (and may be coupled to good isospin). The set $\{l_k\}$ of orbital angular momenta between the clusters is denoted by l_I, including the intermediate couplings. The sum α may run over different fragmentations, different sets of orbital angular momenta, e.g. D-state admixtures, and different sets of width parameters β_h and γ_k. The parameters $\beta_{\alpha h}$ and $\gamma_{\alpha k}$ are determined from the Ritz variational principle together with the coefficients $C_\alpha^{l_I S}$ once the model space has been chosen. For this purpose one chooses the fragmentations and the set $\{l_k\}$ of angular momenta and the number of radial functions and asks for

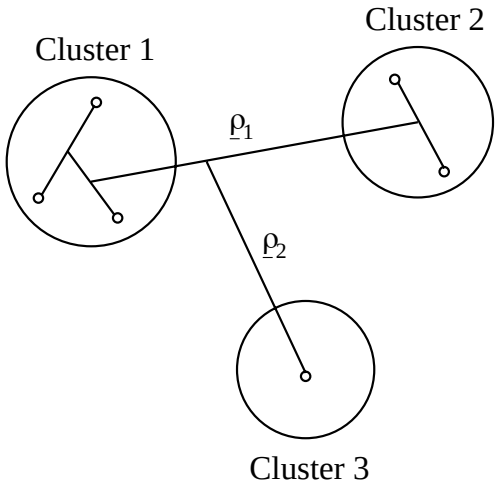

Figure 1: Schematic illustration of the intercluster coordinates ρ used in eq. (2.35).

$$\delta < \phi^{J_1} | H'(1, \ldots, N_1) \; - \; E | \mathcal{A}_1 \phi^{J_1} >= 0 \tag{2.37}$$

where $\mathcal{A}_1$ is the antisymmetriser of the N_1 particles in fragment 1. Therefore, we assume in the following, that ϕ^{J_1} and ϕ^{J_2} are bound states in the chosen model space and fulfill the equations

$$H_i | \mathcal{A}_i \phi_i >= E_i | \mathcal{A}_i \phi_i > \qquad i = 1, 2 \tag{2.38}$$

ϕ_i can be the lowest state but also an excited one, see the example below.

We can now demonstrate that the functional of eq. (2.13) exists and that all integrals exist in a Riemannian sense. Let us consider a fragmentation into N_1 particles in fragment 1 and the rest in fragment 2. Then we can write the total antisymmetriser $\mathcal{A}$ in the form

$$\mathcal{A} = \mathcal{A}_3 \mathcal{A}_1 \mathcal{A}_2 = \sum_{P_3} sign P_3 \;\; P_3 \mathcal{A}_1 \mathcal{A}_2 \tag{2.39}$$

where P_3 permutes particles across the fragment boundaries including $P_3 = id$. Choosing the kinetic energy E_k in the channel k to be

$$E_k = E - E_{1,k} - E_{2,k} \tag{2.40}$$

with $E_{i,k}$ from eq. (2.38), we can then decompose the operator in eq. (2.10) as

$$\begin{aligned} H'(1,\ldots,N)-E &= (H_1(1,\ldots,N_1)-E_{1,k})+(H_2(N_1+1,\ldots,N)-E_{2,k}) \\ &+ \sum_{\substack{i\in\{1,\ldots,N\} \\ j\in\{N_1+1,\ldots,N\}}} V_{ij} - Z_1Z_2e^2/R_{rel} \\ &+ T_{rel}+Z_1Z_2e^2/R_{rel}-E_k \end{aligned} \tag{2.41}$$

All the integrals necessary for evaluating eqs. (2.18 - 2.19) are now well behaved, terms containing only square integrable functions in bra or ket cannot lead to divergent integrals. Because of the exponential fall off of the bound state functions, the same is true for all terms in which channels of different fragmentations are connected. Again, due to the properties of the bound state functions, integrals containing identical fragmentations but a genuine exchange of particles between the fragments, i.e. $P_3 \neq id$, are of short range. Hence, the only possibly critical terms involve channels with identical fragmentations in bra and ket of eq. (2.13) with no exchange across the fragment boundaries.

In this case the first line of eq. (2.41) contributes zero, because according to eq. (2.38) the internal functions are solutions of the internal Hamiltonian H_i to just that energy $E_{i,k}$. The potential in the second line of eq. (2.41) is by construction short ranged, hence also this integral is short ranged. The remaining line in eq. (2.41) is the (point-Coulomb) Hamiltonian of relative motion H_{rel} whose solutions are the well-known Coulomb wave functions [15]. If and only if the functions F_k and G_k in eq. (2.12) are eigenfunctions of H_{rel} to the energy E_k, the related integrals are finite, to be precise they are zero. This choice, however, implies that the threshold energies are fixed by the energies of the fragments $E_{i,k}$. Besides choosing a different potential, the only possibility to vary the threshold energies is to modify the model space for the Ritz variation.

Since we have now shown that all integrals in eq. (2.13) and therefore also in eqs. (2.18, 2.19) are short ranged, we expand the regular and regularised irregular (Coulomb) functions in terms of square integrable functions, for simplicity those chosen in eq. (2.12). Hence, we have to calculate matrix elements of the Hamiltonian, or just overlap matrix elements, between anti-symmetrized translationally invariant wavefunctions where the spatial part consists of a superposition of multi-dimensional Gaussian functions and solid

spherical harmonics. In the next chapter we will describe how to calculate a typical matrix element.

3 Evaluation of the matrix elements

From the ansatz of our wave function eq. (2.36) we see that the calculation of the necessary matrix elements can be performed in several steps, after decomposing the antisymmetrizer into a sum over all permutations acting on spatial and spin-isospin coordinates: Since the potential terms in the Hamiltonian can be written as a product of operators acting in coordinate space and spin-isospin space separately

$$\sum_{i<j} \mathbf{w}_{ij} = \sum_{i<j} \sum_{kq} (-1)^q w_{ij}^{\mathbf{O}}(k,-q) w_{ij}^{\mathbf{ST}}(k,q) \tag{3.1}$$

we can also calculate the respective matrix elements of each operator separately. The rank of the interaction is denoted by k, e.g. $k = 1$ for the spin orbit force. Since the multi-dimensional integration in coordinate space is usually by far the most elaborate part of the calculation, we first describe the essential parts of this calculation.

3.1 Calculation of the spatial matrix elements

The spatial part of our wave function eq. (2.36) consists of Gaussian functions and products of solid spherical harmonics. To keep the notation as simple as possible, we disregard in this section the coupling of the various angular momenta. Therefore a single term on the right-hand side of the matrix elements (marked by the index r) is of the structure

$$|L_r \alpha> = \prod_{i=1}^{N-1} e^{-\beta_i \mathbf{s}_i^r \cdot \mathbf{s}_i^r} \prod_{j=1}^{n_{c_r}-1} \mathcal{Y}_{l_j\, m_j}\, (\mathbf{s}_{N-n_{c_r}+j}^r) \tag{3.2}$$

where we have converted the single particle coordinates $\mathbf{r}_i$ in eq. (2.34) into Jacobian coordination $\mathbf{s}_i$ via an orthogonal matrix. The numbering of the Jacobians starts with the internal ones, see fig. 2. The number of clusters on the right-hand side is denoted by n_{c_r}. Note that $\mathbf{s}_N$, proportional to the coordinate of the center-of-mass, is absent in eq. (3.2) due to the translational invariance of our wave function. The index $|L_r \alpha >$ is just a reminder of the fragmentation and the angular momentum structure of the

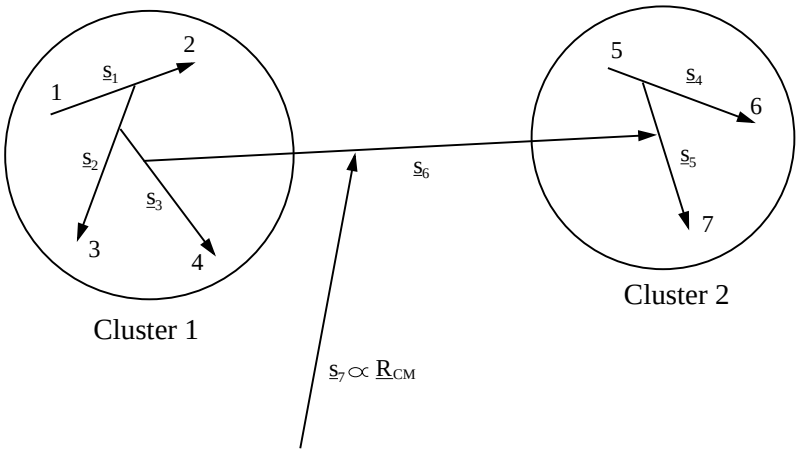

Figure 2: Schematic diagram illustrating the numbering of the Jacobi coordinates of eq. (3.2) for a cluster decomposition into 4 and 3 particles. Note that the arrows shown are only proportional to the Jacobi vectors.

ket wave function. The function on the left-hand side of the matrix element $|L_l\alpha'>$ can be expressed in an analogous way by the Jacobian coordinates $\mathbf{s}_l$ on the left-hand side, which differ in general from those on the right-hand side. So the general spatial matrix element is of the form

$$J^{ij}_{L_l\alpha' L_r\alpha}(P) \equiv < L_l\alpha'|Pw^{\mathbf{O}}_{ij}|L_r\alpha > \tag{3.3}$$

The orbital operators $w^{\mathbf{O}}_{ij}$ contain the coordinates in the form of eq. (3.2), but in addition to that also differential operators may occur, like in the spin-orbit force. We have put the permutation P to the left of the symmetric interaction for convenience, see the discussion below. Since the evaluation of all interactions can be reduced to the calculation of certain overlap matrix elements [16], [17], [4], see also section 3.4, we restrict our considerations to the norm, because there all the essential steps become apparent. We can express the norm matrix element of eq. (3.3) by choosing the Jacobian coordinates on the left-hand side as independent variables in the form

$$\begin{aligned} J^{ij}_{L_l\alpha' L_r\alpha'}(P) &= \int d\mathbf{s}_1 \ldots d\mathbf{s}_{N-1} \exp\left(- \sum_{\mu\mu'}^{N-1} \rho_{\mu\mu'}(P)\mathbf{s}_\mu \cdot \mathbf{s}_{\mu'} \right) \\ & \prod_{n=1}^{z} \mathcal{Y}_{l_n m_n}(\mathbf{Q}_n) \equiv \Gamma_{l_1 m_1 \ldots l_z m_z} \end{aligned} \tag{3.4}$$

Since we used an orthogonal transformation from the single particle coordinates $\mathbf{r}$ to the Jacobian coordinates $\mathbf{s}$, whose index l we suppressed for simplicity, no determinant appears in the integral. The matrix ρ in the exponent results from applying the permutation P to the coordinates on the right-hand side and then expressing these coordinates by those on the left-hand side. The vectors $\mathbf{Q}_n$ are the intercluster coordinates ρ_k, see eq. (2.35) and fig. 1, on the left- and right-hand sides, after applying the permutation P onto the latter. Again these can be expressed as linear combinations of Jacobi coordinates $\mathbf{s}$, the former are just some of these coordinates.

In case of a genuine interaction its radial dependence in Gaussian form is also included into ρ and its angular dependence is then an additional spherical harmonic in eq. (3.4). For treating explicitly other radial dependencies, e.g. the Coulomb interaction, see ref. [4] and the discussion below. The number of angular momenta z is thus the sum of relative coordinates on the left-hand side and those on the right-hand side plus possibly one from the interaction.

Except for the solid spherical harmonics the matrix element eq. (3.4) is just a multi-dimensional Gaussian integral, which can be evaluated by bringing the matrix ρ into diagonal form. For treating the solid spherical harmonics we use their generating function [18]

$$(\mathbf{b}\cdot\mathbf{r})^L = b^L \sum_{m=-L}^{L} C_{Lm}\, b^{-m}\, \mathcal{Y}_{Lm}\,(\mathbf{r}) \tag{3.5}$$

with the vector $\mathbf{b} = (1-b^2, i(1+b^2), -2b)$ being a null vector with respect to a real scalar product, i.e. $\mathbf{b}\cdot\mathbf{b} = 0$ and the scalar product of two vectors given by

$$\mathbf{b}_n \cdot \mathbf{b}_{n'} = 4b_n b_{n'} - 2(b_n^2 + b_{n'}^2) \tag{3.6}$$

The coefficients C_{Lm} are given by [18]

$$C_{Lm} = (-2)^L L! \sqrt{\frac{4\pi}{(2L+1)(L-m)!(L+m)!}} \quad . \tag{3.7}$$

To evaluate the matrix element eq. (3.4) we now consider the generating integral

$$I(a_1 b_1 \ldots a_z b_z) = \int d\mathbf{s}_1 \ldots d\mathbf{s}_{N-1} \exp\left(-\sum_{\mu\mu'} \rho_{\mu\mu'} \mathbf{s}_\mu \cdot \mathbf{s}_{\mu'} + \sum_{n=1}^{z} a_n \mathbf{b}_n \cdot \mathbf{Q}_n \right) . \tag{3.8}$$

Expanding the expression $\exp(\sum \alpha_n \mathbf{b}_n \cdot \mathbf{Q}_n)$ into a power series in a_n and b_n we find

$$I(a_1 b_1 \dots a_z b_z) = \sum_{l_1 m_1 \dots l_z m_z} \left(\prod_{n=1}^{z} \frac{C_{l_n m_n}}{l_n!} \right) a^{l_n} b^{l_n - m_n} \cdot \Gamma_{l_1 m_1 \dots l_z m_z} \tag{3.9}$$

taking into account eq. (3.5).

Since the generating integral eq. (3.8) is just a Gaussian integral it can be done explicitly and the result can again be expanded in a power series in a_n and b_n to find the desired integrals via eq. (3.9). The transformation

$$\mathbf{s}_\mu = \sum_{\lambda=\mu}^{N-1} T_{\mu,\lambda} \mathbf{t}_\lambda \qquad \mu = 1, \dots, N-1 \tag{3.10}$$

with $T_{\lambda\lambda} = 1$ and $T_{\lambda\lambda'} = 0$ for $\lambda > \lambda'$ brings the matrix ρ into diagonal form. This transformation results in

$$I(a_1 b_1 \dots a_z b_z) = \int d\mathbf{t}_1 \dots d\mathbf{t}_{N-1} \exp\left(- \sum_\lambda \left(\beta_\lambda \mathbf{t}_\lambda^2 - \sum_n^z p_{n\lambda} a_n \mathbf{b}_n \cdot \mathbf{t}_\lambda \right) \right) \tag{3.11}$$

where we expressed the vector $\mathbf{Q}_n$ as

$$\mathbf{Q}_n = \sum_{\mu=1}^{N-1} p_{n\mu} \mathbf{t}_\mu \tag{3.12}$$

and used the properties of the transformation eq. (3.10). Employing the method of completing squares the integral yields

$$\begin{aligned} I(a_1 b_1 \dots a_z b_z) &= \prod_{\lambda=1}^{N-1} \left(\frac{\pi}{\beta_\lambda} \right)^{\frac{3}{2}} \exp\left(\frac{1}{4} \sum_{n>n'}^{z} \sigma_{nn'}\, a_n\, a_{n'}\, \mathbf{b}_n \cdot \mathbf{b}_{n'} \right) \\ &= \prod_{\lambda=1}^{N-1} \left(\frac{\pi}{\beta_\lambda} \right)^{\frac{3}{2}} \prod_{n>n'}^{z} \exp(\sigma_{nn'}\, a_n\, a_{n'}\, b_n\, b_{n'}) \\ &\quad \exp\left(\frac{-\sigma_{nn'}}{2}\, a_n\, a_{n'}\, b_n^2 \right) \exp\left(\frac{-\sigma_{nn'}}{2}\, a_n\, a_{n'}\, b_{n'}^2 \right) \end{aligned} \tag{3.13}$$

with the abbreviation

$$\sigma_{nn'} = 2 \sum_\lambda \frac{p_{n\lambda} p_{n'\lambda}}{\beta_\lambda} \tag{3.14}$$

and taking into account eq. (3.6). Expanding the exponentials into a power series and ordering the terms in the form of eq. (3.9) yields the final result [16], [4]

$$\begin{aligned}\Gamma_{l_1 m_1 \ldots l_z m_z} &= \left(\prod_{\lambda=1}^{N-1}\left(\frac{\pi}{\beta_\lambda}\right)^{\frac{3}{2}}\right)\left(\prod_{j=1}^{z}\frac{l_j!}{C_{l_j m_j}}\right)\cdot \\ &\cdot \sum_{g_{nn'}h_{nn'},k_{nn'}} (-\frac{1}{2})^{h_{nn'}+k_{nn'}} \prod_{n>n'}^{z} \frac{\sigma_{nn'}^{g_{nn'}+h_{nn'}+k_{nn'}}}{g_{nn'}!h_{nn'}!k_{nn'}!} \quad (3.15)\end{aligned}$$

The sums over $g_{nn'}, h_{nn'}, k_{nn'}$ run over all possible combinations of nonnegative integers, which fulfill the following relations for $n' = 1, \ldots, z$

$$\sum_n (g_{nn'} + h_{nn'} + k_{nn'} + g_{n'n} + h_{n'n} + k_{n'n}) = l_{n'} \quad (3.16a)$$

and

$$\sum_n (h_{nn'} - h_{n'n} + k_{n'n} - k_{nn'}) = m_{n'} \quad . \quad (3.16b)$$

Eq. (3.16 a) results from comparing the exponent of $a_{n'}$ in eq. (3.13) and eq. (3.9), whereas eq. (3.16 b) results from that of $b_{n'}$. In these relations $g_{nn'} = h_{nn'} = k_{nn'} = 0$ if $n \leq n'$. If there are more than two angular momenta different from zero, e.g. more than 2 clusters, eqs. (3.16) allow many solutions, which have to be found by trial and error. Starting from group theoretical considerations, Stöwe [19] developed a general scheme to find all solutions, which is realized in a very efficient Fortran program. Since the solution of eqs. (3.16) is independent of the permutation and the width parameters used to describe cluster internal and cluster relative wave functions, it need only be done once.

With this formalism we can now calculate each individual overlap matrix element from eq. (3.15) using eqs. (3.7, 3.10 - 3.12, 3.14 and 3.16). Straightforward extensions cover potentials, whose spatial form is a linear combination of products of Gaussian functions, solid spherical harmonics and powers of r^2. In case of a Gaussian radial dependence, this dependence has to be put into the construction of the matrix $\rho_{\mu\mu'}$ in eq. (3.4), which then modifies the transformation $T_{\mu\lambda}$ in eq. (3.10) and hence also the diagonal elements β_λ (eq. (3.11)) and the final coefficients $\sigma_{nn'}$ (eq. (3.14)). Forces containing explicitly a solid spherical harmonic, like the tensor force, are taken care of by

increasing the number of angular momenta by one by adding an additional vector $\mathbf{Q}_n$. With the relation [20]

$$r^{2l} = \frac{4\pi}{2l+1} \sum_{m=-l}^{l} (-1)^m \mathcal{Y}_{lm}(\mathbf{r}) \mathcal{Y}_{l-m}(\mathbf{r}) \tag{3.17}$$

We can treat even powers of r^2 by just increasing the number of angular momenta by two. Obviously all three radial dependencies can be treated simultaneously by modifying the matrix ρ and the number of angular momenta accordingly. The results are always of the form of eq. (3.14), i.e. of the type norm integral.

The Coulomb potential $Z_1 Z_2/r$ is apparently not of the above form, but it can be written as

$$\frac{1}{r} = 2\sqrt{\frac{\beta}{\pi}} \int_0^\infty dk \exp(-k^2 \beta\, r^2) \tag{3.18}$$

yielding again a Gaussian radial dependency and an additional integration over k. The explicit reduction of the matrix elements of the Coulomb integration in terms of overlap integrals is given in ref. [4]. Other negative powers of r are easily obtained by modifying the integral in eq. (3.18) by the appropriate monomial in k^2. For the tensor potential in the non-relativistic quark model, which contains an $\frac{1}{r^3}$ term, an explicit expression is given in [21].

For potentials containing differential operators, like the spin orbit interaction, the differential operators are applied to the wave function on the right-hand side, resulting in additional polynomials in vectors $\mathbf{r}_i - \mathbf{r}_j$, which can be treated by the method described above. For an explicit calculation of the kinetic energy, see [16]. All the potential terms are finally reduced to linear combinations of certain norm-type matrix elements. Each of these integrals can be evaluated explicitly by hand, the sheer number of matrix elements, however, necessitates the use of a computer program. As will be shown below, we need between 15 and 20 different Gaussian width parameters in order to facilitate the expansion of the Coulomb functions in the interaction region. So for one permutation we have typically 200 - 400 different matrix elements per structure taken into account (neglecting the symmetry of entrance and exit channel). On the other side the number of terms in the antisymmetriser grows rapidly with the increasing number of particles and furthermore in general the number of important configurations grows too.

Therefore one is forced to avoid multiple calculations of the same matrix elements. For this purpose the symmetry of the ansatz for the internal wave function, eq. (2.36), can be utilized. Permutations inside a cluster will not modify the wave function eq. (2.36). Furthermore, interactions between different pairs of particles might yield identical spatial matrix elements.

Let us consider ^{12}C as an illustrative example. Without any symmetry the 12-nucleon antisymmetrizer contains $12! = 479\,001\,600$ terms. Since protons with spin up are distinguishable from protons with spin down, we can reduce the huge number to $(3!)^4 = 1296$ terms. If we group the nucleons in ^{12}C together into three alpha-particles, then only 120 terms survive. Allowing for a two-body interaction, each of the above numbers has to be multiplied by $12 \cdot 13/2 = 78$, the number of possible interactions. Realizing that each of the two interacting particles can be in one of the 3 clusters initially and after interaction (and permutation) in some other one yields $9 \cdot 10/2 = 45$ possibilities, where we assumed a spatially symmetric interaction and did not check if this combination is possible for the permutation considered, thus arriving at $120 \cdot 45 = 5400$ possible interaction terms. The actual calculation yields 2601 different terms under the assumption that the 3 clusters have different width parameters.

What was shown here by an example is a quite general decomposition of a finite group into double cosets of appropriate subgroups [22]. Here we comply with the cluster symmetry of the wave function eq. (2.36) by considering subgroups $S_{n_1} \times S_{n_2} \times \ldots$ of the symmetric group S_N with $\sum n_i = N$. Each double coset can be characterized uniquely by one permutation. It is easy to convince one-self [22] that the overlap matrix elements eq. (3.15) for all permutations belonging to one double coset are identical because the matrix $\rho_{\mu\mu'}$ is unchanged. In the above example we consider the subgroup $S_4 \times S_4 \times S_4$, yielding 120 double cosets. Also the interacting particles can be easily marked within the double coset expansion, which is described in some detail in the following section.

3.2 Calculation of the spin-(isospin) matrix elements

As we have seen in the previous section, the calculation of the spatial matrix elements might be quite involved, therefore we try to reduce the number of spatial matrix elements to be calculated as far as possible but still keeping the procedure so general that different systems can be calculated by the same program without any necessary modifications, i.e. just a new input. With

respect to example ^{12}C we consider only a cluster decomposition into three clusters of four nucleons each, but do not take into account their identity.

The first step is to go from the general matrix element

$$\langle \psi^{J'M'} | \mathcal{A} \sum_{i<j} w_{ij} | \psi^{JM} \rangle \tag{3.19}$$

to the reduced one. Here ψ^{JM} denotes a single term in the total wave function eq. (2.12) allowing for the various fragmentations, the possible different components of the internal wave function eq. (2.36) and the various square integrable functions ψ in eq. (2.12). The wave function ψ^{JM} consists of spatial and spin (-isospin) part according to

$$\psi^{JM} = \sum_{m\sigma} (LmS\sigma|JM) \psi^{Lm}(\text{space}) \psi^{S\sigma}(\text{spin} - \text{isospin}) \tag{3.20}$$

where the coupling of the total orbital angular momentum L and the total spin S of the nucleons is explicitly given by the Clebsch-Gordan coefficient $(LmS\sigma|JM)$. Using Racah algebra the matrix elements eq. (3.19) can be expressed in terms of reduced matrix elements for fixed interacting particles i and j and a given rank of the interaction k [20]

$$\begin{aligned} M_{ijk} &= \sum_P < \psi^{J'M'} \left| \sum_q (-1)^P (-1)^q P w_{ij}^O(kq) w_{ij}^{ST}(k,-q) \right| \psi^{JM} > \\ &= \delta_{JJ'} \delta_{MM'} (-1)^{L+2S+S'-J} \left\{ \begin{array}{ccc} S & L & J \\ L' & S' & k \end{array} \right\} \cdot \sum_P (-1)^P \\ &\quad < L' \parallel P w_{ij}^O(k) \parallel L >< S' \parallel P w_{ij}^{ST}(k) \parallel S > \end{aligned} \tag{3.21}$$

where $\left\{ \begin{smallmatrix} S & L & J \\ L' & S' & k \end{smallmatrix} \right\}$ is a 6j-coefficient. Equation (3.21) has to be evaluated for all permutations by employing the symmetry of the orbital wave function. We will sum the spin-isospin matrix elements over all permutations, which yield the same orbital matrix.

In nuclear physics the spin-isospin operators w_{ij}^{ST} are products of the isospin operators $\mathbf{1}$ = identity resp. $\tau_i \cdot \tau_j$ with the spin operators $\mathbf{1}$ (norm and central potential), $\sigma_i \cdot \sigma_j$ (central potential), $(\sigma_i + \sigma_j)_q$ the spherical component q (spin-orbit potential), and $\sigma_{iq}\ \sigma_{jq'}$ (tensor potential). According to eq. (3.21), we have to calculate the reduced spin-isospin matrix element. Using

Wigner-Eckhart's theorem we find [20]

$$< S' \parallel Pw_{ij}^{ST}(k) \parallel S > = \frac{\sqrt{2S'+1}}{(SSkS'-S|S'S')} < S'S'|Pw_{ij}^{ST}(k, S'-S)|SS > \tag{3.22}$$

By using maximal projections of the spin functions the matrix element is guaranteed to be different from zero, if the triangular conditions are fulfilled. The easiest way to calculate the r.h.s. of eq. (3.22) is to decompose the coupled spin functions $|SS >$ into linear combinations of products of elementary single particle spin functions by using again Clebsch-Gordan coefficients. Then the operators acting on the product wave functions yield (linear combinations of) product wave functions. The permutation P can be easily applied to a product and the matrix element is straightforward to evaluate. Since usually many of these matrix elements vanish, it is more economic to start from the product functions in bra and ket and determine all permutations P with non-vanishing matrix element, for details see [16], [17]. The reduced matrix element itself requires only the sum over the known Clebsch-Gordan coefficients. Restricting our considerations for the moment to the overlap matrix element, where $w_{ij} \equiv \mathbf{1}$, we can sum all spin-isospin matrix elements belonging to one double coset including the sign of the permutation. Thus eq. (3.21) reduces to

$$\begin{aligned} M_{ijk} &= \delta_{JJ'}\delta_{MM'}(-1)^{L+2S+S'-J} \left\{ \begin{array}{ccc} S & L & J \\ L' & S' & k \end{array} \right\} \cdot \\ &\quad \cdot \sum_{dc} < L' \parallel P_{dc} w_{ij}^{O}(k) \parallel L > C_{ij}^{SS'}(dc) \end{aligned} \tag{3.23}$$

where P_{dc} is any permutation representing the double coset dc and $C_{ij}^{SS'}(dc)$ contains the sum over spin matrix elements. In case of an interaction $w_{ij} \neq 1$ one has to extend the double coset decomposition and mark the interacting particles i and j. In the following we will not review the decomposition into double cosets in general, this can be found in [22], [23], but rather discuss an illustrative example, which shows all the complexity but is still transparent. Let us consider the ^7Li nucleus, which can be described very well by a fragmentation into ^4He and ^3H. A small admixture of ^6Li and neutron, however, improves the description of excited states appreciably, see [24]. To be specific, let us decompose a matrix element eq. (3.19) into double cosets where the r.h.s. is the ^4He–^3H fragmentation and the l.h.s. the $^6Li - n$ configuration. This corresponds to a matrix element of the standard reaction ^{6}Li(n,t).

In general the decomposition into double cosets can be illustrated by symbols in matrix form, which are called *dc*-symbols [22]. In our example we decompose into $S_4 \times S_3$ for the r.h.s. and into $S_4 \times S_2 \times S_1$, for the l.h.s., because the ${}^6Li$ containing 6 nucleons has to be described by 2 clusters at least, the main component being ${}^4He - d$. Therefore we have a *dc*-symbol containing 3 rows and 2 columns:

	S_4	S_3
S_4	2	2
S_2	1	1
S_1	1	

(3.24)

where the decompostion into clusters reflects the symmetry of the spatial wave functions in bra and ket. In the example of a *dc*-symbol given above, the fact that particle numbers are conserved so that they can just be exchanged from a cluster in the bra (ket) into all clusters in the ket (bra) is taken care of by the sum of the entries in a row (column) being equal to the number of nucleons in that cluster. There is a one-to-one correspondence of *dc*-symbols and double cosets [22], therefore we can use the *dc*-symbol to construct a permutation characteristic of the double coset. For this we write the digits 1 to N row-wise into the *dc*-symbol, as many digits as indicated per site, and then read this scheme column-wise. Writing the digits found in this procedure below the digits 1 to N in natural order we find a permutation representing the double coset. In our example this will read

	S_4	S_3
S_4	12	34
S_2	5	6
S_1	7	

$$\Longrightarrow \quad \begin{pmatrix} 1 & 2 & 3 & 4 & 5 & 6 & 7 \\ 1 & 2 & 5 & 7 & 3 & 4 & 6 \end{pmatrix} = P_{dc} \tag{3.25}$$

We can now interpret this result: There is at least one permutation in the double coset, maybe the one given, which maps the spin functions in the ket onto those of the bra. The entries in (3.24) indicate how many of the particles are exchanged from the cluster given on the left side into the cluster started above by the permutation. Note that exchanging particles and permuting wave functions are inverse operations to each other. To construct the *dc*-symbol from the permutation, we write the digits 1 to N in natural order and group them according to $S_4 \times S_2 \times S_1$, i.e. 1234 56 7 and then group the second line of the P_{dc} in (3.25) according to $S_4 \times S_3$, i.e. 1257 346 and ask how many digits in the various combinations of clusters in bra and ket

agree. For example the 7 in cluster 3 of the bra agrees with the 7 in cluster 1 of the ket.

If we consider an interaction, we have to mark the interacting particles either before or after applying the permutation. We have put the permutation after the interaction, because the potential could contain an exchange operator, therefore it is more convenient to mark the permuted digit of the interacting particles with a point. For a two-body interaction we find for interacting particles 4 and 5 in our example:
$7(= P_{dc}(4))$ and $3(= P_{dc}(5))$

$$\left(\begin{array}{c|c} 12 & \overset{\bullet}{3}\,4 \\ \hline 5 & 6 \\ \hline \overset{\bullet}{7} & \end{array}\right) \equiv \left(\begin{array}{c|c} 2 & \overset{\bullet}{2} \\ \hline 1 & 1 \\ \hline \overset{\bullet}{1} & \end{array}\right) \tag{3.26}$$

where we have omitted the group configurations for convenience. The above example shows that also interacting particles $6(= P_{dc}^{-1}(4))$ and 4 would yield the same orbital matrix element. We sum the spin matrix elements belonging to these two terms. Thus we arrived at a classification scheme for matrix elements of any two body interaction in terms of 2-point *dc*-symbols, over which the sum in eq. (3.23) runs. The above classification scheme can be extended easily to one-body or three-body interactions.

3.3 Electromagnetic Transitions

Electromagnetic transitions are a reliable tool to study the structure of nuclear systems, because of the weakness of the electromagnetic interaction compared to the strong one. Such transitions, however, cannot be calculated by the techniques developed so far, because the transition operators contain besides spin operators and operators treated in chapter 3.1 also a plane wave in one of the particle coordinates measured from the center-of-mass, for details see [25].

A possibility is to expand the plane wave in a power series, keeping only the lowest orders, which is the so-called long wavelength limit, and then proceed along the lines of chapter 3.1, as given in [26]. This procedure allows to describe radiative capture reactions quite well, see e.g. [27], however, in (e, e')- or $(e, e'x)$-reactions the momentum transfer is usually much too large for this approximation to be a reasonable one. Therefore, we are not allowed

to make the long wavelength approximation, when describing electron scattering experiments. In order to illustrate the essential points, we follow [28] and strip the various electromagnetic transition operators, see [25], of all its parts, which can be treated by the methods described so far and consider in the following only the essential spatial part in a multipole expansion

$$w_j(LM) = j_L(kr'_j)Y_{LM}(\hat{\mathbf{r}}'_j) \tag{3.27}$$

where $j_L(kr)$ is a spherical Bessel function [15] and $\mathbf{r}'_j$ denotes the coordinate of the particle j with respect to the center-of-mass. Expanding the plane wave into spherical harmonics [20] we convert the operator $w_j(LM)$ into

$$w_j(LM) = \frac{1}{4\pi i^L} \int Y_{LM}(\hat{\mathbf{k}}) e^{i\mathbf{k}\cdot\mathbf{r}'_j} d\hat{\mathbf{k}} \tag{3.28}$$

It is now straightforward to define matrix elements analogous to eq. (3.4)

$$\begin{aligned} \tilde{\Gamma}^j_{l_1 m_1 \ldots l_z m_z} &= \int d\mathbf{s}_1 \ldots d\mathbf{s}_{N-1} \exp(-\sum_{\mu\mu'}^{N-1} \varrho_{\mu\mu'}(P)\mathbf{s}_\mu \cdot \mathbf{s}_{\mu'}) \\ &\cdot \quad e^{i\mathbf{k}\cdot\mathbf{Q}_0} \prod_{n=1}^{z} Y_{l_n m_n}(\mathbf{Q}_N) \end{aligned} \tag{3.29}$$

with $\mathbf{Q}_0 = \mathbf{r'}_{P(j)}$ being the coordinate of the interacting particle, after the permutation P has been applied. The generating integral eq. (3.8) is easily generalized to

$$\begin{aligned} &\tilde{I}(a_1 b_1 \ldots a_z b_z) = \\ &\int d\mathbf{s}_1 \ldots d\mathbf{s}_{N-1} \exp\left(-\sum_{\mu\mu'} \varrho_{\mu\mu'} \mathbf{s}_{\mu'} \mathbf{s}_{\mu'} + \sum_{n=1}^{z} a_n \mathbf{b}_n \cdot \mathbf{Q}_n + i\mathbf{k}\mathbf{Q}_0 \right) \end{aligned} \tag{3.30}$$

yielding by expansion again the expression (3.9). Now the generating integral $\tilde{I}$ can be calculated directly and comparing like terms we find the desired integrals $\tilde{\Gamma}$. Following along the lines of eqs. (3.10 - 3.12) we find

$$\begin{aligned} &\tilde{I}(a_1 b_1 \ldots a_z b_z) = \\ &\int d\mathbf{t}_1 \ldots d\mathbf{t}_{N-1} \exp\left[-\sum_{\lambda} \left(\beta_\lambda \mathbf{t}_\lambda^2 - t_\lambda \cdot \left(\sum_{n=1}^{z} p_{n\lambda} a_n \mathbf{b}_n + i\mathbf{k} w_{o\lambda} \right) \right) \right] \end{aligned} \tag{3.31}$$

with the relation

$$\mathbf{Q}_0 = \sum_{\lambda} w_{o\lambda} \mathbf{t}_\lambda \quad . \tag{3.32}$$

The integral is solved in the usual way by completing squares. Since the function e^{-z} is holomorphic the path of integration can be chosen arbitrarily, yielding

$$\tilde{I}(a_1 b_1 \dots a_z b_z) = \prod_{\lambda=1}^{N-1} \left(\frac{\pi}{\beta_\lambda}\right)^{\frac{3}{2}} \exp\left[\sum_{\lambda=1}^{N-1} \frac{1}{4\beta_\lambda} \left(\sum_{n=1}^{z} a_n \mathbf{b}_n p_{n\lambda} + i w_{o\lambda} \mathbf{k}\right)^2\right] . \tag{3.33}$$

Expanding the square in the exponent, we find a result analogous to eq. (3.13)

$$\begin{aligned} &\tilde{I}(a_1 b_1 \dots a_z b_z) = \prod_{\lambda=1}^{N-1} \left(\tfrac{\pi}{\beta_\lambda}\right)^{\frac{3}{2}} \exp\left(-\tfrac{w_{o\lambda}^2 k^2}{4\beta_\lambda}\right) \cdot \\ &\prod_{n>n'}^{z} \exp(\sigma_{nn'} a_n a_{n'} b_n b_{n'}) \exp(-\tfrac{\sigma_{nn'}}{2} a_n a_{n'} b_n^2) \exp(-\tfrac{\sigma_{nn'}}{2} a_n a_{n'} b_{n'}^2) \cdot \\ &\prod_{r=1}^{z} \exp(i a_r \gamma_r \mathbf{b}_r \cdot \mathbf{k}) \end{aligned} \tag{3.34}$$

with the abbreviation

$$\gamma_r = \sum_{\lambda=1}^{N-1} \frac{w_{o\lambda} p_{r\lambda}}{2\beta_\lambda} \tag{3.35}$$

All the exponents in eq. (3.34) are again expanded in a power series. For the terms $(\mathbf{b}_r \cdot \mathbf{k})^{d_r}$ eq. (3.5) is used, yielding

$$\begin{aligned} &\tilde{I}(a_1 b_1 \dots a_z b_z) = \prod_{\lambda=1}^{N-1} \left(\tfrac{\pi}{\beta_\lambda}\right)^{\frac{3}{2}} \exp\left(-\tfrac{w_{o\lambda}^2 k^2}{4\beta_\lambda}\right) \cdot \textstyle\sum_{g_{nn'} h_{nn'} k_{nn'} d_r e_r} \\ &\prod_{n>n'}^{z} \prod_{r=1}^{z} \tfrac{\sigma_{nn'}^{g_{nn'}+h_{nn'}+k_{nn'}}}{g_{nn'}! h_{nn'}! k_{nn'}!} \; i^{d_r} \tfrac{\gamma_r^{d_r}}{d_r!} \left(-\tfrac{1}{2}\right)^{h_{nn'}+k_{nn'}} C_{d_r e_r} \mathcal{Y}_{d_r e_r}(\mathbf{k}) \cdot \\ &a_n^{g_{nn'}+h_{nn'}+k_{nn'}} a_r^{d_r} a_{n'}^{g_{nn'}+h_{nn'}+k_{nn'}} \quad b_n^{g_{nn'}+2h_{nn'}} b_r^{d_r-e_r} b_{n'}^{g_{nn'}+2k_{nn'}} \end{aligned} \tag{3.36}$$

Comparing like terms in both power series analogous to eq. (3.9) yields the

final result.

$$\tilde{\Gamma}_{l_1m_1\ldots l_zm_z} = \prod_{\lambda=1}^{N-1}\left(\frac{\pi}{\beta_\lambda}\right)^{\frac{3}{2}}\exp\left(-\frac{w_o^2k^2}{4\beta_\lambda}\right)\left(\prod_{j=1}^{z}\frac{l_j!}{C_{l_jm_j}}\right)$$

$$\cdot\sum_{\substack{g_{nn'}h_{nn'}k_{nn'}\\ d_re_r}}\prod_{n>n'}^{z}\prod_{r}^{z}\frac{\sigma_{nn'}^{g_{nn'}+h_{nn'}+k_{nn'}}}{g_{nn'}!h_{nn'}!k_{nn'}!}\left(-\tfrac{1}{2}\right)^{h_{nn'}+k_{nn'}}\cdot i^{d_r}\,\frac{\gamma_r^{d_r}}{d_r!}C_{d_re_r}\mathcal{Y}_{d_re_r}(\mathbf{k}) \tag{3.37}$$

The summations run over all possible combinations of $g_{nn'}, h_{nn'}, k_{nn'}, d_r$, and e_r with the former being non-negative integers fulfilling now the relations

$$l_{n'} = d_{n'} + \sum_n (g_{nn'} + h_{nn'} + k_{nn'} + g_{n'n} + h_{n'n} + k_{n'n}) \tag{3.38a}$$

$$m_{n'} = e_{n'} + \sum_n (h_{nn'} - h_{n'n} + k_{n'n} - k_{nn'}) \tag{3.38b}$$

and

$$-d_r \le e_r \le d_r \tag{3.38c}$$

Introducing $L_n = l_n - d_n$ and $M_n = m_n - e_n$ reduces eqs. (3.38) to eqs. (3.16) and hence can be solved as before. What remains to be done is to determine all combinations (d_n, e_n) for given (l_n, n_n). Since g, h and k are non-negative, d_n is restricted to

$$0 \le d_n \le l_n \qquad n = 1, \ldots, z \tag{3.39}$$

and an obvious solution of eqs. (3.38) is

$$\begin{aligned} d_n &= l_n \quad , \\ e_n &= m_n \quad , \\ g_{nn'} &= h_{nn'} = k_{nn'} = 0 \quad \text{for} \quad n, n' = 1, \ldots z \quad . \end{aligned} \tag{3.40}$$

Summing eqs. (3.38a) and (3.38b) over n' yields two other equations, restricting the choice for d_n and e_n :

$$\sum_{n'} l_{n'} = \sum_{n'} d_{n'} + 2\sum_{nn'}(g_{nn'} + h_{nn'} + k_{nn'}) \tag{3.41a}$$

$$\sum_{n'} m_{n'} = \sum_n e_{n'} \tag{3.41b}$$

To solve eqs. (3.38) we now start from the solution (3.40) and look for all combinations of $e_{n'}$, which fulfill eq. (3.38c) and (3.41b). For each such combination $(d_n e_n)$ we solve (3.38a) and (3.38b) like eqs. (3.16) and then start with a new d_n combination till all combinations $(d_1, d_2, \ldots d_z) \in (0, \ldots, l_1) \otimes \cdots \otimes (0, \ldots, l_z)$ have been tried. Some further conditions allow to restrict the choice of (d_n, e_n) combinations appreciably, e.g. from eq. (3.41a) we deduce that the sum of all d_n is even (odd) if the sum l_n is even (odd).

What remains to be done is to integrate over the angles of the vector $\mathbf{k}$ according to eq. (3.28) leading to integrals of the form

$$\tau = \frac{1}{4\pi i^L} \int d\hat{\mathbf{k}} Y_{LM}(\hat{\mathbf{k}}) \prod_{r=1}^{z} i^{d_r} \mathcal{Y}_{d_r e_r}(\mathbf{k}) \tag{3.42}$$

Because of the above condition these integrals are always real. By combining successively two spherical harmonics to one [20], the integrals can be reduced to Clebsch-Gordan coefficients and trivial factors yielding

$$\begin{aligned} \tau \quad = \quad & (-1)^M i^{\sum_r d_r - L} k^{\sum_j d_j} \sqrt{\frac{\prod_m (2d_m + 1)}{(2L+1)(4\pi)^{z-1}}} \\ & \cdot \sum_{p_1, \ldots, p_{z-1}} \prod_{s=2}^{z-1} (d_s e_s p_{s-1} \mu_{s-1} | p_s \mu_s)(d_s 0 p_{s-1} 0 | p_s 0) \\ & \cdot \ (d_z e_z p_{z-1} \mu_{z-1} | L - M)(d_z 0 p_{z-1} 0 | L 0) \end{aligned} \tag{3.43}$$

where $p_1 = d_1, \mu_1 = e_1$ and $\mu_s = e_s + \mu_{s-1}, s = 2, \ldots z-1$. The symmetry properties of the Clebsch-Gordan coefficients lead to the following conditions for a non-vanishing τ

$$\sum_j d_j + L = \quad \text{even}$$

and

$$\max_{k \epsilon \{1, \ldots, z\}} \left\{ 2d_k - \sum_{j=1}^{z} d_j, 0 \right\} \leq L \leq \sum_{j=1}^{z} d_j \quad . \tag{3.44}$$

With this expression we have now a complete prescription how to calculate matrix elements of electromagnetic transition operators, like eq. (3.42). Additional differential operators can be treated as described in chapter 3.1. An extension to meson-exchange-currents is given in [29].

In summary, all matrix elements, be it overlap, or potential, or electromagnetic transitions ones, can be calculated by using the methods described in this chapter, provided the radial dependencies are in the form of Gaussian, positive and negative powers in r, solid spherical harmonic, powers of the differential operator, and plane waves. Since combinations of these dependencies are possible, a wide variety of operators can be treated, so that the above restriction is no practical restriction. In addition it is possible to deal with special operators, like the relativistic kinetic energy $\sqrt{p^2+m^2}$ and find analytic expressions for arbitrary number of clusters [30].

4 Determination of physical quantities

With the methods described in the previous chapter, we can now calculate all matrix elements of the Hamiltonian H or the norm matrix N in a basis, where the radial dependence of the relative wave function of two fragments is given by $r^{L_{rel}}\exp(-\beta r^2)$ for an relative orbital angular momentum L_{rel}. Choosing a model space and solving the generalized eigenvalue problem determines the eigenfunctions Γ_ν of eqs. (2.15) and (2.16). In case of a bound state calculation, these wave functions, given as an expansion in terms of Gaussians, are a variational solution. For a scattering calculation more has to be done.

4.1 Construction of physical channels

The wave functions considered so far have a definite total spin S and a definite total orbital angular momentum L, since only reduced matrix elements in spin-space and orbital space were calculated, see eq. (3.21). If one wants to describe scattering, the various clusters have to be combined to two fragments with angular momentum $\mathbf{j}_1$ and $\mathbf{j}_2$. This leads to new quantum numbers, the relative orbital angular momentum between the fragments $\mathbf{L}_{rel}$, the channel spin $\mathbf{S}_c = \mathbf{j}_1 + \mathbf{j}_2$, and the total angular momentum $\mathbf{J} = \mathbf{L}_{rel} + \mathbf{S}_c$. Hence, a physical channel is characterized by the two fragments; their internal energy if one takes excited states into account, their spin $\mathbf{j}_1$ and $\mathbf{j}_2$, $\mathbf{S}_c$, $\mathbf{L}_{rel}$, and $\mathbf{J}$.

So far the wave functions have been characterized by the spins of the fragments s_1 and s_2, the total spin $\mathbf{S} = \mathbf{s}_1 + \mathbf{s}_2$, the internal orbital angular momenta $\mathbf{l}_1$ and $\mathbf{l}_2$ and their coupling to $\mathbf{L}_3 = \mathbf{l}_1 + \mathbf{l}_2$, and finally the total orbital angular momentum $\mathbf{L} = \mathbf{L}_3 + \mathbf{L}_{rel}$. This means till now we have

worked in an LS-coupling scheme, by calculating spin and orbital matrix elements separately, but for scattering reactions we have to use the jj-coupling scheme. This change requires a recoupling via standard procedures. In an obvious notation we find

$$|[L_{rel}[[l_1 s_1]j_1[l_2 s_2]j_2]S_c]J>=\sum_{SL_3L}\ \hat{j}_1\hat{j}_2\hat{L}_3\hat{S}\hat{S}_c^2\hat{L}^2(-1)^{S_c-L_{rel}-J}$$

$$*\left\{\begin{array}{ccc} l_1 & l_2 & L_3 \\ s_1 & s_2 & S \\ j_1 & j_2 & S_c \end{array}\right\}\left\{\begin{array}{ccc} J & S & L \\ L_{rel} & L_3 & L \\ S_c & S_c & 0 \end{array}\right\}\ |\ [\ [\ [\ [l_1 l_2]L_3 L_{rel}]L[s_1 s_2]S]J> \tag{4.1}$$

where $\hat{j}=\sqrt{2j+1}$ and the curly bracket symbols are 9 j-symbols [20].

If a fragment contains different orbital angular momenta, like the S- and D-wave component in the deuteron, then this linear combination can also be performed in eq. (4.1) with the appropriate coefficients. This is another meaning of the index α in eq. (3.3).

The generalized eigenvalue problem is then solved on the basis of physical channels, eq. (4.1). An essential point is that during solution no states appear which have norm equal to zero, be they Pauli-forbidden states or states which cannot be coupled to the required quantum numbers. This is in contrast to the treatment of ref. [3] where the Pauli-forbidden states are used as a test for a correct calculation. Here another test can be performed: Collecting all diagonal overlap matrix elements (and those of the Hamiltonian), which do not have permutation across fragment boundaries (nor interaction across fragment boundaries), the calculated norm is just the product of the internal norm of the fragments times the norm of the Gaussian function on the relative coordinate, which can easily be calculated. Hence, dividing by the norm of the relative motion, the calculated internal norms have to be independent of the width used for the relative motion. A further test are the matrix elements of the Hamiltonian described above, they contain all interactions of the fragments times the relative norm. Hence dividing these matrix elements by the corresponding norm matrix elements yields the internal energy of the two fragments, the threshold energy, which again has to be independent of the width parameters used for the radial motion. In most cases these two checks are a very stringent test on the correctness of the calculation.

In order to calculate the reactance matrix a_{mn} eq. (2.31), the matrix elements for regular and irregular Coulomb functions are still missing.

4.2 Numerical procedure for the Coulomb functions

As discussed below eq. (2.41), all integrals are of short range, therefore the Coulomb functions, $f_l(r)$ and $\tilde{g}_l(r)$, see eq. (2.3), can be expanded in terms of the functions χ_ν, eq. (2.5), or Γ_ν, eq. (2.15), in an appropriately chosen finite interval Δ. Since f_l and g_l are solutions to the point Coulomb Hamiltonian, Δ has to cover the range of the interactions folded with the size of the fragments. In addition to that, the range where $\tilde{g}_l(r)$ deviates from $g_l(r)$ due to the regularisation factor $T_l(r)$, eq. (2.3), has to be considered.

The starting point is to minimize the integral

$$\int_0^\infty \left(f_L(x) - \sum_k c_k \chi_{kL}(x) \right)^2 W_L(x) dx \tag{4.2}$$

The function f_L is calculated numerically according to ref. [15]. The expansion functions χ_{kL} are given in eq. (2.5). Two sets of width parameters β_k are given in [26]. The variational parameters c_k are determined from a system of linear equations. The weight function $W_l(x)$ is chosen in such a way that the internal region dominates and the total interval becomes finite. A typical expression is

$$W_L(x) = x^{-(L+1)}\, e^{-\epsilon x^2} \tag{4.3}$$

with $\epsilon \approx 0.01 fm^{-2}$.
Thus a typical expansion interval is of the order of 20 - 50 fm. The parameter ϵ is numerically very critical: If it is chosen too large the interval will become too small and the small width parameter β_k are strongly suppressed. On the other hand if ϵ is too small, then the expansion interval will become larger and it gets numerically very difficult to reproduce the oscillating function f_L by a finite number of Gaussians centered around the origin. Increasing the number of Gaussian width parameters may lead to numerical dependencies, due to the non-orthogonality of these functions, especially as one set of parameters is used irrespective of the orbital angular momentum L.

The expansion can be improved, if in addition to the functional eq. (4.2) also the derivative of f_L is included in an obvious way. Outside the interval determined by the weight function W_L the values of the sum must not become too large. Modifications of this type are discussed in [31]. An analogous procedure is used for $\tilde{g}_l$.
Depending on the kinetic energy of the fragments we found up to 100 MeV

15 to 20 width parameters sufficient to obtain a good representation of the Coulomb functions. The choice of parameters β_k is not critical to scattering calculations. We can easily omit some of them without changing the results. Changing the parameter β_0 of the regularisation factor, eq. (2.4), in a wide range does not modify the final results either, as long as T_L approaches unity outside the interaction range.

4.3 Asymptotic contributions of the Hamiltonian

In order to determine the reaction matrix a_{mn} from eq. (2.24) and eq. (2.31) we need the matrix elements of $\tilde{H}$ between regular and irregular Coulomb functions. Hence, we need matrix elements of $\hat{H}$, eq. (2.18 - 2.19) between $F_L, \tilde{G}_L$ and Γ_ν, respectively. Since F_L and G_L are not square-integrable functions, some care is necessary. In the discussion below eq. (2.41), F_L and G_L, but obviously not $\tilde{G}_L$, had to be solutions to the point-Coulomb Hamiltonian, or to the total Hamiltonian for large separation of the fragments so that the identity operator from the antisymmetrizer between fragments could not lead to infinite contributions. Hence, one has to correct for the fact that $\tilde{G}_L$ is not a solution in just this case.

All matrix elements of $\hat{H}$, containing F_L in the ket can be calculated using the expansion coefficients determined from eq. (4.2). Using eq. (2.29) the only critical matrix elements are $< \tilde{G}|\hat{H}|\tilde{G} >$ and $< \Gamma_k|\hat{H}|\tilde{G} >$. Operating with the r.h.s. of eq. (2.41) onto $\tilde{G}_L$ we find that the regularisation factor T_L can be factored out from all terms except the kinetic energy of the relative motion. Hence, it suffices to consider this term in detail.

Since there are no permutations across fragment boundaries we can restrict the discussion to just the relative coordinate. Omitting all unnecessary factors we arrive at

$$\begin{aligned} < \tilde{g}|\frac{d^2}{dr^2}|\tilde{g} > &= \int_0^\infty dr\ g(r)T(r)\frac{d^2}{dr^2}\ [g(r)T(r)] = \\ &= \int_0^\infty dr\ \left[g(r)T^2(r)g''(r) - (g(r)T'(r))^2\right] \end{aligned} \tag{4.4}$$

where the first term is already taken care of by g being a solution to the point-Coulomb Hamiltonian and the ' denotes derivation with respect to r.

Taking into account eq. (4.2) we can write in the obvious notation

$$< \tilde{G}|H|\tilde{G} > \;=\; \sum_{mn} g_m g_n < \chi_m|\hat{H}|\chi_n > - \\ -C\int_0^\infty (GT')^2 dr \tag{4.5}$$

here g_m denote the expansion coefficients of $\tilde{G}$ and the constant C contains essentially the internal norm of the fragments.

In an analogous way we find

$$< \chi_m|\hat{H}|\tilde{G} > \;=\; \sum_n g_n < \chi_m|\hat{H}|\chi_n > - \\ -\quad C'\int_0^\infty \chi_m(2G'T' + GT'')\, dr \tag{4.6}$$

Note that the point Coulomb contribution has to be taken out of $< \chi_m|\hat{H}|\chi_n >$. The correction terms of eqs. (4.5) and (4.6) sometimes exceed the expansion terms appreciably.

Now we have all the necessary ingredients to calculate the reactance matrix a_{mn} according to eq. (2.31). Since the Hamiltonian is symmetric, the eigenvalues ϵ_ν, eq. (2.16), are real and therefore depending on the number of expansion functions χ_ν there are certain energies E for which the denominator in eq. (2.21) or (2.31) vanishes. It is easy to convince oneself, that this factor is cancelled against a corresponding one in the numerator, see also ref. [2]. There could be a slight numerical problem, if the energy E is too close to one of the eigenvalues ϵ_ν, due to division by a very small number or even zero. This difficulty can, however, be overcome quite easily by omitting the corresponding eigenvector Γ_ν, or by reducing the number of expansion functions just by one, so changing the eigenvalues ϵ_ν slightly.

It can, however, not be excluded that accidentally the denominator in eqs. (2.21) or (2.31) becomes zero, without the existence of a physical resonance. Therefore it is argued [32, 33] that using a variational principle for e.g. the S-matrix, i.e. using complex scattering functions, this problem can be avoided. This might be true in practice, but there exist counter examples [34].
Since the position of the pole depends also on the regularization parameter β_0, these accidental poles can always be avoided by changing β_0, a procedure which needs only a small amount of computing time, compared to the calcu-

lation of the matrix elements as described in chapter 3.1. Also the measures taken to avoid division by a small number, discussed above, can be used.

Following along the general lines discussed in [5] it is possible to construct various variational principles, out of which the described K-matrix, K^{-1}-matrix or the S-matrix, are just certain limiting cases. One can show that for all these different cases the matrix elements calculated so far suffice and it is only necessary to form the proper linear combinations [35]. So one could just use different methods to avoid spurious resonances. How to calculate the S-matrix and search for the complex energy poles of the S-matrix is described in [8].

5 Application to Neutron Standard Cross Sections

The region of light nuclei houses some of the neutron standards [36]. Starting from proton-neutron scattering below 20 MeV up to carbon-neutron scattering, all cross sections can be calculated by the methods described above, at least in principle, in case suitable nucleon-nucleon potentials are given. In the form of the RGM n-p scattering is just potential scattering, hence, any calculation just reflects how well the extracted potential was fitted to the original data.

The next simplest reaction is ^{3}He (n,p)^{3}H, which has ^{4}He as compound nucleus. For this A = 4 system realistic nucleon-nucleon forces are feasible, whereas for all heavier systems one has to rely on simplified, so-called effective forces. To demonstrate the differences, advantages and disadvantages I discuss in some detail in the following the ^{4}He-system and the ^{7}Li-system, which contains another standard reaction ^{6}Li (n,t)^{4}He. The reaction ^{10}B(n,α) closes this section.

5.1 The ^{4}He-System

The ^{4}He atomic nucleus is one of the best studied few-body systems, both experimentally and theoretically, as summarized in the recent A = 4 compilation [37]. Besides the many textbook examples of gross structure, there are subtle points yielding large effects that are only qualitatively understood. Except for [38] none of the existing calculations aims at a complete understanding of the many features of ^{4}He, which is not surprising in view of the number of different phenomena studied so far [37]. Here we are interested

potential	E bin		E thres	
	^{3}H	^{3}He	^{3}He-p	d - d
av18	-7.068	-6.370	0.698	3.227
av18, large	-7.413	- 6.588	0.725	3.572
av18+UIX	-7.586	-6.875	0.710	3.745
av18+UIX, large	-8.241	-7.493	0.748	4.400
exp.	-8.481	-7.718	0.763	4.033

Table 1: Comparison of experimental and calculated total binding energies and relative thresholds (in MeV) for the various potential models used.

in the ^{3}He (n,p) reaction, which connects the two lowest fragmentations in energy.

To use the above described techniques, the potentials must also be given in terms of Gaussians. Here we use realistic nucleon-nucleon forces, suitably parametrized, the Bonn [40] and the Argonne AV18 potential [39] and even a three-nucleon interaction (TNI) Urbana IX [41]. The inclusion of the additional TN1 requires almost two orders of magnitude more computing power than the realistic NN-forces alone.

In the ^{4}He system we use a model space with six two-fragment channels, namely the p-^{3}H, the n-^{3}He, the ^{2}H-^{2}H, the singlet deuteron and deuteron $đ$ -^{2}H, the $đ - đ$, and the (nn)- (pp) channels. The last three are an approximation to the three- and four-body breakup channels that cannot in practice be treated within the RGM. The ^{4}He is taken as four clusters in the framework of the RGM to allow for the required internal orbital angular momenta of ^{3}He, ^{3}H or ^{2}H.

For the scattering calculation we include S, P, and D wave contributions to the $J^\pi = 0^+$, 1^+, 2^+, 0^-, 1^-, 2^- channels. From the R-matrix analysis these channels are known to give essentially the experimental data. The full wave-functions for these channels contain over 200 different spin and orbital angular momentum configurations, hence, they are too complicated to be given in detail. For the deuteron we use a type similar to that given in [38]

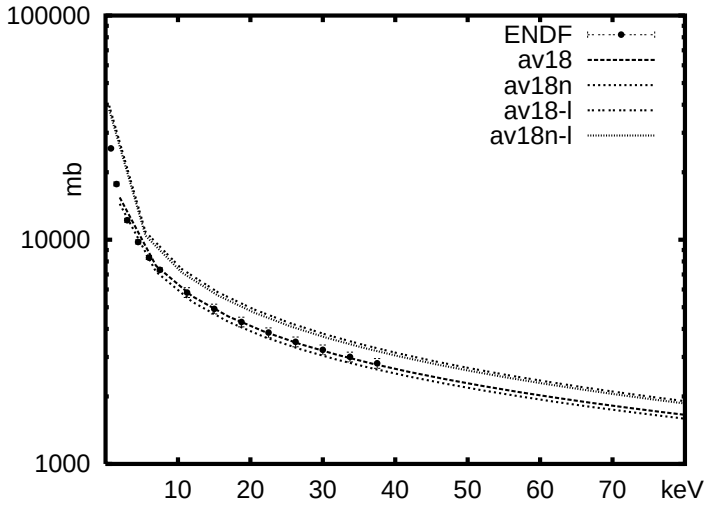

Figure 3: Comparison of the ENDF/B ^{3}He(n,p) cross section and calculations employing AV18 in the small model space (av18), adding negative parity distortion channels (av18n), for the large model space (av18-l) and adding negative parity distortion channels (av18n-l).

yielding the binding energy of - 1.921 MeV, whereas for ^{3}He and triton, we use an analogue to [42] for two model spaces, 29 and 35 dimensional, called small and large, respectively. For the triton AV18 yields -7.068 and -7.413 MeV binding energy, respectively, falling short of the experimental datum of -8.481 MeV. Adding the TNI improves the binding energies to -7.586 MeV and -8.241 MeV respectively, see table 1. The binding energy of the deuteron could be easily improved, but then the threshold energies deteriorate and thus yield worse results. All the Gaussian width parameters were obtained by a non-linear optimization using a genetic algorithm [43] for the combination of AV18 and Urbana IX. The model space described above (consisting of four to ten physical scattering channels for each J^π) is by no means sufficient to find reasonable results. So-called distortion or pseudo-inelastic channels [3] have to be added to improve the description of the wave function within the interaction region. Accordingly, the distortion channels have no asymptotic part. For practical purposes it is obvious to re-use some of the already calculated matrix elements as additional distortion channels. In that way we include all the positive parity states of the three-nucleon subsystems with $J^\pi_3 \leq 5/2^+$ in our calculation. However, it was recently pointed out by A. Fonseca [44] that states having a negative parity J^-_3 in the

three-nucleon fragment increase the n-^{3}H cross section noteably. Therefore we also added the appropriate distortion channels in a similar complexity as in the J_3^+ case to our calculation, thereby roughly doubling the size of the model space.

In fig. 3 we compare the standard ^{3}He(n,p) cross section as given in the ENDF/B-VI evaluation [36] with various calculations using the AV18 potential alone. The calculation using the smallest model space reproduces the data surprisingly well. (The kink in the calculated curves below 10 keV is due to a loss in precision of the energy.) Since the threshold energy is almost 70 keV too low, this result should not be overestimated. Especially as the calculated 0^+ triton-proton phase shifts close to threshold and below demonstrate large differencies between themselves and to the R-matrix analysis, see fig. 4.

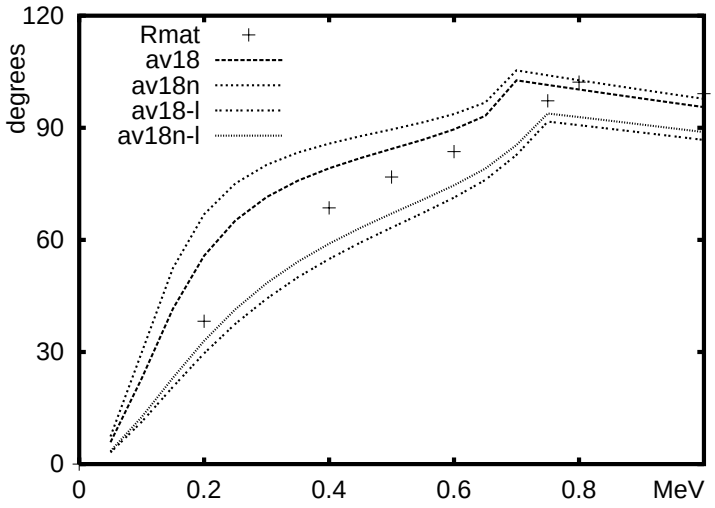

Figure 4: Comparison of the 0^+ triton-proton phase shifts from the R-matrix analysis (crosses) and calculations employing AV18 in the small model space (av18), adding negative parity distortion channels (av18n), for the large model space (av18-l) and adding negative parity distortion channels (av18n-l).

The corresponding figure 5 including three-nucleon forces reveals a much better agreement, also for the threshold energies, see table 1. Unfortunately the ^{3}He(n,p) cross sections including TNI are not yet available, due to the large amount of CPU time necessary.

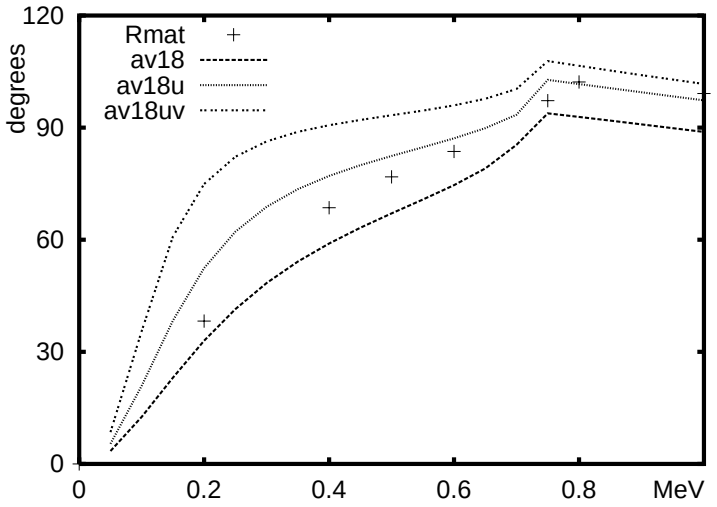

Figure 5: As fig. 4, but R-matrix results (crosses) are compared to the full NN-calculation (av18), adding UIX (av18u) and adding V_3^* (av18uv).

Since the ^{3}He(n,p) data at higher energy are usually deduced via detailed balance from the more easily accessible ^{3}H(p,n) reaction we display in the following the results of a few calculations. In fig. 6 the results for the Bonn potential and a semi-realistic one, which will be used later on on the ^{6}Li(n,t) reaction, are compared to data and the R-matrix analysis. At forward and backward angles large discrepancies between data and calculation are visible. In fig. 7 we change from using the Bonn potential to the Argonne AV18. Obviously the calculations reproduce the data much better. Again the calculation employing the smallest model space is by far the best, missing the data only close to the minimum around 90 degrees. Additional three-nucleon forces do not improve the situation. Considering the fact that the calculations start ab initio from NN- and NNN-potentials the agreement between data, R-matrix analysis, and microscopic calculation is remarkably good. At the time being, any extension to heavier nuclei using the above forces fails due to lack of computing power.

5.2 The ^{7}Li System

The ^{6}Li(n,t) reaction is a standard neutron cross section from thermal energies to 1 MeV [36]. In this energy range is a well developed $\frac{5}{2}^-$ resonance

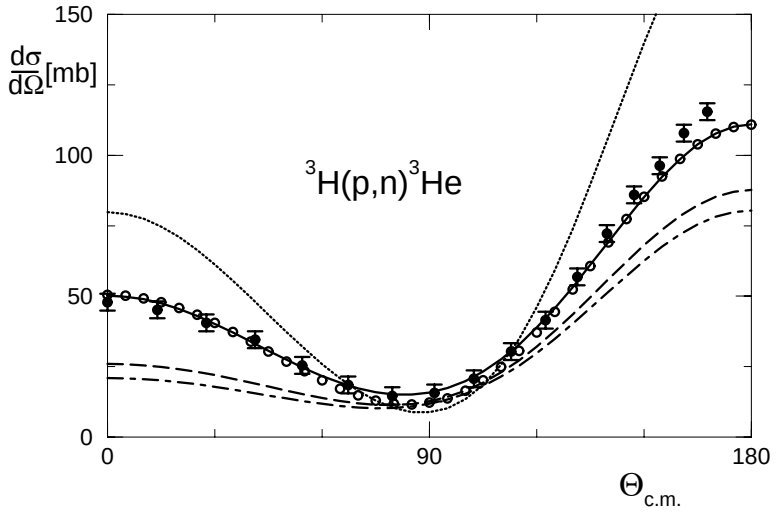

Figure 6: Differential cross section of the reaction ^{3}H(p,n)^{3}He calculated for $E_{cm} = 3.0$ MeV. The data are for 4.101 MeV protons from Perry. The full line represents the R-matrix analysis, the dashed one the full calculation using the Bonn potential, the dot-dashed one the small calculation, and the dotted one the semi-realistic calculation. The open circles denote the full calculation with the $^3P_2$ matrix element replaced by the corresponding R-matrix one, for details see [38].

around 2.40 MeV neutron energy [45]. An RGM calculation using realistic NN-forces is no more feasible. Even a calculation using a semi-realistic potential form [26] poses a major task, due to the many possible fragmentations, like ^{4}He-^{3}H and ^{6}Li-n for the standard reaction, but additional fragmentations ^{6}Li (excited)-n, ^{5}He-d and ^{5}Li-(nn) [45] are necessary to reproduce the position of the $\frac{5}{2}^-$-resonance reasonably well [46, 26]. The the first task is to determine the internal wave functions of all fragments together with the excited states such that the many thresholds are reproduced reasonably well. As all effective forces share a reduced core, they tend to overbind, in case the model space is increased by using more and more width parameters or configurations with internal orbital angular momenta. Therefore any such calculation is a compromise between reproducing the size of the various fragments, the relative threshold energies and the total binding energy of the system, in this case the ^{7}Li ground state $\frac{3}{2}^-$ and first excited state $\frac{1}{2}^-$, well below the ^{4}He - ^{3}H threshold. Increasing the model space too far, leads to overbinding and to tiny fragments, reducing the binding energy might yield too large fragments and then too strong interactions at low energies. Typ-

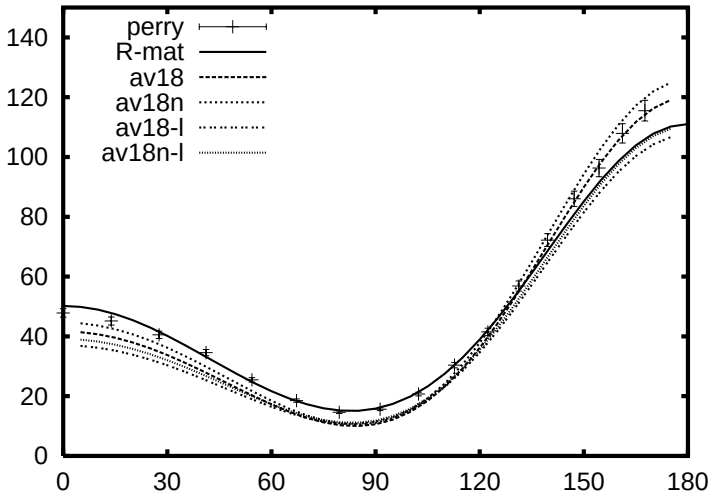

Figure 7: As fig. 6, but data and R-matrix results (crosses) are compared and calculations employing AV18 in the small model space (av18), adding negative parity distortion channels (av18n), for the large model space (av18-1) and adding negative parity distortion channels (av18n-1).

ical examples for the charge conjugate system ^{7}Be are given in [47]. The potential is described in [26]. What can be achieved for the corresponding elastic scattering ^{6}Li(n,n) is displayed in fig. 8, taken from [48].
It should be noted, however, that this effective potential overbinds neutron halo nuclei, like ^{6}He and ^{8}He [49].

To cure this problem a realistic NN interaction has to be used for the NN-P-wave configurations, see [49], whereas for the positive parities still the effective force [26] with the reduced core is taken. A calculation using this potential also in the ^{7}Li-system is under way, see [50].

5.3 The ^{11}B System

The next heavier standard neutron cross sections are ^{10}B(n,α)^{7}Li and ^{10}B(n,α,γ)^{7}Li from thermal energies to 250 keV. As can be seen from the energies of light nuclei [51] there are many resonances in the compound system ^{11}B close to the ^{10}B-n threshold. There are already many channels open, like ^{10}Be-p, ^{8}Be - ^{3}H, and ^{7}Li - ^{4}He together with the first excited state, and furthermore the ^{11}B nucleus has many particle stable states below the

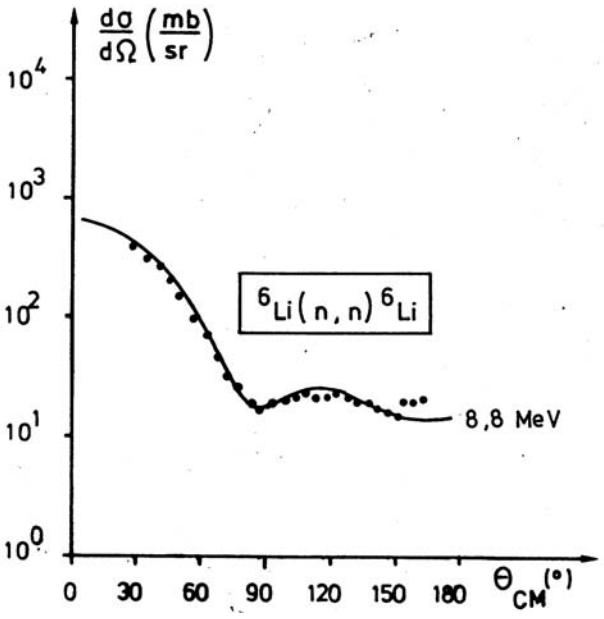

Figure 8: Comparison of a microscopic multi-channel calculations with data for elastic neutron scattering off ^{6}Li.

lowest break-up threshold. Therefore describing the reactions ^{10}B (n,$\alpha_{0,1}$) microscopically poses a major problem. For the potential described in the previous section this task seems to be feasible, but the outcome is unknown.

6 Limitations of the method and conclusion

In the previous chapter various examples demonstrated the great flexibility of the resonating group method. Finally I will discuss some limitations of the method. Of a principle nature are breakup channels into three or more fragments. If the direct coupling to such channels is indeed strong, then the recipe of approximating these channels by effective two fragment channels will not yield good results. Attempts [52] to connect the resonating group method with Faddeev type approaches face the very complex interacting potentials between the fragments. A straightforward approach by expanding the wave function is not possible, because the boundary condition depends on the coordinates. Fortunately, however, most strong breakup channels proceed via sequential decay and thus can be well approximated.

The technical limitations fall into several classes. The most obvious one is the number of particles. Depending on the cluster structure the double coset classification of chapter 3 is feasible on modern workstations up to 12 or even 16 particles, as long as only the highest orbital symmetry is considered. In case of lower symmetries playing an essential role, which means that the number of clusters is increased, the maximum number is around 12. A typical example for such cases are the neutron-halo nuclei like ^{11}Li and ^{11}Be, which can be described by $\alpha - {}^3\mathrm{H} - n - n - (nn)$ and $\alpha - \alpha - n - n - n$ configurations respectively. Larger nuclei can be much better described in the framework of the Generator coordinate method [53, 3], where shell-model techniques can be utilised to reduce the calculation of A-body matrix elements to 2-body matrix elements.

Another obvious limitation is the expansion of the bound state wave function in terms of Gaussians. Even though the number of width parameters may be chosen quite high, the asymptotic behaviour is never that of an exponential function. Hence, if the bound state wave function is needed far beyond the root-mean-square radius, like in the radiative capture at very low energies, approaches where the asymptotic form of the wave function can be utilised [54, 55] are preferable. These methods, however, have to solve the integro-differential equations and therefore have to calculate the kernels, so far by hand or computer algebra and are therefore restricted to mostly 2-, at most 3-cluster systems.

A further limitation lies in the expansion of the scattering wave function in the interaction region in terms of Gaussian functions. Since the Gaussians are all centered at the origin, they will become numerically dependent if too many of them are used. On the other side if the kinetic energy becomes higher and higher more and more zeros of the relative motion wave function move into the interaction region, thus requiring more and more Gaussians. In model studies we found numerically stable sets of Gaussians for up to three zeros. In principle one could use eq. (3.17) and multiply the Gaussians by even powers of r. In model studies this procedure works quite well in practical calculations, however, the following limitations do not allow to reach such an energy range.

With increasing energy usually the number of open channels increases rapidly. The diagonalisation of the resulting large matrices can be done easily. The threshold energies, however, are no more well reproduced, introducing some uncertainties. Furthermore, near thresholds the numerical procedures tend

to be less stable, thus increasing the uncertainties. A typical example on this limit is the reaction ^{4}He (^{2}H, ^{3}He) ^{3}H studied in [56]. By carefully choosing the Gaussian parameters and the weight function, eq. (4.2), the situation can be improved appreciably.

The most serious limitation in energy is, however, related to the potential used. Since one wants to utilise the symmetry of the dominant structures, one needs simple wave functions for the lightest nuclei, i.e. deuteron, triton, ^{3}He and ^{4}He. In practice these light nuclei are just described by pure S-waves, using linear combinations of some Gaussian functions of the internal coordinates. For a nucleon-nucleon potential such wave functions only yield binding, if the short-ranged repulsive core is reduced appreciably. This procedure on the other hand does not yield enough repulsion at higher energies, where the short range behaviour of the potential is tested more closely. The potential we usually employ [26] gives reasonable cross sections up to 35 till 50 MeV centre-of-mass energy above the lowest threshold, depending on the system. The simple cure of using a realistic nucleon-nucleon potential, like [39, 40], leads to such complicated bound state wave functions, that any calculation beyond A = 5 seems to be no more technically feasible [38].

In conclusion, the resonating group model provides the means to study a wide range of few body problems, if an interaction exists which allows to describe the systems with sufficient accuracy. So far nuclear systems have been studied predominantly, but also atomic [14] or molecular problems may be investigated.

Acknowledgments

This work would not have been possible without the dedicated effort of many diploma and Ph.D. students, contributing in various ways. The financial support of the Deutsche Forschungsgemeinschaft and the BMBF is greatfully acknowledged.

References

[1] J. A. Wheeler, Phys. Rev. **52** (1937) 1083-1106 and 1107-1122

[2] H. H. Hackenbroich, in: The Nuclear Many Body Problem, (F. Calogero and C. Cioffi degli Atti, eds.) pp 706-747, Editrice Compositori, Bologna (1973)

[3] Y. C. Tang, in: Topics in Nuclear Physics, (T. T. S. Kuo and S. S. M. Wong, eds.) Lect. Notes in Physics **145**, pp 572-693, Springer, Heidelberg (1981)

[4] H. M. Hofmann, in: Models and Methods in Few-Body Physics, (L. S. Ferreira, A. C. Fonseca and L. Streit) Lect. Notes in Physics **273**, pp 241-282, Springer, Heidelberg (1987)

[5] E. Gerjuoy, A. R. P. Rau, and L. Spruch, Rev. Mod. Phys. **55** (1983) 725-774

[6] W. Kohn, Phys. Rev. **74** (1948) 1763-1772

[7] O. Flebbe, Hadronen mit Strangeness im Quark Cluster Modell, diploma thesis, Erlangen 1989, unpublished

[8] A. Thielmann, Bestimmung der S-Matrix Pole in der komplexen Energieebene, diploma thesis, Erlangen 2001, unpublished

[9] S. Weinberg, Phys. Rev. **131** (1963) 440-460

[10] T. Kato, Prog. Theor. Phys. (Japan) **6** (1951) 394-407

[11] G. John, Anwendung der Theorie der symmetrischen Gruppe auf Zustände und Reaktionen der leichtesten Kerne, BMBW-FB K 71-20, ZAED, Leopoldshafen (1971)

[12] K. T. Hecht, E. J. Reske, T. H. Seligman, and W. Zahn, Nucl. Phys. **A 356** (1981) 146-222

[13] K. T. Hecht, H. M. Hofmann, and W. Zahn, Phys. Lett. **103 B** (1981) 92-98

[14] H. Aulenkamp, Eine mikroskopische Behandlung der niederenergetischen Elektron-Atom-Streuung, Burg Monographs in Science, Vol.**10**, Burg Verlag, Basel (1978)

[15] M. Abramowitz and I. A. Stegun (eds.) Handbook of Mathematical Functions, National Bureau of Standards, Washington D.C. (1964)

[16] H. H. Hackenbroich, Z. Phys. **231** (1970) 216-224

[17] H. M. Hofmann and T. Mertelmeier, Die Berechnung von Matrixelementen im Refined Resonating Group Modell, Internal report, Erlangen 1984 (unpublished)

[18] M. E. Rose, Elementary Theory of Angular Momentum, Wiley, New York (1957)

[19] H. Stöwe, Radien und Übergangswahrscheinlichkeiten von ^{6}Li im verallgemeinerten Clustermodell, Diploma thesis, Cologne (1970) unpublished

[20] A. R. Edmonds, Angular Momentum in Quantum Mechanics, Princeton University Press (1960)

[21] J. Burger, Nukleon-Nukleon Streuung in einem nichtrelativistischen Quarkmodell, Ph.D. thesis Erlangen (1985) unpublished

[22] T. H. Seligman, Double Coset Decomposition of Finite Groups and the Many Body Problem, Burg Monographs in Science, Vol.**1**, Burg Verlag, Basel (1975)

[23] A. Ludwig, Gruppentheoretische Methoden im Clustermodell der Atomkerne - allgmeine Prinzipien und deren Anwendung bei der Berechnung spektroskopischer Faktoren, Diploma thesis Erlangen (1981) unpublished

[24] M. Unkelbach and H. M. Hofmann, Phys. Lett. **261 B** (1991) 211-216

[25] J. Eisenberg and W. Greiner, Excitation Mechanism of the Nucleons, Vol. **2** North Holland, Amsterdam (1970)

[26] T. Mertelmeier and H. M. Hofmann, Nucl. Phys. **A 459** (1986) 387-416

[27] B. Wachter, T. Mertelmeier, and H. M. Hofmann, Phys. Rev.**C 38** (1988) 1139-1144

[28] T. Schmeidl, Mikroskopische Beschreibung photonuklearer Prozesse in leichten Kernen, diploma thesis, Erlangen (1987) unpublished

[29] M. Unkelbach and H. M. Hofmann, Nucl. Phys. **A 549** (1992) 550-576

[30] T. Schmeidl, Ein konsistentes Quark Potentialmodell und seine Anwendung auf die Meson-Meson Streuung, Ph. D. thesis, Erlangen (1990) unpublished

[31] W. Schütte, Eine mikroskopische ^{6}Li-Streurechnung zur Untersuchung der Ladungsenergieeigenschaft der Reaktion ^{4}He + d $\rightarrow$ ^{3}He + ^{3}H, Ph. D. thesis, Cologne (1977) unpublished

[32] W. H. Miller, Comments At. Mol. Phys.**22** (1988) 115-131

[33] J. Z. H. Zhang, S.-I. Chu, and W. H. Miller, J. Chem. Phys. **88** (1988) 6233-6239

[34] R. L. Lucchese, Phys. Rev. **A 40** (1989) 6879-6885

[35] C. Winkler, Vergleich von Kohnschen Variationsprinzipien, diploma thesis, Erlangen (1994) unpublished

[36] A. D. Carlson, W. P. Poenitz, G. M. Hale, R. W. Peelle, D. C. Dodder, C. Y. Fu, and W. Mannhart, the ENDF/B-VI Neutron Cross Section Measurement Standards, Nistir 5177, US Department of Commerce (1993)

[37] D. R. Tilley, H. R. Weller, and G. M. Hale, Nucl. Phys. **A 541** (1992) 1

[38] H. M. Hofmann and G. M. Hale , Nucl. Phys. **A 613** (1997) 69-106

[39] R. B. Wiringa, V. G. J. Stokes, and R. Schiavilla, Phys. Rev. **C 51** (1995) 38

[40] H. Kellermann, H. M. Hofmann, and Ch. Elster, Few Body Syst. **7** (1989) 31-53

[41] B. S. Pudliner, V. R. Pandharipande, J. Carlson, S. C. Pieper, and R. B. Wiringa, Phys. Rev. **C 56** (1997) 1720

[42] B. Pfitzinger, H. M. Hofmann and G. M. Hale, Phys. Rev. **C 64** (2001) 044003

[43] C. Winkler, H. M. Hofmann, Phys. Rev. **C 55** (1997) 684

[44] A. C. Fonseca, Phys. Rev. Lett. **83** (1999) 4021

[45] F. Ajzenberg-Selove, Nucl. Physik **A 490** (1988) 1

[46] H. M. Hofmann, Nucl. Phys. **A 416** (1984) 363

[47] H. M. Hofmann, T. Mertelmeier and W. Zahn, Nucl. Phys. **A 410** (1983) 202

[48] M. Herman, unpublished 1985, and H. M. Hofmann in "Use of the Optical Model for the Calculation of Neutron Cross Sections below 20 MeV", NEADC-222 'U', page 77, OECD Paris 1986

[49] J. Wurzer and H. M. Hofmann, Phys. Rev. **C 55** (1997) 688

[50] T. Michler, diploma thesis, Erlangen 2002

[51] F. Ajzenberg-Selove, Nucl. Phys. **A 506** (1990) 1

[52] K. Hahn, Beobachtbare off-shell-Effekte und das Pauli-Prinzip in den Reaktionen ^{4}He + Deuteron $\rightarrow$ ^{4}He + Deuteron und ^{4}He + Deuteron $\rightarrow$ ^{4}He + Neutron + Proton, Ph.D. thesis, Tübingen (1983) unpublished

[53] D. Baye and P. Descouvemont, Nucl. Phys. **A 407** (1983) 77-97

[54] T. Kajino and A. Arima, Phys. Rev. Lett. **52** (1984) 739-742

[55] Q. K. K. Liu, H. Kanada, and Y. C. Tang, Phys. Rev. **C 23** (1981) 645-656

[56] M. Bruno, F. Cannata, M. D'Agostino, M. L. Fiandri, M. Herman, and H. M. Hofmann, Phys. Rev. **C 41** (1990) 2435-2437 and reference therein

Parameters for Nuclear Reaction Calculations - Reference Input Parameter Library (RIPL-2)

M. Herman*

International Atomic Energy Agency, Vienna, Austria

Lectures given at the
Workshop on Nuclear Reaction Data and
Nuclear Reactors: Physics, Design and Safety
Trieste, 25 February - 28 March 2002

LNS0520002

*mwherman@bnl.gov

Abstract

The status and contents of the Reference Input Parameter Library (RIPL) are summarised. This input library provides an extensive database of model parameters for theoretical calculations of nuclear reactions. It was developed to facilitate use of reaction codes and increase the accuracy of theoretical predictions.

1 Introduction

Increased use of nuclear reaction theory for predicting cross sections, spectra, and angular distributions, as required for a large variety of applications, is an important trend in the evaluation of neutron and charged-particle nuclear data. The model codes offer important advantages such as ensuring internal consistency of the data by preserving the energy balance and the coherence of the partial cross sections with the total or the reaction cross sections. These features are essential for transport calculations. In addition, theoretical calculations represent the only approach that can fill gaps in the experimental results and predict data for unstable nuclei. Nuclear astrophysics and the design of Accelerator Driven Systems are typical applications that depend strongly on theoretical calculations.

With recent formulation of nuclear reaction models (triple-integral form of the statistical model [1], quantum mechanical Multistep Direct and Multistep Compound [2, 3, 4]) and existing approaches to direct reactions, nuclear reaction theory is believed to be in a position to meet most of the requirements for practical applications. The major sources of uncertainty are, the input parameters needed to perform theoretical calculations, including nuclear masses, deformations, nuclear levels and their decay characteristics, γ-strength functions, neutron resonances and level densities, optical model parameters, and fission barriers. The IAEA has addressed these needs through a Coordinated Research Project on the Reference Input Parameter Library (RIPL), which involves the difficult task of collecting, evaluating and recommending the vast amounts of various nuclear parameters. RIPL is targeted at users of nuclear reaction codes and, in particular, at nuclear data evaluators. The first phase of the project was completed in 1999, with the production of a Starter File and related documentation [5]. A second phase of the project was initiated in 1999 to test the RIPL-1 database and produce interfaces between RIPL and commonly used nuclear reaction codes.

Substantial improvements and extensions to the original database have been made, resulting in a more accurate and reliable library. All files selected for RIPL-2 have been prepared in the unified RIPL-2 format, which facilitates their use in the reaction codes. The RIPL-2 library is expected to be released in July 2002. The contents of the RIPL-2 library are outlined below, with possible improvements that could be made to the current database through new measurements at the SNS.

2 Contents of RIPL-2

2.1 Segment 1: MASSES

The mass segment contains basic ground state properties of nuclei, along with two theoretical predictions of masses and deformations. On the basis of the Hartree-Fock-Bogolubov (HFB) theory, a 10-parameter Skyrme force, along with a 4-parameter delta-function pairing force (with blocking for odd nuclei) and a 3-parameter Wigner term, was fitted to all 1888 measured masses of nuclei with N and Z $\geq$ 8. The second file contains predictions obtained within the Finite Range Droplet Model (FRDM) [6]. The atomic mass excesses and nuclear ground-state deformations are tabulated for 8979 nuclei ranging from ^{16}O to A=339. These calculations are based on the finite-range droplet macroscopic model and the folded-Yukawa single-particle microscopic model. The most recent evaluated experimental masses by Audi and Wapstra [7] are included as a separate column. A third possibility is provided by a subroutine implementing the Duflo-Zuker formula [8] for nuclear masses in which, the nuclear Hamiltonian is separated into a monopole term and a residual multipole term. The monopole term is responsible for saturation and single-particle properties, and is fitted phenomenologically while the multipole part is derived from realistic interactions. The latest version of the mass formula made of 10 free parameters reproduces the 1950 experimental masses above ^{4}He with an rms error of 574 keV.

RIPL-2 also provides natural abundancies according to the Wallet Cards and HFB matter densities. The data are necessary for calculation of optical model parameters within the semi-microscopic approach (code MOM) in segment 4.

2.2 Segment 2: LEVELS

This segment contains 110 files (one for each element) with all known level schemes available from ENSDF in 1998. These files are arranged and preprocessed into an easy-to-read format for nuclear reaction codes. During preprocessing all missing spins were inferred uniquely for each level from spin distributions extracted from the existing data. Electromagnetic and γ-ray decay probabilities were estimated. Missing internal conversion coefficients (ICC) were calculated using the inferred or existing spin information, in which existing multipole mixing ratios were also taken into account. Particle decay modes are also given whenever measured. In all cases, the total

decay probability was normalized to unity, including particle decay channels.

This segment also contains the results of constant temperature fit of nuclear level schemes. The main purpose of this file is to provide cut-off energies U_{max} and U_c for completeness of levels and spins in each level scheme. Furthermore, the nuclear temperature inferred from the discrete levels and intended for use in the level density estimation is provided.

2.3 Segment 3: RESONANCES

The average resonance parameters recommended for RIPL-2 were prepared on the basis of the evaluations performed by the Obninsk group, taking into account the analysis of discrepancies between similar evaluations of other groups. Good agreement was found for Γ_γ among the three RIPL-1 files (Obninsk, Mughabghab and Beijing) [5]. However, the comparison is less favorable for the neutron strength functions, especially for those cases with a large number of resonances. The revised average resonance parameters were obtained for 20 additional nuclei for which the data on resolved resonance parameters are available in the Sukhoruchkin compilation [9], bringing the total number of D_{obs} in RIPL-2 to 301. Generally, the accuracy of these additional data is rather poor due to the low number of resonances available for analysis. New evaluations of the average parameters for p-wave neutron resonances, prepared by the Obninsk group, have been included in the updated version of the RIPL-2 file. These resonances provide a good check of consistency since they are known to be about a factor of 3 smaller than the s-wave spacings, which is particularly relevant for magic nuclei.

Careful attention was paid to the estimation of uncertainties for the recommended parameters, based on experienced guesswork of systematic errors beside statistical uncertainties.

2.4 Segment 4: OPTICAL

The optical model parameter (OMP) segment is provided in two forms: full library (archival form) and shorter library with all single-energy potentials removed (user file). Currently, the user (archival) file contains 258 (258) potentials for incident neutrons, 98 (143) potentials for incident protons, 8 (11) for deuterons, 1 (26) for tritons, 3 (53) for ^{3}He particles, and 10 (10) for incident α-particles. Of the neutron potentials, 229 are spherical potentials, 28 are coupled-channels potentials, and 1 is a vibrational model. There are 6 coupled-channels and 92 spherical potentials for incident protons in the

user library, and a total of 5 dispersive optical potentials for incident neutrons. Additions to the OMP library were made including new potentials from JENDL and from the Chinese Nuclear Data Center, as well as several new potentials from Bruyeres and Los Alamos. The new global potential for neutrons and protons from Koning and Delaroche [10] was incorporated, as were the new dispersive potentials from Capote. Where there are not enough experimental data to define phenomenological OM parameters, one has to resort either to global parameterizations or to new microscopic approaches. The semi-microscopic model developed at Bruyeres is now part of the OM segment, incorporating a revised version of the MOM code which relies on the Jeukenne, Lejeune, and Mahaux nuclear matter approach.

A compilation of 1708 deformation parameters (β_2 and β_3) for collective levels has been retrieved from the JENDL-3.2 evaluations, ENSDF and literature to be used in direct reaction calculations. These deformations are in addition to those provided explicitly for the Coupled-Channels potentials in the OMP library.

2.5 Segment 5: LEVEL DENSITIES

2.5.1 Total level density

A revised version of the Back Shifted Fermi Gas (BSFG) model parameters was prepared by the Obninsk group to be consistent with both the recommended RIPL-2 neutron resonance parameters and the evaluated parameters of the recommended low-lying levels. The new BSFG systematics developed by the Brussels group is consistent with the recommended RIPL-2 neutron resonance parameters, and will be included in the RIPL-2 TECDOC. The Gilbert-Cameron (GC) and Generalized Super-fluid Model (GSM) parameters were revised by the Obninsk group in accordance with changes in the RIPL-2 resonance segment. The microscopic HF-BCS calculations of the nuclear level densities are based on the realistic microscopic single-particle level scheme [11] determined within the HF-BCS mass model obtained with the MSk7 Skyrme force, and were supplied by Goriely and made available from the RIPL-2 library. Also, the single-particle schemes used in the HF-BCS calculations were provided by the Brussels group. In addition, the FRDM single-particle schemes are included as corresponding to the accepted FRDM mass table.

2.5.2 Partial level densities

A critical review was undertaken of the methods for calculating partial level densities to be used in pre-equilibrium model calculations. A code for a combinatorial calculation of particle-hole state densities, based on a convolution of shell-model single particle-states with BCS pairing, is included in RIPL-2 along with the corresponding tools for retrieving single-particle levels from Segment I. The most useful analytical approaches in the frame of the equidistant single-particle model are implemented in the revised AVRIGEANU code [12]. The finite hole-depth and binding energy restrictions are taken into account in these calculations.

2.6 Segment 6: GAMMA

This segment contains parameters that quantify Giant Resonances, experimental γ-strength functions and methods for calculating γ-emission in statistical model codes.

The experimental Giant Dipole Resonance parameters were provided by the Chinese group, as represented by Lorentzian fits to the total photoneutron cross sections for 102 nuclides ranging from ^{51}V to ^{239}Pu as compiled by Dietrich and Berman [13]. Additional data for ^{12}C, ^{14}N, ^{16}O, ^{27}Al and ^{28}Si were estimated by Liu Jianfeng and Su Zongdi in 1995 [14].

New compilations of calculated GDR widths and energies for about 6000 nuclei with $14 \leq Z \leq 110$ lying between the proton and the neutron driplines have been provided by Goriely. The table gives the predicted GDR energies [15] with a renormalized np-interaction of strength derived from a least-square fit to the experimental GDR energies [16]. The expression for the shell-dependent GDR width is taken from [17] using the newly-determined GDR energies and the ETFSI shell correction energies. Such predictions include the shell-dependent GDR broadening due to the coupling between the dipole oscillations and the quadrupole surface vibrations.

Theoretical predictions of the E1-strength functions for 3317 nuclei with $8 \leq Z \leq 84$ lying between the proton and the neutron drip-lines have been supplied by Goriely [18, 19]. These strength functions were determined within the QRPA model based on the SLy4 Skyrme force. The ground state was consistently calculated within the Hartree-Fock+BCS model based on the same SLy4 force. QRPA equations were solved in the configuration space so as to exhaust the energy weighted sum rule. All QRPA calculations are performed in the spherical approximation. A folding procedure is applied to

the QRPA strength distribution to take the damping of the collective motion into account. In the case of deformed nuclei, a phenomenological splitting of the QRPA resonance strength is performed in the folding procedure. The resulting E1-strength function is found to be in close agreement with photo-absorption data as well as the available experimental E1 strength at low energies.

A theory-supported practical approach, based on a micro-canonical description of initial states (modified Lorentzian (MLO)) for the calculation of the dipole radiative strength function, was compared with experimental data as well as with the SLO end EGLO models, and included in the library. The strength functions for other multi-polarities will be carried over from RIPL-1.

2.7 Segment 7: FISSION

Fission is a new RIPL-2 segment, which retains the RIPL-1 recommendation and, in addition, includes global prescription for barriers and nuclear level densities at saddle points.

Fission barrier parameters for the trans-thorium nuclei were recommended by Maslov [5] and for the preactinides by Smirenkin [20]. The fission barrier parameters are strongly correlated with the corresponding level density description and the symmetry of the fission barriers should always be taken into account for the consistent description of the fission cross sections. For nuclei with Z¡80 the liquid drop barriers described by Sierk's code [21] are recommended with the addition of the ground-state shell corrections estimated by the Moeller-Nix (Segment 1) or the Mayer-Swiatecki (Segment 5) mass formulae. Sierk's code provides fits to the fission barriers calculated using Yukawa-plus-exponential double folded nuclear energy, exact Coulomb diffuseness corrections, and diffuse-matter moments of inertia.

Another option is to predict the fission barriers and saddle point deformations obtained within the Extended Thomas-Fermi plus Strutinsky Integral (ETFSI) method of Goriely. The ETFSI approach is a semi-classical approximation to the Hartree-Fock method in which the shell corrections are calculated with the 'integral' version of the Strutinsky theorem. BCS corrections are added with a delta-pairing force. Fission barriers are derived in terms of the SkSC4 Skyrme force on which the ETFSI-1 mass formula is based. Experimental primary barriers can be reproduced within plus or minus 1.5 MeV (except for elements with $Z < 87$ which have barriers above 10

MeV). The present ETFSI compilation includes 2301 nuclei with 78≤Z≤120. Their masses range from slightly neutron deficient to very neutron rich nuclei (close to the calculated neutron drip line) up to A = 318. For each nucleus a maximum of two barriers are given ("inner" and "outer"). In addition to these calculated barriers, the deformation parameters at the corresponding saddle points are also included. The nuclear shapes are limited to axially symmetrical deformations.

The ETFSI fission barriers are complemented with nuclear level densities (NLD) at the fission saddle points [22] for some 2300 nuclei with 78≤Z≤120. At each saddle point, the NLD is estimated within the statistical partition function approach. The NLD calculation is based on the realistic microscopic single-particle level scheme [11] determined by means of the HF-BCS mass model obtained with the MSk7 Skyrme force. For each saddle point, the single-particle level scheme is calculated consistently by the HF-BCS model constrained on the corresponding quadrupole, octupole and hexadecapole moments. The same pairing strength (within the constant-G approximation) is used as for the NLD calculation at the ground-state equilibrium deformation (segment 5). No damping of the collective effects at increasing excitation energies is considered. The NLD for nuclei with left-right asymmetric fission barriers is increased by a factor of 2.

3 Testing

Tests have been performed on the optical, resonance and levels segments. A number of misprints and erroneous coding have been detected and corrected.

Several RIPL participants tested the preliminary version of the levels database by using the data in calculations. A new simple test was worked out for checking nuclear temperature (T) derived from the analysis of cumulative plots of discrete levels, yielding temperature values which are remarkably similar to the T(A) function obtained in the global fitting procedure. Ignatyuk tested the performance of the T(A) function by comparing the results with the temperature obtained by Gilbert and Cameron; he found reasonable agreement and recommended the use of T(A) in cases for which no direct estimation is possible. Herman has extensively tested N_{max} values for nearly 500 nuclei using the Gilbert-Cameron procedure and level densities specific to the EMPIRE code. Perfect fits were obtained for about 50% of all analyzed cases, fair agreement was found for about 25%, and poor for the remaining 25%. The quality of the fit depends on the model used for

level densities. No formatting errors were detected while reading files with discrete levels.

Global testing of the RIPL-2 database has been performed in three separate exercises. Large numbers of nuclear reaction cross sections were calculated by means of the nuclear model codes EMPIRE-II, UNF and TALYS. Herman performed calculations for the most important neutron-induced reactions on 22 targets from ^{40}Ca up to ^{208}Pb in the energy range from 1 keV up to 20 MeV. The 2-17-beta version of the statistical model code EMPIRE-II has been used with all default parameters except those differentiating the 3 series of runs. In all cases TUL MSD and Heidelberg MSC models were used for pre-equilibrium emission of neutrons, and exciton model (DEGAS) for pre-equilibrium emission of protons and γs. These studies were complemented with Hauser-Feshbach calculations including widths fluctuations at incident energies below 5 MeV (HRTW model). The results were converted into ENDF-6 format and compared with experimental data available from the EXFOR library. Three sets of calculations were performed in order to test new levels segment, Koning's global optical potential and HF-BCS level densities. No problems were encountered while processing the new RIPL-2 files, which indicates that the files are formally correct. Comparison with experimental data shows reasonable overall agreement for most of the calculations. There is a clear indication that calculations using the new RIPL-2 files fit experimental data better than those with default EMPIRE-II parameters, which demonstrates the improvements brought about by RIPL-2. The HF-BCS microscopic level densities were found to perform comparably to the phenomenological level densities and in some cases even better. However, significant discrepancies among the results of the three sets of calculations were observed in a number of cases. These findings illustrate the importance of the model parameters and prove the practical usefulness of the RIPL-2 library for basic research and applications. The second exercise was carried out by the Beijing group, using the recently developed UNF code to study 103 nuclei from the mass region 69-160 in the incident energy range from 0.1 to 20 MeV. All input parameters were taken from the RIPL database. Agreement with the experimental data was found to be very good for total and elastic cross sections (within 3%). For other main reaction channels, calculations reproduced the shape, but some parameter adjustments were necessary in order to fit the absolute cross sections. TALYS calculations were performed for various neutron-induced reactions on 5 isotopes from ^{52}Cr to ^{208}Pb. Default input parameters originated from RIPL-2. This

exercise concentrated on the comparison of Ignatyuk-type and microscopic level densities and provided very reasonable agreement with experimental data for both formulations.

4 Code Interfaces

The work on interfaces between selected nuclear model codes and RIPL-2 segments has been facilitated by the standard RIPL-2 format. The two optical model codes (ECIS and SCAT2) and two statistical model codes (EMPIRE-II and UNF) use RIPL-2 library to a significant extent. Interface codes preparing inputs for ECIS and SCAT2 have been written by Young and is available in the optical segment.

The statistical model code UNF (PR China) makes use of RIPL optical potentials, masses, levels, level densities and GDR parameters. EMPIRE-II accesses RIPL-2 database directly and retrieves optical model parameters, discrete levels and microscopic level densities (HF-BCS). Built-in systematics for GDR parameters and prescriptions for γ-strength functions follow RIPL-2 recommendations. EMPIRE-II library of masses and ground state deformations is numerically identical to the mass-frdm.dat in the mass segment of RIPL-2. TALYS uses a dedicated format for the input parameter library but numerical data are based on RIPL-2.

An interface code (OM-RETRIEVE) is provided to generate input files for SCAT2000 and ECIS96 from the OMP library. Utility codes for editing and summarizing the OMP library content are also available.

5 Conclusions

The RIPL-2 library is close to completion, with public release expected in July 2002. Users of reaction codes will benefit considerably from the generation of a complete and consistent set of starting parameters to give sensible results for cross sections and spectra. However, RIPL-2 should be further extended and continuously updated in order to retain the relevance and value of the library to the users. At the recent co-ordination meeting in Vienna, December 2001, the CRP participants discussed possible improvements of the current project and formulated recommendations for further activities. These finding are summarized below:

- RIPL-2 provides valid sets of parameters for spherical and near-spherical nuclei. On the other hand, data for the deformed nuclei are scarce and less accurate. In particular there is a need for more Coupled-Channels potentials and γ-ray strength functions for the deformed nuclei.

- Special techniques should be applied for the determination of parameters for nuclei far from the stability line for which there are usually no experimental data available. These nuclei are important for ADS and astrophysics.

- New experimental data from the recently initiated projects (HINDAS and N-TOF at CERN) should become available within a year or two, offering possibilities for testing RIPL-2 parameters. The same is true for the SNS facility at Oak Ridge at a somewhat longer time scale.

- RIPL-2 library should be complemented with a set of routines for the calculation of certain input parameters (such as level densities, binding energies, γ-strength functions, etc.) in order to facilitate user access to the database and to avoid misuse of the parameters.

- More attention should be dedicated to the use of microscopic models for producing parameters. Parameters related to the fission channel contained in RIPL-2 need more accurate analysis and improvement.

- The problem of collective enhancement of level densities should be addressed in more detail in order to provide a reliable prescription for calculating level densities in deformed nuclei. The latter are often needed for ADS and new reactor concepts.

- RIPL-2 studies focused on incident energies below 20 MeV, a typical limit for standard nuclear data files. However, new applications such as ADS, medical radioisotope production and radiation treatment require reliable data at much higher energies (up to 1.5 GeV in the case of ADS). Most of the parameters available from RIPL-2 cannot be extrapolated to such high energies (e.g., temperature dependence of the GDR width). In particular, there should be consistency between statistical model calculations at low energies and the intra-nuclear cascade model commonly used at high energies.

- Use of the results obtained in heavy ion induced reactions could be helpful in determining model parameters, especially for nuclei far from the stability line.
- Medical applications require charged particle reactions, which could be better represented in the parameter library.

6 Participants

The following scientists contributed to the RIPL-2 library: T. Belgya (IIS-CCR, Budapest, Hungary), O. Bersillon (Bruyres-le-Chtel, France), R. Capote (NCEADNC, Havana , Cuba), T. Fukahori (JAERI, Tokai-mura, Japan), S. Goriely (Univ. of Brussels, Belgium), M. Herman (IAEA, Vienna, Austria), A. V. Ignatyuk (IPPE, Obninsk, Russia), S. Kailas (Bhabha, Trombay-Mumbai, India), A. Koning (Petten, Holland), P. Oblozinsk (BNL, Brookhaven, USA), V. Plujko (Univ. of Kiev, Ukraine), P. G. Young (LANL, Los Alamos, USA), Ge Zhigang (CNDC, Beijing, China).

References

[1] J. J. M. Verbaarschot, H. A. Weidenmueller, and M. R. Zirnbauer, Phys. Rep. **129**, 367 (1985).

[2] H. Feshbach, A. Kerman, and S. Koonin, Ann. Phys. **125**, 429 (1980).

[3] T. Tamura, T. Udagawa, and H. Lenske, Phys. Rev. **C26**, 379 (1982).

[4] H. Nishioka, J. J. M. Verbaarschot, H. A. Weidenmüller, and S. Yoshida, Ann. Phys. **172**, 67 (1986).

[5] *Handbook for calculations of nuclear reaction data: reference input parameter library* (International Atomic Energy Agency, Vienna, Austria, 1998, http://www-nds.iaea.or.at/ripl), No. IAEA-TECDOC-1034.

[6] P. Moller, J. R. Nix, W. D. Myers, and W. J. Swiatecki, At. Data Nucl. Data Tables **59**, 185 (1995).

[7] G. Audi and A. H. Wapstra, Nucl. Phys. **A595**, 409 (1995).

[8] J. Duflo and A. Zuker, Phys. Rev. **C52**, 23 (1995).

[9] S. Sukhoruchkin, Z. N. Soroko, and V. V. Deriglazov, in *Low Energy Neutrons Physics, Tables of Neutron Resonance Parameters*, edited by H. Schopper (Springer-Verlag, Darmstadt, 2000), Vol. 16B.

[10] A. Koning and J. Delaroche, to be published (2002).

[11] S. Goriely, F. Tondeur, and J. Pearson, At. Data Nucl. Data Tables **77**, 311 (2001).

[12] M. Avrigeanu and V. Avrigeanu, Comput. Phys. Commun. **112**, 191 (1998).

[13] S. S. Dietrich and B. L. Berman, At. Data and Nucl. Data Tables **38**, 199 (1988).

[14] Liu Jianfeng and Su Zongdi, Chinese J. Nucl. Phys. **17**, 336 (1995).

[15] P. Van Isacker *et al.*, Phys. Rev. **C45**, R13 (1992).

[16] S. Goriely, Phys. Lett. **B436**, 10 (1998).

[17] F.-K. Thielemann and M. Arnould, in *Conf. on Nuclear Data for Science and Technology*, Antwerp, 6-10 September, 1982, edited by K. Bockhoff (Reidel, Dordrecht, The Netherlands, 1983), p. 762.

[18] S. Goriely and E. Khan, Nucl. Phys. A submitted for publication (2002).

[19] E. Khan *et al.*, Nucl. Phys. **A694**, 103 (2001).

[20] G. Smirenkin, Report INDC(CCP)-359, IAEA, Vienna (unpublished).

[21] A. J. Sierk, *BARMOM*, no.967 ed., National Energy Software Center (Argonne National Laboratory, IL60439).

[22] A. Mamdouh, J. Pearson, M. Rayet, and F. Tondeur, Nucl. Phys. **A679**, 337 (2001).

Nuclear Data Requirements for Decay Heat Calculations

A.L. Nichols*

International Atomic Energy Agency, Nuclear Data Section,
Department of Nuclear Sciences and Applications,
Vienna, Austria

Lectures given at the
Workshop on Nuclear Reaction Data and
Nuclear Reactors: Physics, Design and Safety
Trieste, 25 February – 28 March 2002

LNS0520003

* A.Nichols@iaea.org

Abstract

A sound knowledge of the time-dependent energy release resulting from the decay of the radioactive nuclides formed in the reactor core is extremely important in formulating safe procedures for the operation of nuclear facilities and the handling of irradiated fuel. Accurate estimates of this resulting decay heat are needed for a wide range of applications, including safety assessments of all types of nuclear plant, the handling of fuel discharges, the design and transport of fuel-storage flasks, and the management of the resulting radioactive waste. More specifically, the nuclear power community must ensure accurate and reliable calculations of the decay heat of irradiated fuel in order to maintain credibility and confidence in the safe and reliable performance of the various nuclear fuel cycles.

Neutron cross sections, fission yields and radionuclidic decay data represent the input to the summation calculations used to determine the release of decay heat over an extended period of time after reactor shutdown (i.e., following termination of neutron-induced fission). Nuclear data requirements for these summation calculations have been assessed, and a summary is given of their status. Associated uncertainties are examined, and specific inadequacies explored.

1. INTRODUCTION

Neutron-induced fission within the fuel of a reactor core, and the subsequent conversion of mass to energy constitutes a principal means of generating power. The resulting energy arises from the following phenomena:

> kinetic energies of the fission products and neutrons;
> prompt gamma radiation from highly-excited fission fragments, including short-lived isomeric states;
> gamma and beta energy released through the delayed natural decay of the various radioactive products, particularly the fission products.

The last energy source contributes approximately 8% to 12% of the total energy generated through the fission process, and is commonly referred to as "decay heat".

The author has focused on the decay heat that continues to be generated after the fission process has been terminated; the fission process is not considered directly, and the reader is referred to a number of dedicated publications on this phenomenon (Gönnenwein, 1991; Wagemans, 1991; Denschlag, 1997). The prompt sources of energy decline rapidly when a reactor is shutdown, but radioactive decay continues to heat the reactor core. Hence, coolant operation needs to be maintained after termination of the fission process, on the basis of reliable decay-heat calculations. Decay heat varies as a function of cooling time, and can be determined in theory from known nuclear data, based on computations of the inventory of the resulting radionuclides (primarily fission products, and actinides) created during the fission process and after reactor shutdown, and their radioactive decay characteristics.

Decay heat has been reviewed in detail by others from a technical perspective and also through the use of decay-heat equations as standards (ANS, 1979; Tobias, 1980; GNS, 1990; Dickens *et al*, 1991; Tasaka *et al*, 1991); the reader is referred to these publications for authorative assessments of the analytical procedures. Rather, the author has focused on the basic nuclear data of relevance to the decay heat generated in fission power-reactor systems, including the means of defining the initial radioactive inventory of controlled nuclear fission and other modes of decay within the core.

Cross-section, fission-yield and decay-data libraries are maintained for national and international usage. While this article avoids recommending specific sources of such data, Appendix A provides the reader with a brief summary of the means of accessing the most relevant data files via the acquisition of CD-ROMs or through the Internet. The latter method has become increasingly powerful, and provides the user with an extremely rapid route to virtually all of the highest quality nuclear data.

2. IRRADIATED FUEL INVENTORY

Several computer programs are commonly used to compute the changing inventory of nuclides during reactor operation and at any time after shutdown (for example, ORIGEN (Bell, 1973), FISP (Clarke, 1972; Tobias, 1978) and FISPIN (Burstall and Thornton, 1977; Burstall, 1979). Fission-product yields for each fissioning nuclide are used in conjunction with the effective group-averaged fission cross sections, decay constants and mean alpha, beta and gamma energy releases to calculate decay heat. Thus, substantial quantities of data are required to determine core inventories and define their decay characteristics. The nuclides listed in Tables 1, 2 and 3 represent the fission products, structurally-based activation products and actinides (and their decay-chain nuclides) respectively, that would normally be included within inventory calculations.

The resulting fission products can undergo transformation by several modes of radioactive decay, neutron absorption, or a combination of these processes. A series of linear decay chains can be defined that include a number of short-lived fission products that have not been experimentally observed or adequately characterised; theoretical data can be adopted (half-lives denoted in parentheses in Appendix B. 1, which also provides a reasonable summary of the fission products associated with decay-heat calculations). All such data are subject to significant modifications throughout future years.

The effective yield of fission product i (α) is given by the equation:

$$\alpha_i = \sum_a \sum_{k=1}^{N} \sigma_{a,k}^F \phi_k N_a(t) Y_{a,k}^i$$

where $\sigma_{a,k}^F$ is the effective group-averaged fission cross section of actinide a in the k^{th} neutron group (of N groups $_i$), ϕ_k is the neutron flux in the k^{th} neutron group, $N_a(t)$ is the number of atoms of fissile actinide a at time t of irradiation, and $Y_{a,k}^i$ represent the independent yields for fission product i. A period of reactor operation may be represented as a series of time steps in which time-dependent quantities are constant for an individual step, but vary between steps.

Consider a linear decay chain

$$N_1 \rightarrow N_2 \rightarrow N_3 \rightarrow \ \ldots\ldots N_i \rightarrow \ \ldots\ldots$$

with effective fission yields α_i, decay constants λ_i per sec, and effective neutron-capture cross sections σ_i cm^2. The number of atoms N_i as a function of time is given by

$$\frac{d}{dt}\left(N_1\right) = -\left(\lambda_1 + \sigma_1 \phi\right)N_1 + \alpha_1 F$$

where ϕ (n cm^{-2} s^{-1}) is the effective neutron flux, and F is the fission rate (s^{-1})

$$\frac{d}{dt}(N_2) = -(\lambda_2 + \sigma_2 \phi)N_2 + \alpha_2 F + \gamma_1 N_1$$

and

$$\frac{d}{dt}(N_i) = -\left(\lambda_i + \sigma_i \phi\right)N_i + \alpha_i F + \gamma_{i-1} N_{i-1}$$

in which $\gamma_{i-1} = (k_{i-1})(\lambda_{i-1})$ or $(k_{i-1})(\sigma_{i-1})\phi$, depending on the coupling between *(i-1)* and *i*, and k_{i-1} is the relevant branching fraction. The set of equations represented by $\frac{d}{dt}(N_i)$ can be solved by either an analytical method or numerical integration.

Actinide inventories can be calculated in a similar manner on the basis of the following processes:

(a) radioactive decay,

(b) total neutron absorption and production from (n, γ) and (n, 2n) reactions,

(c) production from alpha and beta decay of parent nuclides.

Appendix B. 2 outlines the formation of these actinides in irradiated fuel (particularly Pu, Am and Cm radionuclides) and their decay-chain products. The number of atoms $N_{Z,A}$ of nuclide of atomic number Z and mass number A is given by the equation:

$$\begin{aligned}\frac{d}{dt}\left(N_{Z,A}\right) = &-\lambda^{T}_{Z,A} N_{Z,A} - N_{Z,A} \times \int \sigma^{A}_{Z,A}(E)\phi(E)\,dE \\ &+ N_{Z,A-1} \times \int \sigma^{n,\gamma}_{Z,A-1}(E)\phi(E)\,dE \\ &+ N_{Z,A+1} \times \int \sigma^{n,2n}_{Z,A+1}(E)\phi(E)\,dE \\ &+ k_{\alpha}\lambda^{\alpha}_{Z-2,A+4} \times N_{Z+2,A+4} \\ &+ k_{\beta^-}\lambda^{\beta^-}_{Z-1,A} N_{Z+1,A} + k_{\beta^+}\lambda^{\beta^+}_{Z+1,A} N_{Z+1,A}\end{aligned}$$

where $\sigma_{i,j}^{A}$(E), $\sigma_{i,j}^{(n,\gamma)}$(E) and $\sigma_{i,j}^{(n,2n)}$(E) are the total neutron absorption, (n, γ) and (n, 2n) cross sections respectively, at neutron energy *E* for a nuclide of atomic number *i* and mass number *j*; $\lambda_{i,j}^{\alpha}$, $\lambda_{i,j}^{\beta^-}$, $\lambda_{i,j}^{\beta^+}$, $\lambda_{i,j}^{T}$ are the alpha, negatron, positron and total decay constants for the nuclide of atomic number *i* and mass number *j*; k_{α}, k_{β^-} and k_{β^+} are the branching fractions for α, β^- and β^+ decay to nuclide Z, A; and $\phi(E)$ is the neutron flux at neutron energy *E*. The coupling of the linear system of first-order differential equations is complex, and they are normally solved by means of numerical integration.

After reactor shutdown, the fission products and actinides formed during reactor operation will undergo radioactive decay. The number of atoms at time *t* following shutdown can be expressed as a series of equations:

$$\frac{d}{dt}N_i = -\lambda_i N_i + \lambda_{i-1}N_{i-1}$$

that are coupled in a much less complex manner after shutdown than for reactor operation.

When the actinide and fission-product inventories have been calculated for the specified conditions of reactor operation and subsequent cooling period, the decay heat can be derived by summing the products of the nuclear activities in terms of the mean alpha, beta and gamma energy releases per disintegration of that nuclide:

$$H_{\alpha}(t) = \sum_{i=1}^{M} \lambda_i^T \, N_i(t) \, E_{\alpha}^i$$

$$H_{\beta}(t) = \sum_{i=1}^{M} \lambda_i^T \, N_i(t) \, E_{\beta}^i$$

$$H_{\gamma}(t) = \sum_{i=1}^{M} \lambda_i^T \, N_i(t) \, E_{\gamma}^i$$

where E_{α}^i, E_{β}^i and E_{γ}^i are the mean alpha, beta and gamma energy releases respectively per disintegration of nuclide *i*; λ_i^T is the total decay constant of nuclide *i*, and $H_{\alpha}(t)$, $H_{\beta}(t)$ and $H_{\gamma}(t)$ are the total alpha, beta and gamma decay heat respectively at time t after reactor shutdown.

The nuclear data requirements for decay-heat calculations can be determined from the information given above:

$\sigma_{a,k}^{F}$ - effective group-averaged fission cross section of actinide *a* in the k^{th} neutron group,

$\sigma_{i,j}^{A}$ - total neutron absorption cross section of fission product *i*,

$\sigma_{i,j}^{(n,\gamma)}$ - (n, γ) cross section of fission product *i*,

$\sigma_{i,j}^{(n,2n)}$ - (n, 2n) cross section of fission product *i*,

$Y_{a,k}^{i}$ - independent yields for fission product *i*,

λ_i - decay constant(s) of fission product *i*,

k_α, k_{β^-}, k_{β^+} - branching fractions for α, β^- and β^+ decay to nuclide Z, A,

E_α^i, E_β^i, E_γ^i - mean alpha, beta and gamma energy releases per disintegration of nuclide *i*.

Table 1: Fission products (1038 nuclides) – representative listing for inventory calculations

1-H-1, **H-2**, H-3;
2-He-3, **He-4**, He-6, He-8;
3-Li-6, **Li-7**, Li-8, Li-9;
4-Be-7, **Be-9**, Be-10, Be-11, Be-12;
5-B-11, B-12;
6-C-12, C-14, C-15;
7-N-14, **N-15**;
10-Ne-21;
21-Sc-50, Sc-51;
22-Ti-50, Ti-51, Ti-52, Ti-53;
23-V-51, V-52, V-53, V-54, V-55;
24-Cr-52, **Cr-53**, **Cr-54**, Cr-55, Cr-56, Cr-57;
25-Mn-55, Mn-56, Mn-57, Mn-58, Mn-58m, Mn-59, Mn-60;
26-Fe-56, **Fe-57**, **Fe-58**, Fe-59, Fe-60, Fe-61, Fe-62, Fe-63;
27-Co-59, Co-60, Co-60m, Co-61, Co-62, Co-62m, Co-63, Co-64, Co-65, Co-66;
28-Ni-60, **Ni-61**, **Ni-62**, Ni-63, **Ni-64**, Ni-65, Ni-66, Ni-67, Ni-68, Ni-69;
29-Cu-63, Cu-64, **Cu-65**, Cu-66, Cu-67, Cu-68, Cu-68m, Cu-69, Cu-70, Cu-70m, Cu-71, Cu-72, Cu-73, Cu-74, Cu-75, Cu-76, Cu-78;
30-Zn-64, Zn-65, **Zn-66**, **Zn-67**, **Zn-68**, Zn-69, Zn-69m, **Zn-70**, Zn-71, Zn-71m, Zn-72, Zn-73, Zn-73m, Zn-74, Zn-75, Zn-76, Zn-77, Zn-77m, Zn-78, Zn-79, Zn-80;
31-Ga-67, Ga-68, **Ga-69**, Ga-70, **Ga-71**, Ga-72, Ga-72m, Ga-73, Ga-74, Ga-74m, Ga-75, Ga-76, Ga-77, Ga-78, Ga-79, Ga-80, Ga-81, Ga-82, Ga-83, Ga-84;
32-Ge-70, Ge-71, Ge-71m, **Ge-72**, **Ge-73**, Ge-73m, **Ge-74**, Ge-75, Ge-75m, **Ge-76**, Ge-77, Ge-77m, Ge-78, Ge-79, Ge-79m, Ge-80, Ge-81, Ge-81m, Ge-82, Ge-83, Ge-84, Ge-85, Ge-86;
33-As-72, As-73, As-74, **As-75**, As-75m, As-76, As-77, As-78, As-79, As-80, As-81, As-82, As-82m, As-83, As-84, As-85, As-86, As-87, As-88;

34-Se-74, Se-75, **Se-76**, **Se-77**, Se-77m, **Se-78**, Se-79, Se-79m, **Se-80**, Se-81, Se-81m, **Se-82**, Se-83, Se-83m, Se-84, Se-85, Se-86, Se-87, Se-88, Se-89, Se-90, Se-91, Se-92;

35-Br-77, Br-77m, Br-78, **Br-79**, Br-79m, Br-80, Br-80m, **Br-81**, Br-82, Br-82m, Br-83, Br-84, Br-84m, Br-85, Br-86, Br-87, Br-88, Br-89, Br-90, Br-91, Br-92, Br-93, Br-94;

36-Kr-79, **Kr-80**, Kr-81, Kr-81m, **Kr-82**, **Kr-83**, Kr-83m, **Kr-84**, Kr-85, Kr-85m, **Kr-86**, Kr-87, Kr-88, Kr-89, Kr-90, Kr-91, Kr-92, Kr-93, Kr-94, Kr-95;

37-Rb-82, Rb-82m, Rb-83, Rb-84, Rb-84m, **Rb-85**, Rb-86, Rb-86m, **Rb-87**, Rb-88, Rb-89, Rb-90, Rb-90m, Rb-91, Rb-92, Rb-93, Rb-94, Rb-95, Rb-96, Rb-97, Rb-98, Rb-99, Rb-100, Rb-101, Rb-102;

38-Sr-84, Sr-85, Sr-85m, **Sr-86**, Sr-87, Sr-87m, **Sr-88**, **Sr-89**, Sr-90, Sr-91, Sr-92, Sr-93, Sr-94, Sr-95, Sr-96, Sr-97, Sr-98, Sr-99, Sr-100, Sr-101, Sr-102;

39-Y-86, Y-86m, Y-87, Y-87m, Y-88, **Y-89**, Y-89m, Y-90, Y-90m, Y-91, Y-91m, Y-92, Y-93, Y-93m, Y-94, Y-95, Y-96, Y-96m, Y-97, Y-97m, Y-98, Y-98m, Y-99, Y-100, Y-100m, Y-101, Y-102, Y-103;

40-Zr-88, Zr-89, Zr-89m, **Zr-90**, Zr-90m, **Zr-91**, **Zr-92**, Zr-93, **Zr-94**, Zr-95, **Zr-96**, Zr-97, Zr-98, Zr-99, Zr-100, Zr-101, Zr-102, Zr-103, Zr-104;

41-Nb-91, Nb-91m, Nb-92, Nb-92m, **Nb-93**, Nb-93m, Nb-94, Nb-94m, Nb-95, Nb-95m, Nb-96, Nb-97, Nb-97m, Nb-98, Nb-98m, Nb-99, Nb-99m, Nb-100, Nb-100m, Nb-101, Nb-102, Nb-102m, Nb-103, Nb-104, Nb-104m, Nb-105, Nb-106, Nb-107, Nb-108;

42-Mo-93, Mo-93m, **Mo-94**, **Mo-95**, **Mo-96**, **Mo-97**, **Mo-98**, Mo-99, **Mo-100**, Mo-101, Mo-102, Mo-103, Mo-104, Mo-105, Mo-106, Mo-107, Mo-108, Mo-110;

43-Tc-96, Tc-96m, Tc-97, Tc-97m, Tc-98, Tc-99, Tc-99m, Tc-100, Tc-101, Tc-102, Tc-102m, Tc-103, Tc-104, Tc-105, Tc-106, Tc-107, Tc-108, Tc-109, Tc-110, Tc-111, Tc-112;

44-Ru-98, **Ru-99**, **Ru-100**, **Ru-101**, **Ru-102**, Ru-103, Ru-103m, **Ru-104**, Ru-105, Ru-106, Ru-107, Ru-108, Ru-109, Ru-109m, Ru-110, Ru-111, Ru-112, Ru-113, Ru-114;

45-Rh-101, Rh-101m, Rh-102, Rh-102m, **Rh-103**, Rh-103m, Rh-104, Rh-104m, Rh-105, Rh-105m, Rh-106, Rh-106m, Rh-107, Rh-108, Rh-108m, Rh-109, Rh-110, Rh-110m, Rh-111, Rh-112, Rh-113, Rh-114, Rh-114m, Rh-115, Rh-116, Rh-116m, Rh-117, Rh-119;

46-Pd-102, Pd-103, **Pd-104**, **Pd-105**, **Pd-106**, Pd-107, Pd-107m, **Pd-108**, Pd-109, Pd-109m, **Pd-110**, Pd-111, Pd-111m, Pd-112, Pd-113, Pd-113m, Pd-114, Pd-115, Pd-116, Pd-117, Pd-118, Pd-119, Pd-120, Pd-122;

47-Ag-106, Ag-106m, **Ag-107**, Ag-107m, Ag-108, Ag-108m, **Ag-109**, Ag-109m, Ag-110, Ag-110m, Ag-111, Ag-111m, Ag-112, Ag-113, Ag-113m, Ag-114, Ag-114m, Ag-115, Ag-115m, Ag-116, Ag-116m, Ag-117, Ag-117m, Ag-118, Ag-118m, Ag-119, Ag-120, Ag-120m, Ag-121, Ag-122, Ag-122m, Ag-123, Ag-124, Ag-125;

48-Cd-108, Cd-109, **Cd-110**, **Cd-111**, Cd-111m, **Cd-112**, **Cd-113**, Cd-113m, **Cd-114**, Cd-115, Cd-115m, **Cd-116**, Cd-117, Cd-117m, Cd-118, Cd-119, Cd-119m, Cd-120, Cd-121, Cd-121m, Cd-122, Cd-123, Cd-124, Cd-125, Cd-126, Cd-127, Cd-128, Cd-130;

49-In-111, In-111m, In-112, In-112m, **In-113**, In-113m, In-114, In-114m, **In-115**, In-115m, In-116, In-116m, In-116n, In-117, In-117m, In-118, In-118m, In-118n, In-119, In-119m, In-120, In-120m, In-121, In-121m, In-122, In-122m, In-123, In-123m, In-124, In-124m, In-125, In-125m, In-126, In-126m, In-127, In-127m, In-128, In-128m, In-129, In-129m, In-130, In-131, In-131m, In-132, In-133;

50-Sn-112, **Sn-114**, **Sn-115**, **Sn-116**, **Sn-117**, Sn-117m, **Sn-118**, **Sn-119**, Sn-119m, **Sn-120**, Sn-121, Sn-121m, **Sn-122**, Sn-123, Sn-123m, **Sn-124**, Sn-125, Sn-125m, Sn-126, Sn-127, Sn-127m, Sn-128, Sn-128m, Sn-129, Sn-129m, Sn-130, Sn-130m, Sn-131, Sn-131m, Sn-132, Sn-133, Sn-134, Sn-135, Sn-136;

51-Sb-118, Sb-118m, Sb-119, Sb-120, Sb-120m, **Sb-121**, Sb-122, Sb-122m, **Sb-123**, Sb-124, Sb-124m, Sb-124n, Sb-125, Sb-126, Sb-126m, Sb-126n, Sb-127, Sb-128, Sb-128m, Sb-129, Sb-129m, Sb-130, Sb-130m, Sb-131, Sb-132, Sb-132m, Sb-133, Sb-134, Sb-134m, Sb-135, Sb-136, Sb-137, Sb-138;

52-Te-118, Te-119, Te-119m, **Te-120**, Te-121, Te-121m, **Te-122**, **Te-123**, Te-123m, **Te-124**, **Te-125**, Te-125m, **Te-126**, Te-127, Te-127m, **Te-128**, Te-129, Te-129m, **Te-130**, Te-131, Te-131m, Te-132, Te-133, Te-133m, Te-134, Te-135, Te-136, Te-137, Te-138, Te-139, Te-140, Te-141;

53-I-121, I-123, I-124, I-125, I-126, **I-127**, I-128, I-129, I-130, I-130m, I-131, I-132, I-132m, I-133, I-133m, I-134, I-134m, I-135, I-136, I-136m, I-137, I-138, I-139, I-140, I-141, I-142;

54-Xe-126, **Xe-128**, **Xe-129**, Xe-129m, **Xe-130**, **Xe-131**, Xe-131m, **Xe-132**, Xe-133, Xe-133m, **Xe-134**, Xe-134m, Xe-135, Xe-135m, **Xe-136**, Xe-137, Xe-138, Xe-139, Xe-140, Xe-141, Xe-142, Xe-143, Xe-144, Xe-145, Xe-147;

55-Cs-130, Cs-131, Cs-132, **Cs-133**, Cs-134, Cs-134m, Cs-135, Cs-135m, Cs-136, Cs-136m, Cs-137, Cs-138, Cs-138m, Cs-139, Cs-140, Cs-141, Cs-142, Cs-143, Cs-144, Cs-145, Cs-146, Cs-147, Cs-148;

56-Ba-132, Ba-133, Ba-133m, **Ba-134**, **Ba-135**, Ba-135m, **Ba-136**, Ba-136m, **Ba-137**, Ba-137m, **Ba-138**, Ba-139, Ba-140, Ba-141, Ba-142, Ba-143, Ba-144, Ba-145, Ba-146, Ba-147, Ba-148, Ba-149;

57-La-135, La-136, La-136m, La-137, **La-138**, **La-139**, La-140, La-141, La-142, La-143, La-144, La-145, La-146, La-146m, La-147, La-148, La-149, La-150, La-151;

58-Ce-137, Ce-137m, **Ce-138**, Ce-138m, Ce-139, Ce-139m, **Ce-140**, Ce-141, **Ce-142**, Ce-143, Ce-144, Ce-145, Ce-146, Ce-147, Ce-148, Ce-149, Ce-150, Ce-151, Ce-152;

59-Pr-139, Pr-140, **Pr-141**, Pr-142, Pr-142m, Pr-143, Pr-144, Pr-144m, Pr-145, Pr-146, Pr-147, Pr-148, Pr-148m, Pr-149, Pr-150, Pr-151, Pr-152, Pr-153, Pr-154, Pr-155;

60-Nd-142, **Nd-143**, **Nd-144**, **Nd-145**, **Nd-146**, Nd-147, **Nd-148**, Nd-149, **Nd-150**, Nd-151, Nd-152, Nd-153, Nd-154, Nd-155, Nd-156;

61-Pm-144, Pm-145, Pm-146, Pm-147, Pm-148, Pm-148m, Pm-149, Pm-150, Pm-151, Pm-152, Pm-152m, Pm-153, Pm-154, Pm-154m, Pm-155, Pm-156, Pm-157, Pm-158;

62-Sm-146, **Sm-147**, **Sm-148**, **Sm-149**, **Sm-150**, Sm-151, **Sm-152**, Sm-153, Sm-153m, **Sm-154**, Sm-155, Sm-156, Sm-157, Sm-158, Sm-159, Sm-160;

63-Eu-149, Eu-150, Eu-150m, **Eu-151**, Eu-152, Eu-152m, Eu-152n, **Eu-153**, Eu-154, Eu-154m, Eu-155, Eu-156, Eu-157, Eu-158, Eu-159, Eu-160, Eu-161, Eu-162;

64-Gd-150, **Gd-152**, Gd-153, **Gd-154**, **Gd-155**, Gd-155m, **Gd-156**, **Gd-157**, **Gd-158**, Gd-159, **Gd-160**, Gd-161, Gd-162, Gd-163, Gd-164;

65-Tb-155, Tb-156, Tb-157, Tb-158, Tb-158m, **Tb-159**, Tb-160, Tb-161, Tb-162, Tb-163, Tb-164, Tb-165, Tb-166;

66-Dy-157, Dy-157m, **Dy-158**, Dy-159, **Dy-160**, **Dy-161**, **Dy-162**, **Dy-163**, **Dy-164**, Dy-165, Dy-165m, Dy-166, Dy-167, Dy-168, Dy-169, Dy-170;

67-Ho-161, Ho-161m, Ho-162, Ho-162m, Ho-163, Ho-163m, Ho-164, Ho-164m, **Ho-165**, Ho-166, Ho-166m, Ho-167, Ho-168, Ho-169, Ho-170, Ho-170m;

68-Er-163, **Er-164**, Er-165, **Er-166**, **Er-167**, Er-167m, **Er-168**, Er-169, **Er-170**, Er-171, Er-172, Er-173;

69-Tm-167, Tm-168, **Tm-169**, Tm-170, Tm-171, Tm-172, Tm-173, Tm-174, Tm-175, Tm-176;

70-Yb-169, **Yb-170**, **Yb-171**, **Yb-172**, **Yb-173**, **Yb-174**, Yb-175, **Yb-176**, Yb-176m, Yb-177, Yb-177m, Yb-178, Yb-179;

71-Lu-172, Lu-173, Lu-174, Lu-174m, **Lu-175**, **Lu-176**, Lu-176m, Lu-177, Lu-177m, Lu-178, Lu-178m, Lu-179, Lu-180, Lu-181, Lu-182, Lu-183;

72-Hf-176, **Hf-177**, **Hf-178**, **Hf-179**, **Hf-180**, Hf-180m, Hf-181, Hf-182, Hf-182m, Hf-183, Hf-184;

73-Ta-181, Ta-182, Ta-183, Ta-184, Ta-185, Ta-186;

74-W-182, **W-183**, W-183m, **W-184**, W-185, **W-186**, W-187;

75-Re-185, **Re-187**;

Naturally-occurring nuclides are listed in bold type.

Table 2: Structural materials and decay products on irradiation (708 nuclides) – representative listing for inventory calculations

1-H-1, **H-2**, H-3, H-4;
2-He-3, **He-4**, He-6;
3-Li-6, **Li-7**, Li-8;
4-Be-8, **Be-9**, Be-10, Be-11;
5-B-10, **B-11**, B-12;
6-C-12, **C-13**, C-14, C-15;
7-N-13, **N-14**, **N-15**, N-16;
8-O-16, **O-17**, **O-18**, O-19;
9-F-19, F-20;
10-Ne-20, **Ne-21**, **Ne-22**, Ne-23;
11-Na-22, **Na-23**, Na-24, Na-24m, Na-25;
12-Mg-24, **Mg-25**, **Mg-26**, Mg-27, Mg-28;
13-Al-27, Al-28, Al-29, Al-30;
14-Si-28, **Si-29**, **Si-30**, Si-31, Si-32;
15-P-31, P-32, P-33, P-34;
16-S-32, **S-33**, **S-34**, S-35, **S-36**, S-37;
17-Cl-35, Cl-36, **Cl-37**, Cl-38, Cl-38m;
18-Ar-36, Ar-37, **Ar-38**, Ar-39, **Ar-40**, Ar-41, Ar-42;
19-K-39, **K-40**, **K-41**, K-42, K-43, K-44;
20-Ca-40, Ca-41, **Ca-42**, **Ca-43**, **Ca-44**, Ca-45, **Ca-46**, Ca-47, **Ca-48**, Ca-49;
21-Sc-45, Sc-46, Sc-46m, Sc-47, Sc-48, Sc-49, Sc-50;
22-Ti-46, **Ti-47**, **Ti-48**, **Ti-49**, **Ti-50**, Ti-51;
23-V-49, **V-50**, **V-51**, V-52, V-53, V-54;

24-Cr-50, Cr-51, **Cr-52**, **Cr-53**, **Cr-54**, Cr-55;

25-Mn-53, Mn-54, **Mn-55**, Mn-56, Mn-57, Mn-58;

26-Fe-54, Fe-55, **Fe-56**, **Fe-57**, **Fe-58**, Fe-59, Fe-60;

27-Co-55, Co-56, Co-57, Co-58, Co-58m, **Co-59**, Co-60, Co-60m, Co-61, Co-62;

28-Ni-58, Ni-59, **Ni-60**, **Ni-61**, **Ni-62**, Ni-63, **Ni-64**, Ni-65, Ni-66;

29-Cu-62, **Cu-63**, Cu-64, **Cu-65**, Cu-66, Cu-67;

30-Zn-63, **Zn-64**, Zn-65, **Zn-66**, **Zn-67**, **Zn-68**, Zn-69, Zn-69m, **Zn-70**, Zn-71, Zn-71m;

31-Ga-69, Ga-70, **Ga-71**, Ga-72, Ga-72m;

32-Ge-70, Ge-71, Ge-71m, **Ge-72**, **Ge-73**, **Ge-74**, Ge-75, Ge-75m, **Ge-76**, Ge-77, Ge-77m;

33-As-75, As-76, As-77;

34-Se-74, Se-75, **Se-76**, **Se-77**, Se-77m, **Se-78**, Se-79, Se-79m, **Se-80**, Se-81, Se-81m, **Se-82**, Se-83, Se-83m;

35-Br-79, Br-80, Br-80m, **Br-81**, Br-82, Br-82m, Br-83;

36-Kr-78, Kr-79, Kr-79m, **Kr-80**, Kr-81, Kr-81m, **Kr-82**, **Kr-83**, Kr-83m, **Kr-84**, Kr-85, Kr-85m, **Kr-86**, Kr-87, Kr-88;

37-Rb-85, Rb-86, Rb-86m, **Rb-87**, Rb-88, Rb-89;

38-Sr-84, Sr-85, Sr-85m, **Sr-86**, **Sr-87**, Sr-87m, **Sr-88**, Sr-89, Sr-90, Sr-91, Sr-93;

39-Y-89, Y-89m, Y-90, Y-90m, Y-91, Y-92, Y-93, Y-94, Y-96;

40-Zr-89, **Zr-90**, **Zr-91**, **Zr-92**, Zr-93, **Zr-94**, Zr-95, **Zr-96**, Zr-97;

41-Nb-91, Nb-92, **Nb-93**, Nb-93m, Nb-94, Nb-94m, Nb-95, Nb-95m, Nb-96, Nb-97, Nb-97m, Nb-98, Nb-100;

42-Mo-92, Mo-93, Mo-93m, **Mo-94**, **Mo-95**, **Mo-96**, **Mo-97**, **Mo-98**, Mo-99, **Mo-100**, Mo-101;

43-Tc-97, Tc-97m, Tc-98, Tc-99, Tc-100, Tc-101;

44-Ru-96, Ru-97, **Ru-98**, **Ru-99**, **Ru-100**, **Ru-101**, **Ru-102**, Ru-103, **Ru-104**, Ru-105, Ru-106, Ru-107;

45-Rh-102, **Rh-103**, Rh-104, Rh-104m, Rh-105, Rh-105m, Rh-106, Rh-106m, Rh-107;

46-Pd-102, Pd-103, **Pd-104**, **Pd-105**, **Pd-106**, Pd-107, Pd-107m, **Pd-108**, Pd-109, Pd-109m, **Pd-110**, Pd-111, Pd-111m;

47-Ag-106, **Ag-107**, Ag-108, Ag-108m, **Ag-109**, Ag-109m, Ag-110, Ag-110m, Ag-111, Ag-111m, Ag-112;

48-Cd-106, Cd-107, **Cd-108**, Cd-109, **Cd-110**, **Cd-111**, Cd-111m, **Cd-112**, **Cd-113**, Cd-113m, **Cd-114**, Cd-115, Cd-115m, **Cd-116**, Cd-117, Cd-117m, Cd-119, Cd-121;

49-In-113, In-113m, In-114, In-114m, **In-115**, In-116, In-116m, In-117, In-117m, In-118, In-119, In-119m, In-120, In-120m, In-121;

50-Sn-112, Sn-113, Sn-113m, **Sn-114**, **Sn-115**, **Sn-116**, **Sn-117**, Sn-117m, **Sn-118**, **Sn-119**, Sn-119m, **Sn-120**, Sn-121, Sn-121m, **Sn-122**, Sn-123, Sn-123m, **Sn-124**, Sn-125, Sn-125m, Sn-126;

51-Sb-121, Sb-122, Sb-122m, **Sb-123**, Sb-124, Sb-124m, Sb-125, Sb-126, Sb-126m;

52-Te-120, Te-121, Te-121m, **Te-122**, **Te-123**, Te-123m, **Te-124**, **Te-125**, Te-125m, **Te-126**, Te-127, Te-127m, **Te-128**, Te-129, Te-129m, **Te-130**, Te-131, Te-131m;

53-I-125, I-126, **I-127**, I-128, I-129, I-130, I-130m, I-131, I-132, I-135;

54-Xe-124, Xe-125, Xe-125m, **Xe-126**, Xe-127, Xe-127m, **Xe-128**, **Xe-129**, Xe-129m, **Xe-130**, **Xe-131**, Xe-131m, **Xe-132**, Xe-133, Xe-133m, **Xe-134**, Xe-135, Xe-135m, **Xe-136**, Xe-137;

55-Cs-131, Cs-132, **Cs-133**, Cs-134, Cs-134m, Cs-135, Cs-136, Cs-137, Cs-138;

56-Ba-130, Ba-131, Ba-131m, **Ba-132**, Ba-133, Ba-133m, **Ba-134**, **Ba-135**, Ba-135m, **Ba-136**, Ba-136m, **Ba-137**, Ba-137m, **Ba-138**, Ba-139, Ba-140, Ba-141;

57-La-137, **La-138**, **La-139**, La-140, La-141;

58-Ce-136, Ce-137, Ce-137m, **Ce-138**, Ce-139, Ce-139m, **Ce-140**, Ce-141, **Ce-142**, Ce-143, Ce-144, Ce-145;

59-Pr-141, Pr-142, Pr-142m, Pr-143, Pr-144, Pr-145;

60-Nd-142, **Nd-143**, **Nd-144**, **Nd-145**, **Nd-146**, Nd-147, **Nd-148**, Nd-149, **Nd-150**, Nd-151;

61-Pm-145, Pm-146, Pm-147, Pm-148, Pm-148m, Pm-149, Pm-150, Pm-151, Pm-152;

62-Sm-144, Sm-145, Sm-146, **Sm-147**, **Sm-148**, **Sm-149**, **Sm-150**, Sm-151, **Sm-152**, Sm-153, **Sm-154**, Sm-155, Sm-156;

63-Eu-151, Eu-152, Eu-152m, **Eu-153**, Eu-154, Eu-155, Eu-156, Eu-157;

64-Gd-152, Gd-153, **Gd-154**, **Gd-155**, Gd-155m, **Gd-156**, **Gd-157**, **Gd-158**, Gd-159, **Gd-160**, Gd-161, Gd-162;

65-Tb-157, Tb-158, **Tb-159**, Tb-160, Tb-161, Tb-162;

66-Dy-156, Dy-157, **Dy-158**, Dy-159, **Dy-160**, **Dy-161**, **Dy-162**, **Dy-163**, **Dy-164**, Dy-165, Dy-165m, Dy-166;

67-Ho-163, **Ho-165**, Ho-166, Ho-166m;

68-Er-162, Er-163, **Er-164**, Er-165, **Er-166**, **Er-167**, Er-167m, **Er-168**, Er-169, **Er-170**, Er-171, Er-172;

69-Tm-169, Tm-170, Tm-170m, Tm-171, Tm-172, Tm-173;

70-Yb-168, Yb-169, **Yb-170**, **Yb-171**, **Yb-172**, **Yb-173**, **Yb-174**, Yb-175, Yb-175m, **Yb-176**, Yb-177;

71-Lu-175, **Lu-176**, Lu-176m, Lu-177, Lu-177m;

72-Hf-174, Hf-175, **Hf-176**, **Hf-177**, **Hf-178**, Hf-178m, **Hf-179**, Hf-179m, **Hf-180**, Hf-180m, Hf-181, Hf-182;

73-Ta-180, **Ta-181**, Ta-182, Ta-182m, Ta-183;

74-W-180, W-181, **W-182**, **W-183**, W-183m, **W-184**, W-185, W-185m, **W-186**, W-187, W-188, W-189;

75-Re-185, Re-186, **Re-187**, Re-188, Re-188m, Re-189;

76-Os-184, Os-185, **Os-186**, **Os-187**, **Os-188**, **Os-189**, **Os-190**, Os-190m, Os-191, Os-191m, **Os-192**, Os-193, Os-194;

77-Ir-191, Ir-192, Ir-192m, **Ir-193**, Ir-194, Ir-194m;

78-Pt-190, Pt-191, **Pt-192**, Pt-193, Pt-193m, **Pt-194**, **Pt-195**, Pt-195m, **Pt-196**, Pt-197, Pt-197m, **Pt-198**, Pt-199, Pt-199m;

79-Au-197, Au-198, Au-199, Au-200;

80-Hg-196, Hg-197, Hg-197m, **Hg-198**, **Hg-199**, Hg-199m, **Hg-200**, **Hg-201**, **Hg-202**, Hg-203, **Hg-204**, Hg-205;

81-Tl-203, Tl-204, **Tl-205**, Tl-206;

82-Pb-204, Pb-205, **Pb-206**, **Pb-207**, **Pb-208**, Pb-209, Pb-210;

83-Bi-208, **Bi-209**, Bi-210, Bi-210m, Bi-211;

84-Po-210, Po-211, Po-211m;

92-U-234, **U-235**, U-236, **U-238**, U-239;

93-Np-239;

Naturally-occurring nuclides are listed in bold type.

Table 3: Actinides and heavy elements (129 nuclides) – representative listing for inventory calculations

80-Hg-206;
81-Tl-206, Tl-206m, Tl-207, Tl-207m, Tl-208, Tl-209, Tl-210;
82-Pb-205, **Pb-206**, **Pb-207**, **Pb-208**, Pb-209, Pb-210, Pb-211, Pb-212, Pb-214;
83-Bi-209, Bi-210, Bi-210m, Bi-211, Bi-212, Bi-212m, Bi-212n, Bi-213, Bi-214, Bi-215;
84-Po-209, Po-210, Po-211, Po-211m, Po-212, Po-212m, Po-213, Po-214, Po-215, Po-216, Po-218;
85-At-215, At-217, At-218, At-219;
86-Rn-217, Rn-218, Rn-219, Rn-220, Rn-222;
87-Fr-221, Fr-223;
88-Ra-223, Ra-224, Ra-225, Ra-226, Ra-228;
89-Ac-225, Ac-227, Ac-228;
90-Th-227, Th-228, Th-229, Th-230, Th-231, **Th-232**, Th-233, Th-234, Th-235;
91-Pa-231, Pa-232, Pa-233, Pa-234, Pa-234m, Pa-235;
92-U-232, U-233, **U-234**, **U-235**, U-235m, U-236, U-237, **U-238**, U-239, U-240;
93-Np-236, Np-236m, Np-237, Np-238, Np-239, Np-240, Np-240m, Np-241;
94-Pu-236, Pu-237, Pu-238, Pu-239, Pu-240, Pu-241, Pu-242, Pu-243, Pu-244, Pu-245, Pu-246;
95-Am-240, Am-241, Am-242, Am-242m, Am-243, Am-244, Am-244m, Am-245, Am-246, Am-246m;
96-Cm-241, Cm-242, Cm-243, Cm-244, Cm-245, Cm-246, Cm-247, Cm-248, Cm-249, Cm-250;
97-Bk-249, Bk-250;
98-Cf-249, Cf-250, Cf-251, Cf-252, Cf-253;
99-Es-253;

Naturally-occurring nuclides are listed in bold type.

3. DECAY HEAT CALCULATIONS: DATA UNCERTAINTIES

Nuclear data files are normally based on statistical analyses and evaluations of all relevant measured data reported in the open literature. Unfortunately, there may be omissions in the resulting data libraries that need to be filled to avoid serious impact on the ability to undertake the desired calculations with confidence. Setting this issue aside until Sections 4 and 5, some consideration is given below to data uncertainties and the value of sensitivity studies in identifying the main parameters to be improved in order to increase the accuracy and reliability of decay-heat calculations.

3.1. Neutron Cross Sections

Uncertainties in the neutron-absorption cross sections of the fission products have only a marginal effect on decay-heat predictions for cooling times $< 10^4$ sec. Changes in decay heat at longer cooling times are dependent on the flux level and irradiation time, and no simple estimate can be made of the uncertainty in decay heat at these cooling times that arises from uncertainties in the cross-section data. Nevertheless, the conservative assumption is normally made that the desired accuracy of decay-heat calculations can be achieved with uncertainties in the cross sections of 10-30% for the important capture products over long decay times (leading up to 10^8 sec).

3.2. Fission Yields

There are extensive gaps in the charge distribution data for fission, and in the chain yields for the more important fission reactions; there are also significant discrepancies between chain-yield measurements. Many fission products of importance in decay-heat calculations are short-lived, and their decay characteristics are either poorly defined or entirely unknown because of the difficulties associated with their direct study. Under such circumstances, sound theoretical extrapolation procedures and modelling techniques have been adopted to generate comprehensive fission-yield data sets, while various methods have been successfully explored to derive beta-strength functions and use these approximations to estimate half-lives and mean beta and gamma energies.

Isomeric states are normally low-lying metastable states (< 1 MeV) that occur when the angular momentum differences between this nuclear level and all lower levels are large. Electromagnetic transition probabilities are significantly reduced under such circumstances, and the lifetimes of the states are long (i.e., metastable). The half-lives of both the ground and metastable states can span many orders of magnitude ($\sim 10^{15}$ sec) due to variations in the form of β^- decay (end-point energies and beta-strength functions). Over 150 of the fission products formed in the thermal-neutron fission of ^{233}U, ^{235}U and ^{239}Pu have known isomeric states with half-lives ≥ 0.1 sec.

These isomeric states play an important role in decay-energy release, since this time-dependent phenomenon depends on the relative populations between the ground and metastable states. Madland and England (1977) have developed a simple model to calculate the independent yield branching ratios between the ground and metastable states, and this approach has been extended by Rudstam *et al* (IAEA-CRP, 2000).

3.3. Decay Data

Most experimental measurements of nuclear structure and decay-scheme data focus on the emission of discrete gamma-rays. This type of spectral measurement dominates fission-product decay-scheme studies because of the difficulties and scarcity of facilities throughout the world to measure the corresponding beta-transition energies and emission probabilities accurately. However, the inability to detect weak high-energy gamma-ray emissions satisfactorily has been noted by Hardy *et al* (1977), and this problem impacts on the β^- decay data calculated from such measurements. A generalised assessment was made of a radionuclide with a complex decay scheme (labelled "pandemonium"): approximately 20% of the gamma-ray emissions above 1.7 MeV were estimated to remain undetected within the background, and would be omitted from the proposed decay scheme. Under these conditions, every complex β^- decay scheme derived through gamma-ray studies must be regarded with some doubt – the recommended β^--decay scheme may be inaccurate (Fig. 1), and might explain anomalies that sometimes occur between calculated and measured decay heat.

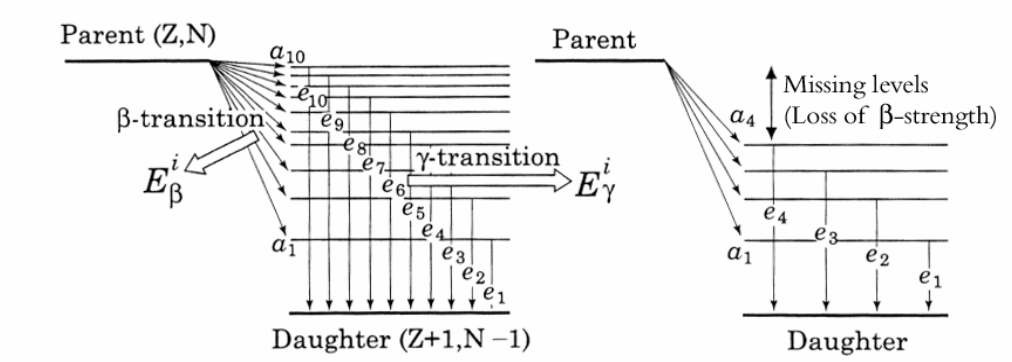

Fig. 1. Effect of missing nuclear levels: loss of γ-ray energy release ($E^i\gamma$)

The β^- decay of ^{87}Br represents a good example of the problems faced by evaluators of complex decay schemes (Reich, 1987). This nuclide has a half-life of 55.7 sec, and an extremely thorough study by Raman *et al* (1983) has revealed the existence of 126 bound levels and 12 levels in the unbound region. Approximately 220 gamma rays were detected in a series of singles and coincidence measurements, and β^-

emission probabilities were calculated from the measured gamma-ray intensities: 160 beta branches were defined, with evidence of broad resonance-like structure in the overall beta-strength distribution. These measurements have resulted in significant changes in the mean beta and gamma energies for this radionuclide. Unfortunately, few short-lived fission products with such complex decay schemes are likely to be studied in such a comprehensive manner. Many short-lived fission products are very poorly characterised because their gamma-ray spectra have been incompletely measured or remain undetermined; under these circumstances, theoretical models have been adopted to calculate mean beta and gamma energies (and half-lives).

3.4. Sensitivity Studies

3.4.1. Fission products

Schmittroth (1976) studied the impact of the uncertainties in fission-product yields, half-lives, decay energies and the assignment of isomeric states. Thermal-neutron fission of ^{235}U was considered in detail, and this assessment indicated that decay heat can be calculated to an accuracy of 7% or better for cooling times > 10 sec. The major sources of uncertainty at cooling times < 1000 sec arise from ill-defined decay energies and fission-product charge distributions. This work was extended further by Schmittroth and Schenter (1977) who undertook a sensitivity analysis of the calculated decay heat associated with the thermal fission of ^{235}U and the fast fission of ^{238}U and ^{239}Pu. Both burst and 10^7 sec exposures were considered (Figs. 2 and 3).

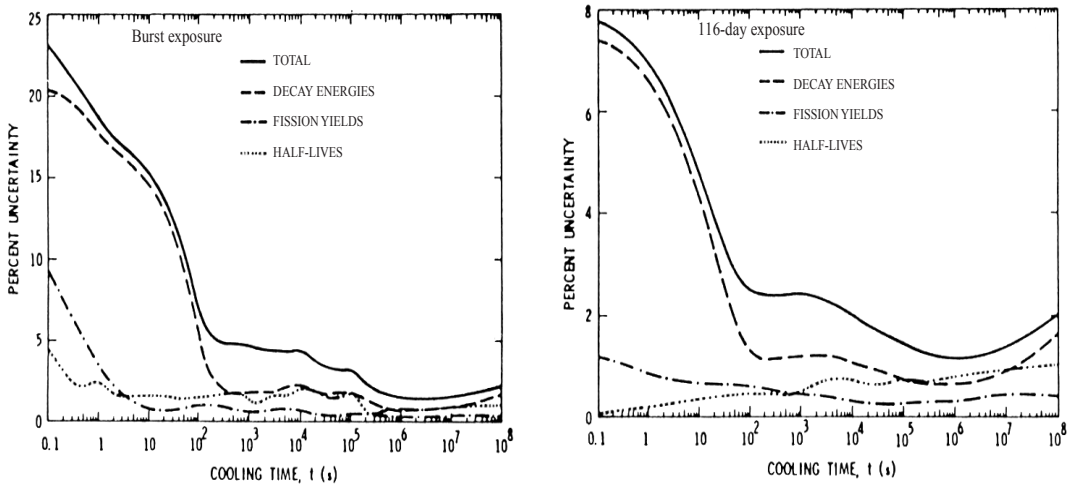

Fig. 2. Total decay-heat uncertainties for thermal fission of ^{235}U (Schmittroth and Schenter, 1977)

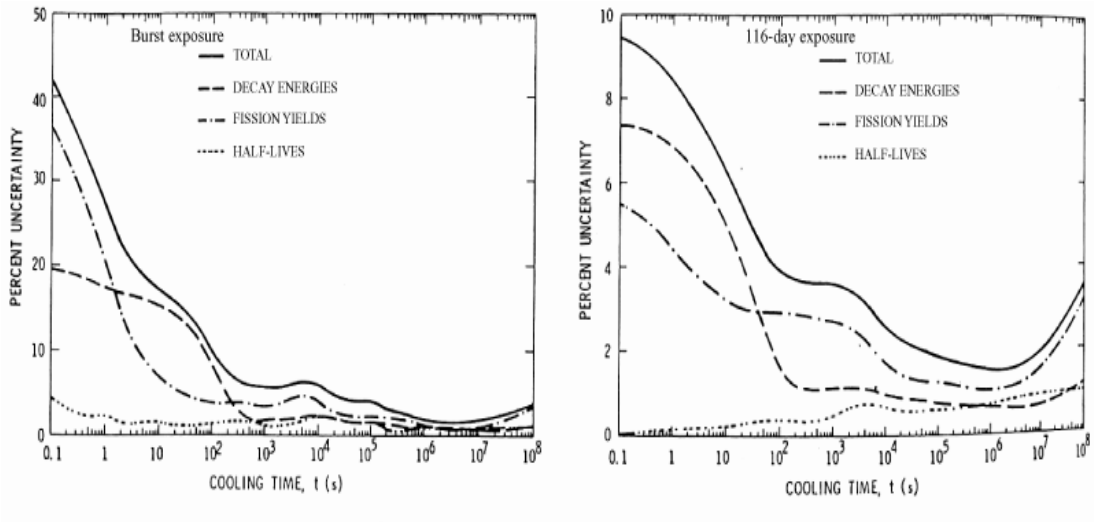

Fig. 3. Total decay-heat uncertainties for fast fission of ^{239}Pu (Schmittroth and Schenter, 1977)

Schmittroth and Schenter were able to attribute the main sources of uncertainty in decay-heat summation calculations to existing uncertainties in the fission-product yields and decay energies. Uncertainties in fission-product half-lives were judged to be relatively unimportant for most cooling times in decay-heat calculations. Overall, decay energies were found to be the major source of decay-heat uncertainties, especially for short cooling times (< 100 sec). These studies underline the sensitivity of decay heat to the mean energies of decay; various efforts have been made to improve these data by measurement and theoretical modelling, as outlined in Section 5.

A similar sensitivity analysis has been made of the uncertainties in decay heat when using the nuclear data contained within the JEF-2.2 library (Storrer, 1994). The calculated decay heat is dominated by radionuclides with well-defined decay schemes for cooling times > 3 x 10^6 sec, while the largest contributions come from poorly-defined nuclides for cooling times < 3 x 10^5 sec. Finally, at cooling times less than ~10 sec, fission products based completely on theoretical data contribute approximately 25% to the resulting decay heat.

Developments of the gross theory of beta decay form the main source of decay data for poorly-defined radionuclides in the JNDC-FP and US ENDF/B-VI libraries (see Sections 5.3 and 5.5). Oyamatsu *et al* (1997) have undertaken extensive studies of the suitability of these data libraries in decay-heat calculations. Their sensitivity analyses were extremely detailed, and highlighted a series of specific inadequacies.

For example, Fig. 4 shows the variation in uncertainty of the total $\beta+\gamma$ decay heat as a function of cooling time, following the thermal-neutron fission of ^{235}U:

(a) at short cooling times, the uncertainty in decay heat is dominated by uncertainties in specific independent yields and decay constants, although there is also a increasingly significant contribution from uncertainties in the decay energies up to 1000 sec cooling time;

(b) particular peaks in the uncertainty profile contain significant contributions from the uncertainties of specific parameters (see Table 4) – for example, peak 4 contains significant contributions from uncertainties in the decay energies of ^{93}Sr and ^{102}Tc, and peak 7 is dominated by uncertainties in the independent fission yields of $^{97,97m}Y$.

These analyses are extremely informative for a wide range of fissioning nuclides, and a further example is given in Fig. 5 and Table 5, for the fast fission of ^{238}Pu. Particular nuclear parameters appear regularly in the assessments (e.g., independent yields of ^{97}Sr and ^{97m}Y in peak 1, decay constant for ^{101}Zr in peaks 1 and 2, decay energies of ^{103}Mo and ^{103}Tc in peak 3, and cumulative yields for $^{102,102m}Nb$ in peak 4). The main contributors to the decay-heat uncertainties are highlighted in the tables with respect to each numbered peak, providing clear indications of the specific needs for improved fission-product data.

3.4.2. Actinides

Actinide decay contributes a maximum of approximately 20-30% of the total decay heat for a wide range of irradiation conditions up to cooling times of ~ 10^8 sec. (Fig. 6). The most significant contributions to actinide decay heat arise from ^{239}U and ^{239}Np for cooling times < 10^6 sec, while the α decay of ^{238}Pu, ^{241}Am, ^{242}Cm and ^{244}Cm become more important at much longer times (Fig. 7). Assuming a decay-heat contribution of 30% by ^{239}U and ^{239}Np gives rise to a maximum uncertainty in the total decay-heat predictions of 2% for uranium-based thermal reactors at cooling times up to 10^6 sec. At longer cooling times, the actinide contribution to decay heat is dominated by ^{242}Cm, and the contribution to the overall uncertainty in decay heat ranges from 0.5% to 6% over the cooling time 10^8 to 3 x 10^9 sec. Overall, there would appear to be no serious problems associated with the actinides in decay-heat calculations.

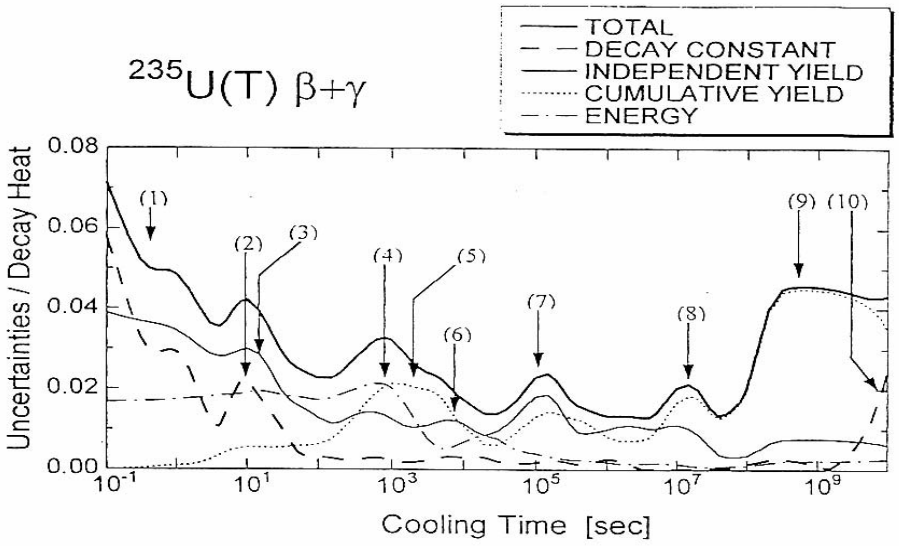

Fig. 4. Uncertainties in total decay heat for ^{235}U(T) without taking correlation effects into account

No.	t [sec]	Parameter	Nuclide
(1)	0~1	Independent Yield	^{88}As
			^{100}Y
			^{97m}Y
		Decay Constant	^{86}Ge
			^{101}Zr
(2)	10	Decay Constant	^{101}Zr
(3)	10~	Independent yield	^{100}Zr
(4)	10^3	Decay Energy	^{93}Sr
			^{102}Tc
(5)	10^3~	Cumulative Yield	^{102}Nb
(6)	~10^4	Independent yield	^{134}Te
			^{130m}Sn
			^{134m}I
(7)	10^5	Independent yield	^{97}Y
			^{97m}Y
(8)	10^7	Cumulative Yield	^{95}Y
(9)	10^8~	Cumulative Yield	^{90m}Rb
(10)	~10^{10}	Decay Constant	^{90}Sr
			^{137}Cs

Table 4: Main parameters contributing to the uncertainties in total decay heat for ^{235}U(T)

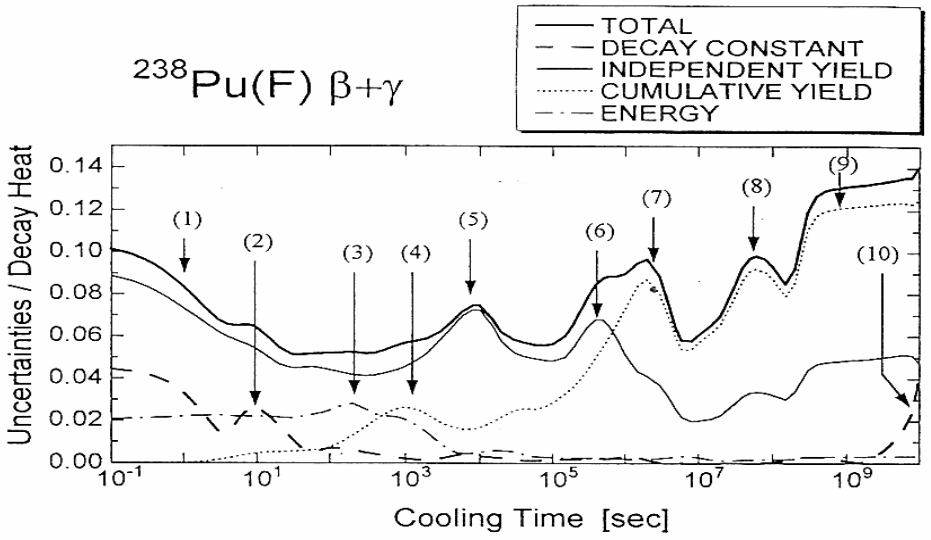

Fig. 5. Uncertainties in total decay heat for ^{238}Pu(F) without taking correlation effects into account

No.	t [sec]	Parameter	Nuclide
(1)	0~1	Independent Yield	^{97}Sr
			^{97m}Y
		Decay Constant	^{101}Zr
			^{104m}Nb
(2)	10	Decay Constant	^{101}Zr
(3)	10^2~	Decay Energy	^{103}Mo
			^{103}Tc
(4)	10^3	Cumulative Yield	^{102}Nb
			^{102m}Nb
(5)	10^4	Independent Yield	^{134}Te
			^{138}Xe
			^{142}Ba
(6)	~10^6	Independent Yield	^{132}Te
(7)	10^6~	Cumulative Yield	^{140}Cs
(8)	~10^8	Cumulative Yield	^{106}Tc
			^{144}La
(9)	10^8~	Cumulative Yield	^{137}Xe
(10)	~10^{10}	Decay Constant	^{126}Sn
			^{137}Cs

Table 5: Main parameters contributing to the uncertainties in total decay heat for ^{238}Pu(F)

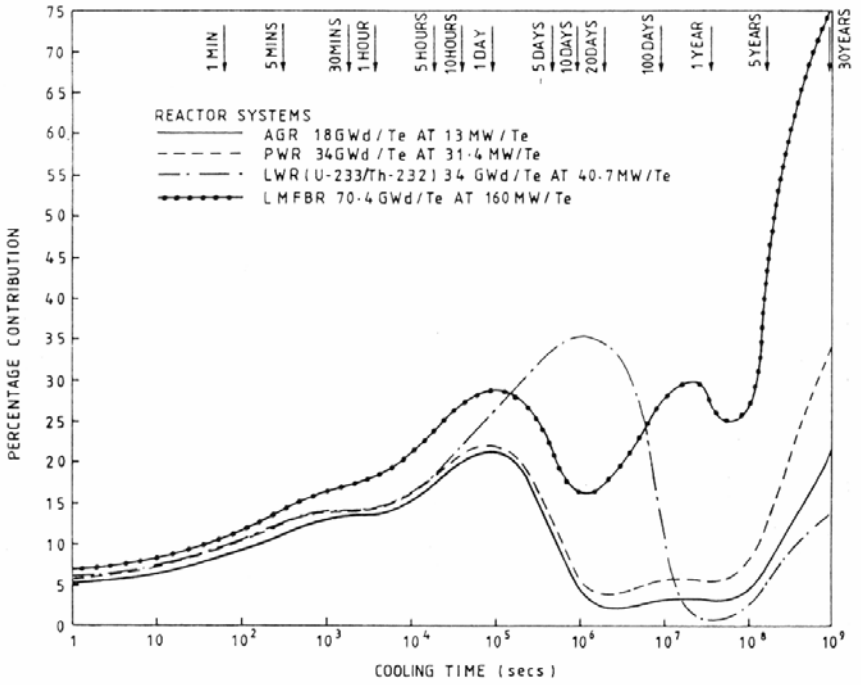

Fig. 6. Percentage contribution of actinides to total decay heat from typical fuel of different reactor systems

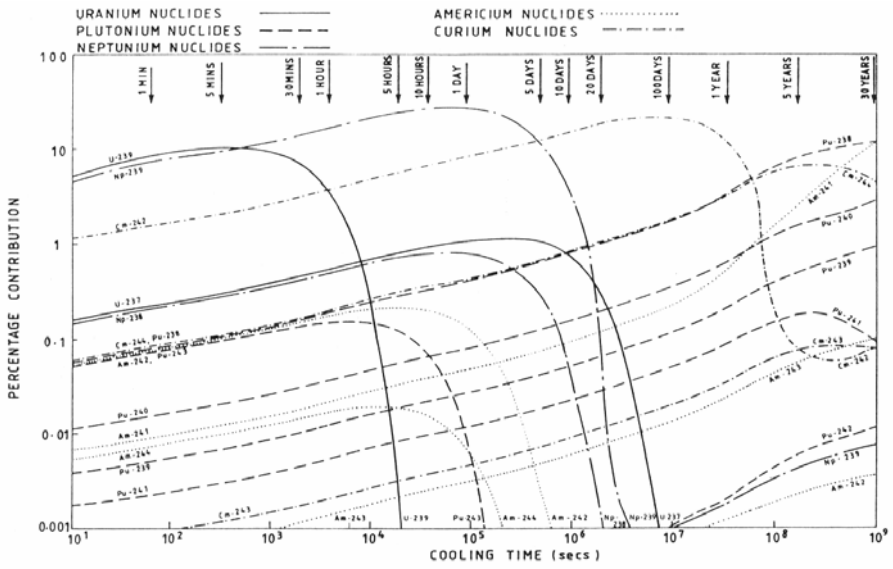

Fig. 7. Percentage contribution from individual actinides to total decay energy release rates [5 MW/Te(U) end of life rating 30 GWd/Te(U)] for gas-cooled reactor fuel (AGR)

3.4.3. Activation products

A few comments are merited concerning the impact of activation products on decay-heat calculations for fission-based reactors. The radioactive decay of the activation products generated from the structural materials of a thermal-reactor core represents an extremely minor contribution to the resulting decay heat. This source is more significant following shutdown of a fast reactor, with the formation of ^{22}Na and ^{24}Na by activation of the sodium coolant, and ^{58}Co and ^{60}Co from the activation of the nickel content of the steel structures in the reactor core:

$$^{58}\text{Ni(n, p)}^{58}\text{Co(n, }\gamma\text{)}^{59}\text{Co(n, }\gamma\text{)}^{60}\text{Co}$$

Up to ~ 10% of the decay heat at 5 years cooling time arises primarily from ^{60}Co. However, the production cross sections and decay data of all the main contributors are sufficiently well known that uncertainties in these parameters pose no problems in summation calculations. Hence, the activation products will be considered no further.

4. FISSION YIELDS

Complete fission product inventories need to be known as accurately as possible, and yield distributions are required as input to the summation calculations of decay heat. Emphasis is placed on the methods adopted to derive comprehensive yield data for the various fission processes – this requirement involves a significant amount of modelling, as discussed below. Ternary fission is only mentioned briefly, although this particular process has been extensively studied to improve the fundamental understanding of scission – the impact on decay heat of producing a third light fragment (such as ^{3}H and ^{4}He) is negligible.

The fission process is complex, and different definitions of fission yield are used (IAEA-CRP, 2000):

(a) Independent fission yield [*Y(A, Z, I)*] – number of atoms of a specific nuclide formed directly in fission (excludes radioactive decay of precursors)

$$Y(A,Z,I) = Y(A)\times f(A,Z)\times R(A,Z,I)$$

where *Y(A)* is the total sum of independent yields (before delayed-neutron emission) of all fission products of mass number *A*,
f(A, Z) is the fractional independent yield of all isomers of *A, Z*,
R(A, Z, I) is the fraction of *A, Z* produced directly as isomer *I* (i.e., isomeric yield ratio).

(b) Cumulative fission yield [*Cu(A, Z, I)*] – total number of atoms of a specific nuclide that accumulate from fission, the decay of precursor(s), and via delayed-neutron emission (but excluding neutron reactions on fission products)

$$Cu(A,Z,I) = Y(A,Z,I) + \sum_{A',Z',I'} b(A',Z',I' \rightarrow A,Z,I).Cu(A',Z',I')$$

The majority of fission products undergo β^- and IT decay, and therefore $A' = A$. However, difficulties arise in the determination of $Cu(A,Z,I)$ for β^- n decay, when $A' = A+1$ and $Z' = Z-1$.

(c) Chain yield [*Ch(A)*] – sum of the cumulative yields of the last (stable or long-lived) members of a chain.

(d) Mass yield – sum of all independent yields of a particular mass chain.

Although the sum of the independent yields cannot be determined in most measured yield distributions, this parameter is important in the development of fission yield systematics. The accepted procedure for recommending each yield set (combination of fissionable nucleus and neutron energy) is to evaluate measured relative and absolute independent and cumulative yields. These data are combined with estimated yields (when no measurements are available), and the complete yield distributions are adjusted by applying physical constraints (conservation of mass and charge in fission). This method of evaluation produces comprehensive yield distributions (Fig. 8).

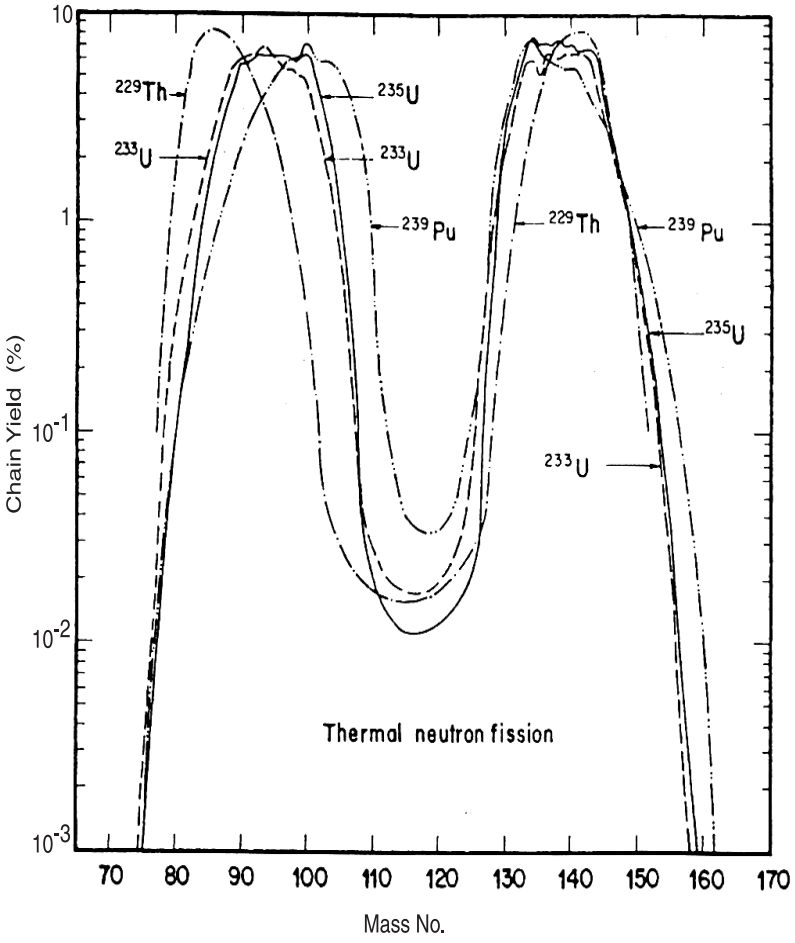

Fig. 8. Mass distribution curves in the thermal-neutron induced fission of ^{229}Th, ^{233}U, ^{235}U, and ^{239}Pu

Until the mid-1970s, several fission yield evaluations had been undertaken on only a limited number of yield sets. Crouch (1977), and Meek and Rider (1972, 1974 and 1978)/Rider (1981) produced their UK and US fission yield libraries in the late 1970s, and the Chinese began fission yield compilation and evaluation efforts in 1976. These files have been extended as the requirements for evaluated fission yield data have increased dramatically in recent years:

- number of yield sets has increased significantly,
- addition of isomeric yields for decay heat calculations,
- energy dependence of fission yields to permit more accurate burn-up calculations for fast reactor neutron spectra,
- development of new techniques for fission yield measurements (for example, on-line mass spectrometry), and incorporation of these data in new evaluations,
- models and calculation methods were developed to determine charge and mass distributions and isomeric yield ratios for unmeasured yields.

Much of this work was reviewed in detail during the course of an IAEA Coordinated Research Programme on the Compilation and Evaluation of Fission Yield Nuclear Data (IAEA-CRP, 2000). Furthermore, these commendable studies have continued under the auspices of another IAEA Coordinated Research Programme on Fission Yield Data Required for Transmutation of Minor Actinide Nuclear Waste (1997 to date).

4.1. Modelling

Various equations and model parameters have been derived from studies of the systematic trends in measured yield distributions. Although these theoretical data are not sufficiently reliable for applied purposes, they have been used to obtain numerical values where no yields have been measured, or to check and adjust experimental data to the expected distribution. Wahl (1987 and 1988) has carried out a thorough evaluation of independent fission yields in order to obtain best values for a set of empirical model parameters. These model parameters have been subsequently used by fission-yield evaluators to calculate charge distributions and estimate unmeasured yields.

4.1.1. Mass distribution

Mass distributions are normally obtained from measurements, but models can be used to fill gaps that are too large for linear interpolation. A variable number of

Gaussian functions can be used to represent the mass distributions of different fission reactions and neutron energies, from Th to Es (Z = 90–99) and for excitation energies < 20 MeV (e.g., Figs. 9 and 10). Thus, the sum of 2 to 5 Gaussian functions can be fitted to the experimental chain yield data [Y(A)] of products from the fission of these nuclei, using the method of least squares. The Gaussian functions can then be characterised against mathematical functions of the atomic numbers (Z_F), mass numbers (A_F), and excitation energies (E*) of the fissioning nuclei. Reciprocal variance weighting is used in both types of calculation, and the resulting functions provide a means of determining complete mass distributions for fissioning nuclei.

The central Gaussian curve is not needed to represent chain yields from spontaneous fission reactions (SF), in agreement with experimental observations that show the valley yields from spontaneous fission to be more than an order-of-magnitude less than those from thermal-neutron induced fission reactions. Furthermore, one Gaussian curve per peak can be adopted to represent the chain-yield data reasonably well for both 14 MeV neutron-induced fission and thermal-neutron induced fission of the heavier actinides ($Z_F > 94$). Other modifications can be made to improve the chain-yield representations: for example, fission of heavier actinides - modify the peak Gaussian functions to include an exponential drop in Y(A) for $A_H < 130$ and in the complementary range for the light peak (these modified peak functions are then renormalized to achieve a 200% sum for all yields).

Equations have also been developed to calculate the uncertainties in fission yields obtained from these model estimates. Uncertainties in the calculated yields can be estimated from the following empirical equation proposed for the percentage uncertainty (PER):

$$PER = (25)\exp\{-0.25[\ln Y(A)]\}$$

with an estimated range of uncertainty of $Y(A)/(1 + PER/100)$ to $Y(A)(1 + PER/100)$.

Most experimental chain yields fall within the estimated range of uncertainties, implying that most of the calculated chain yields should be reliable.

Many of the measured chain yields have fine structure that cannot be fully reproduced by summing smooth Gaussian functions (Figs. 9 and 10), although complementary single Gaussian curves can represent the experimental data reasonably well for high excitation energies and $Z_F > 94$. Thus, an empirical multi-Gaussian model has been successfully developed to calculate the chain yields [Y(A)] of fission reactions, with a nuclear charge [Z_F] from 90 to 99 and excitation energy $E^* \leq 20$ MeV. There are many other features of these mass distribution curves that will not be considered in any further detail within this review.

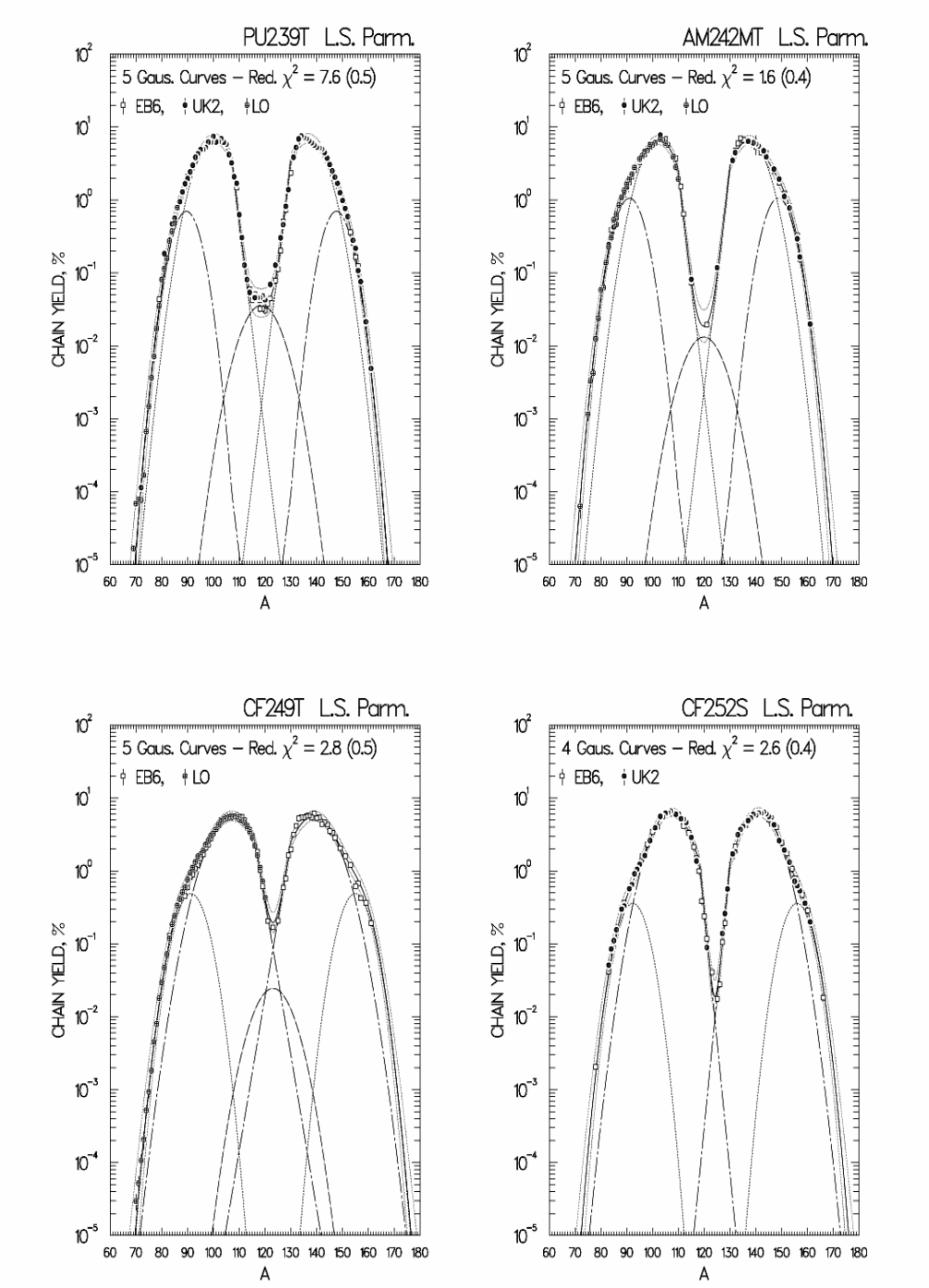

Fig. 9. Various Gaussian curves fitted to mass distributions of fission processes: thermal-neutron fission of ^{239}Pu, ^{242m}Am and ^{249}Cf, and spontaneous fission of ^{252}Cf

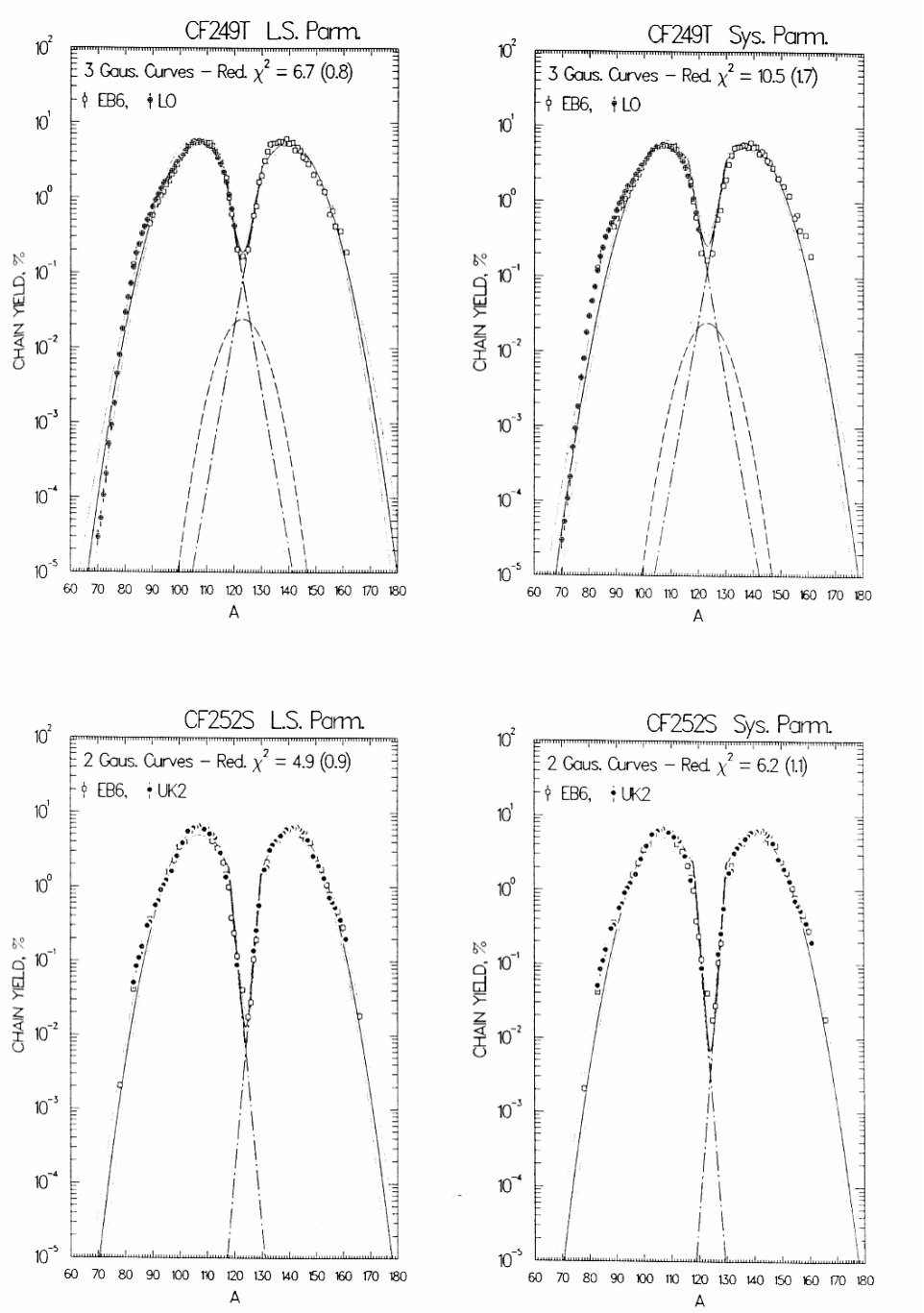

Fig. 10. Various Gaussian curves fitted to mass distributions of fission processes: thermal-neutron fission of ^{249}Cf, and spontaneous fission of ^{252}Cf

4.1.2. Nuclear-charge distribution

Nuclear-charge distributions describe the dispersion of yields with mass and atomic numbers (A and Z) of ~1000 primary fission products from each of the many fission reactions (yields are for the fission products after prompt-neutron emission and before beta decay). However, only a small fraction of the yields have been measured, and theoretical models are not sufficiently advanced to give reliable yield estimates. Therefore, two empirical models have been proposed that include mathematical functions derived from the available experimental data (Wahl, 1988).

While the Z_P and A'_P models give different perspectives on the nuclear-charge distribution from fission, comparisons of the results have been helpful in improving both models. The Z_P model treats the dispersion of fractional independent yields [FI] with Z for each A of primary fission products; the A'_P model considers the dispersion of independent yields [IN] with A' for each Z of primary fission products, where A' is the average mass number of the precursor primary fragments that give products with A by prompt-neutron emission ($A' = A + \bar{\nu}_A$).

Experimental independent yields can be supplemented by yields calculated from the Z_P or A'_P models for the fission reaction of interest, prior to dividing amongst the isomeric states (Madland and England, 1977). The spins of the states need to be defined for both treatments, and the isomeric cumulative yields can be calculated by summation of the independent yields based on the spins and branching fractions to the isomeric states.

(a) $\boldsymbol{Z_p}$ model

The Z_P model has been used for charge distribution calculations in the two major fission yield evaluations (US ENDF/B-VI and UKFY2 (and UKFY3)). Z_P-model parameters are defined as F_Z, F_N, σ_Z and ΔZ, and are either constant or linear functions of A' in each of the regions considered (as shown in Fig. 11). Fractional independent yields are expressed in terms of these parameters:

$$FI(A,\ Z) \ = \ (0.5)\ [F(A)]\ [N(A)]\ [erf(V)\ -\ erf(W)]$$

$$\text{where} \quad V \ = \ \frac{Z(A)\ -\ Z_p(A)\ +\ 0.5}{\sqrt{2}\ \ [\sigma_Z(A')]}$$

$$\text{and} \quad W \ = \ \frac{Z(A)\ -\ Z_p(A)\ -\ 0.5}{\sqrt{2}\ \ [\sigma_Z(A')]}$$

$$\text{in which} \quad Z_p(A_H) \ = \ A'_H[Z_F / A_F] \ + \ \Delta Z(A'_H)$$

0.Fig. 10 Various Gaussian curves fitted to mass distributions of fission processes: thermal-neutron fission of ^{249}Cf, and spontaneous fission of ^{252}Cf

$$\text{and} \quad Z_p(A_L) = A'_L[Z_F / A_F] - \Delta Z(A'_{Hc})$$

where Z_F and A_F are the atomic number and mass number of the fissioning nuclide, A_H and A_L are the mass numbers for the heavy and light fission peaks respectively, $A'_{Hc} = A_F - A'_L$, and

	for Z	for N
$F(A) = [F_Z(A')][F_N(A')]$	even	even
$F(A) = [F_Z(A')/[F_N(A')]$	even	odd
$F(A) = [F_N(A')]/[F_Z(A')]$	odd	even
$F(A) = \dfrac{1}{[F_Z(A')][F_N(A')]}$	odd	odd
$F(A) = 1.00$ near symmetry		

N(A) is the normalisation factor to achieve *Σ(FI)* = 1.00 for each *A*, which has to be implemented because *F(A)* destroys the inherent normalisation of the Gaussian distributions; values of *N(A)* seldom deviate by more than 10% from unity.

All of the parameters $\Delta Z(A'), \sigma_Z(A'), F_Z(A')$ and $F_N(A')$ depend on A', and the region in which A' falls. Apart from distributions close to symmetry, all of the parameters are constant except ΔZ, which has a small negative slope (ΔZ is the displacement of Z_P from an unchanged charge distribution):

$$\Delta Z = \{Z_P - A'[Z_F/A_F]\}_H = \{A'[Z_F/A_F] - Z_P\}_L$$

Near to symmetry, the width parameter [σ_z] changes abruptly twice to a lower value, the even-odd proton and neutron factors [F_Z and F_N] equal 1.0, and the ΔZ function undergoes a zig-zag transition from positive values for light fission products to negative values for heavy fission products. The Z_P model has been modified to include parameter slopes vs. A' and slope changes in the wing regions.

Values of the Z_P-model parameters have been determined for each of twelve fission reactions (^{229}Th thermal, ^{232}Th fast, ^{233}U thermal, ^{235}U thermal, ^{238}U fast, ^{238}U 14 MeV neutrons, ^{238}Np thermal, ^{239}Pu thermal, ^{241}Pu thermal, ^{242}Am thermal, ^{249}Cf thermal, and ^{252}Cf sf) by the method of least squares. However, all of the model parameters can only be determined by this method for the thermal fission of ^{235}U. Other fission reactions require the following equation to estimate Z_P-model parameter values [PM]:

$$PM = P(1) + P(2)(Z_F - 92) + P(3)(A_F - 236) + P(4)(E^* - 6.551)$$

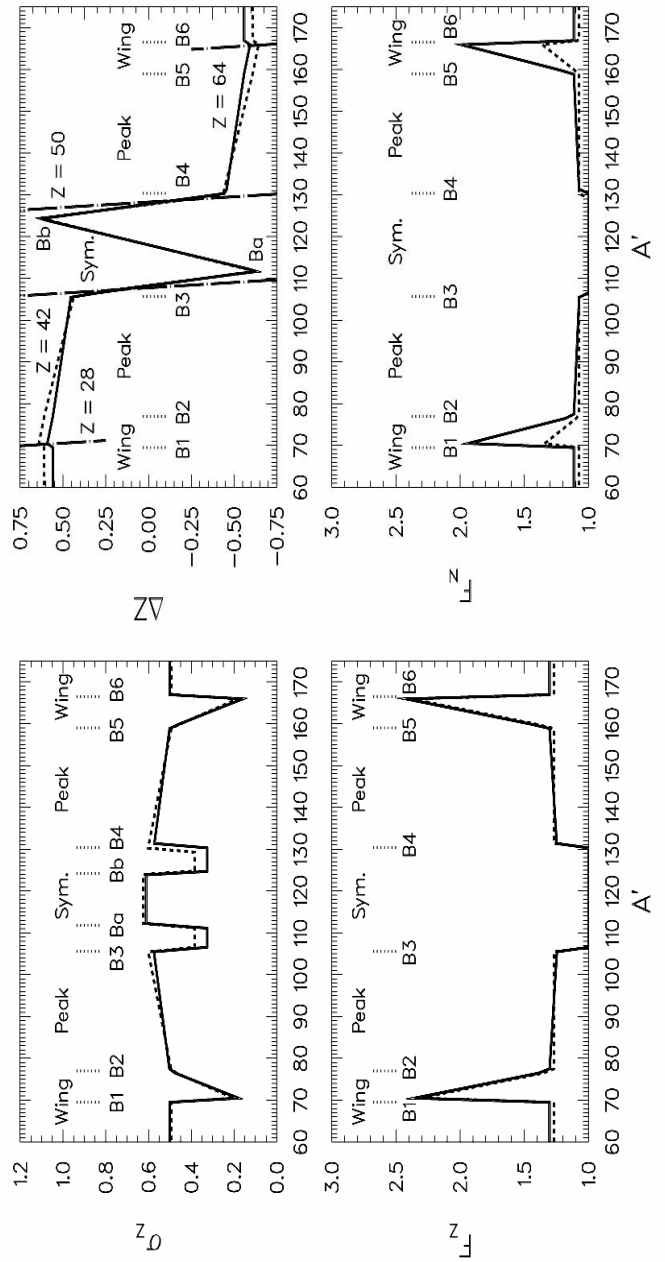

Fig. 11. Z_p functions for thermal fission of ^{235}U
Solid lines calculated by L.S., red. $\chi^2 = 3.6(0.7)$
Dashed lines from systematics, red. $\chi^2 = 6.6(0.6)$

where E* is the excitation energy above the ground state of the fissioning nuclide. *P(i)* values were calculated by the method of least squares from the PM values that could be determined by least squares for individual fission reactions. Fig. 12 shows the adopted parameter values as points and the derived functions as lines.

Checks have been made on the validity and usefulness of the Z_P-model parameters obtained from the PM calculations for each of the 12 fission reactions investigated. The reduced χ^2 values were within a factor of approximately 2 of those determined by the method of least squares with variation of as many parameters as possible. Further details of these studies can be found in IAEA-CRP (2000).

b) A'_p model

Studies are underway to determine whether a simplified A'_P model can be used with only five Gaussian functions to represent the element yields, rather than the many needed for the association of one model parameter with each element yield (IAEA-CRP, 2000). Fig. 13 shows the results of calculations for the thermal-neutron fission of ^{235}U close to symmetry (Z = 42–50).

The data include independent yields for individual elements or for complementary element pairs when the data are available from radiochemical and on-line mass-separator measurements. Solid-black symbols represent $_{43}$Tc yields, while open symbols represent the yields for heavy fission products. The Gaussian width parameters [$\sigma = \sigma_{A'}$] are close to the average global parameter of 1.50 for $_{47}$Ag and the $_{50}$Sn–$_{42}$Mo pair. However, the values of σ are considerably larger for $_{48}$Cd and $_{43}$Tc-$_{49}$In pair, implying that these radionuclides could be formed by more than one process. The data for $_{48}$Cd and the $_{43}$Tc–$_{49}$In pair can be represented better by two Gaussian functions (symmetric and asymmetric), each with a σ value of 1.50 and peak separation of about 4 A' (Fig. 14). Significant deviations occur for the curve of the $_{43}$Tc–$_{49}$In pair, underlining the need for a re-evaluation of these data.

4.1.3. Isomeric fission yields

The independent fission yields of isomeric states are important in the definition of inventories for decay-heat calculations. However, these data are sparse for all fission processes apart from the thermal fission of ^{235}U. Modelling calculations are normally used to derive values, based on the partition of the independent fission yields of nuclides among their isomeric states using the spin distributions of the fission fragments and nuclear levels as fitting parameters.

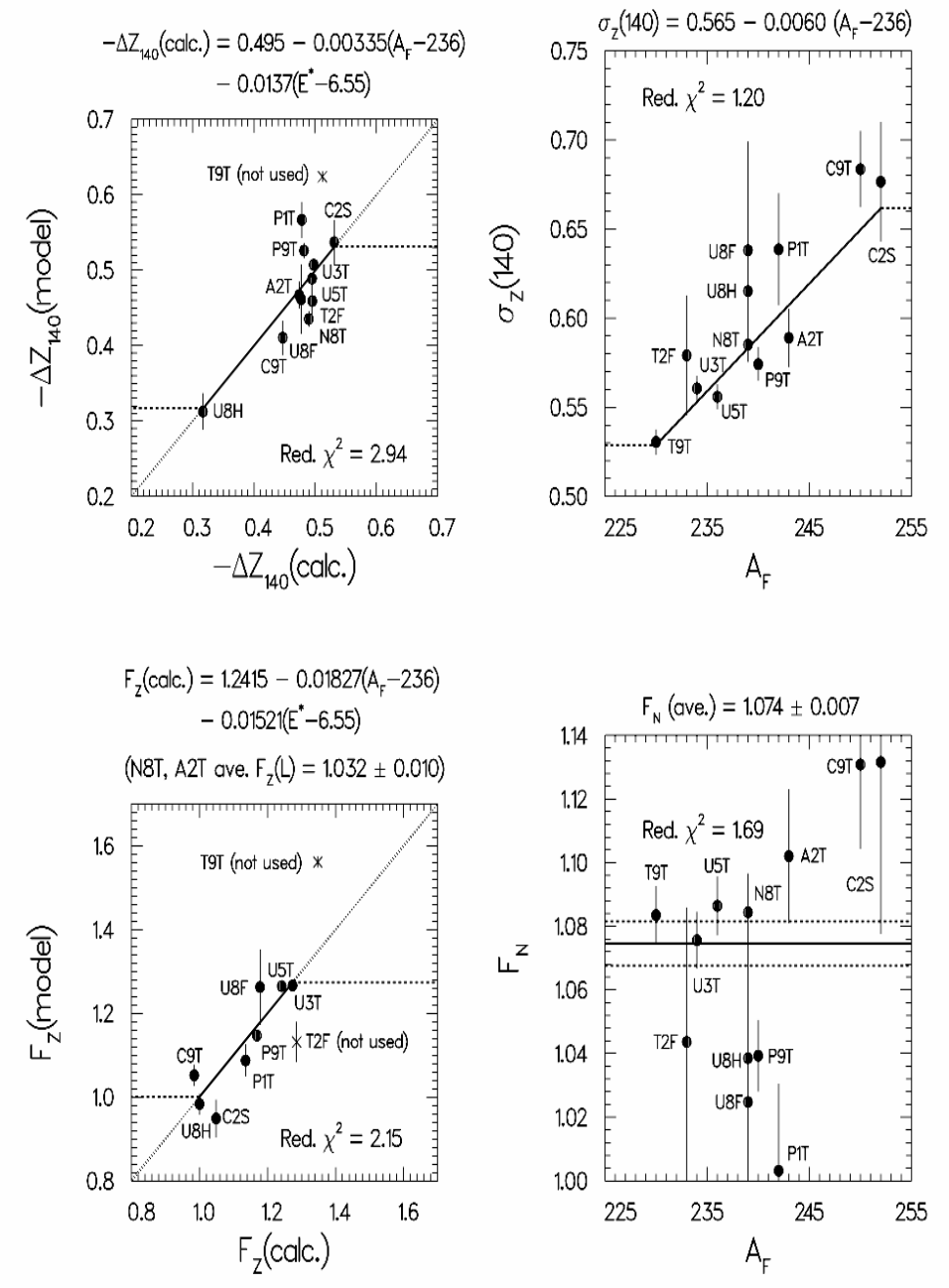

Fig. 12. Peak parameters for A'(140)

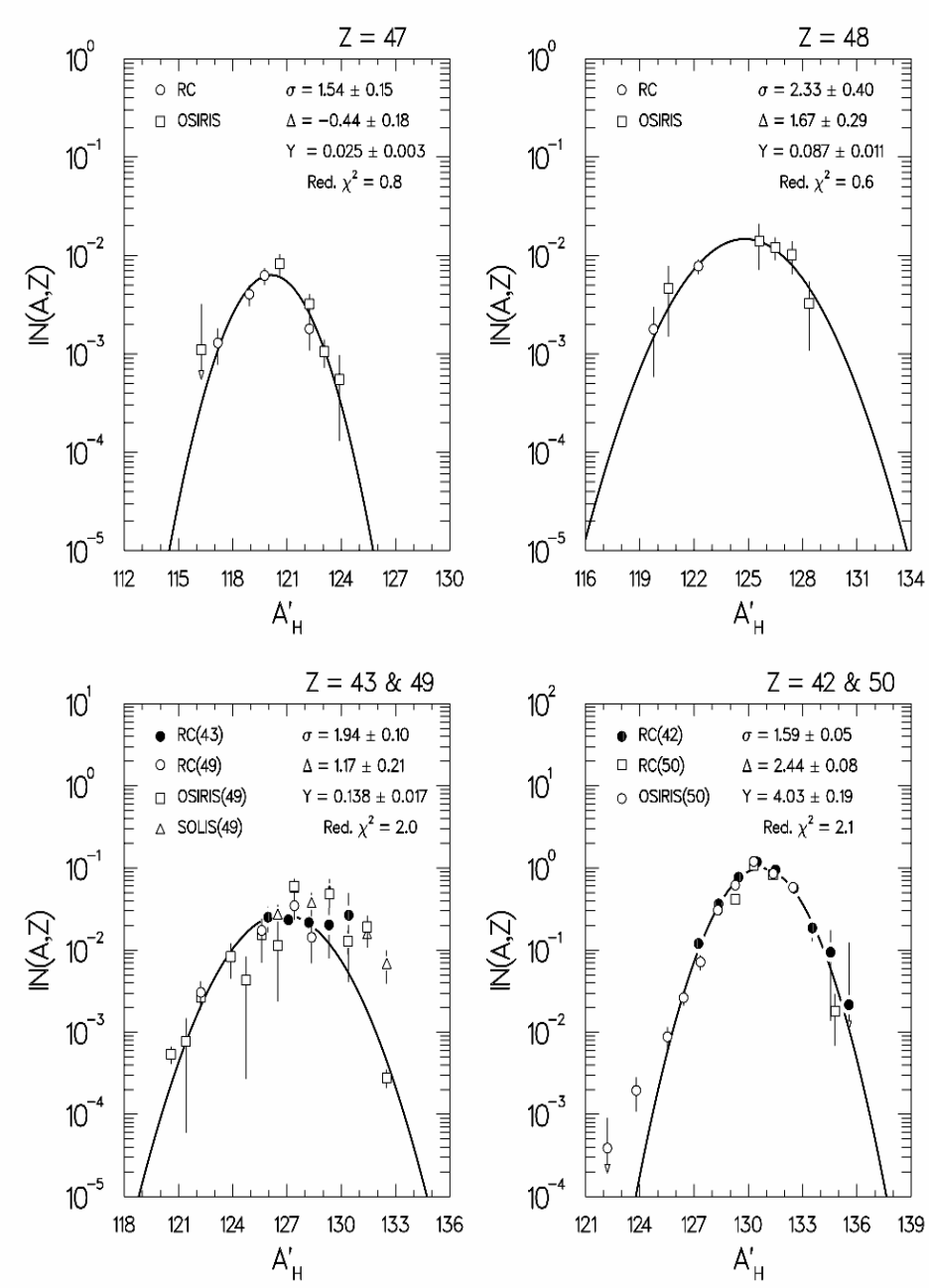

Fig. 13. Thermal fission of ^{235}U - A'_p model near symmetry: single Gaussian curve

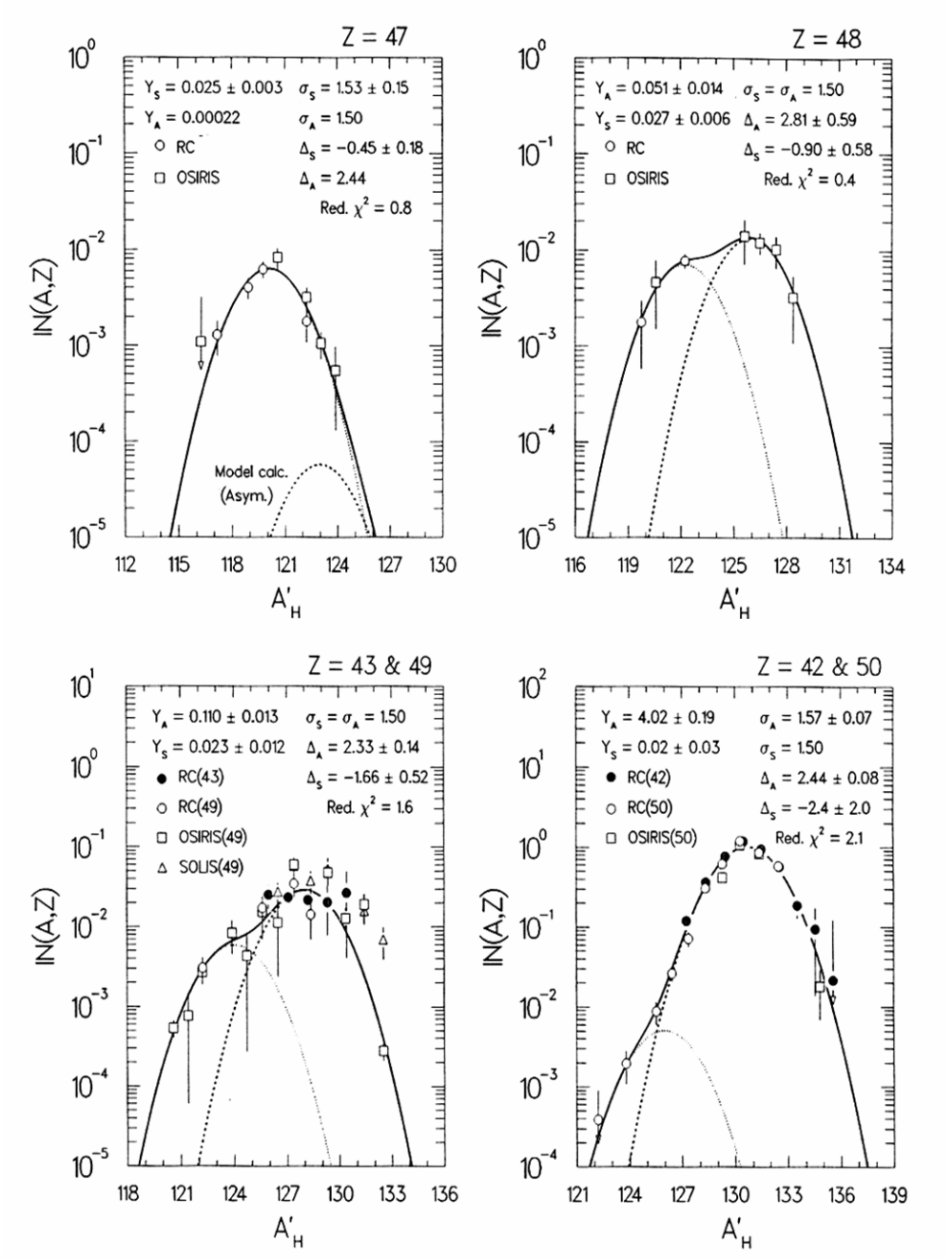

Fig. 14. Thermal fission of ^{235}U - A'$_p$ model near symmetry: two Gaussian curves

Madland and England (1977) assumed that the spin distribution of the fission fragments after prompt-neutron emission could be represented by the equation:

$$P(J) = C \times (2J+1) e^{-[(J+1/2)/Jrms]^2},$$

in which J_{rms} defines the state of the spin distribution, and C is a constant. Fragments with J nearer the spin of a particular isomer state are defined as feeding that state. This model has been developed further by Rudstam and co-workers (IAEA-CRP, 2000): the probability that the spin will decrease by one unit is proportional to the density of nuclear states of spin *J-1*, while the probability that the spin will increase is proportional to the density of nuclear states of spin *J+1*. The ratio between the number of nuclear states of spin *J-1* and those of spin *J+1* is given by *Z(J)*:

$$Z(J) = \frac{(2J-1)}{(2J+3)} e^{(4J+2)/J_{nuc}^2}$$

in which J_{nuc} is another spin parameter (defined effectively by the above equation). This approach results in a relative probability of *Z/(1+Z)* to decrease the spin by one unit, and a relative probability of *1/(1+Z)* to increase the spin by one unit. Erroneous results will occur when the isomeric state is at a much higher energy than the ground state.

Equations have been derived to calculate the fractional independent isomeric yields (*fiiy*), and they can be modified to accommodate reductions in the excitation energy caused by the gamma-ray emissions. The available experimental data have been compared with the calculated *fiiy* values, particularly for the thermal fission of ^{235}U. Various combinations of J_{rms} and J_{nuc} were adopted, and the best combinations were found to be:

J_{rms} of 6.50, and J_{nuc} of 6.00 for odd-mass nuclides;

J_{rms} of 6.00, and J_{nuc} of 1.00 to 2.00 for even-mass nuclides.

A value of 6.25 has been adopted for J_{rms}, and values of 6.00 (odd mass) and 2.00 (even mass) for J_{nuc} in comparing the *fiiy* data for the high-spin isomers listed in Table 6. Agreement between experimental and calculated values is judged to be satisfactory, although some nuclides exhibit significant discrepancies (e.g., ^{82}As, ^{99}Nb, ^{119}Cd, ^{128}Sb and ^{146}La).

Table 6: Experimental and calculated fractional independent yields of the high-spin isomers of nuclides formed in the thermal-fission of ^{235}U

Nuclide	*fiiy(high)*		**Nuclide**	*fiiy(high)*	
	experimental	**calculated**		**experimental**	**calculated**
^{79}Ge	1.00 ± 0.11	0.829	^{127}In	0.87 ± 0.06	0.814
^{81}Ge	0.70 ± 0.06	0.835	^{127}Sn	0.90 ± 0.11	0.626
^{82}As	0.17 ± 0.07	0.597	^{128}In	0.30 ± 0.07	0.190
^{83}Se	0.89 ± 0.07	0.816	^{128}Sn	0.11 ± 0.07	0.209
^{84}Br	0.30 ± 0.04	0.504	^{128}Sb	0.61 ± 0.06	0.192
^{84}Br	0.38 ± 0.04	0.504	^{129}In	0.76 ± 0.07	0.815
^{90}Rb	0.58 ± 0.05	0.659	^{129}Sn	0.43 ± 0.06	0.621
^{90}Rb	0.90 ± 0.01	0.659	^{130}Sn	0.13 ± 0.02	0.212
^{99}Nb	0.06 ± 0.14	0.819	^{130}Sb	0.45 ± 0.11	0.190
^{113}Ag	~1.00	0.847	^{132}Sb	0.20 ± 0.02	0.190
^{115}Ag	~1.00	0.846	^{132}Sb	0.19 ± 0.03	0.190
^{116}Ag	~1.00	0.391	^{133}Te	0.78 ± 0.04	0.590
^{117}Ag	~1.00	0.848	^{133}Te	0.57 ± 0.04	0.590
^{118}Ag	0.44 ± 0.10	0.388	^{133}Te	0.61 ± 0.08	0.590
^{119}Cd	0.39 ± 0.20	0.724	^{133}I	0.07 ± 0.02	0.140
^{120}Ag	0.85 ± 0.15	0.382	^{133}Xe	0.75 ± 0.04	0.603
^{121}Cd	0.89 ± 0.11	0.730	^{134}Sb	0.19 ± 0.05	0.279
^{123}Cd	0.68 ± 0.02	0.614	^{134}I	0.20 ± 0.02	0.183
^{123}In	0.94 ± 0.11	0.817	^{135}Xe	0.65 ± 0.04	0.575
^{123}Sn	1.00 ± 0.28	0.627	^{136}I	0.79 ± 0.14	0.391
^{124}In	0.86 ± 0.80	0.215	^{138}Cs	0.58 ± 0.08	0.392
^{125}Cd	0.66 ± 0.08	0.614	^{146}La	0.06 ± 0.03	0.391
^{125}In	0.88 ± 0.08	0.813	^{148}Pr	0.12 ± 0.03	0.660
^{126}In	0.42 ± 0.17	0.215	^{148}Pm	0.71 ± 0.06	0.388

4.2. Evaluated Fission Yield Libraries

The fission-yield data sets in the most recent evaluations are listed in Table 7. Thermal (**T***)* yields cover all measurements at 0.025 eV, or in well-moderated thermal reactor spectra. Fast **(F***)* yields include all measurements in fast reactor spectra (mean neutron energies of 150–500 keV) and fission neutron spectra (mean energies around 1 MeV and above). **H** means neutron energies around 14–15 MeV, while **S** stands for spontaneous fission.

Measurements of the energy dependence of fission yields are too scarce to derive systematic trends and develop a semi-empirical model for obtaining reliable predictions; many more systematic measurements are required before a reliable model can be developed. Therefore, ‘thermal’, ‘fast’ and ‘high’ (around 14 MeV) yields continue to be evaluated for data files and are used in applied calculations.

(a) The US evaluation has increased from 10 to 60 yield sets, each yield set consisting of cumulative and independent yields (total of about 132,000 yield values and their uncertainties). Corrections have been applied, models have been used to estimate unmeasured yields, and adjustments have been made to all yield sets in ENDF-6 format (England and Rider, 1994).
(b) UKFY2 includes 39 yield sets (UKFY3 is in the process of being assembled, and also contains 39 sets of cumulative and independent yields). Both UKFY2 and UKFY3 are in ENDF-6 format (James *et al*, 1991a, 1991b and 1991c; Mills, 1995), and have been adopted as the fission yield files for different versions of the NEA-OECD Joint Evaluated File (NEA-OECD, 2000). A number of important short-lived fission products are absent from the decay data files (with greater than 10% of the yield in some mass chains of specific fissioning systems) – while assembling this library for JEF-2.2, correction terms were applied to adjust the independent yields for each mass, so that calculations gave the recommended chain yield values. An improved method of calculation of the correction terms has subsequently been developed for UKFY3, and decay-data evaluations have been undertaken for the most significant missing fission products in order to avoid this problem.
(c) The Chinese fission yield file was released in 1987 as part of the CENDL library (Wang Dao and Zhang Dongming, 1987); a new evaluation is in progress that will be converted into ENDF-6 format.

Fission yields adopted in other applications files have been taken from these sources (for example, the Japanese JENDL library and the French files have adopted US ENDF/B-VI fission yields).

The facilitating role of a recent IAEA-CRP on the compilation and evaluation of fission yield nuclear data should be noted and acknowledged (IAEA-CRP, 2000); specific facets of this work are described below. Co-operation has been established between internationally-respected fission yield experts, and resulted in considerable improvements to the evaluation process (e.g., cleanup of data bases, analyses of experimental data, model development, and evaluation procedures). A PC-based program has also been written and made available through the Internet to calculate mass yields, fractional independent and cumulative yields for 12 fission reactions [YCALC (Gromes, Kling and Denschlag), based on the studies of Wahl, 1988; see also IAEA-CRP, 2000]:

^{252}Cf(sf), ^{229}Th(T), ^{233}U(T), ^{235}U(T), ^{238}Np(T), ^{239}Pu(T), ^{241}Pu(T), ^{242}Am(T), ^{249}Cf(T), ^{232}Th(F), ^{238}U(F) and ^{238}U(H);

sf, T, F and H refer to spontaneous fission, thermal, fast and 14 MeV neutron-induced fission, respectively. Results can be displayed and down-loaded in graphic and tabulated forms via LINKS on the University of Mainz Website

http://www.kernchemie.uni-mainz.de

Empirical models are available for mass and charge distributions and for ternary fission yields that allow the reliable derivation of fission yields for neutron energies from thermal to 15 MeV. Computer programs have also been developed for the introduction of correlations and covariance matrices in future fission yield evaluations.

Table 7: Evaluated fission yield libraries, 2000

Fissioning	**US ENDF/B-VI**				**UKFY2 (JEF-2.2)**				**CENDL**		
Nuclide	**S**	**T**	**F**	**H**	**S**	**T**	**F**	**H**	**T**	**F**	**H**
^{227}Th		x									
^{229}Th		x									
^{232}Th			x	x			x	x		x	
^{231}Pa			x								
^{232}U		x									
^{233}U		x	x	x		x	x	x	x		
^{234}U			x	x			x				
^{235}U		x	x	x		x	x	x	x	x	x
^{236}U			x	x			x				
^{237}U			x								
^{238}U			x	x			x	x		x	x
^{237}Np	x	x	x	x		x	x				
^{238}Np			x			x	x				
^{238}Pu			x			x	x				
^{239}Pu		x	x	x		x	x		x	x	
^{240}Pu		x	x	x			x				
^{241}Pu		x	x			x	x		x		
^{242}Pu		x	x	x			x				
^{241}Am		x	x	x		x	x				
^{242m}Am		x				x	x				
^{243}Am			x			x	x				
^{242}Cm			x		x						
^{243}Cm		x	x			x	x				
^{244}Cm	x		x		x	x	x				
^{245}Cm		x				x	x				
^{246}Cm	x		x								
^{248}Cm	x		x								
^{249}Cf		x									
^{250}Cf	x										
^{251}Cf		x									
^{252}Cf	x				x						
^{253}Es	x										
^{254}Es		x									
^{254}Fm	x										
^{255}Fm		x									
^{256}Fm	x										

5. DECAY DATA

5.1. Decay Parameters

Decay data are defined in this review as those parameters relating to the normal radioactive decay modes of a nuclide, and include:

- half-life,
- total decay energies (Q-values) and branching fractions,
- alpha-particle energies and emission probabilities,
- beta-particle energies, emission probabilities, and transition types,
- electron-capture (and positron) energies, transition probabilities, and transition types,
- gamma-ray energies, emission probabilities and internal conversion coefficients,
- Auger and conversion-electron energies and emission probabilities,
  x-ray energies and emission probabilities,
- characteristics of spontaneous fission (branching fraction(s) and recoil energies, while setting aside the physics associated with the mass and nuclear-charge distributions of the resulting fragments),
- delayed-neutron energies and emission probabilities,
- delayed-proton energies and emission probabilities.

Over recent years, more exotic modes of decay have been detected with increasing regularity, specifically the emission of nuclear clusters (such as Ne and Mg nuclei from ^{234}U, and ^{30}Mg nuclei from ^{236}U) and double beta decay. These more complex and low-probability entities are not addressed in this review, which focuses on α, β^- and gamma-ray decay. Electron capture (and positron) decay occurs when the nucleus is neutron deficient, and is not normally observed in the decay of neutron-rich fission-products and the actinides.

5.1.1. Half-life

Radioactive decay is largely insensitive to conditions outside the nucleus (although not always so), and the resulting behaviour can be characterised by fixed modes of decay, transition energies and probabilities. The number of atoms decaying per unit time is the activity (A) given by the equation:

$$A = N\lambda = \frac{-dN}{dt}$$

where N is the number of atoms at time t, λ is the decay constant (probability that an atom will decay in unit time), and dN is the number of spontaneous nuclear transitions from that energy state in time interval dt. Activity is expressed in Becquerels (Bq) in which 1 Bq is one disintegration per second (dps). Integration of the above equation and substitution results in the expression:

$$N = N_0 e^{-\lambda t}$$

where N_0 is the number of atoms at time t = 0. Each radionuclide has a characteristic decay constant that is related to the half-life ($t_{½}$), the time taken for the number of original radionuclides to reduce by a factor of two:

$$t_{½} = \frac{\ln 2}{\lambda}$$

The half-life of a radionuclide is a primary parameter in any radioactive decay process.

5.1.2. Decay Modes

Nuclides with high *N/Z* ratios are neutron rich, and undergo radioactive decay to reduce this value by the emission of an electron (representing the conversion of a neutron to a proton within the nucleus). Conversely, nuclides with low *N/Z* ratios will decay by the emission of a positron (representing the conversion of a proton to a neutron); electron capture decay is an alternative process to positron emission, in which the unstable nucleus captures an orbiting electron to produce the same daughter nuclide.

Alpha decay becomes a dominant process above *Z* = 80, with the emission of an alpha particle (helium nucleus). Other relatively common modes of decay include isomeric transition (gamma-ray decay from a well-defined energy state of a radionuclide to a lower energy state in the same nuclide), spontaneous fission and delayed-neutron emission.

(a) Beta Decay

The mass number remains unchanged, and the atomic number *Z* increases by one unit when a radionuclide undergoes β^- decay. An electron and an antineutrino are emitted, as a neutron in the nucleus is transformed into a proton:

$$n \rightarrow p + \beta^- + \bar{\nu}$$

$${}^{A}_{Z}X \rightarrow {}^{A}_{Z+1}Y + \beta^- + \bar{\nu}$$

The maximum β-energy is represented by the equation:

$$E_{\beta^-_{\max}} = Q^- - E_l$$

where Q^- is the overall disintegration energy, equal to the difference in atomic masses between the ground states of the parent and daughter, and E_l is the energy level to which the decay occurs. Similarly, β^+ decay is described by:

$$p \rightarrow n + \beta^+ + \nu$$

$${}^{A}_{Z}X \rightarrow {}^{A}_{Z-1}Y + \beta^+ + \nu$$

and $$E_{\beta^+_{\max}} = Q^+ - 2m_0c^2 - E_l$$

where ν is a neutrino, Q^+ is the overall disintegration energy, and

$$2m_0c^2 = 1.021998 \text{ MeV}$$

in which m_0 is the mass of an electron at rest.

β^+ emission occurs when

$$Q^+ - E_i > 2m_0c^2$$

The β transition energy is shared between the electron (or positron) and antineutrino (or neutrino), as a continuous distribution for the two particles extending from 0 up to $E_{\beta_{\max}}$.

(b) Alpha decay

A nucleus of atomic number *Z* and mass number *A* disintegrates by the emission of an α particle to give a daughter nucleus with atomic number $Z - 2$ and mass number $A - 4$:

$${}^{A}_{Z}X_N \rightarrow {}^{A-4}_{Z-2}Y_{N-2} + {}^{4}_{2}He_2$$

The α disintegration energy can be represented by the equation:

$$Q_\alpha = E_{\alpha_1} + E_l + E_{r_1}$$

where E_{α_i} is the energy of the emitted α particle, E_l is the nuclear-level energy of the daughter nuclide, and E_{r_i} is the recoil energy:

$$E_{r_i} = \frac{M_\alpha}{M_N + M_\alpha}\left(Q_\alpha - E_l\right)$$

in which M_N is the mass of the recoiling daughter nucleus, and M_α is the mass of the α particle. The α particle is held within the nucleus by the Coulomb potential barrier, and escapes from the nucleus by means of a tunnelling mechanism.

(c) Gamma transitions

A gamma transition occurs when a nucleus in an excited state de-excites to a lower energy level, leading to the emission of a γ ray and conversion electron (and an electron-positron pair when energy conditions permit). The gamma transition probability is defined as:

$$P_{TP} = P_\gamma + P_{ce} + P_{e^\pm}$$

where P_γ, P_{ce} and $P_{e^\pm}$ are the γ -ray, conversion-electron and electron-positron pair emission probabilities, respectively.

The energy of the emitted γ-ray can be represented by the equation:

$$E_\gamma = \left(E_i - E_f\right) - E_r$$

where $E_i - E_f$ is the energy difference between the initial and final levels of the γ transition, and E_r is the recoil energy of the nucleus in the final state:

$$E_r = \frac{\left(E_\gamma\right)^2}{2 M_N c^2}$$

where M_N is the mass of the recoiling daughter nucleus. The recoil energy is negligible, except for high γ energies and nuclei with low atomic number.

Gamma transitions can be classified in terms of multipole order, which is a function of the orbital angular momentum and quantum number L carried by the photon: L = 0, monopole; L = 1, dipole; L = 2, quadrupole, etc… If J_i and J_f are the total angular momenta quantum numbers of the initial and final levels connected by the γ transition, the vectorial relationship between the angular momenta is given by the formulation:

$$\left|J_i - J_f\right| \leq L \leq \left|J_i + J_f\right|$$

Moreover, the angular momentum carried off by the photon cannot be zero, and consequently a $0 \rightarrow 0$ transition cannot occur except by internal conversion or internal-pair creation.

Gamma transitions are divided into electric and magnetic radiations:

electric radiation (emitted by the oscillation of electrical charges), with a parity change of $(-1)^L$;

magnetic radiation (caused by the magnetic moment of the nucleus), with a parity change of $(-1)^{(L+1)}$.

A gamma transition can be a mixture of two (or sometimes three) multipole transitions. Two transitions in competition will have multipole order 2^L and 2^{L+1}, one electric and the other magnetic (e.g., mixture of M1 + E2).

The de-excitation energy of the nucleus can also be transferred directly to an electron (K, L, M..) which is ejected from the atom in preference to a gamma-ray emission:

$$E_{\mathrm{ce_X}} = E_\gamma - E_\mathrm{x}$$

where E_x is the binding energy of the electron in the X shell.

The internal conversion coefficient of the electron in the K shell is defined as:

$$\alpha_\mathrm{K} = \frac{P_{\mathrm{ce_K}}}{P_\gamma}$$

where $P_{\mathrm{ce_K}}$ and P_γ are the K conversion-electron and γ-ray emission probabilities, respectively; similar terms are also defined for the L, M, N … shells.

The total conversion coefficient is:

$$\alpha_\mathrm{total} = \alpha_\mathrm{K} + \alpha_\mathrm{L} + \alpha_\mathrm{M} + \ldots = \frac{P_\mathrm{ce}}{P_\gamma}$$

where P_ce is the total conversion-electron emission probability of the related transition.

5.2. Decay Data Requirements

Decay-data requirements for decay-heat calculations are parametrically limited to half-lives (through the decay constants, λ_i ($t_{½}$ = ln2/λ)) and the mean alpha, beta and gamma energy releases per disintegration of the nuclides ($\overline{E}_\alpha, \overline{E}_\beta$ and $\overline{E}_\gamma$). Ideally, the mean energies are systematically determined from the discrete alpha, beta and gamma transitions and other relevant emissions, which extends the decay-data needs dramatically.

(a) The mean alpha energy is the mean energy of all heavy particles (alpha particles, recoil nuclei, protons, neutrons, and spontaneous fission fragments):

$$\overline{E}_\alpha = \sum_i^{all\,\alpha} \overline{E}_{\alpha_i} P_{\alpha_i} + \sum_j^{all\,recoil} \overline{E}_{R_j} P_{R_j} + \sum_k^{all\,protons} \overline{E}_{p_k} P_{p_k} + \sum_l^{all\,neutrons} \overline{E}_{n_l} P_{n_l} + \sum_m^{fission\,frag} \overline{E}_{F_m} P_{F_m}$$

where $\overline{E}_{\alpha_i}$, $\overline{E}_{R_j}$, $\overline{E}_{p_k}$, $\overline{E}_{n_l}$ and $\overline{E}_{F_m}$ are the mean alpha, recoil nucleus, proton, neutron and fission fragment energies of the ith, jth, kth, lth and mth component of each type respectively, and P_{α_i}, P_{R_j}, P_{p_k}, P_{n_l} and P_{F_m} are the corresponding absolute emission probabilities per disintegration.

(b) The mean beta energy is the mean energy of all electron emissions:

$$\overline{E}_\beta = \sum_i^{all\,\beta^-} \overline{E}_{\beta_i^-} P_{\beta_i^-} + \sum_j^{all\,\beta^+} \overline{E}_{\beta_j^+} P_{\beta_j^+} + \sum_k^{all\,Auger} \overline{E}_{A_k} P_{A_k} + \sum_l^{all\,conversion} \overline{E}_{ce_l} P_{ce_l}$$

where $\overline{E}_{\beta_i^-}$, $\overline{E}_{\beta_j^+}$, $\overline{E}_{A_k}$, and $\overline{E}_{ce_l}$ are the mean negatron, positron, Auger electron and conversion-electron energies of the ith, jth, kth and lth transition of each type respectively, and $P_{\beta_i^-}$, $P_{\beta_j^+}$, P_{A_k} and P_{ce_l} are the corresponding absolute emission probabilities per disintegration.

(c) The mean gamma energy includes all the electromagnetic radiation such as gamma rays, x-rays, annihilation radiation and bremsstrahlung:

$$\overline{E}_\gamma = \sum_i^{all\,\gamma} \overline{E}_{\gamma_i} P_{\gamma_i} + \sum_j^{all\,X-rays} \overline{E}_{X_j} P_{X_j} + \sum_k^{all\,\beta^+} 1.022\, P_{\beta_k^+} + \sum_l^{all\,\beta^+\beta^-} \overline{E}_{\beta_l} P_{\beta_l}$$

where $\overline{E}_{\gamma_i}$ and $\overline{E}_{X_j}$ are the mean gamma and x-ray energies of the ith and jth transition of each type respectively, and P_{γ_i} and P_{X_j} are the corresponding

emission probabilities per disintegration; $\overline{E}_{\beta_l}$ is the mean internal bremsstrahlung energy of the l^{th} beta transition with absolute emission probability P_{β_l}, and $P_{\beta_k^+}$ is the absolute emission probability of positron transition k.

Data files containing these nuclear parameters have been assembled over many years to assist analysts and spectroscopists to identify and quantify radionuclides. As the emissions from nuclides have been characterised in greater detail and their decay-scheme data defined with increased confidence, extended libraries of nuclear data have been compiled in agreed formats for use by the nuclear industry. These libraries are also used in decay-heat calculations, and are updated at regular intervals through either international consensus, or more localised efforts based on specific national needs.

The contents of a decay-data library need to be complete and consistent in order to model decay heat with confidence. The normal procedure would be to evaluate and prepare individual files of decay data that have been internally tested for consistency between the various decay-scheme parameters (i.e., α, β and γ transitions), and to validate the complete library against benchmark experiments.

Evaluated decay-data libraries are used for many different purposes, as well as decay-heat calculations. Files of discrete decay data can aid in the measurement and quantification of the radionuclidic composition of a sample, and provide spectroscopists with the necessary high-quality standards data for detector efficiency calibration. Ideally, a comprehensive set of such data files should encompass all of the important fission products, actinides and their decay-chain nuclides, and provide the user with the necessary half-lives, mean energies and isomeric branching ratios to carry out decay-heat calculations with confidence. Unfortunately, this requirement cannot be realised because of the difficulty of measuring comprehensively the discrete data for the many short-lived fission products, along with the added complications that occur when studying some of the more complex decay schemes (pandemonium (Hardy *et al*, 1977)).

5.3. Modelling β^- Decay

A serious lack of suitable decay data for many of the short-lived fission products has necessitated the adoption of theoretical half-lives and mean energies, based on a number of modelling methods that focus on the derivation of beta-strength functions. These models are outlined below.

(a) Gross theory: smooth beta-strength functions

The gross theory of β^- decay has been used by Takahashi *et al* (1973) to predict beta-strength functions, and calculate the half-lives and other relevant decay parameters averaged over the final daughter states. The decay constant and average beta and gamma energies per disintegration can be expressed in terms of the sum of each partial decay to the i[th] final state of energy ε_i:

$$\lambda = \sum_{i=0}^{n} \lambda_i \ ,$$

$$\overline{E}_\beta = \sum_{i=0}^{n} \ \frac{\lambda_i}{\lambda} \left(Q - \varepsilon_i\right) C_i \ ,$$

$$\overline{E}_\gamma = \sum_{i=0}^{n} \ \frac{\lambda_i}{\lambda} \ \varepsilon_i \ ,$$

in which C_i is the ratio of the average kinetic energy of the beta emission to the i[th] state to the maximum kinetic energy of the beta decay ($Q - \varepsilon_i$).

The equation for λ can be reformulated to include the beta-transition matrix element (ψ_i, $\Omega\psi$):

$$\lambda = \frac{1}{2\pi^3} \sum_{i=0}^{n} \sum_{\Omega} \left|g_\Omega\right|^2 . \left|(\psi_i, \Omega\psi)\right|^2 \ f\left(E_i\right),$$

where f is the integrated Fermi function, and E_i is the maximum energy available for the emitted electron; Ω represents the transition operator, and g_Ω is the coupling constant. A major assumption in the evolution of the gross theory is that the density of the final levels is sufficiently high to replace this summation with an integration function:

$$\lambda = \frac{1}{2\pi^3} \int_{-Q}^{0} \sum_{\Omega} \left|g_\Omega\right|^2 \ . \ \left|M_\Omega\left(E_g\right)\right|^2 \ f\left(-E_g + 1\right) dE_g \ ,$$

in which $|M_\Omega(E_g)|^2$ is the product of the square of the transition matrix and the level density of the final states (also referred to as the beta-strength function, and sometimes denoted by the term $S_\beta(E)$). Similar manipulations can lead to gross theory expressions for the mean beta and gamma energies:

$$\overline{E}_\beta = \frac{1}{2\pi^3 \lambda} \int_{-Q}^{0} \sum_{\Omega} \left|g_\Omega\right|^2 \ . \ \left|M_\Omega\left(E_g\right)\right|^2 \int_{1}^{-E_g+1} mc^2 (E-1)\, p\, E \left(-E_g + 1 - E\right)^2 \ F(E)\, dE\, dE_g \ ,$$

$$\overline{E}_\gamma = \frac{1}{2\pi^3 \lambda} \int_{-Q}^{0} \sum_{\Omega} \left|g_\Omega\right|^2 \ . \left|M_\Omega\left(E_g\right)\right|^2 \ mc^2 \left(Q + E_g\right) \int_{1}^{-E_g+1} p\, E \left(-E_g + 1 - E\right)^2 \ F(E)\, dE\, dE_g \ ,$$

where *F* is the Fermi function, and *p* is the momentum of the electron. The beta-strength function is assumed to be smooth in this model; any structural features are deemed to be unimportant in deriving half-lives and mean energies.

The gross theory has been systematically applied to calculate β^- decay half-lives, and these data compared with known experimental values (Table 8). Half-lives were predicted within a factor of 5 for 70% of 100 fission products with half-lives less than 1 min, and within a factor of 10 for 90% of the same set of fission products (Yoshida, 1977). Good agreement was also obtained for the mean beta and gamma energies, although the theory failed to predict these decay parameters for ^{82}As and ^{92}Rb (odd-odd nuclei).

Table 8: Mean beta-particle and gamma-ray energies for nuclides with Q > 4.5 MeV: comparison of gross theory calculations with evaluated measurements (Yoshida, 1977)

Nuclide	Mean beta-particle energy (MeV)			Mean gamma-ray energy (MeV)			Half-life (sec)
	UK evaluation (1973)	US evaluation (1975)	Gross theory	UK evaluation (1973)	US evaluation (1975)	Gross theory	
^{74}Ga	1.072	1.070	1.350	3.043	3.040	2.471	500
^{76}Ga	1.675	1.680	1.832	2.808	2.810	2.136	27
^{80}As	2.468	2.523	2.584	0.554	0.606	0.347	17
^{82}As	3.137	3.211	1.888	0.336	0.288	2.909	23
^{86}Br	1.765	1.775	1.946	3.296	3.318	2.936	59
^{87}Br	2.087	2.136	1.757	1.727	1.726	2.387	56
^{88}Rb	2.000	2.083	1.156	0.677	0.674	2.463	1100
^{90}Rb	1.789	1.659	1.673	2.560	2.660	2.814	150
^{91}Rb	1.320	1.334	1.533	2.871	2.733	2.533	59
^{92}Rb	3.714	3.459	2.526	0.260	0.261	2.696	4.5
^{94}Y	1.193	1.717	1.039	1.043	0.986	2.417	1100
^{95}Y	1.713	1.745	0.968	0.523	0.488	2.111	650
^{97}Y	1.612	2.162	2.294	0.935	0.935	1.055	1.1
^{99}Zr	1.586	1.621	1.651	0.794	0.794	0.719	2.4

Yoshida and Nakasima (1981) have used the gross theory to determine mean beta and gamma energies for fission products that undergo high-energy β^- decay. Approximately 170 radionuclides with known half-lives and decay schemes were assessed in this manner (Q-values ≥ 3 MeV), and the calculated mean energies were compared with available experimental data. There was a reasonable degree of overlap between theory and experiment for the mean beta energy data, but the mean gamma energies exhibited much less satisfactory agreement. This same approach was also adopted for a significant number of poorly-defined nuclides:

(i) measured half-lives, but unknown decay schemes;
(ii) unknown half-lives and decay schemes (as defined in 1980).

Nuclides in category (i) include some radionuclides that contribute significantly to decay heat at short cooling times (e.g., ^{89}Br, ^{94}Rb, ^{101}Nb, ^{102}Zr, ^{102}Nb, ^{103}Mo, ^{145}Ba and ^{145}La). Yoshida and Katakura (1986) combined a cascade gamma transition model with the gross theory of beta decay in a further attempt to improve predictions of the mean gamma energy data for short-lived fission products.

When all of the theoretical decay data were incorporated into decay-heat assessments, good agreement was observed between experiments and calculation (Figs. 15 and 16). Decay-heat measurements of Dickens *et al* (1980) have been compared with summation calculations in which theoretical mean energies were included. The original JNDC-FP decay-data library overestimated

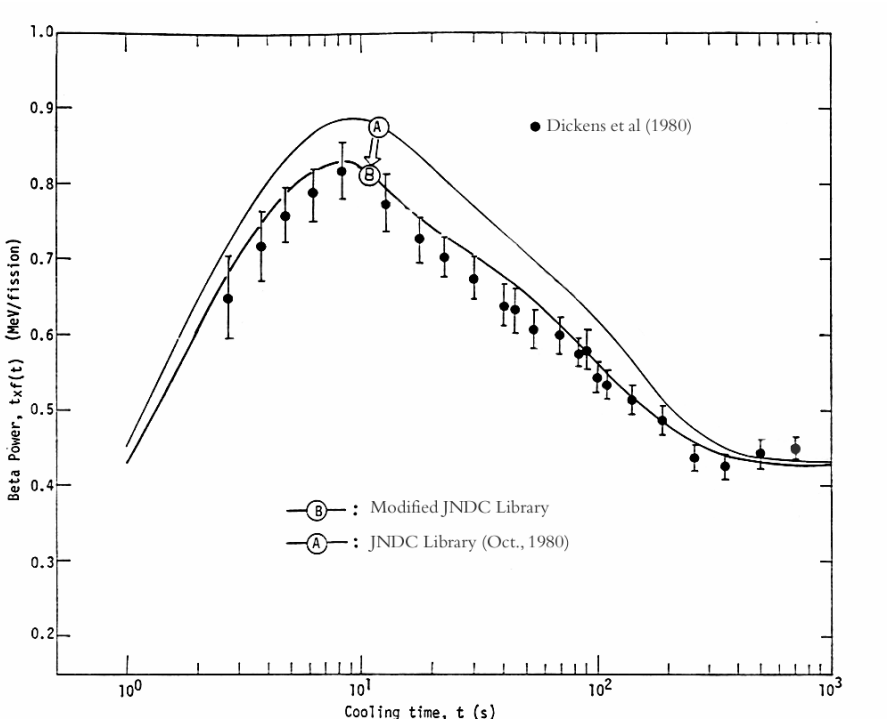

Fig. 15. Beta energy emission rate after instantaneous pulse of thermal-neutron fission of ^{235}U

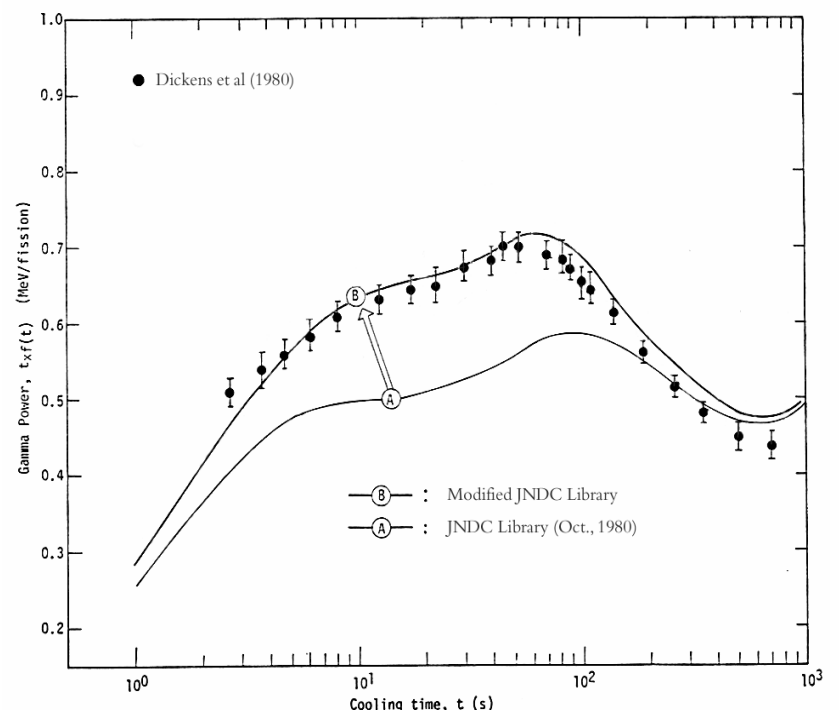

Fig. 16. Photon energy emission rate after instantaneous pulse of thermal-neutron fission of ^{235}U

the beta energy release and underestimated the gamma energy release; when the theoretical data were introduced, the decay-heat calculations reproduced the measurements extremely well.

Tachibana *et al* (1990) extended the gross theory by modifying the one-particle strength function and introducing the ΔQ_0 term. When the Q-value is relatively small, the β^- decay is sensitive to the forbiddenness of the transitions to the low-lying states, and the ΔQ_0 term was used to modify the resulting strength functions of these nuclides (and others). Nakata *et al* (1995) have also refined the gross theory further for odd-odd nuclei, taking into account the selection rule for the beta transition to the ground state. This refined approach gives half-lives in better agreement with the experimental data than the values obtained by the unmodified gross theory (except for parents with a spin and parity of 1^-). Furthermore, Nakata *et al* (1997) have taken the shell effects of the parent nuclei into consideration to produce the semi-gross theory of β^- decay; the one-particle strength functions are dependent on the principal quantum numbers and spin-parity of the initial state of the decaying nuclide. This modification also involves raising the beta strengths to a level defined by the ΔQ_0

term (subsequently referred to as Q_{00}) when the transitions to low-lying levels are highly forbidden.

Yoshida and Tachibana (2000) adopted the concept of Q_{00} to reproduce experimental half-lives:

$$Q_{00} = \begin{cases} 0.25\,MeV \;\; for\, even-even\, parent \\ 1.0\;\; MeV \;\; for\, odd-A\, parent \\ 1.75\,MeV \;\; for\, odd-odd\;\; parent \end{cases}$$

in which these Q_{00}-values were subsequently multiplied by a parameter that depends on the even/odd properties of each nuclide to give the Q_{00}-factor. The ratio between the calculated and experimental half-lives is given in Fig. 17 on a logarithmic scale; the best agreement is observed when the Q_{00}-factor is unity. Similar analyses of the beta and gamma decay components indicate that a Q_{00}-factor of approximately 0.4 is most appropriate for the calculation of the mean beta and gamma energies (Figs. 18 and 19).

(b) Structural beta-strength functions

Klapdor (1983) has argued that the neglect of any structure within beta-strength functions is an oversimplification that is inconsistent with experimental observations. Structure is found at high-level densities, and can significantly affect the half-lives and branching ratios of β^--delayed processes. Klapdor and Metzinger (1982a and 1982b) included this structure when determining the electron and antineutrino spectra generated after the fission process. Their method involved microscopic calculations of $S_\beta(E)$ for all fission products:

$$S_\beta(E)\,dE = \sum_i B_i(E_i)\,dE / D$$

where B(E) is the reduced beta transition probability to a state at excitation energy E_i in the daughter nucleus, and D is the vector coupling constant. However, a major source of uncertainty in the calculation of the electron and antineutrino spectra is the effect the fission products with unknown or poorly-defined decay schemes will have on the shape of the beta-strength function.

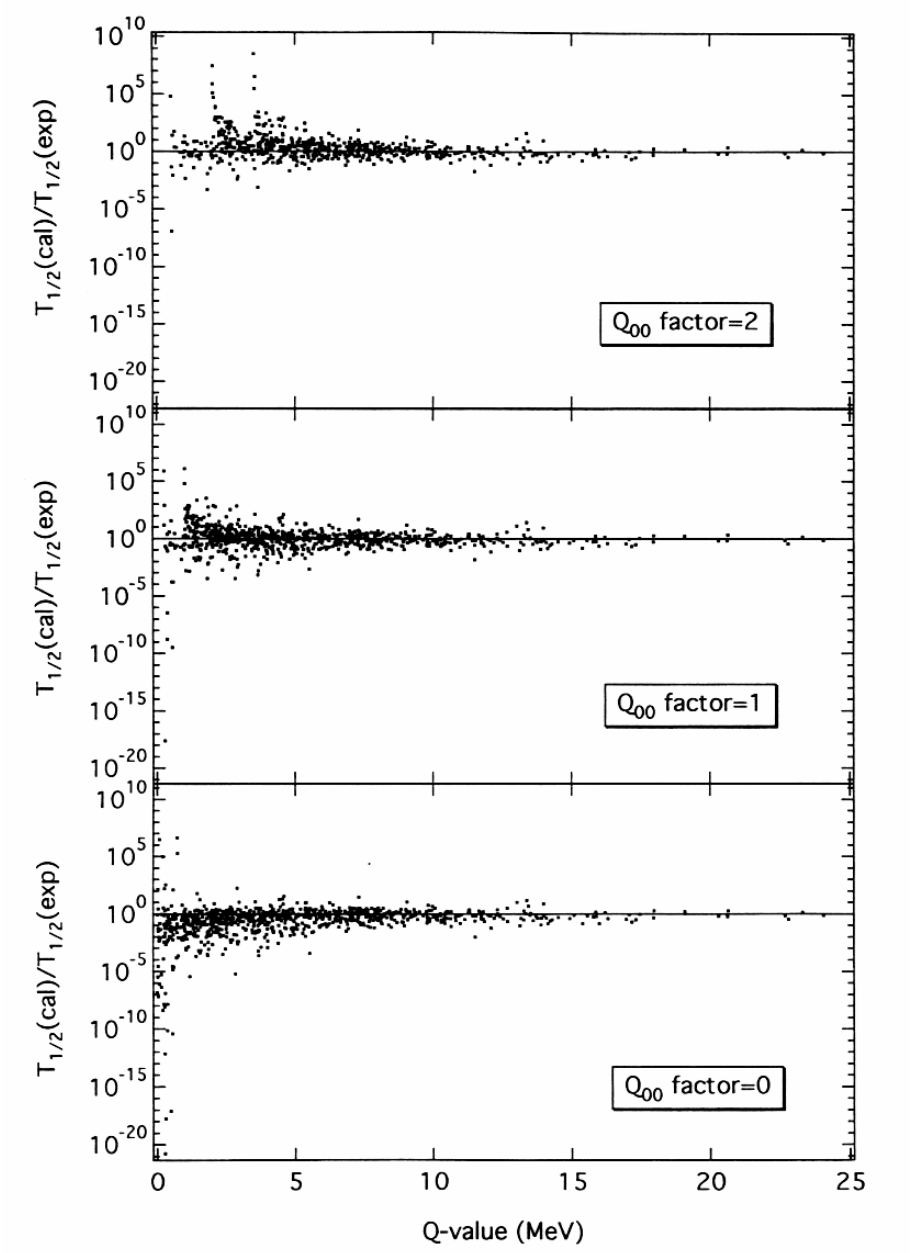

Fig. 17. Ratios of the half-lives between gross theory calculations and experimental results (Yoshida and Tachibana, 2000)

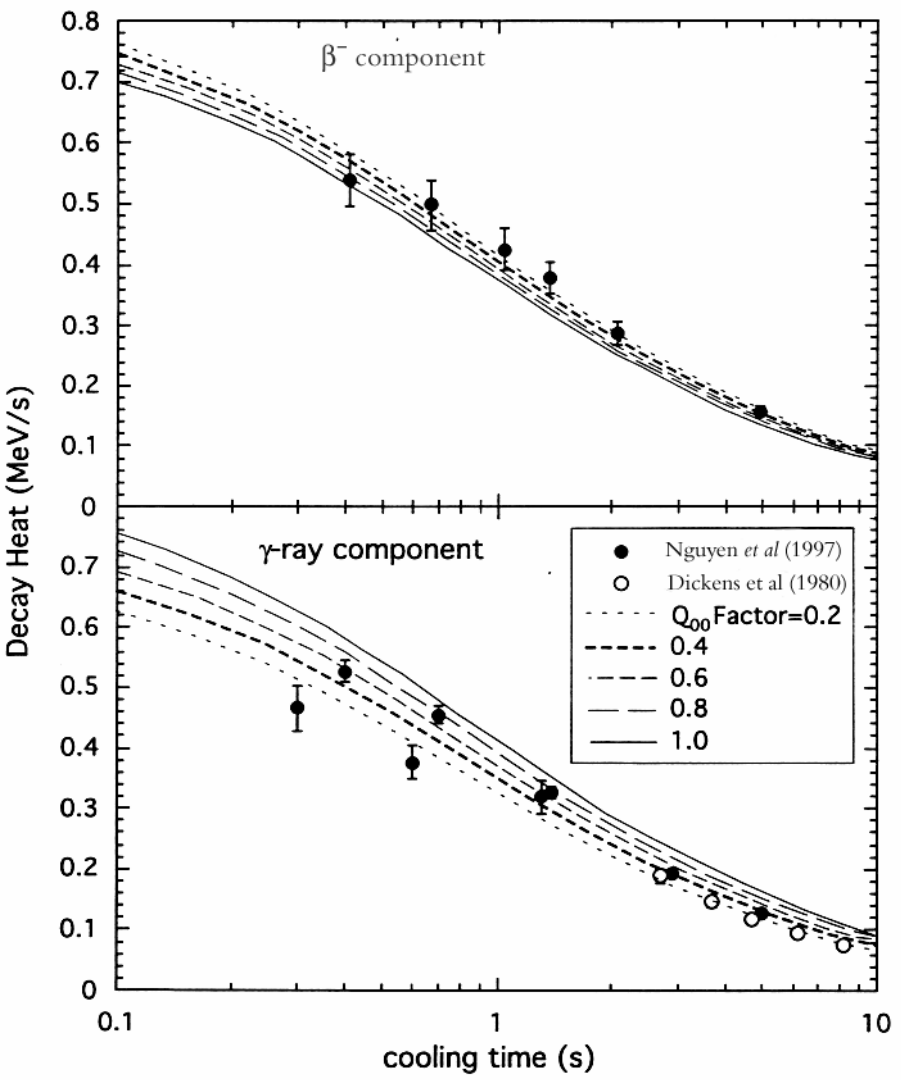

Fig. 18. Calculated β-and γ-ray components of ^{235}U decay heat compared with experiments at very short cooling times (Yoshida and Tachibana, 2000)

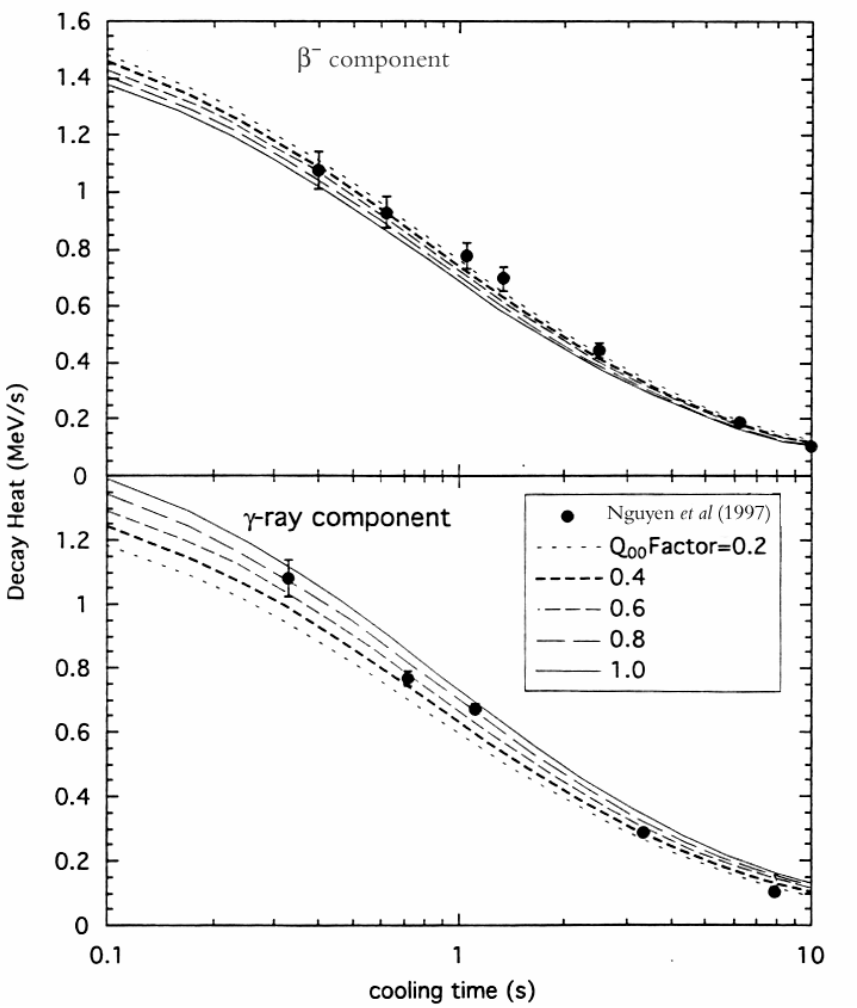

Fig. 19. Calculated β- and γ-ray components of ^{238}U decay heat compared with experiments at very short cooling times (Yoshida and Tachibana, 2000)

Despite a lack of reliable decay-scheme data for a significant number of fission-product nuclides, β^--spectra have been calculated by Davis *et al* (1979), Avignone and Greenwood (1980), Kopeykin (1980) and Vogel *et al* (1981) on the assumption that the resulting beta-strength function is smooth. These particular calculations do not reproduce the precise β-spectrum measurements of the fission products from ^{235}U fission (Schreckenbach *et al*, 1981). Klapdor and Metzinger (1982b) undertook a microscopic analysis of $S_\beta(E)$ for all fission products with unknown and uncertain decay schemes: considerable improvement was obtained against the measurements,

with a deviation from experiments of less than 4%. Figs. 20 and 21 compare the electron and antineutrino spectra obtained from the various methods of calculating $S_\beta(E)$, normalised against the equivalent measurements of Schreckenbach *et al* (1981); calculation/experiment ratio (C/E = R) for method 4 (i.e., Klapdor and Metzinger, 1982b) is much closer to unity over the full energy range. Table 9 lists the different sets of data as a function of electron and antineutrino energy. Studies have also been made of the thermal fission of ^{239}Pu, with similar results (Klapdor and Metzinger, 1982a).

Further microscopic modelling studies by Hirsch *et al* (1992) have resulted in the successful use of the proton-neutron quasiparticle random phase approximation (pn-QRPA) to calculate the beta-strength functions. Single particle energies are calculated, taking into account nuclear deformation and pairing interaction; subsequent RPA calculations include proton-neutron residual interactions. The resulting theoretical half-lives and mean beta and gamma energies are in good agreement with experimental measurements across the full range of Z, and these data have been adopted to extend the range of radionuclidic coverage of a number of decay-data libraries.

(c) Simplified statistical definition

Mann *et al* (1982) have advocated that accurate predictions can be made of β-decay properties using a statistical model with only one free parameter (implying that any intrinsic structure is not important). The beta-strength function for a transition to a daughter level at energy E via a multipole λ is given by the equation:

$$S_\beta^\lambda(E)\,dE = \sum_{J,\pi} \rho(E,J,\pi)\beta_\lambda(E)\,dE / D$$

where $\rho(E,J,\pi)$ is the density of levels with spin J and parity π at excitation energy E, β_λ is the average reduced transition probability per level for moment λ in the interval $(E, E+dE)$, and D is the vector coupling constant.

The half-life can be expressed by the following equation:

$$t_{1/2} = 1/\sum_\lambda \int_0^{Q_\beta} S_\beta^\lambda(E)\, f_\lambda(Z, Q_\beta - E)\,dE$$

where f contains the kinematic factors and Fermi function. Similar integrals can be derived for the mean beta and gamma energies. Energy-dependent β_λ values were found for all of the allowed transitions in the β-decay of the fission products (log ft values of 4.3 to 5.6), while β_λ corresponded to log ft of 7.1 for first forbidden transitions. Beta rates were calculated by multiplying the level density parameter by $N/(N+Z)$, where N is the number of neutrons and Z is the number of protons in the daughter nucleus; this factor represents the only free global parameter in this model.

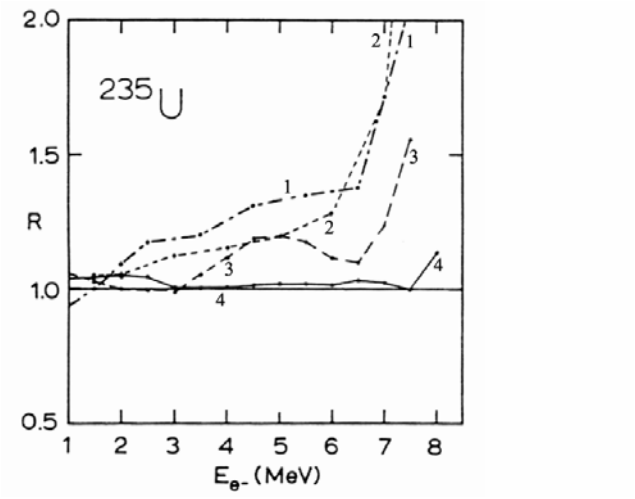

Fig. 20. Electron spectrum from thermal fission of ^{235}U (Klapdor, 1983) R is ratio C/E:
1 $S_\beta(E)$ Avignone and Greenwood (1980)
2 $S_\beta(E)$ Kopeykin (1980)
3 $S_\beta(E)$ Vogel *et al* (1981)
4 $S_\beta(E)$ Klapdor and Metzinger (1982b)

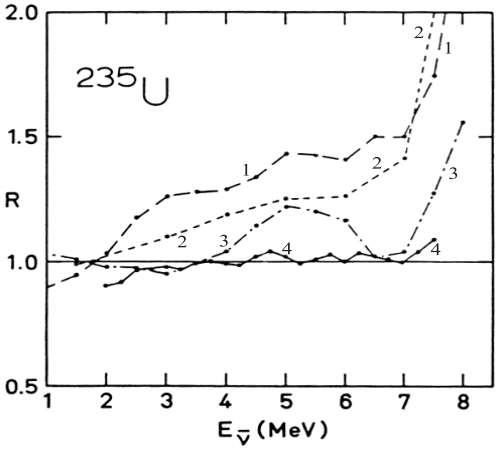

Fig. 21. Antineutrino from thermal fission of ^{235}U (Klapdor and Metzinger, 1982b) R is ratio C/E:
1 $S_\beta(E)$ Avignone and Greenwood (1980)
2 $S_{\beta(}E)$ Kopeykin (1980)
3 $S_{\beta(}E)$ Vogel *et al* (1981)
4 $S_{\beta(}E)$ Klapdor and Metzinger (1982b)

Table 9: Calculated electron and antineutrino spectra from the thermal fission of ^{235}U in secular equilibrium compared with measurements of Schreckenbach *et al*, 1981 (Klapdor and Metzinger, 1982b; Klapdor, 1983).

E_{kin} (MeV)	N_β (per fission per MeV)					
	Experiment, Schreckenbach *et al* (1981)[a]	Davis *et al* (1979)[b]	Avignone and Greenwood (1980)[c]	Kopeykin (1980)[c]	Vogel *et al* (1981)[c]	Klapdor and Metzinger (1982b)[c]
1.00	1.91	1.92	-	-	2.01	1.98
1.50	1.31	1.28	1.31	1.37	1.35	1.36
2.00	0.88	0.867	-	0.925	0.880	0.923
2.50	0.587	0.595	0.689	-	0.586	0.612
3.00	0.399	-	-	0.449	0.396	0.400
3.50	0.252	0.256	0.303	-	0.265	0.253
4.00	0.154	-	-	0.178	0.172	0.155
4.50	0.091	0.0946	0.119	-	0.108	0.0925
5.00	0.0550	-	-	0.0659	0.0655	0.0561
5.50	0.0314	0.0318	0.0424	-	0.0369	0.0321
6.00	0.0172	-	-	0.0221	0.0192	0.0175
6.50	0.0088	0.00904	0.0121	-	0.00966	0.00909
7.00	0.00380	-	-	0.00652	0.00468	0.00389
7.50	0.00132	0.00171	0.0027	-	0.00205	0.00132
8.00	0.000260	-	-	0.00147	-	0.000296
8.50	0.000043	-	0.000482	-	-	0.000131
9.00	< 0.000030	-	-	0.000242	-	0.0000365
E_{kin} (MeV)	$N\bar{\nu}$ (per fission per MeV)					
	Deduced from experiment, Schreckenbach *et al* (1981)[a]	Davis *et al* (1979)[b]	Avignone and Greenwood (1980)[c]	Kopeykin (1980)[c]	Vogel *et al* (1981)[c]	Klapdor and Metzinger (1982b)[c]
1.00	-	2.38	2.12	-	2.44	2.36
1.50	-	1.65	1.62	1.70	1.73	1.71
2.00	1.18	1.21	1.35	1.35	1.28	1.31
2.50	0.86	0.842	1.04	-	0.860	0.888
3.00	0.60	0.595	0.769	0.669	0.580	0.613
3.50	0.406	-	0.526	-	0.410	0.412
4.00	0.265	0.273	0.349	0.321	0.282	0.268
4.50	0.163	-	0.212	-	0.181	0.160
5.00	0.099	0.103	0.139	0.121	0.118	0.0970
5.50	0.060	-	0.0857	-	0.0720	0.0596
6.00	0.0345	0.0350	0.0493	0.0442	0.0408	0.0346
6.50	0.0192	-	0.0287	-	0.0195	0.0189
7.00	0.0099	0.0101	0.0150	0.0141	0.0104	0.0100
7.50	0.00432	-	0.00693	-	0.00506	0.00399
8.00	-	0.00187	0.00310	0.00400	0.00204	0.00131
8.50	-	-	-	-	-	0.000312
9.00	-	-	-	-	-	0.000141

[a] Exposure time of 1.5 d.
[b] Exposure time of 3 y.
[c] Infinite exposure time.

Fig. 22 shows the experimental data compared with the predicted half-lives of a series of Rb nuclides:

(i) calculated by gross theory (Takahashi *et al*, 1973);
(ii) determined on the basis of the microscopic structure of the beta-strength function (Klapdor, 1983);
(iii) from statistical analysis (Mann *et al*, 1982).

The simple statistical method can be seen to generate data in closer agreement with the measurements than the more rigorous theoretical approaches.

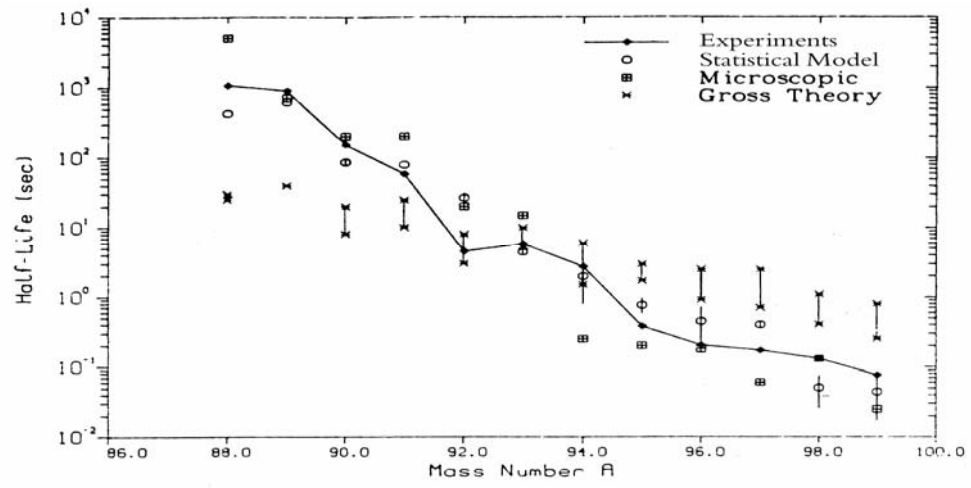

Fig. 22. Half-lives of Rb nuclides (Mann *et al*, 1982)

5.4. Spectral Measurements of Short-lived Fission Products

(a) Continuous beta and gamma spectra

The detailed decay data required to construct a complex decay scheme that is correct, and the difficulties experienced in obtaining the discrete decay data of short-lived fission products represent considerable challenges when producing decay-data files for decay-heat summation calculations. However, the OSIRIS and ISOLDE facilities have been used in tandem to address the problem of recommending adequate decay data for such nuclides (Rudstam *et al*, 1990). Radionuclides of interest with high β^--decay rates and sufficiently significant fission yields have been studied, focusing on nuclides with half-lives in the range from a fraction of a second to 1 hour.

The gamma-ray measurements were carried out by means of a low-resolution detection system (NaI(Tl)) and a high-resolution Ge(Li) detector. Mass-separated beams from OSIRIS impinged on an aluminised Mylar tape located directly in front of the NaI(Tl) spectrometer, which was well characterised up to an energy of 4.5 MeV (an extrapolation process was adopted for higher energies, although there is considerable doubt about the accuracy of this approach). These samples could also be monitored by the Ge(Li) detector. A large range of fission products was simultaneously released from the target-ion source, and the resulting mass-separated beam contained several isobars (also non-isobaric nuclides formed through the delayed-neutron emission from isobar components).

The cyclic procedure involved a background measurement, sample collection, waiting period, and sample measurement in a chosen manner that allowed a particular component to be favourably studied and quantified. This process was repeated several hundred times for each nuclide of interest in order to generate good statistics.

The number of decays of each fission-product nuclide was determined by means of the Ge(Li) detector, using the most prominent gamma rays. Pulse spectra measured by the NaI(Tl) detector can be defined by the following equation:

$$N_{kj} = \sum_i D_{ki} P_{ij}$$

where N_{kj} is the number of counts in energy channel j for experiment k, D_{ki} is the number of decays of component i during experiment k, and P_{ij} is the pulse spectrum of component i. This equation is a linear combination of contributions from components i for each channel j. Hence, with k equations, P_{ij} can be solved exactly for $k = i$, and can be determined by the least squares method for $k > i$. Individual pulse spectra (P_{ij}) can be converted to gamma-ray spectra from the response function of the spectrometer. Integration produces the mean gamma energy per decay, and the mean number of gamma rays per decay. The overall uncertainties are quantified in terms of three components: statistics (number of counts), uncertainties in the absolute branching ratios (sometimes large), and the absolute calibration of the two spectrometers.

Beta spectra were measured in a similar manner on the OSIRIS and ISOLDE facilities, using high-purity Ge and Si(Li) detectors. Both sets of spectra can be used to check the validity of the recommended decay schemes constructed from detailed gamma-ray measurements. Examples are given in Figs. 23 - 25 of a number of important fission-product nuclides that have complex decay schemes. Whenever possible, the gamma-ray data have been compared with equivalent decay data from the ENSDF files (see Section 5.5.1); the regular “shortfall” of the ENSDF solid line in many of the figures demonstrates the inadequacies in these discrete decay-data

files (particularly with respect to high-energy gamma rays). This observation underlines the assessment of Hardy *et al* (1977) concerning the incomplete nature of complex decay schemes derived from gamma-ray measurements (pandemonium).
Rudstam *et al* (1990) and Johansson *et al* (1994) have generated an extremely important set of mean-energy data for fission-product nuclides that contribute ~70% of the beta decay heat for short irradiations, and between 60% and 25% for long irradiations followed by cooling times of 0 to 1000 sec. These radionuclides have a similar impact as major contributors to the gamma decay heat at short cooling times. Examples of the resulting data for a limited set of these nuclides are given in Table 10. The mean beta and gamma data for over 100 nuclides determined by this method have been incorporated into many of the decay-data files used for decay-heat calculations in order to address the problem of recommending suitable data for those nuclides with high-energy β^- decay and incomplete decay schemes. Such gross adjustments to the mean energies may result in the creation of inconsistencies with the discrete spectral data.

The OSIRIS on-line mass separator has also been used to prepare sources of short-lived fission products for the measurement of their half-lives and delayed-neutron branching fractions by means of a neutron counter and beta detector (Rudstam *et al*, 1993). Over 60 radionuclides in the mass range 70 to 150 have been studied, and the branching fractions for a significant number of these nuclides were reported for the first time. Improved half-lives were determined for many of these radionuclides, including ^{84}Ge, ^{84}As, ^{85}As, ^{86}As, ^{87}As, ^{133}Sn, ^{134}Sn, ^{135}Sb, ^{136}Sb, ^{137}Te, ^{138}I, ^{147}Ba, ^{148}Cs, ^{148}La and ^{150}La.

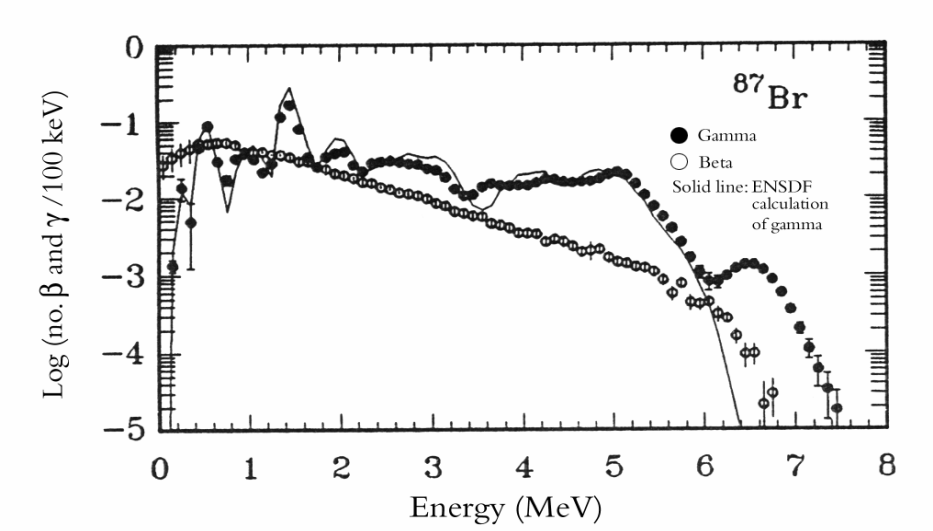

Fig. 23. Beta and gamma spectra of short-lived fission product ^{87}Br (Rudstam *et al*, 1990)

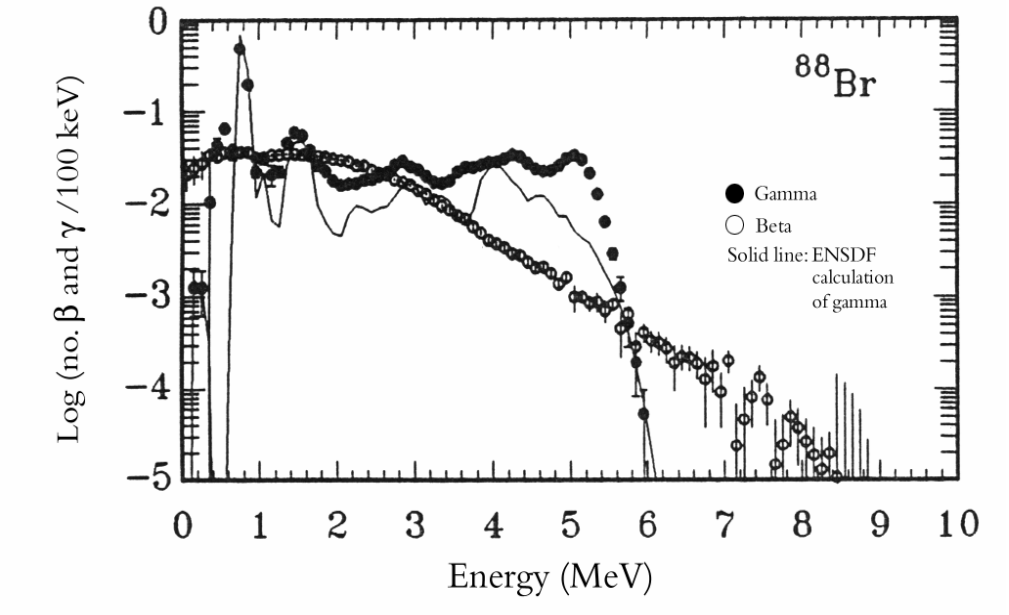

Fig. 24. Beta and gamma spectra of short-lived fission product ^{88}Br (Rudstam *et al,* 1990)

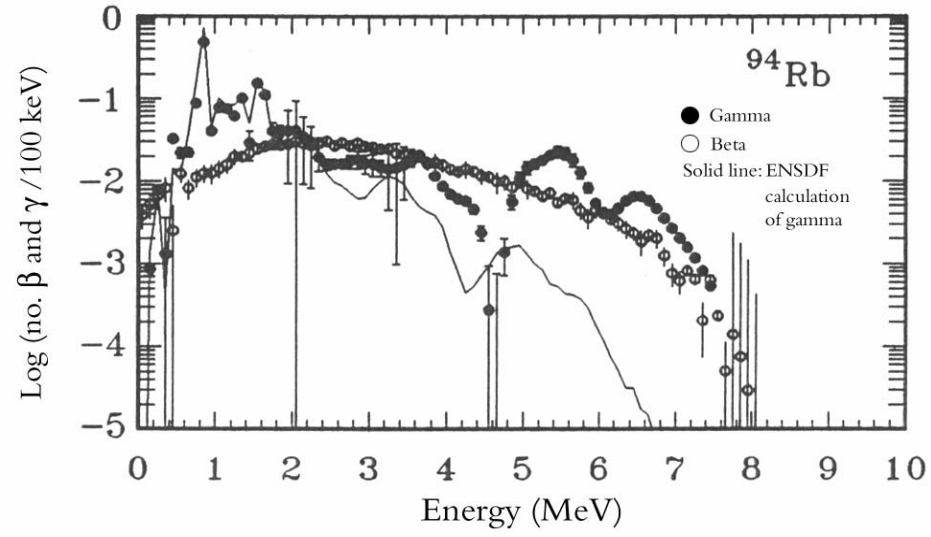

Fig. 25. Beta and gamma spectra of short-lived fission product ^{94}Rb (Rudstam *et al*, 1990)

Table 10: Mean beta, gamma and antineutino energies compared with known Q_β-values (Rudstam *et al*, 1990)

Nuclide	Mean E_γ (keV)	Mean E_β (keV)	Mean $E\nu$ (keV)	Neutron (keV)	Sum (keV)	Q_β (keV)[a]
^{85}As	920(280)	2600(140)	3140(220)	3210(580)	9870(690)	8910(410)
^{87}Br	3560(130)	1410(10)	1820(50)	153(1)	6940(140)	6830(120)
^{88}Br	4290(180)	1680(10)	2120(50)	460(4)	8550(190)	8970(130)
^{89}Br	3220(260)	2180(40)	2680(140)	720(17)	8800(300)	8300(400)
^{90}Br	-	2500(50)	3030(50)	-	-	10700(400)
^{93}Rb	1920(100)	2630(30)	3140(60)	76(1)	7690(120)	7443(13)
^{94}Rb	4120(250)	2830(70)	3370(160)	718(4)	11040(320)	10307(27)
^{95}Rb	3370(220)	2850(150)	3300(180)	383(6)	9900(320)	9280(60)
^{98}Y	870(90)	2540(80)	3080(170)	16(1)	6510(210)	8890(70)
^{99}Y	1340(150)	2480(70)	3030(130)	94(2)	6950(210)	7610(80)
^{135}Sb	1600(200)	2290(60)	2900(110)	578(35)	7370(230)	7540(220)
^{137}I	1230(150)	2050(40)	2620(30)	309(2)	6210(160)	5880(80)
^{138}I	1560(90)	2510(40)	3150(40)	332(4)	7550(100)	7820(70)
^{139}I	1400(150)	2430(40)	3040(60)	340(13)	7210(170)	6820(100)

[a] Q_β values from Firestone *et al* (1996), ENSDF (NNDC, 1987), and earlier versions of these two sources of data.
Uncertainties are given in parentheses (for example, 920(280) means 920 ± 280)

(b) Total absorption gamma-ray spectrometry

Greenwood and co-workers have developed total absorption gamma-ray spectrometry (TAGS) in order to determine the intensity distributions of a wide range of β^--emitting radionuclides (Greenwood *et al*, 1994; Helmer *et al*, 1994; Greenwood *et al*, 1996; Greenwood *et al*, 1997). The TAGS system consists of a NaI(Tl) detector with a deep axial counting well to allow almost complete summing of the gamma-ray cascades from the source. A Si detector is also located in the well so that β^--particle-gated coincidence gamma rays can be measured in addition to singles gamma-ray spectra. Spontaneous fission of ^{252}Cf generated the fission-product radionuclides, and a He gas-jet transported these nuclides to a mass separator. The selected fission-product mass fraction was collected on a tape for a pre-set time, before moving to the Si detector in the well of the TAGS system. Although only relative β^--intensity distributions are obtained from the TAGS gamma-ray cascade-summed spectral data, the detector system can be used in $4\pi\gamma$-β^- coincidence mode to obtain the β^--branching intensity to the ground state; the measurement of this key parameter provides a simple means of converting the relative β^--intensity distributions to absolute values.

The resulting singles spectra were compared with simulated spectra derived from the evaluated decay data to be found in Nuclear Data Sheets (Bhat, 1992): examples are shown in Figs. 26 and 27 for ^{138g}Cs and ^{138m}Cs, respectively. Measured and

calculated spectra for ^{138g}Cs are in good agreement below ~3200 keV, but the simulated spectrum exhibits serious deficiencies in the postulation of beta-particle emission probabilities above this energy. Additional pseudolevels have been introduced to the decay scheme in order to achieve the good fit shown in Fig. 28 (see also Table 11); these additions and increased populations to other high-energy levels increase the beta-particle emission probabilities above 3200 keV from 2.65% to 5.9%. Similar procedures can be applied to the spectrum of ^{138m}Cs (Fig. 29), with the addition of a considerable number of pseudolevels above 2500 keV as listed in Table 12.

The TAGS method of spectral measurement and analysis would appear to be an extremely powerful means of modifying inadequate decay-scheme data in a quantitative manner. This approach is very welcome, and should be encouraged further in order to eliminate serious gaps in our detailed knowledge of the discrete decay data of many important short-lived fission products.

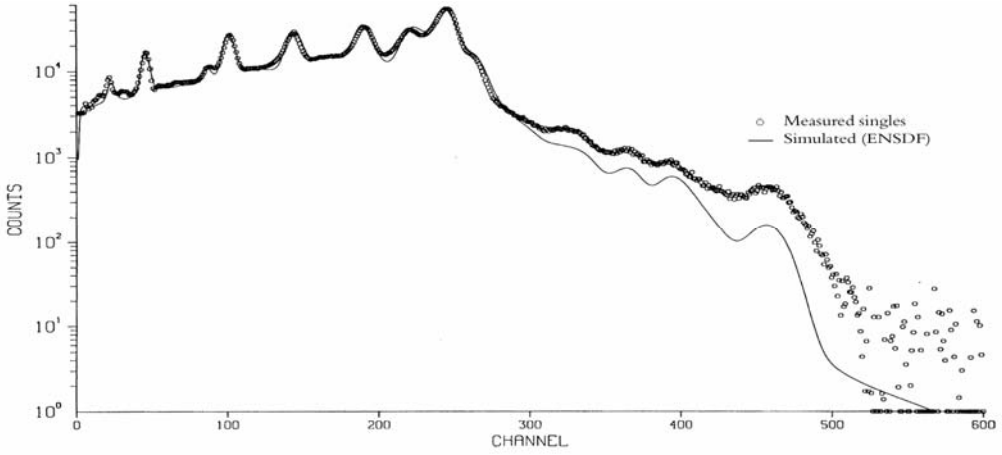

Fig. 26. Comparison of measured singles spectrum for ^{138g}Cs with the simulated spectrum for the evaluated decay scheme (Greenwood *et al*, 1994)

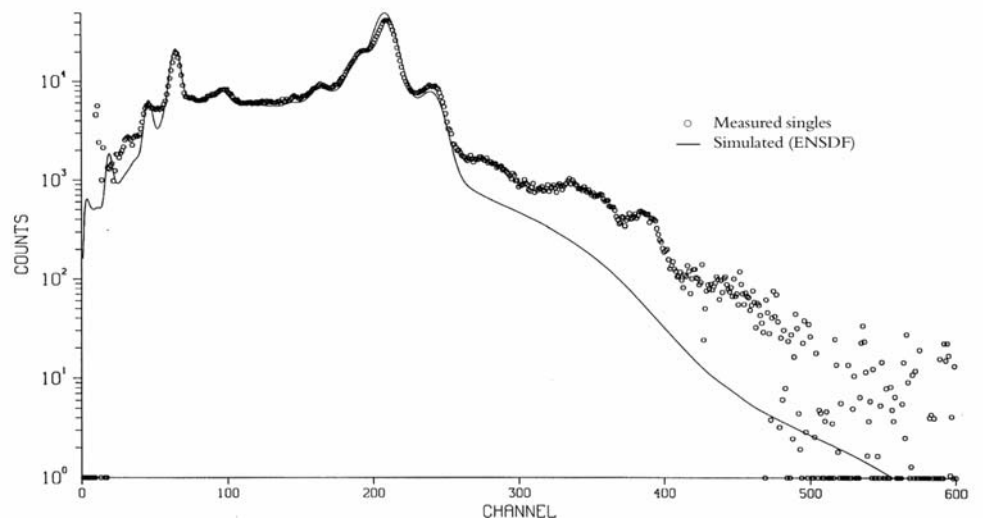

Fig. 27. Comparison of measured singles spectrum for ^{138m}Cs with the simulated spectrum for the evaluated decay scheme (Greenwood *et al*, 1994)

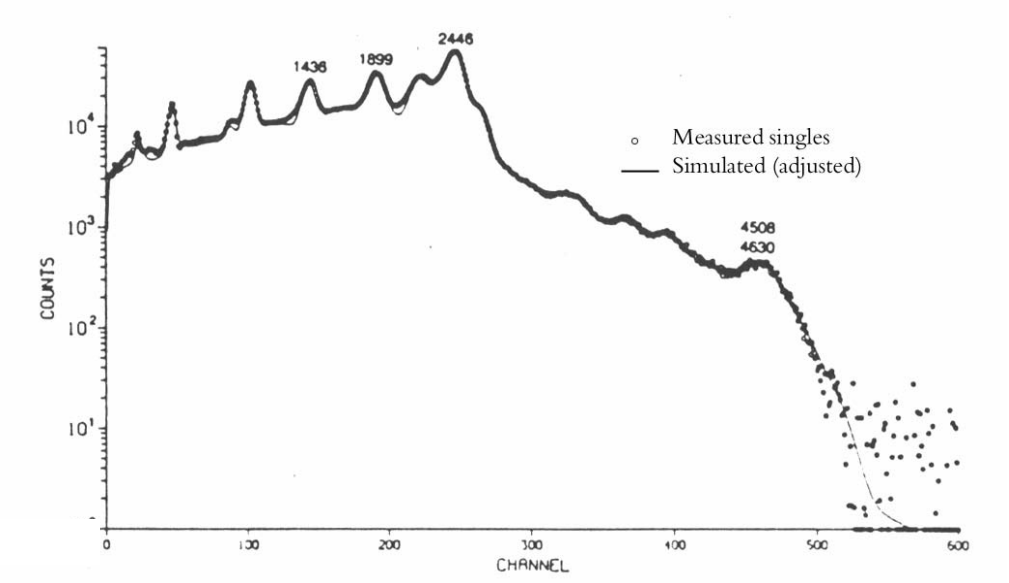

Fig. 28. Comparison of measured singles spectrum for ^{138g}Cs with the simulated spectrum for the re-adjusted decay scheme (Greenwood *et al*, 1994)

Table 11: ^{138g}Cs β^- emission probabilities, P_β (Greenwood *et al*, 1997)

Level energy (keV)	**P_β(%)**	
	NDS	**TAGS**
0.0	0.0	0.0
1435.9	4.3	3.76
1898.7	13.7	13.94
2217.9	13.0	13.23
2307.6	7.3	6.10
2415.5	0.63	0.64
2445.7	44.0	44.76
2583.1	1.67	1.42
2639.5	8.80	7.32
2779.5	1.59	0.81
2851.6	0.20	0.20
2880.9	0.54	0.55
2931.5	0.21	0.21
2991.2	0.64	0.61
3049.9	0.17	0.17
3163.6	0.34	0.35
3242.6	0.27	0.54
3257.7	0.06	0.33
3339.0	0.17	0.33
3352.6	0.035	0.036
3367.0	0.23	0.23
3437.4	0.011	0.011
3442.3	0.011	0.011
3510 P	-	0.25
3647.0	0.43	0.66
3652.6	0.005	0.005
3694.0	0.30	0.46
3825 P	-	0.15
3922.6	0.21	0.25
3935.2	0.47	0.61
4012.3	0.08	0.08
4080.1	0.18	0.18
4242.5	0.10	0.28
4370 P	-	0.10
4508.1	0.16	0.41
4629.8	0.26	0.72
4850 P	-	0.20
5080 P	-	0.046

NDS: Nuclear Data Sheets, **69**(1993)69.
P: placement of pseudolevel.

Table 12: ^{138m}Cs β^- emission probabilities, P_β (Greenwood *et al*, 1997)

Level energy (keV)	**P_β(%)[a]**	
	NDS	**TAGS**
0.0	0.0	0.0
1436.0	0.0	0.0
1899.0	0.0	3.63
2090.7	75.3	64.69
2203.2	10.3	8.89
2307.8	0.0	0.0
2415.2	14.4	15.88
2600 P	-	0.272
2730 P	-	0.59
2800 P	-	0.59
2900 P	-	0.45
3300 P	-	0.41
3400 P	-	0.82
3500 P	-	0.82
3600 P	-	0.64
3800 P	-	0.59
3900 P	-	1.00
4100 P	-	0.073
4200 P	-	0.073
4300 P	-	0.073
4400 P	-	0.136
4500 P	-	0.109
4600 P	-	0.109
4700 P	-	0.064
4800 P	-	0.054
4900 P	-	0.032
5000 P	-	0.018

[a]Contribution to the total ^{138m}Cs decay is obtained by multiplying P_β by 0.19.
NDS: Nuclear Data Sheets, **69**(1993)69.
P: placement of pseudolevel.

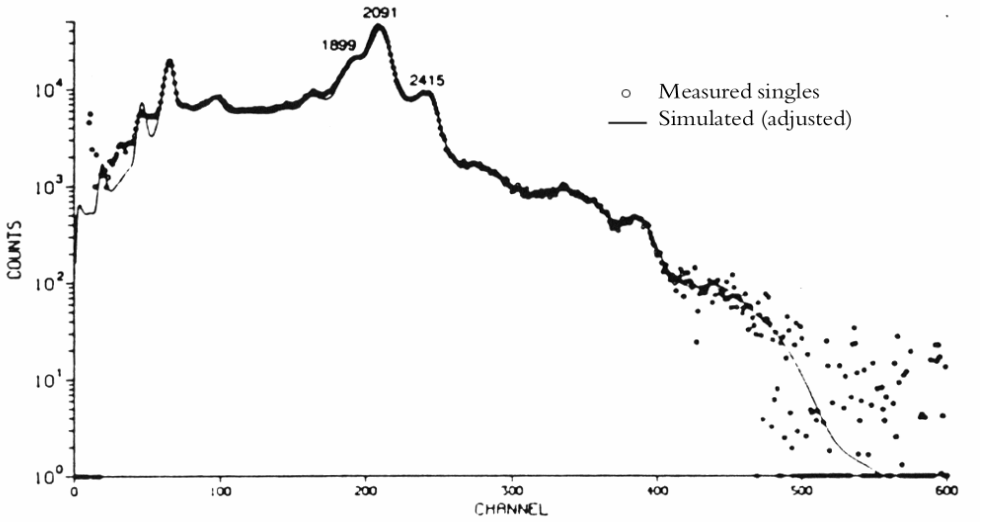

Fig. 29. Comparison of measured singles spectrum for ^{138m}Cs with the simulated spectrum for the re-adjusted decay scheme (Greenwood *et al*, 1994)

(c) Endpoint energies (Q_β-values)

Accurate measurements of Q_β aid considerably the determination of the energies of individual β^- emissions, and in the derivation of the mean beta energies (and gamma energies) of short-lived fission products. Rapid mass-separation techniques are used to alter the isobaric composition of the ion beams after their emission from fission targets, and high-purity Ge detectors measure the β-γ coincidence and β singles spectra of the resulting sample (Wünsch *et al*, 1978; Przewloka *et al*, 1992a and 1992b; Ikuta *et al*, 1994).

The beta endpoints are determined from Fermi-Kurie plots of the measured β^- spectrum (Fermi-Kurie plot with good statistics is shown in Fig. 30 for ^{92}Rb (Przewloka *et al*, 1992a)). Equivalent data for a number of neutron-rich nuclides are listed in Table 13 (Ikuta *et al*, 1994), and are compared with the recommended values of Audi and Wapstra (1995). Discrepancies do occur (^{147}La, ^{147,149,150}Ce and ^{150}Pr), and underline the need to refine theoretical calculations in this particular region.

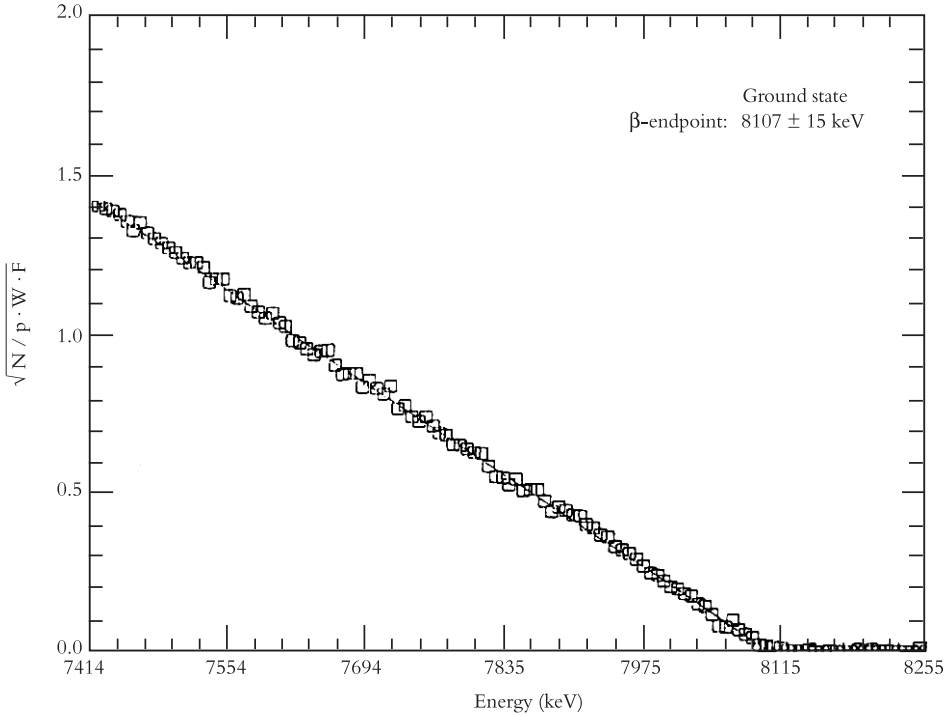

Fig. 30. β-endpoint spectrum of ^{92}Rb (Przewloka *et al*, 1992a)

Table 13: Q_β values of neutron-rich nuclei in the mass region 147≤A≤152 (Ikuta *et al*, 1994)

Nuclide	**Half-life**	**Measured Q_β (keV)**	**Q_β (keV)** Audi and Wapstra, 1995
^{147}La	4.015 s	5130(80)	4945(55)
^{147}Ce	56.4 s	3426(28)	3290(40)
^{147}Pr	13.3 m	2710(50)	2686(37)
^{148}Ce	56 s	2140(30)	2060(75)
^{148}Pr	2.27 m	4880(50)	4932(89)
^{149}Ce	5.2 s	4386(27)	4190(75)
^{149}Pr	2.26 m	3430(90)	3397(10)
^{150}Ce	4.0 s	3470(60)	3010(90)
^{150}Pr	6.19 s	5390(30)	5690(80)
^{151}Pr	18.90 s	4200(40)	4101(35)
^{151}Nd	12.44 m	2460(100)	2442(4)
^{152}Pr	3.24 s	6340(120)	6444(300)
^{152}Nd	11.6 m	1100(40)	1110(78)
^{152}Pm	4.1 m	3520(60)	3504(72)

Uncertainties are given in parentheses (for example, 4945(55) means 4945 ± 55).

5.5. Decay Data Libraries

5.5.1. Nuclear structure

A number of teams around the world are engaged in the co-ordinated evaluation and compilation of nuclear structure data, under the auspices of the International Atomic Energy Agency. This International Network for Nuclear Structure Data Evaluation generates updated Evaluated Nuclear Structure Data Files (ENSDF), and is responsible for the evaluation of all the mass-chains on a regular basis (NNDC, 1987; Bhat, 1992). The resulting files are maintained by the National Nuclear Data Centre at Brookhaven National Laboratory, along with other services (Dunford, 1994; Kinsey *et al*, 1994). Available databases include ENSDF, atomic masses, NuDat (basic nuclear data extracted from ENSDF, including radionuclidic decay data), RADLST (calculated decay parameters from ENSDF), CSISRS (experimental cross-section data) and ENDF-6 (evaluated nuclear reaction and decay data in ENDF-6 format for applications in the nuclear industry). Details of the methods of data retrieval from NNDC are given in Appendix A, including access to the ENDF-6 files (Dunford, 1992). Theoretical decay data have been incorporated into this library for a number of important short-lived fission products, including delayed-neutron data and continuum spectra (Brady and England, 1989).

NUBASE is a database that contains the main nuclear and decay properties of nuclides in their ground and isomeric states (Audi *et al*, 1996 and 1997). These data have been primarily derived from ENSDF and the atomic mass evaluation of Audi and Wapstra (1995). Experimentally-measured nuclear parameters have been compiled for virtually all known nuclides, with some values estimated by systematic extrapolation. Recommended data are listed for mass excess, excitation energy of isomeric states, half-life, spin and parity, decay modes and branching fractions, as well as isotopic abundances for the stable nuclei and a list of relevant references.

The Table of Isotopes has a long and respected history, culminating in the release of the eighth edition in 1996 (Firestone *et al*, 1996). A CD-ROM is also included that contains all of the recommended decay-scheme data, and this vehicle will be preferentially used to communicate updates (Firestone *et al*, 1998). The main table is initially ordered by mass number and then by atomic number, with abbreviated mass-chain decay schemes that give the adopted half-lives, spin-parity and Q-values. Data are listed for each ground state and isomer with half-lives $\geq$ 1 sec. ENSDF evaluations have been adopted whenever the authors judged this data source to be appropriate. Significant amounts of nuclear data are contained within this immense document/file, and the reader is referred to the original publication for greater detail. Other specialised decay-data compilations have been published (e.g., Reus and Westmeier, 1983; Westmeier and Merklin, 1985; Rytz, 1991; Nichols, 1996), but few appear to have been maintained in the same rigorous manner as ENSDF and the Table of Isotopes. Both are comprehensive and contain decay data for approximately

2500 radionuclides, effectively covering all nuclides that have been observed and characterised to some degree. The ability to inspect and use these data via a CD-ROM and the World Wide Web adds considerable strength to their commonality of use.

5.5.2. Nuclear applications

The US ENDF/B-VI nuclear data library was released to the international community in the early 1990s (Dunford, 1992). An initial point of note is the development over many years of an internationally-accepted data format (ENDF-6), including the potential to accommodate uncertainties in the form of covariance matrices. Specific aims included the production of a self-consistent set of evaluated neutron cross sections, updated decay-data files (extracted from the ENSDF files, and supplemented with new measurements and theory), and the addition of charged-particle and high-energy reaction files. Many of the neutron-reaction cross sections were completely re-evaluated, including ^{238}U(n, f), ^{239}Pu(n, f) and the resonance parameters for ^{235,238}U and ^{239,241}Pu. Adjustments were also made to the neutron-capture cross sections of ^{151,153}Eu, ^{165}Ho and ^{197}Au (latter as standard). Both the decay-data and fission-yield files of ENDF/B-VI have been supplemented with the beta and gamma energies and Pn values of Rudstam *et al* (1990 and 1993) and the chain yields derived by Wahl (1988). This resulting data base was tested in a series of decay-heat calculations and shown to reproduce the experimental results in a satisfactory manner (Rudstam and England, 1990). ENDF/B-VI gamma-ray data for the short-lived fission products were also augmented by spectra calculated from the gross theory for beta-strength functions to form mixed files of discrete and theoretical decay data (Katakura and England, 1991).

The Joint Evaluated File (JEF) is a collaborative project between member states of the NEA-OECD to produce a nuclear data library for industrial applications and research (Nordborg *et al*, 1992; Nordborg and Salvatores, 1994). Various decay-data files have been assembled by staff at the NEA Data Bank from other sources (particularly ENSDF, UKPADD-2 (Nichols, 1993) and UKHEDD-2 (Nichols, 1991)). This JEF-2.2 library consists of a general purpose file, radioactive decay-data files and fission-yield files. A number of adjustments were made to the JEF-2.2 decay-data starter files:

(a) mean beta and gamma energies of 109 short-lived fission products measured by Rudstam *et al* (1990) were added to the files;

(b) theoretical data were based on the p-n QRPA model of Hirsch *et al* (1992): 16 half-lives, 101 mean beta and gamma energies, and 32 P_n values.

The contents of the JEF-2.2 files have been summarised in hardcopy, and represent a definitive data set for nuclear applications (NEA-OECD, 1994 and 2000).

Efforts are underway to amalgamate the NEA fission (JEF) and fusion (EAF) data libraries, and to improve and expand the contents of the resulting files (Finck *et al*, 1997; Jacqmin *et al*, 2001; Bersillon *et al*, 2001). A Joint Evaluated Fission and Fusion project has been formulated to combine JEF and EAF database activities. Other sources of updated decay-data for JEFF-3 include NUBASE, ENSDF, UKPADD and UKHEDD. Various studies are also underway or completed to improve the contents of specific decay data files judged to be inadequate for fission and fusion reactor applications (e.g., Backhouse and Nichols, 1998; Nichols *et al*, 1999a and 1999b).

Other libraries have been developed for nuclear power applications that contain decay-data files. Staff at the Chinese Nuclear Data Centre, have assembled files of basic nuclear data and model parameters (Su Zongdi *et al*, 1994 and 1997). This nuclear parameter library (CENPL) contains atomic masses and constants for ground states, nuclear level properties and gamma-ray data extracted from ENSDF.

The JNDC-FP (Japanese Nuclear Data Committee - Fission Product) library contains decay and fission yield data for 1087 unstable and 142 stable fission products, and neutron cross-section data for 166 nuclides (Tasaka *et al*, 1990; Katakura *et al*, 2001). Recommended decay data include half-lives, branching ratios, and total beta and gamma-ray energies released per decay of every radionuclide. Significant emphasis has been placed on producing a comprehensive set of fission-product decay data, with the introduction of theoretical half-lives and mean energies for over 500 radionuclides with no known discrete decay data.

The contents of the various national and international decay-data files are difficult to summarise with respect to their technical origins (i.e., discrete decay-data or mean beta-decay measurements; file supplemented with calculated decay data from gross theory of β decay, microscopic analyses or p-n QRPA). Table 14 focuses on the fission-product nuclides to be found in the US ENDF/B-VI, JENDL-FP and JEF-2.2 libraries.

"Estimated decay energies" refers to a combination of data that originate from Rudstam *et al* (1990), Hirsch *et al* (1992) and others. The inclusion of estimated and theoretical decay data is considerably more extensive in US ENDF/B-VI and JENDL-FP than in JEF-2.2 (latter includes more recommended data based on direct measurements (with the concomitant problem of pandemonium (Hardy *et al*, 1977)).

Table 14: Evaluated decay-data libraries, 2000/2001: contents and origins of fission-product decay energies (NEA-OECD, 2000; Katakura *et al*, 2001)

Fission products	**ENDF/B-VI**	**JENDL-FP**	**JEF-2.2**
Evaluated nuclides	891	1229	860
Radioactive nuclides	764	1087	730
Stable nuclides	127	142	130
Evaluated decay energies[a]	443[c]	536[d]	611
Estimated decay energies[b]	384[c]	551[d]	119

[a] Evaluations of discrete decay data.
[b] Mean decay energies from gross measurements and theory.
[c] Some files contain both evaluated discrete data and estimated theoretical data (including continuum spectra).
[d] Uncertain - defined by number balance only.

5.5.3. Electronic access

The advent of personal computers (leading to the emergence of the CD-ROM and the World Wide Web) has revolutionised the ability to communicate with and access large data bases rapidly and efficiently. Examples of the provision of CD-ROMs and the implementation of the Web are listed in Appendix A (ENSDF, NUBASE and the Table of Isotopes). A significant number of these data bases have been adapted so that PCs can interrogate, extract, compare and use their contents. Both the Internet and the utilisation of CD-ROMs have given users world-wide access to all of the most recently evaluated nuclear data libraries via a number of routes including the IAEA Network of Nuclear Data Centres. Communications between laboratories have improved beyond all recognition over the previous 10 years, and have revolutionised the speed with which data can be provided for various calculations (including decay-heat analyses).

5.6. Inadequate and Discrepant Decay Data

The evolution of the various decay-data libraries for nuclear applications has resulted in programmes of intensive testing to re-assure users that the recommended data sets are reliable and comprehensive. During the course of these benchmark exercises, errors and inadequacies have inevitably been discovered. Many can be dealt with rapidly, but some problems have proved more difficult to overcome without a significant amount of additional work. Although the assessments given below are not comprehensive, a number of important discrepancies are noted, along with known efforts to improve the contents of the decay-data libraries. Sometimes the analyses required to highlight and identify the culprit radionuclide(s) can be as taxing as subsequent attempts to correct the problematic data. Furthermore, attempts to improve the quality of the recommended decay data in this manner may be seriously undermined by the increasing lack of expertise available to undertake such work.

After much consultation and debate in the mid-1990s, a number of important radionuclides were judged to be inadequately characterised for various applications (ranging from estimates of radiotoxicity and input data for reprocessing flowsheets, to nuclides that undergo delayed-neutron emission). A set of 27 fission products (plus short-lived daughters and related metastable/ground states) was identified as important for various thermal reactor studies, including decay-heat calculations (Table 15). The majority of these radionuclides are short-lived fission products with half-lives significantly less than 3 hours. Considerable improvements were made in their recommended decay data as a consequence of including a number of relatively recent measurements in the evaluations, although the complexity of many of the decay schemes may still pose mean energy problems (Nichols, 1998; Nichols *et al*, 1999a).

Various decay parameters and continuum spectra have also been theoretically derived for 35 neuton-rich nuclides deemed to be important at short cooling times in decay-heat calculations (Table 16). While each of these fission products contributes significantly to the decay heat of irradiated fuel (>0.01 of the fractional cumulative yield), they have proved extremely difficult (if not impossible) to prepare, isolate and study experimentally, and are not included in the JEF-2.2 decay-data library. The US ENDF/B-VI decay-data library contains files of theoretical data for 33 of these nuclides, and they were considered as possible candidates for incorporation into the JEFF library, with supportive data from Takahashi *et al* (1973) and Audi *et al* (1997).

The precise content of any data library for decay-heat calculations is based on subjective judgements, although the desire for completeness can overcome many constraints. While the nuclides contained within Appendix B provide a reasonably comprehensive set of fission products and actinides for this type of study, changes can always be made to improve and expand the data base (Storrer, 1994). The addition of further isomeric states is a particular good example of this form of improvement; recent experimental studies have furnished evaluators with evidence for further short-lived radionuclides of this type that could be incorporated into the decay-data (and fission yield) libraries:

^{81m}Ge; ^{84m}As; ^{96m}Rb; ^{97n}Y; ^{103m}Ru, ^{109m}Ru; ^{112m}Rh, ^{114m}Rh, ^{116m}Rh; ^{113m}Pd, ^{115m}Pd, ^{117m}Pd; ^{107m}Ag, ^{119m}Ag, ^{120n}Ag, ^{122m}Ag; ^{123m}Cd, ^{125m}Cd; ^{120n}In, ^{122n}In, ^{126m}In, ^{130m,130n}In, ^{131m,131n}In; ^{114m}Sn, ^{128m}Sn; ^{129m}Sb; ^{132m}I; ^{132m}Xe; ^{144m}Cs; ^{146m}La; ^{148m}Pr; ^{153m}Sm; ^{155m}Gd.

While the postulated decay schemes for many of these radionuclides are simple (e.g., ^{107m}Ag, ^{113m}Pd and ^{128m}Sn), others are relatively complex (e.g., ^{112m}Rh, ^{122n}In, ^{125m}Cd and ^{146m}La). Their decay data can be found in ENSDF, and could be assessed and transferred to nuclear applications libraries.

Table 15: Evaluation of discrete decay data - consistency of data sets requested for JEFF-3

Radionuclide	**Consistency (% Deviation)**	**Radionuclide**	**Consistency (% Deviation)**
33-As-85	0.0988*	(51-Sb-126)	-0.0653
34-Se-79	0.0000	(51-Sb-126m)	-0.1714
(34-Se-79m)	-0.0962	(51-Sb-126n)	-0.3560
35-Br-87	-0.1976*	51-Sb-127	-0.0431
35-Br-88	0.2554*	51-Sb-135	-0.0198*
35-Br-89	0.0534*	(52-Te-127)	-0.0037
35-Br-90	0.1331*	(52-Te-127m)	-0.0908
35-Br-91	0.0274*	52-Te-132	0.1077
37-Rb-93	-0.0182*	53-I-132	-0.0832
37-Rb-94	-0.0527*	(53-I-132m)	-0.3723
37-Rb-95	-0.2394*	53-I-137	0.1276*
(39-Y-98)	-0.0432*	53-I-138	-0.1955*
39-Y-98m	-0.2944*	53-I-139	-0.0552*
39-Y-99	-0.0741*	57-La-140	-0.0108
40-Zr-93	1.2384	59-Pr-143	0.0000
(41-Nb-93m)	-0.3678	59-Pr-144	0.0382
45-Rh-106	-0.0243	(59-Pr-144m)	-0.0860
(45-Rh-106m)	-0.0487	62-Sm-147	-0.0023
50-Sn-126	0.0293	65-Tb-161	-0.0324

Additional short-lived daughter and related metastable/ground state radionuclides are in parentheses, and were also evaluated.
*Beta-decay mode only.

Table 16: Short-lived fission products requested for JEFF-3 - US ENDF/B-VI decay data adopted or modified unless stated otherwise

Radionuclide	**Half-life (sec)** ‡	**Continuum Spectra - Energy Range (keV)***		
		Gamma	**Beta**	**Neutron**
39-Y-104	0.13(2)	0(500) - 12730	0 - 12690	0 - 5510
39-Y-105	0.15(2)	0(500) - 10820	0 - 10790	0 - 6840
40-Zr-105	0.6(2)	0(500) - 8290	0 - 8260	0 - 2260✦
40-Zr-106	0.9(2)	0(500) - 6380	0 - 6350	0 - 2570
40-Zr-107	0.24(4)	0(500) - 9230	0 - 9200	0 - 3950
41-Nb-109	0.19(6)	0(500) - 8760	0 - 8730	0 - 5300
42-Mo-109	0.5(2)	0(500) - 6700	0 - 6670	0 - 1200Ψ
42-Mo-111	0.5(2)	0(500) - 8020	0 - 7990	0 - 2210
42-Mo-112	1.0(2)	0(500) - 6020	0 - 5990	0 - 2720
43-Tc-113	0.13(4)	0(500) - 7540	0 - 7510	0 - 4080
43-Tc-114	0 20(4)	0(500) - 10610	0 - 10580	0 - 4790
43-Tc-115	0.27(5)	0(500) - 8870	0 - 8840	0 - 5910
43-Tc-116	0.12(2)	0(500) - 11860	0 - 11830	0 - 6650
44-Ru-115	0.7(2)	0(500) - 7250	0 - 7220	0 - 1400
44-Ru-116	1.7(3)	0(500) - 5510	0 - 5480	0 - 2150
44-Ru-117	0.34(7)	0(500) -8500	0 - 8470	0 - 3180
44-Ru-118	0.7(2)	0(500) - 6530	0 - 6500	0 - 3680
44-Ru-119	0.19(4)	0(500) - 9290	0 - 9260	0 - 4440
45-Rh-118	0.32(6)	0(500) - 9970	0 - 9940	0 - 3410
45-Rh-120	0.17(3)	0(500) - 10770	0 - 10730	0 - 4830
45-Rh-121	0.25(5)	0(500) - 8790	0 - 8760	0 - 5990
46-Pd-121	0.6(1)	0(500) - 7560	0 - 7530	0 - 1520
51-Sb-141	0.3(1)	No entry in US ENDF/B-VI; other theoretical data adopted		
57-La-152	0.28(6)	0(500) - 8810	0 - 8770	0 - 3980
58-Ce-153	1.5(3)	0(500) - 5820	0 - 5790	0 - 1620
58-Ce-154	2.0(4)	0(500) - 5010	0 - 4970	0 - 1640
58-Ce-158	1.0(2)	No entry in US ENDF/B-VI; other theoretical data adopted		
59-Pr-156	0.5(1)	0(500) - 8690	0 - 8660	0 - 2790
59-Pr-157	0.30(6)	0(500) - 8130	0 - 8100	0 - 3590
60-Nd-157	2.5(5)	0(500) - 5560	0 - 5520	None
60-Nd-158	0.7(2)	0(500) - 5000	0 - 4970	0 - 320
60-Nd-159	0.5(1)	0(500) - 7150	0 - 7120	0 - 1230
60-Nd-160	0.30(6)	0(500) - 6350	0 - 6320	0 - 1830
61-Pm-159	3.0(6)	0(500) - 5650	0 - 5620	0 - 410
61-Pm-160	2.0(4)	0(500) - 7800	0 - 7770	0 - 1130

‡ Adopted from a combination of Audi *et al* (1997), Takahashi *et al* (1973) and US ENDF/B-VI (Dunford, 1992); uncertainties are given in parentheses (for example, 0.13(2) means 0.13 ± 0.02).

* Expressed in terms of incremental units of 10 keV starting from zero (first incremental energy step of continuum gamma spectra is from zero to 500 keV, as noted in parentheses).

✦ Neutron spectrum adjusted to 0-1794 keV.

Ψ Neutron spectrum adjusted to 0-620 keV.

An interesting piece of detective work has been carried out by Yoshida *et al* (1997 and 1999) to offer some explanation for the discrepancy between experiments and calculations of the gamma component of decay heat over cooling times between 300 and 3000 sec (Fig. 31, instantaneous fission burst for ^{239}Pu). Experimental data measured by Dickens *et al* (1980 and 1981), Akiyama and An (1983), and Nguyen *et al* (1997) were combined and compared with decay-heat calculations using the JNDC-FP-V2 library (adoption of either fast-neutron or thermal-neutron fission yields had little impact on the resulting curves). Yoshida *et al* introduced a gamma-ray emission that is effectively missing from the decay-data files, and was postulated to belong to an ill-defined fission product (half-life of ~1000 sec). An additional β^- decay chain was artificially added to the JNDC data base (as two radionuclides) on the basis of this proposed omission.

An energy release of 1.5 MeV per decay was assumed to occur (e.g., ^{104}Mo (half-life of 60 sec) $\rightarrow$ ^{104}Tc (half-life of 1092 sec) represents a suitable candidate for such an emission). The results of these artificial calculations are shown in Fig. 32 for ^{233,235,238}U and ^{239}Pu in comparison with the measurements of Akiyama and An (1983): the discrepancies between 300 and 3000 sec disappeared for all four sets of data. Fig. 33 shows the impact on the beta-energy component for the fission burst of ^{239}Pu; there is some decrease against the original calculation, but this change falls well within the error bars of the measurements. Re-assessments have been made of beta-strength functions to identify possible candidates, including ^{102}Tc, ^{104}Tc and ^{105}Tc. Overall, the proposal of Yoshida *et al* would appear to be a reasonable suggestion.

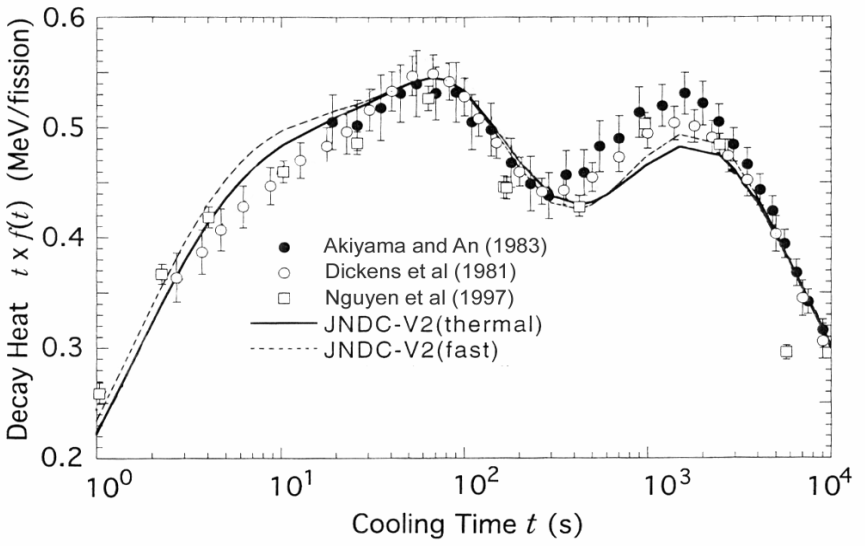

Fig. 31. Gamma-ray discrepancies seen in ^{239}Pu decay heat after a fission burst (Yoshida *et al*, 1999)

The incorrect assignments of ground and metastable states may also play an important role in explaining some of the discrepancy in the gamma component between 300 to 3000 sec. Fig. 34 compares experimental data with decay-heat calculations for ^{239}Pu; improvements can be achieved by adjusting the decay data for ^{108}Rh. The ground and metastable states of ^{108}Rh are assigned half-lives of 17 sec and 6 min respectively in JNDC-V2 (labelled 'JNDC-V2 original' in Fig. 34), while these assignments are reversed in JEF-2.2 (labelled 'Rh108-JEF2.2' in Fig. 34). Adoption of the JEF-2.2 data increases the half-life of ^{108g}Rh by a factor of ~ 20, leading to a considerable rise in decay heat around 1000 sec. Another feature is worthy of note: a lack of gamma-ray transition energy in the ^{102}Tc decay-data file of JEF-2.2 gives rise to a collapse in the gamma energy component (labelled 'Tc102-JEF2.2' in Fig. 34), implying that this radionuclide represents a suitable candidate for the missing gamma energy (as noted earlier). These studies demonstrate that adjustments to the decay-data of only one nuclide can dramatically change the decay-heat predictions, and that beta branching ratios to the ground and metastable states need to be measured with good accuracy in order to define the situation correctly.

6. CONCLUDING REMARKS

Estimates of decay heat can only be calculated with confidence if the neutron cross sections, fission yields and radionuclidic decay data are known with confidence, and extensive data libraries have been assembled at both the national and international levels in an agreed format (ENDF-6) to achieve this objective. All data in these libraries are subjected to comprehensive checking procedures and some form of validation before they are released for general use. Their adoption in decay-heat calculations has shown measurement-based files to be inadequate, and therefore efforts continue to improve and extend their contents (particularly isomeric fission yields and the decay data of short-lived fission products), as requested by users.

Systematic fitting procedures, gross energy measurements and theoretical data have played important roles in addressing the problem of non-existent (unmeasured) fission-yield and decay data. Along with evaluations of measured discrete data, these approaches will continue to be used in order to extend the contents of the data libraries, and so improve decay-heat calculations and increase operational confidence in the results.

Acknowledgments

The author wishes to thank the following for their assistance in formulating specific features of this article:
C.J. Dean (AEA Technology, Winfrith),
M.A. Kellett (NEA Data Bank),
M. Lammer (IAEA Nuclear Data Section),
F. Storrer (CEN Cadarache),
E.B. Webster (AEA Technology, Winfrith).

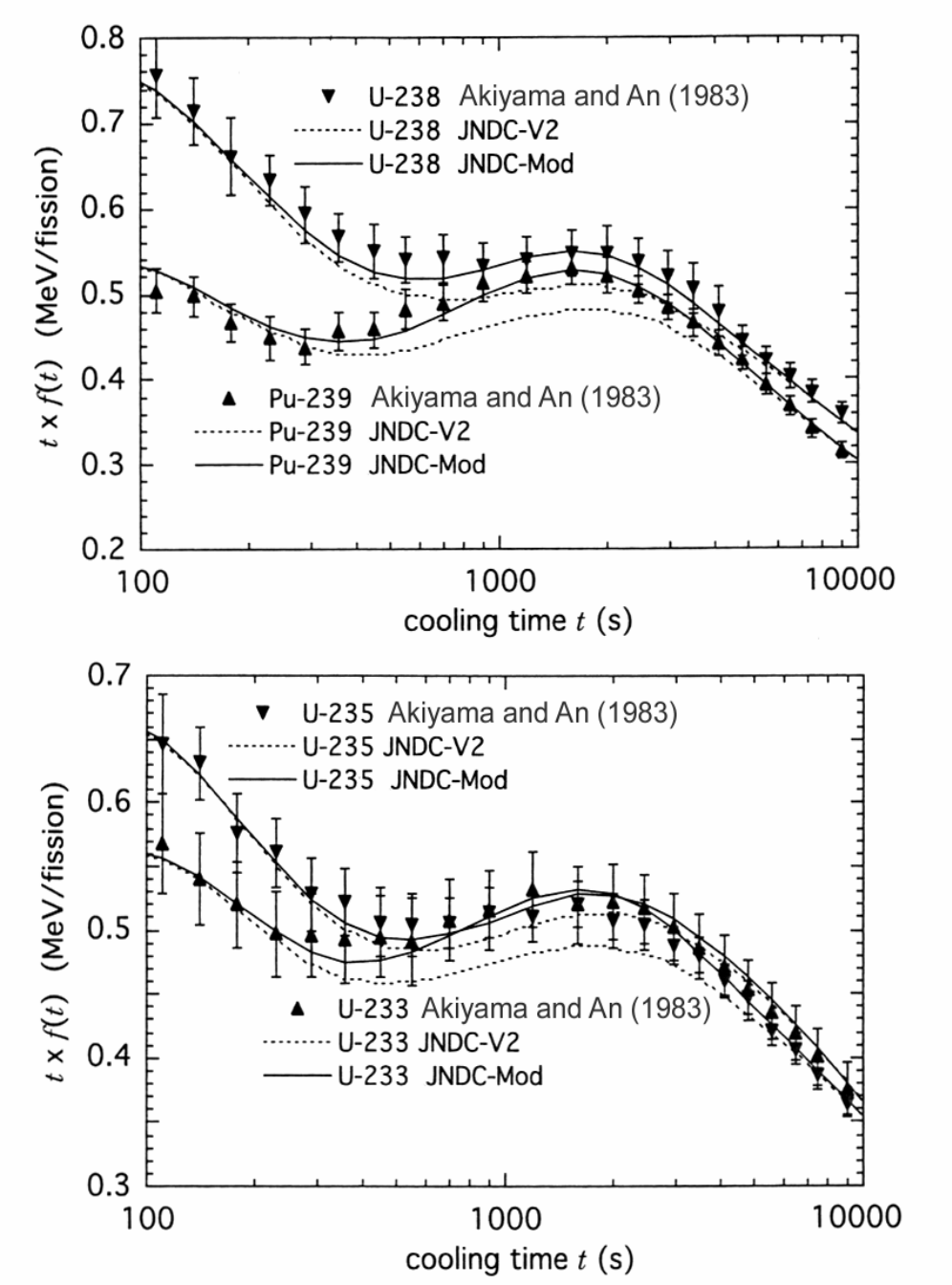

Fig. 32. Removal of γ-ray discrepancy by including 1.5 MeV γ-ray emitter (Yoshida *et al*, 1999)

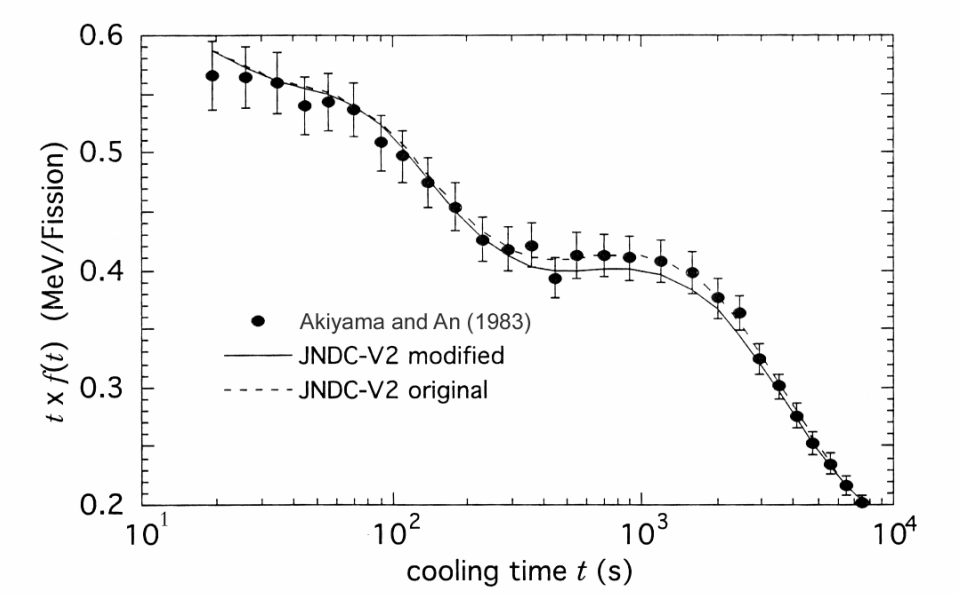

Fig. 33. Beta-ray component of ^{239}Pu decay heat after a burst fission: addition of 1.5 MeV γ-ray emitter (Yoshida *et al*, 1999)

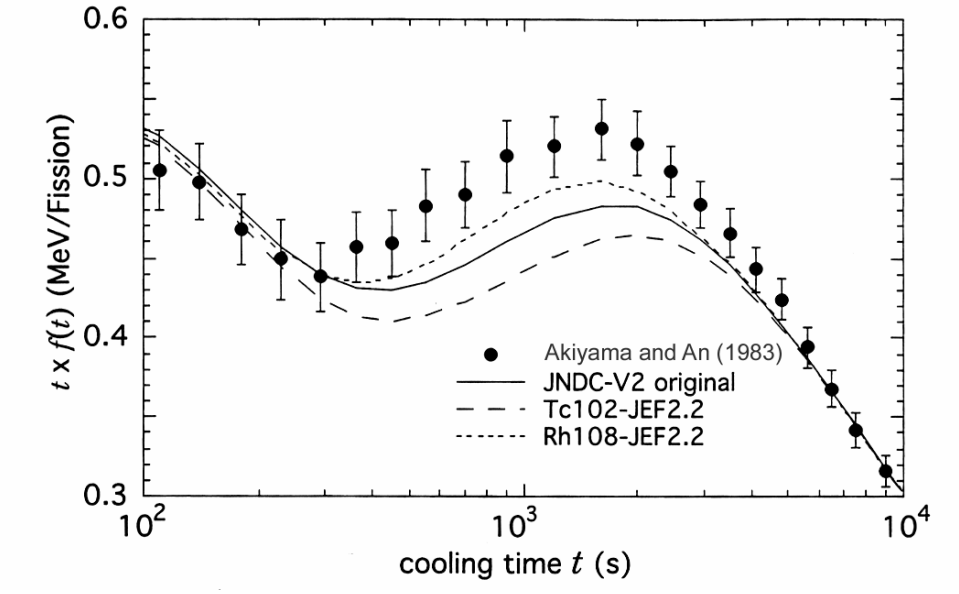

Fig. 34. ^{239}Pu γ-decay heat after a fission burst: ^{102}Tc and ^{108}Rh data adjusted in JEF-2.2 (Yoshida *et al*, 1999)

References

Akiyama, M. and An, S. (1983) Measurements of fission-product decay heat for fast reactors, pp 237-244 in Proc. Int. Conf. Nucl. Data for Science and Technology, Editor: Böckhoff, K. H., D Reidel Publishing Co., Dordrecht, Holland.

ANS (1979) American National Standard: for decay heat power in light water reactors, ANSI/ANS-5.1-1979, American Nuclear Society, USA.

Audi, G. and Wapstra, A.H. (1995) The 1995 update to the atomic mass evaluation, Nucl. Phys., **A595**, 409-480.

Audi, G., Bersillon, O., Blachot, J. and Wapstra, A.H. (1996) NUBASE: a database of nuclear and decay properties, Nucl. Instrum. Meth. Phys. Res., **A369**, 511-515.

Audi, G., Bersillon, O., Blachot, J. and Wapstra, A.H. (1997) The NUBASE evaluation of nuclear and decay properties, Nucl. Phys., **A624**, 1-124.

Avignone, F.T. and Greenwood, Z.D. (1980) Calculated spectra of antineutrinos from the fission products of ^{235}U, ^{238}U and ^{239}Pu, and antineutrino-induced reactions, Phys. Rev., **C22**, 594-605.

Backhouse, J.S. and Nichols, A.L. (1998) Assessment and evaluation of decay data for nuclear reactor applications, Appl. Radiat. Isot., **49**, 1393-1396.

Bell, M.J. (1973) Calculated radiation properties of spent plutonium fuels, Nucl. Technol., **18**, 5-14.

Bersillon, O., Blachot, J., Dean, C.J., Mills, R.W., Nichols, A.L. and Nouri, A. (2001) JEFF-3T: decay data and fission yield libraries, ND2001 Int. Conf. Nucl. Data for Science and Technology, 7-12 October 2001, Tsukuba, Japan.

Bhat, M.R. (1992) Evaluated Nuclear Structure Data File (ENDSF), pp 817-821 in Proc. Int. Conf. Nucl. Data for Science and Technology, Editor: Qaim, S.M., Springer-Verlag, Berlin, Germany; also Nuclear Data Sheets, Academic Press Inc., New York, USA.

Brady, M.C. and England, T.R. (1989) Delayed neutron data and group parameters for 43 fissioning systems, Nucl. Sci. Eng., **103**, 129-149.

Burstall, R.F. (1979) FISPIN – a computer code for nuclide inventory calculations, UK Atomic Energy Authority Report ND-R-328(R).

Burstall, R.F. and Thornton, D.E.J. (1977) Production of fission product and actinide levels in irradiated fuel and cladding, pp 416-424 in Proc. 5th Int. Conf. on Reactor Shielding, Science Press, Princeton, USA.

Clarke, R.H. (1972) FISP, a comprehensive computer program for generating fission product inventories, Health Physics, **23**, 565-572.

Crouch, E.A.C. (1977) Fission-product yields from neutron-induced fission, At. Data Nucl. Data Tables, **19**(5), 417–532.

Davis, B.R., Vogel, P., Mann, F.M. and Schenter, R.E. (1979) Reactor antineutrino spectra and their application to antineutrino-induced reactions, Phys. Rev., **C19**, 2259-2266.

Denschlag, H.O. (1997) Fission Fragment Mass, Charge and Energy Distributions, Chapter 15 in "Experimental Techniques in Nuclear Physics", Editors: Poenaru D.N. and Greiner, W., W. de Gruyter, Berlin, Germany, ISBN 3-11-014467-0.

Dickens, J.K., Love, T.A., McConnell, J.W. and Peelle, R.W. (1980) Fission-product energy release for times following thermal-neutron fission of ^{235}U between 2 and 14000 s, Nucl. Sci. Eng., **74**, 106-129.

Dickens, J.K., Love, T.A., McConnell, J.W. and Peelle, R.W. (1981) Fission-product energy release for times following thermal-neutron fission of ^{239}Pu and ^{241}Pu between 2 and 14000 s, Nucl. Sci. Eng., **78**, 126-146.

Dickens, J.K., England, T.R. and Schenter, R.E. (1991) Current status and proposed improvements to the ANSI/ANS-5.1 American National Standard for decay heat power in light water reactors, Nucl. Safety, **32**(2), 209-221.

Dunford, C.L. (1992) Evaluated Nuclear Data File ENDF/B-VI, pp 788-792 in Proc. Int. Conf. Nucl. Data for Science and Technology, Editor: Qaim, S.M., Springer-Verlag, Berlin, Germany.

Dunford, C.L. (1994) Future directions in nuclear data dissemination, pp 25-30 in Proc. Int. Conf. Nucl. Data for Science and Technology, Vol. 1, Editor: Dickens, J.K., American Nuclear Society Inc., La Grange Park, USA.

England, T.R. and Rider, B.F. (1994) Evaluation and compilation of fission product yields 1993, Los Alamos National Laboratory Report LA-UR-94-3106, ENDF-349.

Finck, Ph., Gruppelaar, H., Konieczny, M., Nordborg, C. and Rowlands, J. (1997) The JEFF project and the JEFF-3 nuclear data library, pp 1002-1007 in Proc. Int.

Conf. Nucl. Data for Science and Technology, Vol 59, Editors: Reffo, G., Ventura, A. and Grandi, C., SIF, Bologna, Italy.

Firestone, R.B., Shirley, V.S., Baglin, C.M., Chu, S.Y.F. and Zipkin, J. (1996) Table of Isotopes, 8th Edition, Vols I and II (includes CD-ROM), John Wiley and Sons Inc., New York, USA, ISBN 0-471-14918-7.

Firestone, R.B., Baglin, C.M. and Chu, S.Y.F. (1998) Table of Isotopes, 8th Edition, 1998 Update with CD-ROM, John Wiley and Sons Inc., New York, USA, ISBN 0-471-24699-9.

GNS (1990) German National Standard, decay heat power in nuclear fuels of light water reactors, DIN 25463, Beuth, Berlin, Germany.

Gönnenwein, F. (1991) Mass, Charge and Kinetic Energy of Fission Fragments, Chapter 8 in "The Nuclear Fission Process", Editor: Wagemans, C., CRC Press, Boca Raton, USA, ISBN 0-8493-5434-X.

Greenwood, R.C., Helmer, R.G., Putnam, M.H. and Watts, K.D. (1994) Beta-decay intensity distributions of fission-product isotopes measured using a total absorption gamma-ray spectrometer, pp 327-330 in Proc. Int. Conf. Nucl. Data for Science and Technology, Vol. 1, Editor: Dickens, J.K., American Nuclear Society Inc., La Grange Park, USA.

Greenwood, R.C., Putnam, M.H. and Watts, K.D. (1996) Ground-state β^--branching intensities of several fission-product isotopes measured using a total absorption γ-ray spectrometer, Nucl. Instrum. Meth. Phys. Res., **A378**, 312-320.

Greenwood, R.C., Helmer, R.G., Putnam, M.H. and Watts, K.D. (1997) Measurement of β^--decay intensity distributions of several fission-product isotopes using a total absorption γ-ray spectrometer, Nucl. Instrum. Meth. Phys. Res., **A390**, 95-154.

Hardy, J.C., Carraz, L.C., Jonson, B. and Hansen, P.G. (1977) The essential decay of pandemonium: a demonstration of errors in complex beta-decay schemes, Phys. Letts., **71B**(2), 307-310.

Helmer, R.G., Putnam, M.H., Greenwood, R.C. and Willmes, H. (1994) Methodology for the measurement of β^--decay intensity distributions from the analysis of total absorption γ-ray spectra, Nucl. Instrum. Meth. Phys. Res., **A351**, 406-422; Erratum, Nucl. Instrum. Meth. Phys. Res., **A361** (1995) 628.

Hirsch, M., Staudt, A., Muto, K. and Klapdor-Kleingrothaus, H. V. (1992) New calculations of beta-decay data of nuclei far from stability, pp 539-541 in Proc. Int.

Conf. Nucl. Data for Science and Technology, Editor: Qaim, S.M., Springer-Verlag, Berlin, Germany.

IAEA-CRP (2000) Compilation and evaluation of fission yield nuclear data, final report of a Co-ordinated Research Project, 1991-1996, IAEA-TECDOC-1168, IAEA Vienna.

Ikuta, T., Taniguchi, A., Yamamoto, H., Kawade, K. and Kawase, Y. (1994) Q_β measurements of neutron-rich isotopes in the mass region $147 \leq A \leq 152$, pp 331-333 in Proc. Int. Conf. Nucl. Data for Science and Technology, Vol. 1, Editor: Dickens, J.K., American Nuclear Society Inc., La Grange Park, USA.

Jacqmin, R., Rowlands, J., Nouri, A. and Kellett, M. (2001) Status of the JEFF-3 project, ND2001 Int. Conf. Nucl. Data for Science and Technology, 7-12 October 2001, Tsukuba, Japan.

James, M.F., Mills, R.W. and Weaver, D.R. (1991a) A new evaluation of fission product yields and the production of a new library (UKFY2) of independent and cumulative yields, Part I: methods and outline of evaluation, AEA Technology Report AEA-TRS-1015.

James, M.F., Mills, R.W. and Weaver, D.R. (1991b) A new evaluation of fission product yields and the production of a new library (UKFY2) of independent and cumulative yields, Part II: tables of measured and recommended fission yields, AEA Technology Report AEA-TRS-1018.

James, M.F., Mills, R.W. and Weaver, D.R. (1991c) A new evaluation of fission product yields and the production of a new library (UKFY2) of independent and cumulative yields, Part III: tables of fission yields with discrepant or sparse data, AEA Technology Report AEA-TRS-1019.

Johansson, P.I., Rudstam, G., Eriksen, J., Faust, H.R., Blachot, J. and Wulff, J. (1994) Average beta and gamma energies of fission products in the mass range 98-108, pp 321-323 in Proc. Int. Conf. Nucl. Data for Science and Technology, Vol 1, Editor: Dickens, J.K., American Nuclear Society Inc., La Grange Park, USA.

Katakura, J. and England, T.R. (1991) Augmentation of ENDF/B fission product gamma-ray spectra by calculated spectra, Los Alamos National Laboratory Report LA-12125-MS, ENDF-352.

Katakura, J., Yoshida, T., Oyamatsu, K. and Tachibana, T. (2001) Development of JENDL FP decay data file 2000, ND2001 Int. Conf. Nucl. Data for Science and Technology, 7-12 October 2001, Tsukuba, Japan.

Kinsey, R.R., McLane, V. and Burrows, T.W. (1994) Nuclear data services in the 90s: responding to expanding technologies and shrinking budgets, pp 745-747 in Proc. Int. Conf. Nucl. Data for Science and Technology, Vol 2, Editor: Dickens, J.K., American Nuclear Society Inc., La Grange Park, USA.

Klapdor, H.V. (1983) The shape of the beta strength function and consequences for nuclear physics and astrophysics, Prog. Part. Nucl. Phys., **10**, 131-225.

Klapdor, H.V. and Metzinger, J. (1982a) Antineutrino spectrum from the fission products of ^{239}Pu, Phys. Rev. Letts., **48**(3), 127-131.

Klapdor, H.V. and Metzinger, J. (1982b) Calculation of the antineutrino spectrum from thermal fission of ^{235}U, Phys. Letts., **112B**(1), 22-26.

Kopeykin, V.I. (1980) Electron and antineutrino spectra from fragments of fission of ^{235}U, ^{239}Pu, ^{241}Pu induced by thermal neutrons and fission of ^{238}U induced by fast neutrons, Yad. Fiz., **32**(6), 1507-1513 (English translation, Sov. J. Nucl. Phys., **32**(6), 780-783).

Madland, D.G. and England, T.R. (1977) The influence of isomeric states on independent fission product yields, Nucl. Sci. Eng., **64**, 859-865.

Mann, F.M., Dunn, C. and Schenter, R.E. (1982) Beta decay properties using a statistical model, Phys. Rev., **C25**, 524-526.

Meek, M.E. and Rider, B.F. (1972, 1974, and 1978) Compilation of fission product yields, Vallecitos Nuclear Center Reports NEDO-12154 (1972), NEDO-12154-1 (1974), NEDO-12154-2E (1978), General Electric Co., USA.

Mills, R.W. (1995) Fission product yield evaluation, PhD thesis, University of Birmingham, UK.

Nakata, H., Tachibana, T. and Yamada, M. (1995) Refinement of the gross theory of β-decay for odd-odd nuclei, Nucl. Phys., **A594**, 27-44.

Nakata, H., Tachibana, T. and Yamada, M. (1997) Semi-gross theory of nuclear β-decay, Nucl. Phys., **A625**, 521-553.

NEA-OECD (1994) JEF-2.2 radioactive decay data, NEA Data Bank JEF Report 13, OECD Publications, Paris, France.

NEA-OECD (2000) The JEF-2.2 nuclear data library, NEA Data Bank JEFF Report 17, OECD Publications, Paris, France, ISBN 92-64-17686-1.

Nguyen, H.V., Li, S., Campbell, J.M., Couchell, G. P., Pullen, D.J., Schier, W.A., Seabury, E.H., Tipnis, S.V. and England, T.R. (1997) Decay heat measurements following neutron fission of ^{235}U and ^{239}Pu, pp 835-838 in Proc. Int. Conf. Nucl. Data for Science and Technology, Vol 59, Editors: Reffo, G., Ventura, A. and Grandi, C., SIF, Bologna, Italy.

Nichols, A.L. (1991) Heavy element and actinide decay data: UKHEDD-2 data files, AEA Technology Report AEA-RS-5219.

Nichols, A.L. (1993) Activation product decay data: UKPADD-2 data files, AEA Technology Report AEA-RS-5449.

Nichols, A.L. (1996) Tables of alpha-particle emitters: energies and emission probabilities, pp 237-247 in Handbook of Nuclear Properties, Editors: Poenaru, D.N. and Greiner, W., Clarendon Press, Oxford, UK.

Nichols, A.L. (1998) Recommended decay data for short-lived fission products: status and needs, pp 100-115 in AIP Conf. Proc. Nuclear Fission and Fission-product Spectroscopy, Second International Workshop, Seyssins, France, April 1998, Editors: Fioni, G., Faust, H., Oberstedt, S. and Hambsch, F-J., American Institute of Physics, Woodbury, USA.

Nichols, A.L., Dean, C.J. and Neill, A.P. (1999a) Extension and maintenance of evaluated decay data files: UKPADD-6, AEA Technology Report AEA-5226.

Nichols, A.L., Dean, C.J., Neill, A.P. and Perry, R.J. (1999b) UKPADD-6: evaluated decay data library, AEA Technology Report AEA-5281.

NNDC (1987) ENDSF: the Evaluated Nuclear Structure Data File, Brookhaven National Laboratory Report BNL-NCS-51655.

Nordborg, C., Gruppelaar, H. and Salvatores, M. (1992) Status of the JEF and EFF projects, pp 782-787 in Proc. Int. Conf. Nucl. Data for Science and Technology, Editor: Qaim, S. M., Springer-Verlag, Berlin, Germany.

Nordborg, C. and Salvatores, M. (1994) Status of the JEF evaluated data library, pp 680-684 in Proc. Int. Conf. Nucl. Data for Science and Technology, Vol. 2, Editor: Dickens, J.K., American Nuclear Society Inc., La Grange Park, USA.

Oyamatsu, K., Ohta, H., Miyazono, T. and Sagisaka, M. (1997) Uncertainties in summation calculations of aggregate decay heat and delayed neutron emission with ENDF/B-VI, pp 756-758 in Proc. Int. Conf. Nucl. Data for Science and Technology, Vol 59, Editors: Reffo, G., Ventura, A. and Grandi, C., SIF, Bologna, Italy.

Przewloka, M., Przewloka, A., Wächter, P. and Wollnik, H. (1992a) Measurements of β-endpoint-energies using a magnetic electron separator, Z. Phys. A – Hadrons and Nuclei, **342**, 23-26.

Przewloka, M., Przewloka, A., Wächter, P. and Wollnik, H. (1992b) New Q_β-values of $^{139-146}$Cs, Z. Phys. A – Hadrons and Nuclei, **342**, 27-29.

Raman, S., Fogelberg, B., Harvey, J.A., Macklin, R.L., Stelson, P.H., Schröder, A. and Kratz, K-L. (1983) Overlapping β decay and resonance neutron spectroscopy of levels in ^{87}Kr, Phys. Rev., **C28**, 602-622; Erratum, Phys. Rev., **C29** (1984) 344.

Reich, C.W. (1987) Review of nuclear data of relevance for the decay heat problem, pp 107-118 in Proc. Specialists' Meeting on Data for Decay Heat Calculations, Studsvik, Sweden, 7-10 September 1987, NEACRP-302L, NEANDC-245U, NEA-OECD, Paris, France.

Reus, U. and Westmeier, W. (1983) Catalog of gamma rays from radioactive decay, At. Data Nucl. Data Tables, **29**(1, 2), 1-406.

Rider, B.F. (1981) Compilation of fission product yields, Vallecitos Nuclear Center Report NEDO-12154-3C, General Electric Co., USA.

Rudstam, G. and England, T.R. (1990) Test of pre-ENDF/B-VI decay data and fission yields, Los Alamos National Laboratory Report LA-11909-MS.

Rudstam, G., Johansson, P.I., Tengblad, O., Aagaard, P. and Eriksen, J. (1990) Beta and gamma spectra of short-lived fission products, At. Data Nucl. Data Tables, **45**(2), 239-320.

Rudstam, G., Aleklett, K. and Sihver, L. (1993) Delayed-neutron branching ratios of precursors in the fission product region, At. Data Nucl. Data Tables, **53**(1), 1-22.

Rytz, A. (1991) Recommended energy and intensity values of alpha particles from radioactive decay, At. Data Nucl. Data Tables, **47**(2), 205-239.

Schmittroth, F. (1976) Uncertainty analysis of fission-product decay-heat summation methods, Nucl. Sci. Eng., **59**, 117-139.

Schmittroth, F. and Schenter, R.E. (1977) Uncertainties in fission product decay-heat calculations, Nucl. Sci. Eng., **63**, 276-291.

Schreckenbach, K., Faust, H.R., von Feilitzsch, F., Hahn, A.A., Hawerkamp, K. and Vuilleumier, J.L. (1981) Absolute measurement of the beta spectrum from ^{235}U fission as a basis for reactor antineutrino experiments, Phys. Letts., **99B**(3), 251-256.

Storrer, F. (1994) Test of JEF-2 decay data and fission yields by means of decay heat calculations, pp 819-821 in Proc. Int. Conf. Nucl. Data for Science and Technology, Vol 2, Editor: Dickens, J.K., American Nuclear Society Inc., La Grange Park, USA.

Su Zongdi, Ge Zhigang, Zhang Limin, Yu Ziqiang, Zuo Yixin, Huang Zhongfu and Liu Jianfeng (1994) Chinese evaluated nuclear parameter library (CENPL), pp 712-714 in Proc. Int. Conf. Nucl. Data for Science and Technology, Vol 2, Editor: Dickens, J.K., American Nuclear Society Inc., La Grange Park, USA.

Su Zongdi, Ge Zhigang, Sun Zhengjun, Zhang Limin, Huang Zhongfu, Dong Liaoyuan, Liu Jianfeng, Zuo Yixin, Yu Ziqiang, Zhang Xiaocheng, Chen Zhenpeng and Ma Gonggui (1997) Chinese evaluated nuclear parameter library (CENPL) and studies on corresponding model parameters, pp 907-909 in Proc. Int. Conf. Nucl. Data for Science and Technology, Vol 59, Editors: Reffo, G., Ventura, A. and Grandi, C., SIF, Bologna, Italy.

Tachibana, T., Yamada, M. and Yoshida, Y. (1990) Improvement of the gross theory of β-decay, II: one-particle strength function, Prog. Theor. Phys., **84**(4), 641-657.

Takahashi, K., Yamada, M. and Kondoh, T. (1973) Beta-decay half-lives calculated on the gross theory, At. Data Nucl. Data Tables, **12**(1), 101-142.

Tasaka, K., Katakura, J., Ihara, H., Yoshida, T., Iijima, S., Nakasima, R., Nakagawa, T. and Takano, H. (1990) JNDC nuclear data library of fission products - second version, Japan Atomic Energy Research Institute Report JAERI 1320.

Tasaka, K., Katoh, T., Katakura, J., Yoshida, T., Iijima, S., Nakasima, R. and Nagayama, S. (1991) Recommendation on decay heat power in nuclear reactors, J. Nucl. Sci. Technol., **28**(12), 1134-1142.

Tobias, A. (1978) FISP5 – an extended and improved version of the fission product inventory code FISP, Central Electricity Generating Board Report RD/B/N4303.

Tobias, A. (1980) Decay heat, Prog. Nucl. Energy, **5**, 1-93.

Vogel, P., Schenter, G.K., Mann, F.M. and Schenter, R.E. (1981) Reactor antineutrino spectra and their application to antineutrino-induced reactions, Phys. Rev., **C24**, 1543-1553.

Wagemans, C. (1991) Ternary Fission, Chapter 12 in "The Nuclear Fission Process", Editor: Wagemans, C., CRC Press, Boca Raton, USA, ISBN 0-8493-5434-X.

Wahl, A.C. (1987) Nuclear-charge distribution and delayed-neutron yields for thermal-neutron-induced fission of ^{235}U, ^{233}U, ^{239}Pu and ^{241}Pu, and the fast-neutron-

induced fission of ^{238}U, pp 9-19 in Proc. Specialists' Meeting on Data for Decay Heat Calculations, Studsvik, Sweden, 7-10 September 1987, NEACRP-302L, NEANDC-245U, NEA-OECD, Paris, France.

Wahl, A.C. (1988) Nuclear-charge distribution and delayed-neutron yields for thermal-neutron-induced fission of ^{235}U, ^{233}U and ^{239}Pu, and for spontaneous fission of ^{252}Cf, At. Data Nucl. Data Tables, **39**(1), 1–156.

Wang Dao and Zhang Dongming (1987) Evaluation of fission product yields, pp 37-68 in Proc. Specialists' Meeting on Data for Decay Heat Calculations, Studsvik, Sweden, 7-10 September 1987, NEACRP-302L, NEANDC-245U, NEA-OECD, Paris, France.

Westmeier, W. and Merklin, A. (1985) Catalog of alpha particles from radioactive decay, Physik Daten/Physics Data, 29-1, Fachinformationszentrum Energie, Physik-Mathematik GmbH, Karlsruhe, Germany.

Wünsch, K.D., Decker, R., Wollnik, H., Münzel, J., Siegert, G., Jung, G. and Koglin, E. (1978) Precision beta endpoint energy measurements of rubidium and caesium fission products with an intrinsic Ge-detector, Z. Phys., **A288**, 105-106.

Yoshida, T. (1977) Estimation of nuclear decay heat for short-lived fission products, Nucl. Sci. Eng., **63**, 376-390.

Yoshida, T. and Katakura, J. (1986) Calculation of the delayed gamma-ray energy spectra from aggregate fission product nuclides, Nucl. Sci. Eng., **93**, 193-203.

Yoshida, T. and Nakasima, R. (1981) Decay heat calculations based on theoretical estimation of average beta- and gamma-energies released from short-lived fission products, J. Nucl. Sci. Technol., **18**(6), 393-407.

Yoshida, T. and Tachibana, T. (2000) Theoretical treatment of the asymptotic behavior of fission product decay heat toward very short cooling time, J. Nucl. Sci. Technol., **37**(6), 491-497.

Yoshida, T., Oyamatsu, K. and Katakura, J. (1997) On a possible level missing in aggregate fission products from the point of decay heat calculations, pp 829-831 in Proc. Int. Conf. Nucl. Data for Science and Technology, Vol 59, Editors: Reffo, G., Ventura, A. and Grandi, C., SIF, Bologna, Italy.

Yoshida, T., Tachibana, T., Storrer, F., Oyamatsu, K. and Katakura, J. (1999) Possible origin of the gamma-ray discrepancy in the summation calculations of fission product decay heat, J. Nucl. Sci. Technol., **36**(2), 135-142.

APPENDIX A

NUCLEAR DATA: COMPUTERISED INFORMATION SYSTEMS

1. INTERNATIONAL INFORMATION SYSTEMS

1.1 Network of Nuclear Data Centres

The Nuclear Data Centres Network is a world-wide co-operation of nuclear data centres established under the auspices of the International Atomic Energy Agency (IAEA) to co-ordinate the collection, compilation and dissemination of nuclear data at an international level. Nearly all nuclear data required for energy, non-energy nuclear applications and basic science are covered, including nuclear cross sections, fission yields and decay data. The Network consists of four 'core' Nuclear Data Centres, and a group of regional, national and/or specialised data centres (second group compiles data from a restricted geographical region and/or for special data types (e.g., nuclear structure data, charged particle or photon induced reactions)). Essential links have been forged through the Network to establish communications between the producers and users of nuclear data. A brief summary is given below of the various communication links for nuclear data users, with listings of standard and Internet addresses.

1.1.1 Data centres

The four main data centres compile and exchange data in the CINDA and EXFOR systems, and maintain and exchange evaluated data files for nuclear reaction, structure and decay data. Evaluated data files include general purpose files as well as specialised data files (e.g., for fission products, activation, thermonuclear fusion, and dosimetry). These data centres compile and disseminate data to customers over a defined geographical area:

National Nuclear Data Centre: United States of America, and Canada;
Nuclear Energy Agency Data Bank: OECD countries in Western Europe and Japan;
Russian Nuclear Data Centre: former Soviet countries in Europe and Asia;
IAEA Nuclear Data Section: all remaining countries in Eastern Europe, South and Central America, Asia, Africa and Australasia.

The reader can contact the responsible data centre (in their relevant geographical area) for further information, or retrieve data directly via the Internet using one of the addresses given below:

Centre name:	***National Nuclear Data Centre***	***Nuclear Energy Agency Data Bank***
Contact:	P. Oblozinsky	C. Nordborg
Address:	Bldg. 197D Brookhaven National Laboratory PO Box 5000 Upton, NY 11973-5000 USA	Le Seine St-Germain 12, boulevard des Iles 92130 Issy-les Moulineaux France
Telephone:	+1 516 344 2902	+33 1 4524 1090
Fax:	+1 516 344 2806	+33 1 4524 1110
E-mail:	nndc@bnl.gov	nea@nea.fr
World Wide Web:	http://www.nndc.bnl.gov	http://www/nea.fr
FTP file transfer:	bnlnd2.dne.bnl.gov username: bnlndc (no password required)	FTP file transfer Username: open Password: neadb

Centre name:	***Nuclear Data Section***	***Russian Nuclear Data Centre***
Contact:	A.L. Nichols	V.N. Manokhin
Address:	IAEA Wagramer Strasse 5, PO Box 100 A-1400 Vienna Austria	Leipunsky Institute of Physics and Power Engineering Centr Jadernykh Dannykh Ploschad Bondarenko 249 020 Obninsk Kaluga Region Russia
Telephone:	+43 1 2600 21709	+7 084 399 8982
Fax:	+43 1 26007	+7 095 883 3112/7 095 230 2326
E-mail:	services@iaeand.iaea.org	manokhin@ippe.rssi.ru
World Wide Web:	http://www-nds.iaea.org	http://rndc.ippe.obninsk.ru
FTP file transfer	username: ndsopen	acjd.ippe.rssi.ru username: cjd

1.2 EXFOR

EXFOR is the **EX**change **FOR**mat used by the Data Centres to exchange compiled experimental data. Designed initially for neutron reaction data, the format is flexible enough to be extended to the compilation of a great variety of data types: neutron, charged-particle and photon-induced reactions, as well as spontaneous fission data. More details can be obtained in brochures from the Data Centres or directly from the appropriate Web pages.

The flexibility of the format as well as the possibility to store all experimental details for evaluator access make EXFOR ideal for the worldwide compilation of experimental data. Furthermore, all the fission yield data from the Meek and Rider files that were missing in EXFOR have been converted and added to the EXFOR data base, which makes the latter almost complete with regard to fission yields.

1.3 CINDA

The **C**omputer **I**ndex of **N**eutron **DA**ta (CINDA) contains bibliographic references to measurements, calculations, reviews and evaluations of neutron reaction and spontaneous fission data. Proposed extensions include charged-particle and photon-induced reaction data. CINDA is also the index for EXFOR entries and the evaluated data libraries available from the Data Centres. Information contained in the CINDA file is available as annually-updated books, and by direct retrievals through the Internet.

1.4 INIS

The **I**nternational **N**uclear **I**nformation **S**ystem (INIS) is a co-operative, decentralised information system which contains bibliographical information on the peaceful uses of nuclear science and technology, as well as on economic, environmental and health aspects of nuclear and other energy sources. An entry into the INIS data base consists of several pieces of information: title of publication, author(s) and reference citation, an abstract, if available, and sets of descriptors, plus some information on the origin and availability of the published information. Searches of the data base can be made either by bibliographic information (author, reference) or by keywords (to be found in title, abstract or descriptors). The information is provided by INIS Liaison Officers in several international organisations as well as to the IAEA Member States, who also have the right to disseminate that information within their restricted areas (as laid down in agreements).

All of the collected information is published by the IAEA on a regular basis in the *INIS Atomindex*, which is available as hard copy, microfiche, magnetic tapes and cartridges, and CD-ROM (INIS services are not cost-free). Further information can be obtained from:

IAEA INIS Section
PO Box 100
A-1400 Vienna
Austria

Telephone:	+43 (1) 2600 22842
Fax:	+43 (1) 26007 22882
E-mail:	INIS.CentralServicesUnit@iaea.org
Web Home Page:	http://www.iaea.org/inis/inis.htm
subscription to INIS Database:	http://www.iaea.org/inis/inisdbm.htm

2. OTHER SYSTEMS AND RETRIEVAL PROGRAMS

A brief summary is given of some of the on-line services (mainly in Europe and the USA), user-friendly PC programs and CD ROMs available to search for, display and retrieve nuclear data:

- ***evaluated nuclear data files*** - include fission yields, nuclear structure, mass, radioactive decay and cross-section data,

- ***scientific works published recently in the literature*** – e.g., NSR (Nuclear Science References, a computer file of indexed references maintained by NNDC, Brookhaven National Laboratory, USA); INIS (International Nuclear Information System) operated by the International Atomic Energy Agency, Vienna, Austria; references system for the NUBASE evaluation (Atomic Mass Data Centre, Orsay, France), with regular updates accessible through the Internet.

Each of these tools may be rapidly used by reactor physicists to access evaluated data (e.g., ENSDF, AME, NUBASE, ENDF/B and JEF), and by nuclear data evaluators as a source of information on new measurements. Such on-line services and PC programs are also extremely useful for research and educational purposes.

The list of accessible data libraries outlined below is not complete – there are numerous special purpose files dedicated to more specific applications that have not been included (e.g., NUCLÉIDE - CD-ROM reference files of decay data for radiometrology (Bé *et al*, 1996); BANDRRI - CD-ROM reference files of decay data for dosimetry applications (Los Arcos *et al*, 2000); CD-ROM containing gamma-ray spectrum catalogues based on the studies of Heath (1974), and expanded by Helmer *et al* (2000)). Many of these specialised data files can be applied to the needs of nuclear medicine, dosimetry and detector calibration, and are accessible through the Internet.

2.1 Software to Display Nuclear Data

Some of the software described below is available on CD-ROM or floppy disk, as well as through the Internet:

2.1.1 US Nuclear Data Network

- CD-ROM version 1.0 of the 8th Edition of the Table of Isotopes (TOI), with Adobe Acrobat viewer to display the hypertext data - released in March 1996 by Richard B. Firestone (LBL), CD-ROM Editor: S.Y. Frank Chu, Editor: Virginia S. Shirley, John Wiley & Sons, Inc. (ISBN 0-471-14918-7 Volume set, ISBN 0-471-16405-5 CD-ROM). Updated in 1998:ISBN 0-471-24699-9 Volume set,ISBN 0-471-29090-4.

Five folders are available on this CD-ROM corresponding to the following:

Table of Isotopes,
Table of Superdeformed Nuclear Bands and Fission Isomers,
Tables of Atoms, Atomic nuclei and Subatomic Particles,
Description of Nuclear Structure and Decay Data Bases,
ENSDF Manual.

- CD-ROM entitled: Nuclear Data and References, PC Applications for Nuclear Science, PCNudat and Papyrus^{TM} NSR by L. P. Ekström, R. R. Kinsey and E. Browne.

  For further information:

  a) contact in the USA:
  Edgardo Browne (email: ebrowne@lbl.gov)

  contact for PCNudat:
  Robert Kinsey (email: kinsey@bnl.gov)

  b) US Nuclear Data Network (USNDN) Home Page via Internet:
  http://www.nndc.bnl.gov/usndp

- EXFOR CD-ROM, see Website: ***http://www-nds.iaea.or.at/***

- MacNuclide project at the San Jose State University.

2.1.2 University of Lund, Sweden

Lund Nuclear Data WWW Service at:
http://nucleardata.nuclear.lu.se/nucleardata/

As well as the normal data services, the Lund Website includes the Isotope Explorer 2.0 program, which can interactively access and display nuclear data and search for literature references. Developed by:

S. Y. F. Chu[a], H. Nordberg[b], R. B. Firestone[a], and L. P. Ekström[b]
[a] Isotopes Project, LBNL, Berkeley
[b]Department of Physics, University of Lund

For further information on the Isotope Explorer:
http://ie.lbl.gov/isoexpl/isoexpl.htm

For further information on the Lund Nuclear Data Centre and Services:

Contact: Peter Ekström
Address: Department of Physics
University of Lund
Box 118, Office: B201
SE-221 00 Lund
Sweden

Telephone: +46 46 22 27647
Mobile phone: +46 073 995 7984
Fax: +46 46 22 24709
E-mail: peter.ekstrom@nuclear.lu.se

Visiting address: Professorsgatan 1, Internal post: Hämtställe 14

2.1.3 Atomic Mass Data Centre, Paris - Orsay

Website of the Atomic Mass Data Centre (AMDC): ***http://csnwww.in2p3.fr/amdc***

AMDC is devoted to nuclear and mass spectroscopic data. The Centre produces a newsletter that describes on-going experimental, theoretical and evaluation work on the atomic masses, and feedback on important conferences. Furthermore, the 1995 update of the atomic mass evaluation by G. Audi and A. H. Wapstra (1995), and the NUBASE data evaluation by G. Audi *et al.* (1997) can be displayed by the NUCLEUS PC program or by the 'jvNubase JAVA applet' on the Web. NUBASE contains the main nuclear and decay properties of the known nuclides in their ground and isomeric states as derived from ENSDF, the Atomic Mass Evaluation, and a critical compilation of recent literature.

For further information, contact Georges Audi:

Address: Atomic Mass Data Centre, CSNSM (IN2P3-CNRS)
Batiment 108
91405 Orsay Campus
France

Telephone: +33 1 6915 5223
Fax: +33 1 6915 5268
E-mail: audi@csnsm.in2p3.fr

2.1.4 OECD/NEA Data Bank, Paris

NEA Data Bank has developed and released the JEF-PC program, in co-operation with CSNSM-Orsay and the University of Birmingham. This jointly-developed program generates a "Chart of the Nuclides" format for the display of data from a number of evaluated libraries, including the Joint Evaluated File (JEF-2.2), ENDF/B-VI.4 and JENDL-3.2 supplied on CD-ROM as part of the package. Three internal modules are devoted to radioactive decay, fission product yields and cross-section data (Konieczny *et al.*, 1997). Evaluated and experimental cross-section data can also be plotted and compared.

JANIS (JAva Nuclear data Information System) is in the process of being developed by the NEA Data Bank on the basis of user feed-back from JEF-PC. All earlier features of JEF-PC have been reproduced, along with several others (e.g., energy and angular distribution, and display of resonance parameters). This new software is more flexible and user-friendly, and is undergoing preliminary tests (Nouri *et al.*, 2001).

Contact the NEA Nuclear Data Service Section for further information:

Mark A Kellett or Ali Nouri:
Address: OECD Nuclear Energy Agency
Le Seine St-Germain
12, boulevard des Iles
92130 Issy-les-Moulineaux
France

Tel:	+33 1 4524 1085	+33 1 4524 1084
Fax:	+33 1 4524 1110	+33 1 4524 1110
E-mail:	kellett@nea.fr	nouri@nea.fr

NEA Data Bank Website: ***http://www.nea.fr/html/databank/***

More information on JANIS is available on the Web at:
http://www.nea.fr/html/dbdata/

2.1.5 Institute for Transuranium Elements (ITU), Karlsruhe, Germany

'Nuclides 2000: an Electronic Chart of the Nuclides' has been developed and released as a CD-ROM by ITU, Karlsruhe. The Nuclide explorer gives access to the radionuclide decay data from JEF-2.2, using either a "Chart of the Nuclides' or Segrè display (Magill, 1999). Derived data include activities, gamma dose rates and annual limits of intake. There are additional features to this package, including background articles that describe various aspects of decay data and related historical publications.

'Nuclides 2000' allows the user to carry out decay calculations: starting from an initial mass or activity, the user can determine the masses, activities, radiotoxicities, gamma dose rates etc for all daughters at any time.

Contact ITU, Karlsruhe for further information:

Joseph Magill
Address: Institute for Transuranium Elements
Postfach 2340
D-76125 Karlsruhe
Germany

Tel: +49 7247 951366
Fax: +49 7247 951591
E-mail: magill@itu.fzk.de

More information on 'Nuclides 2000' is available on the Web (including direct purchase): ***http://www.nuclides.net/***

3. NUCLEAR DATA CENTRES IN EUROPE AND THE USA

3.1 National Nuclear Data Centre (NNDC), Brookhaven National Laboratory (BNL), USA:

- Anonymous FTP server
  Address: ftp.nndc.bnl.gov
  User name: anonymous
  Password: your E-mail address

- Terminal Access (using Telnet)
  Address: telnet.nndc.bnl.gov (IP address: 130.199.112.132)
  User name: NNDC (no password)
  Enter the code when prompted for assigned authorization code. New users may adopt the user name GUEST for a time-limited trial, and can apply for registration by using an electronic form which appears on exiting from the system.

- Home Page through the World Wide Web: ***http://www.nndc.bnl.gov/***

  Nuclear Data and Programs:
  NSR, ENSDF, NUDAT, MIRD, PHYSCO, CINDA, CSISRS/EXFOR and ENDF.

  E-mail for further information: services@bnlnd2.dne.bnl.gov

NNDC Web effort co-ordinator: Thomas W. Burrows
NNDC On-line service co-ordinator: Victoria McLane

Address: On-line Data Service
National Nuclear Data Centre
Brookhaven National Laboratory
Upton, NY 11973
USA

Tel: +1 516-344-2901
Fax: +1 516-344-2806
E-mail: NNDC@BNL.GOV

3.2 IAEA Nuclear Data Section (NDS), Austria

- Services are available through the Web at: ***http://www-nds.iaea.org***

- Telnet access (NDIS - Nuclear Data Information System):
  Address: iaeand.iaea.or.at
  User name: iaeands (no password).
  Enter the code, at the prompt for an assigned authorization code. New users may adopt the user-name GUEST for a time-limited trial, and can apply for registration using an electronic form which appears on exiting from the system.

  Nuclear Data and Programs are basically the same as for US NNDC (see above).

- FTP server:
  Address: iaeand.iaea.or.at
  User names: ANONYMOUS for FTP file transfer
  FENDL2 for FENDL-2.0 files
  RIPL for RIPL files

For further information: Nuclear Data Section
International Atomic Energy Agency
PO Box 100
A-1400 Vienna
Austria

Tel: +43-1 2600-21710
Fax: +43-1 26007
E-mail: services@iaeand.iaea.org

3.3 Nuclear Energy Agency (NEA) Data Bank

NEA On-line Services are open to registered scientific users in the seventeen member states of the NEA Data Bank. New users register via the on-line form at Web address www.nea.fr The site offers access to a wide range of databases (ENSDF, NSR, NUDAT, as well as experimental data (EXFOR), bibliographic reference to neutron induced reactions (CINDA), evaluated data files (including JEF, ENDF/B and JENDL) and the NEA Thermochemical Data Base (TDB)). All data libraries have on-line search and download facilities.

On-line services can be accessed through the Web at the following address:
http://www.nea.fr/

For further information, contact: Pierre Nagel - Network & On-line-services
Telephone: +33 1 4524 1082
E-mail: nagel@nea.fr

References

Audi, G. and Wapstra, A. H. (1995) The 1995 update to the atomic mass evaluation, Nucl. Phys., **A595**, 409-480.

Audi, G., Bersillon, O., Blachot, J. and Wapstra, A. H. (1997) The NUBASE evaluation of nuclear and decay properties, Nucl. Phys., **A624**, 1-124.

Bé, M. M., Duchemin, B. and Lamé, J. (1996) An interactive database for decay data, Nucl. Instrum. Meth. Phys Res., **A369**, 523-526.

Heath, R. L. (1974) Gamma-ray spectrum catalogue, AEC Report ANC-1000-2.

Helmer, R. G., Gehrke, R. J., Davidson, J. R. and Mandler, J. W. (2000) Scientists, spectrometry and gamma-ray spectrum catalogues, 1957-2007, J. Radioanal. Nucl. Chem., **243**, 109-117.

Konieczny, M., Weaver, D. R., Hale, D., Baynham, I., Tagziria, H. and Weaver, R. A. (1997) JEF-PC Version 2.0: a PC program for viewing evaluated and experimental data, pp 1063-1065 in Proc. Int. Conf. Nucl. Data for Science and Technology, Vol. 59, Editors: Reffo, G., Ventura, A. and Grandi, C., SIF, Bologna, Italy.

Los Arcos, J. M., Bailador, A., Gonzalez, A., Gonzalez, C., Gorostiza, C., Ortoz, F., Sanchez, E., Shaw, M. and Williart, A. (2000) The Spanish National Reference Database for Ionizing Radiations (BANDRRI), Appl. Radiat. Isot., **52**, 335-340.

Magill, J. (1999) Nuclides 2000: an electronic Chart of the Nuclides – user's guide, EUR 18737 EN, Office for Official Publications of the European Communities, Luxembourg, ISBN 92-828-6512-6.

Nouri, A., Nagel, P., Amah, F. Le C., Cunin, C., Patrouix, J., Rioland, O., Soppera, N. and Taton, B. (2001) JANIS: new software for nuclear data services, ND2001 Int. Conf. Nucl. Data for Science and Technology, 7-12 October 2001, Tsukuba, Japan.

APPENDIX B

B. 1 FISSION PRODUCTS AND DECAY CHAINS

B. 2 ACTINIDES AND DECAY CHAINS

<u>Health warning</u>: all data within this review (and particularly Appendix B) are subject to change.

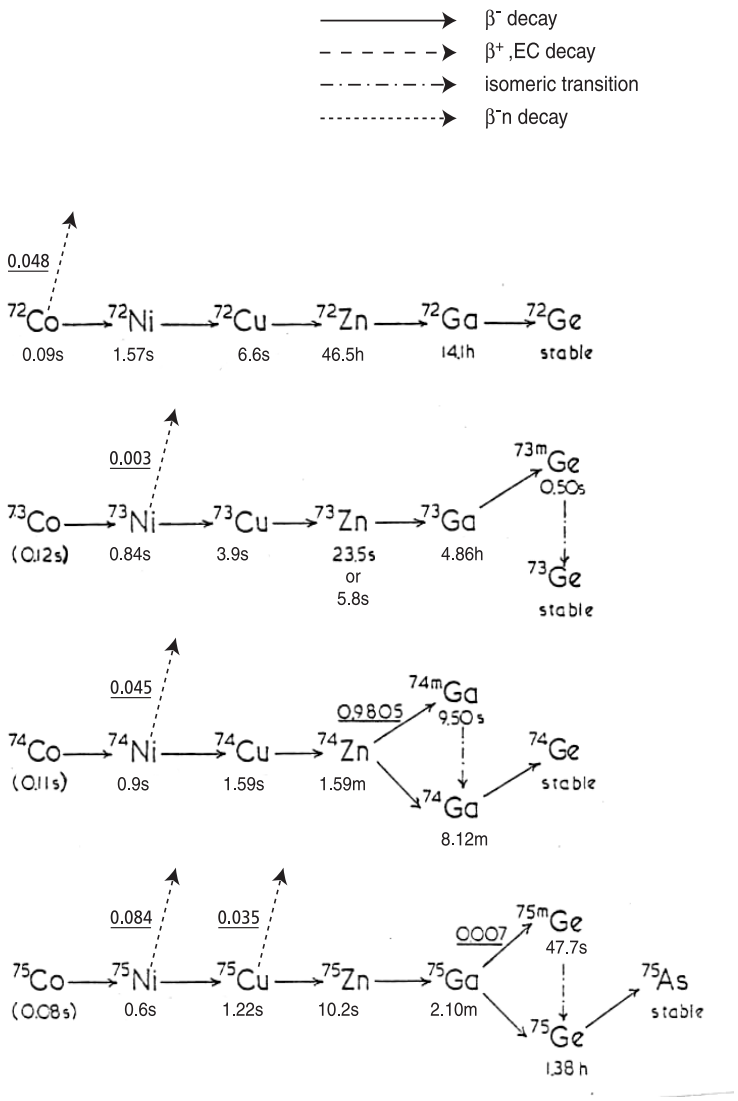

B.1.1 Fission products and decay chains

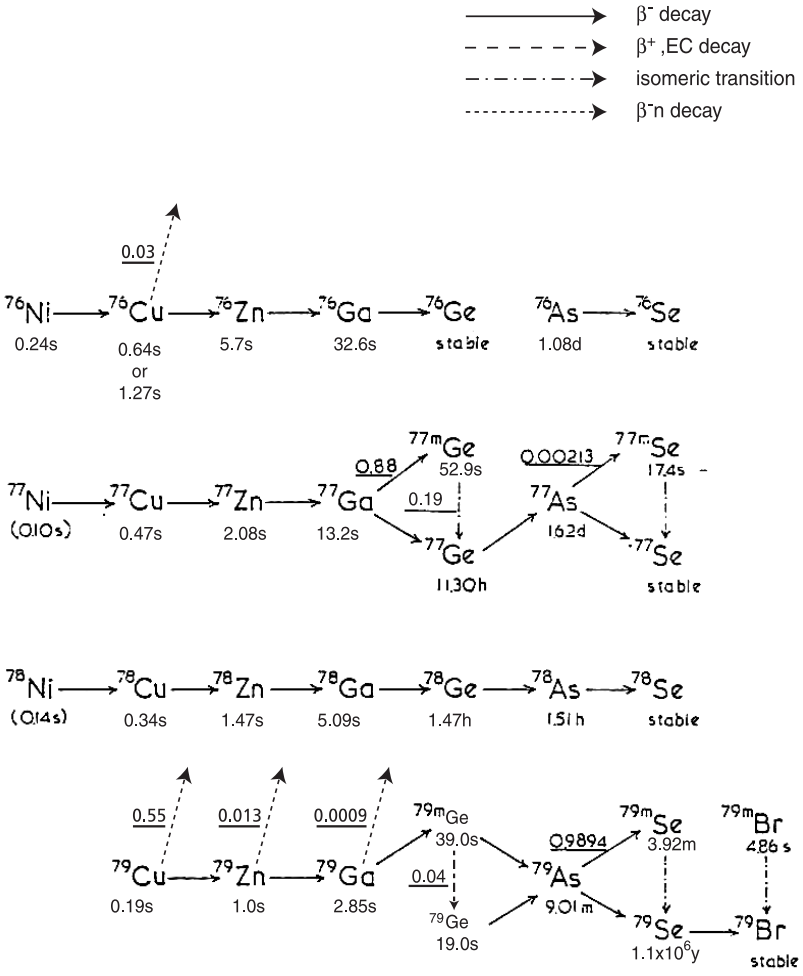

B.1.2 Fission products and decay chains

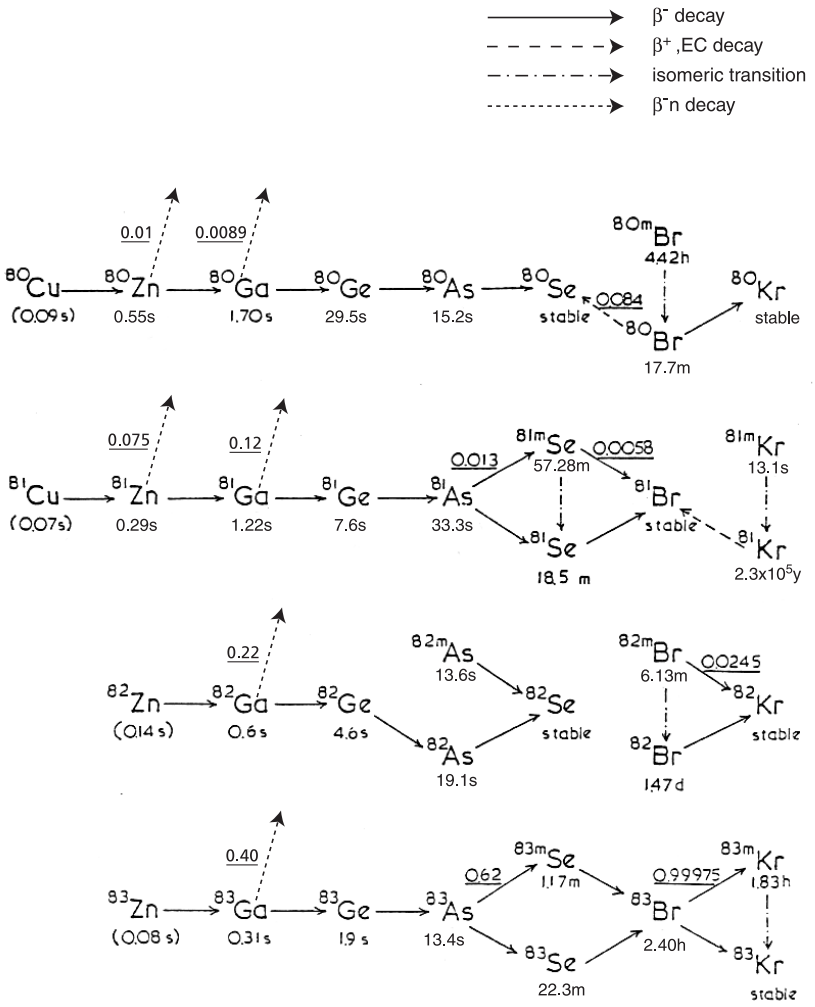

B.1.3 Fission products and decay chains

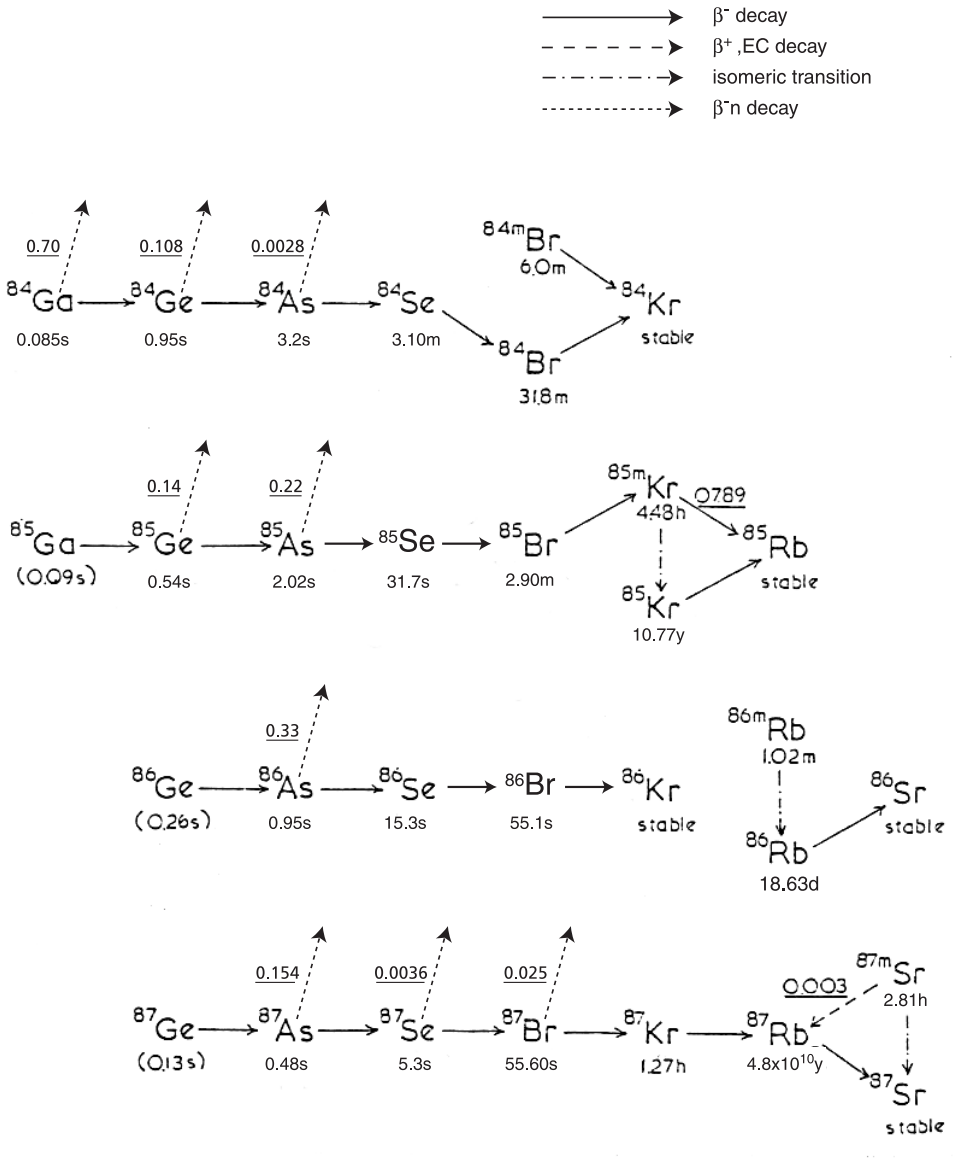

B.1.4 Fission products and decay chains

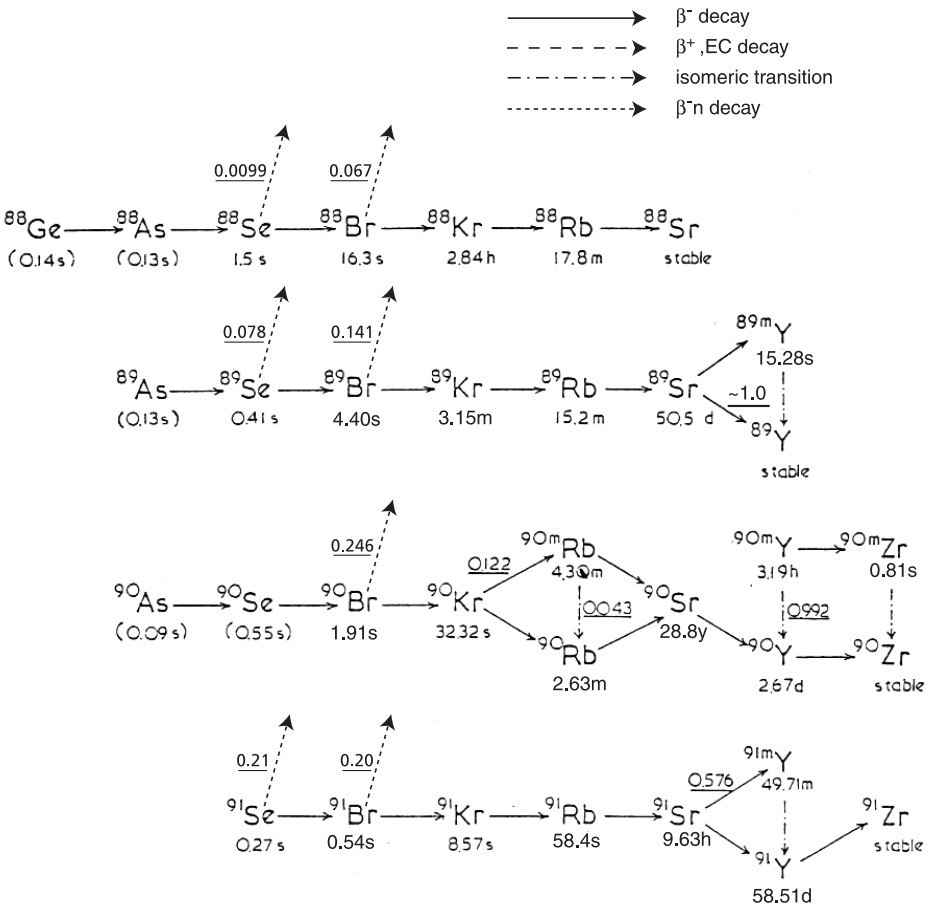

B.1.5 Fission products and decay chains

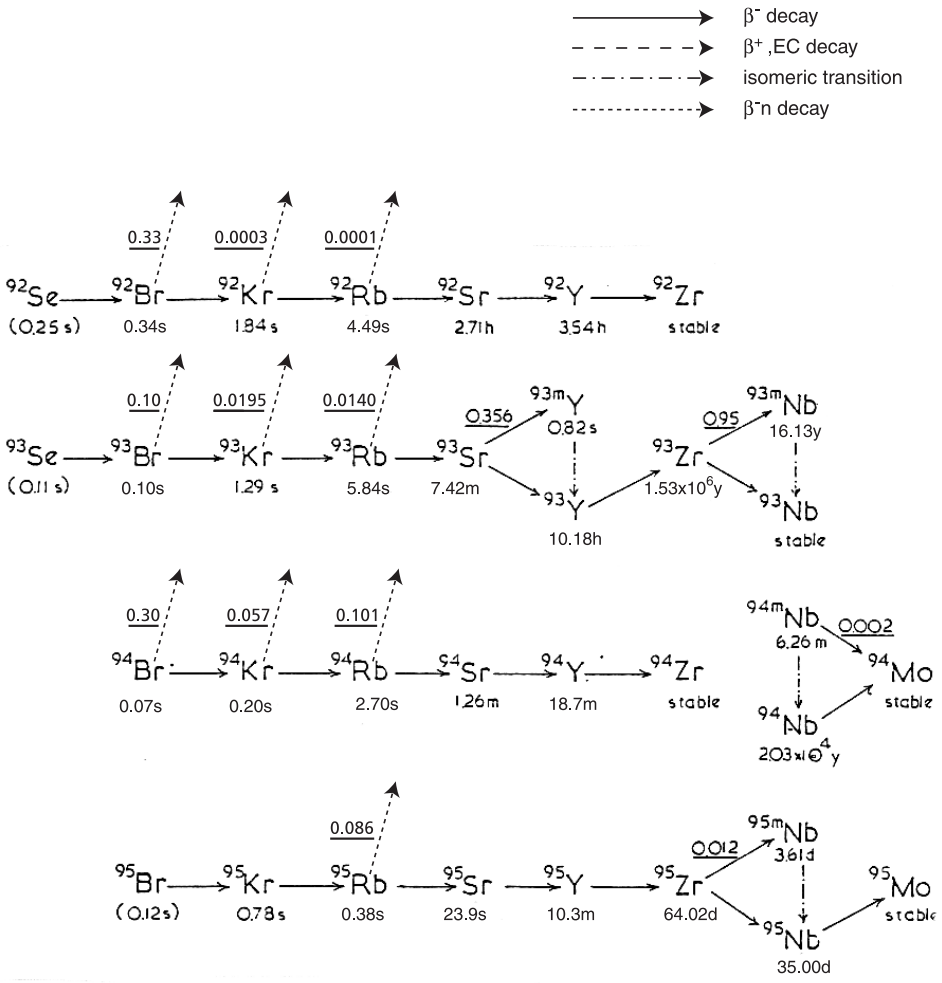

B.1.6 Fission products and decay chains

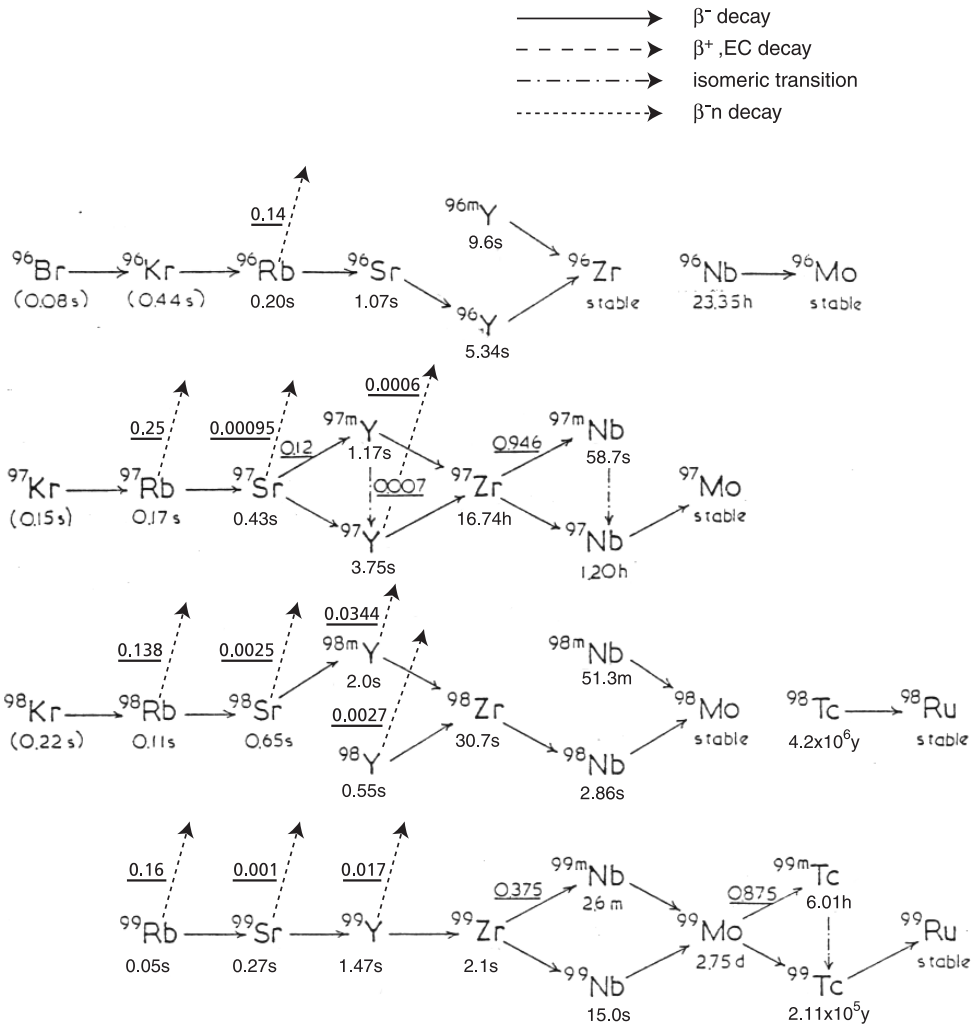

B.1.7 Fission products and decay chains

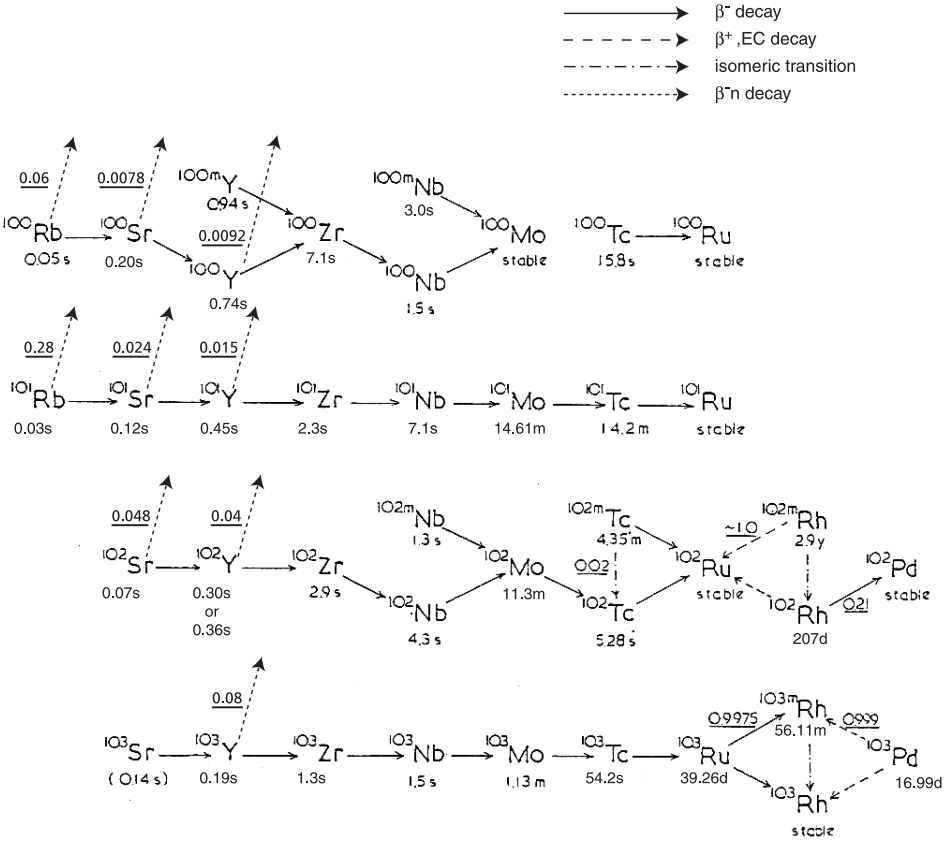

B.1.8 Fission products and decay chains

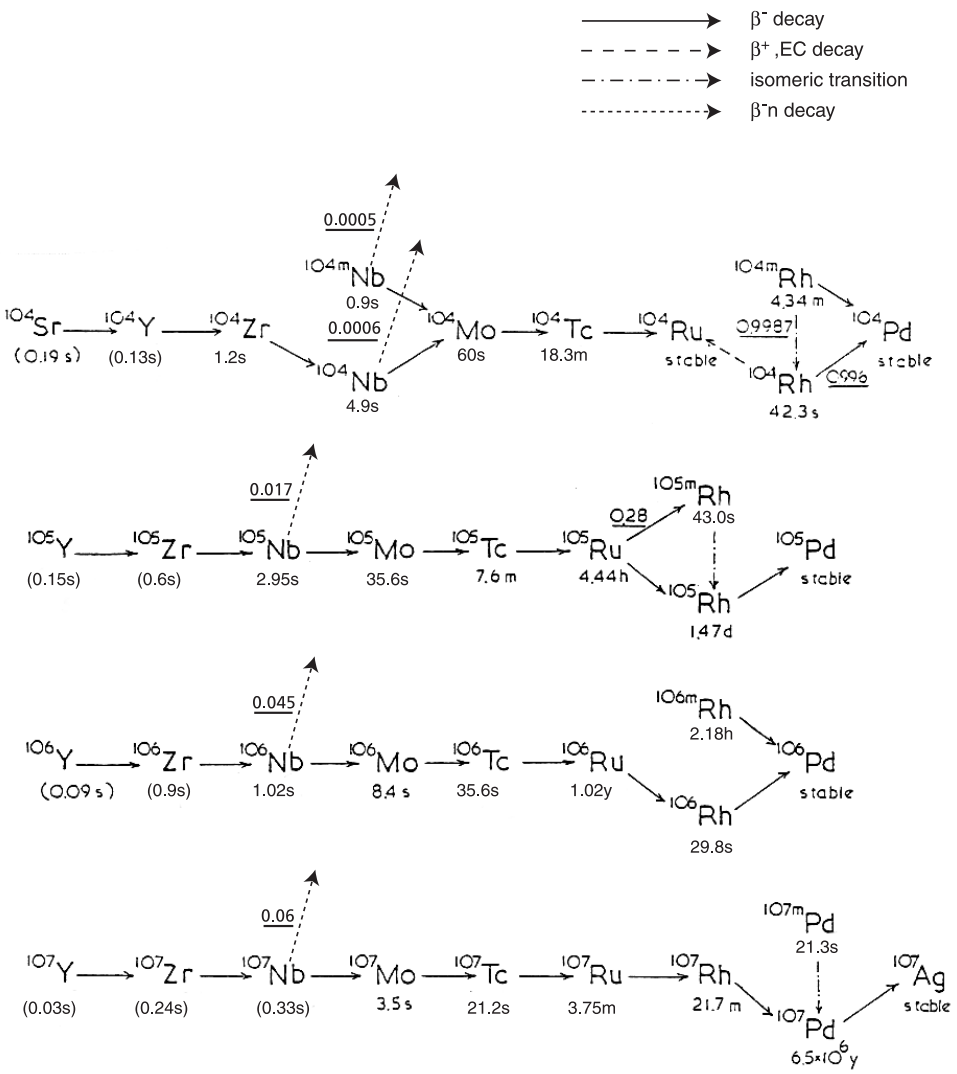

B.1.9 Fission products and decay chains

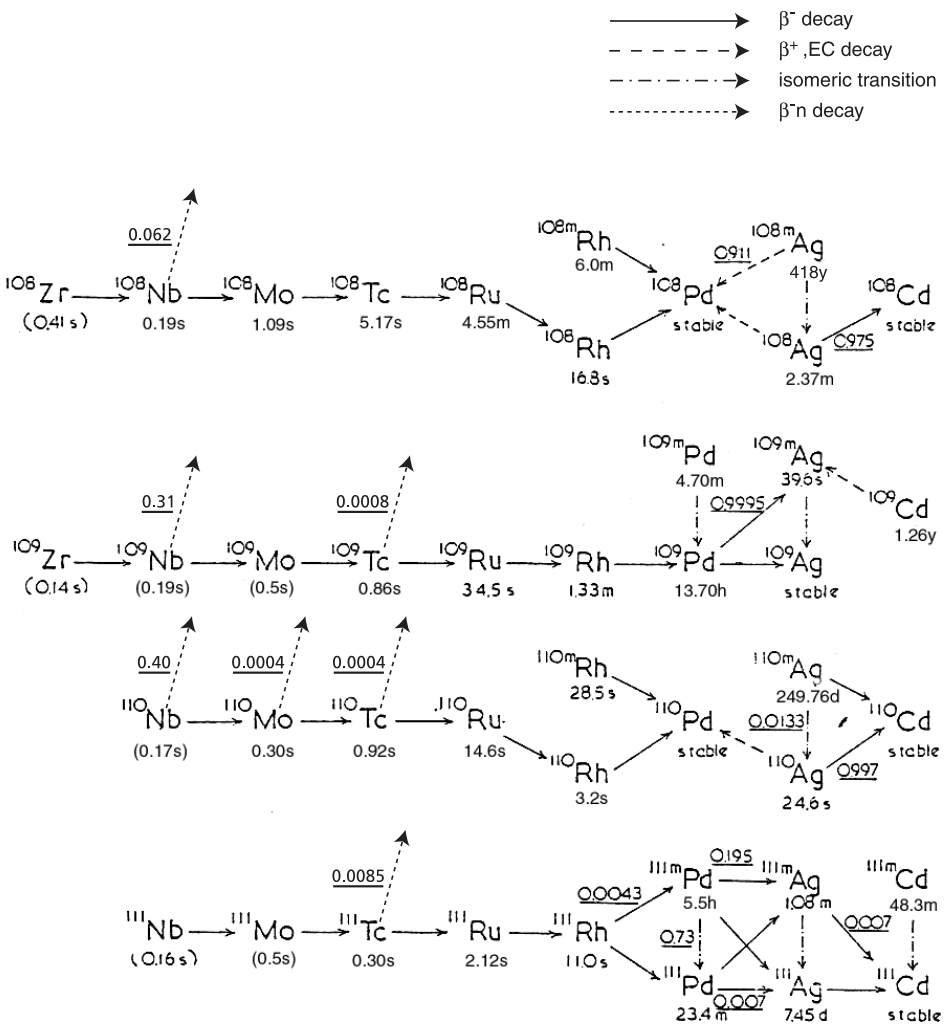

B.1.10 Fission products and decay chains

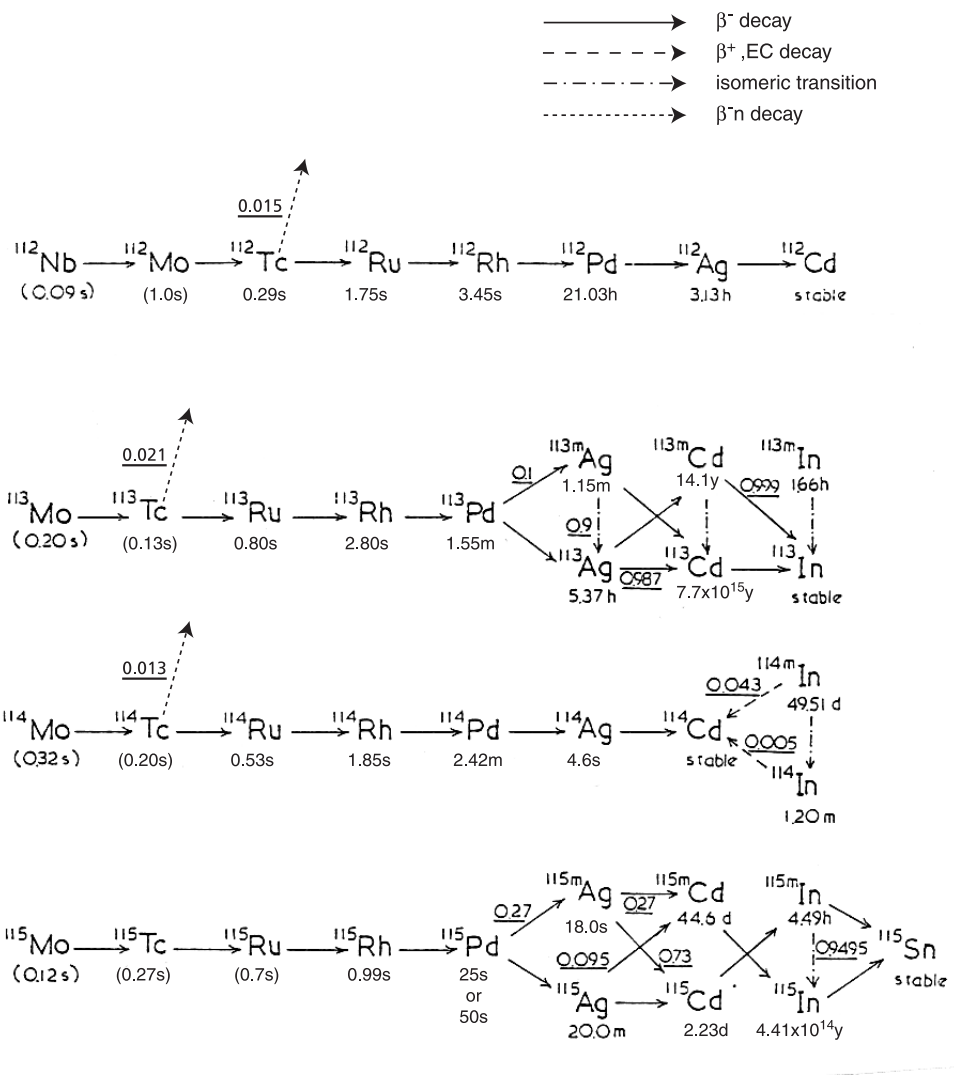

B.1.11 Fission products and decay chains

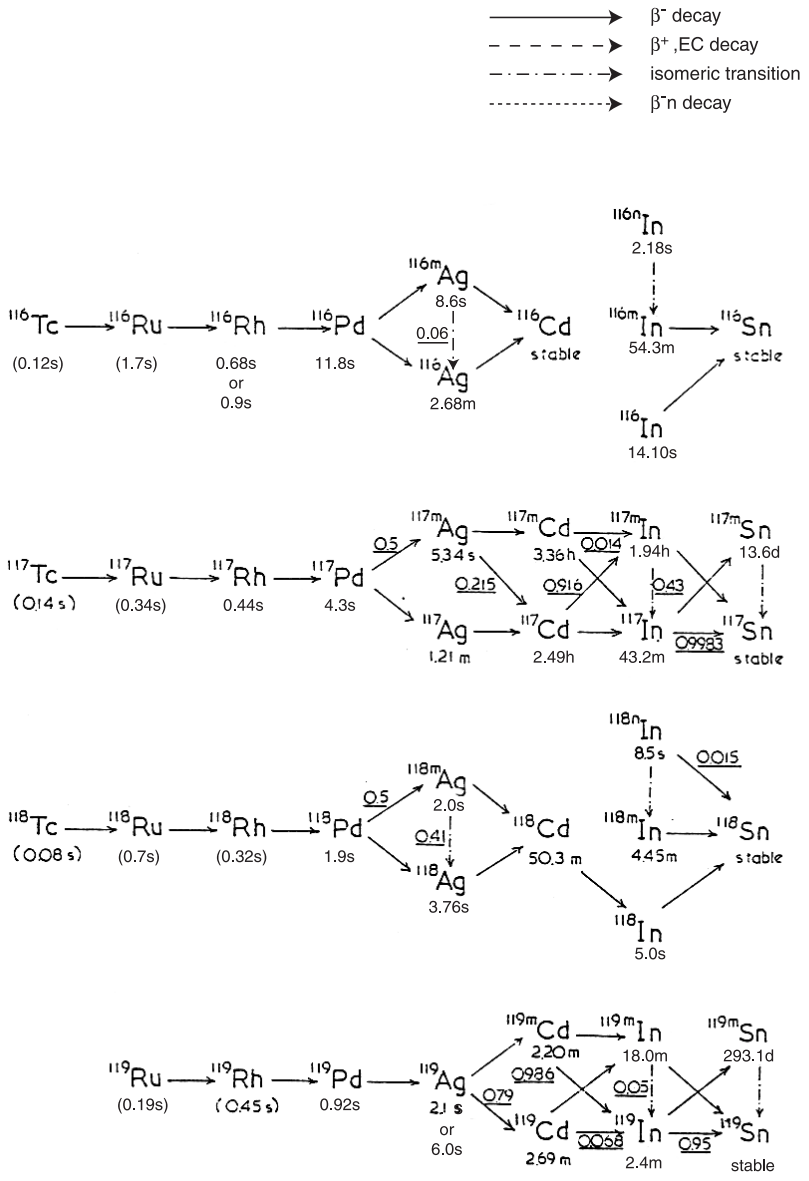

B.1.12 Fission products and decay chains

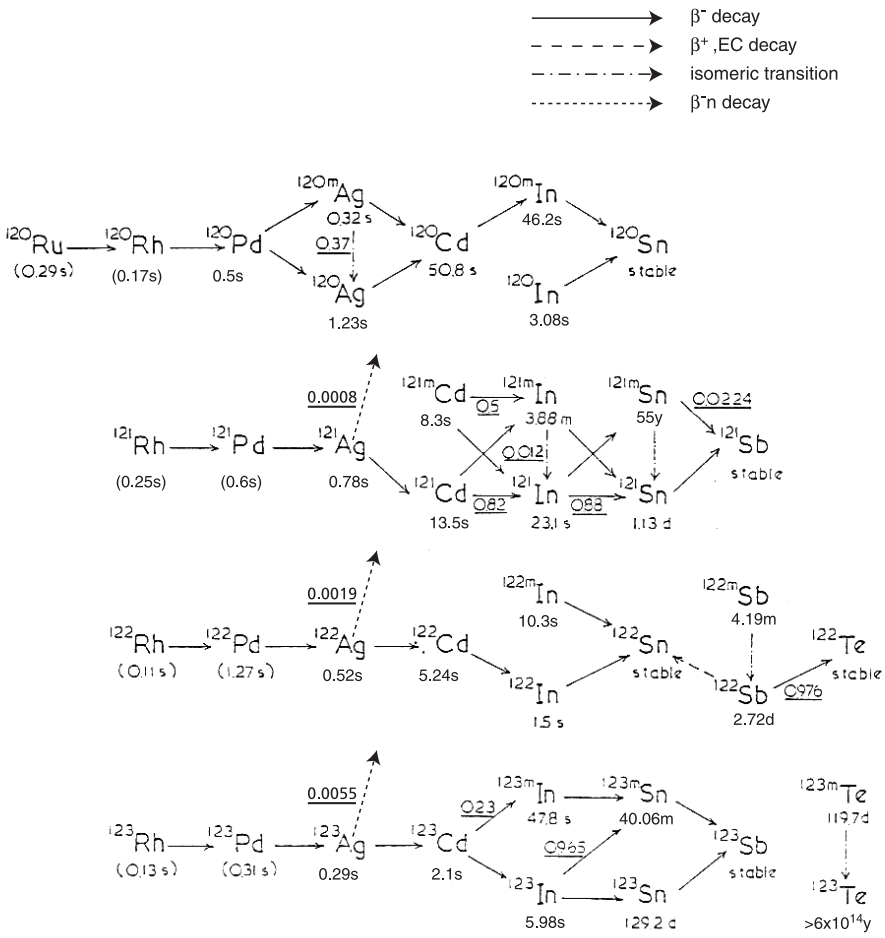

B.1.13 Fission products and decay chains

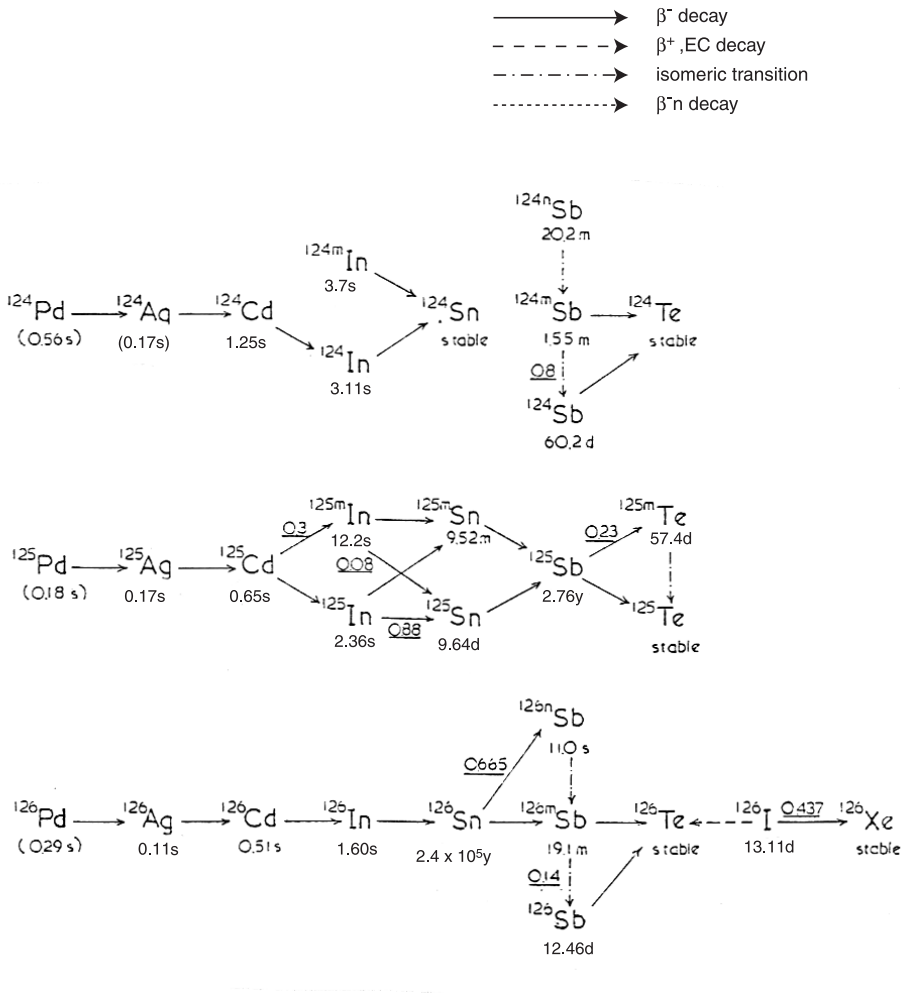

B.1.14 Fission products and decay chains

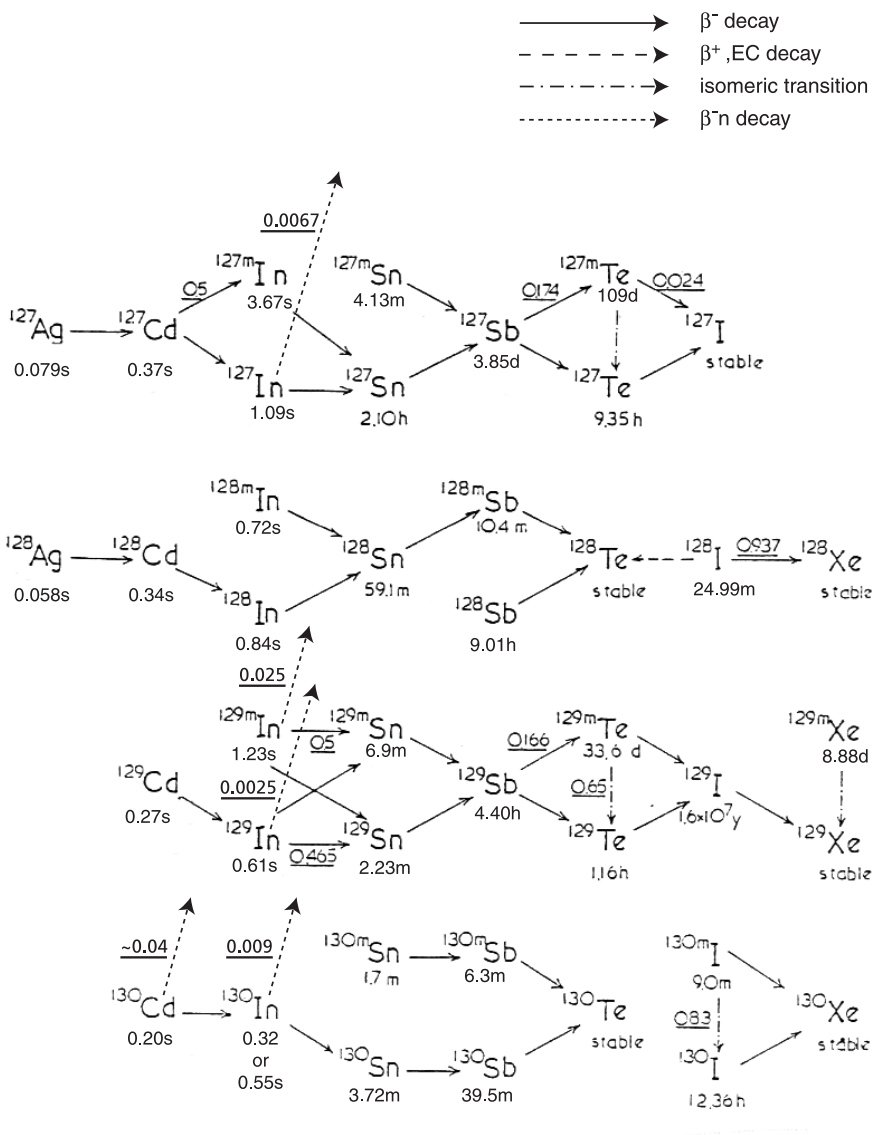

B.1.15 Fission products and decay chains

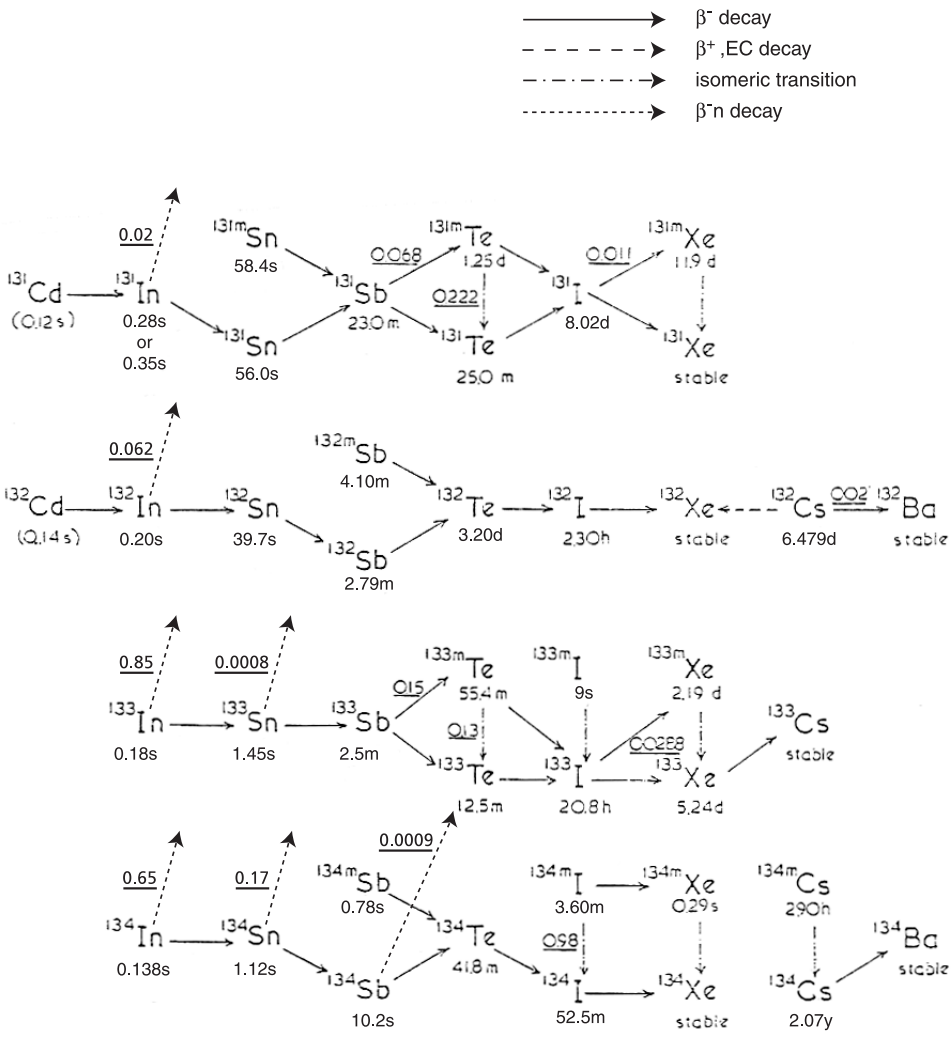

B.1.16 Fission products and decay chains

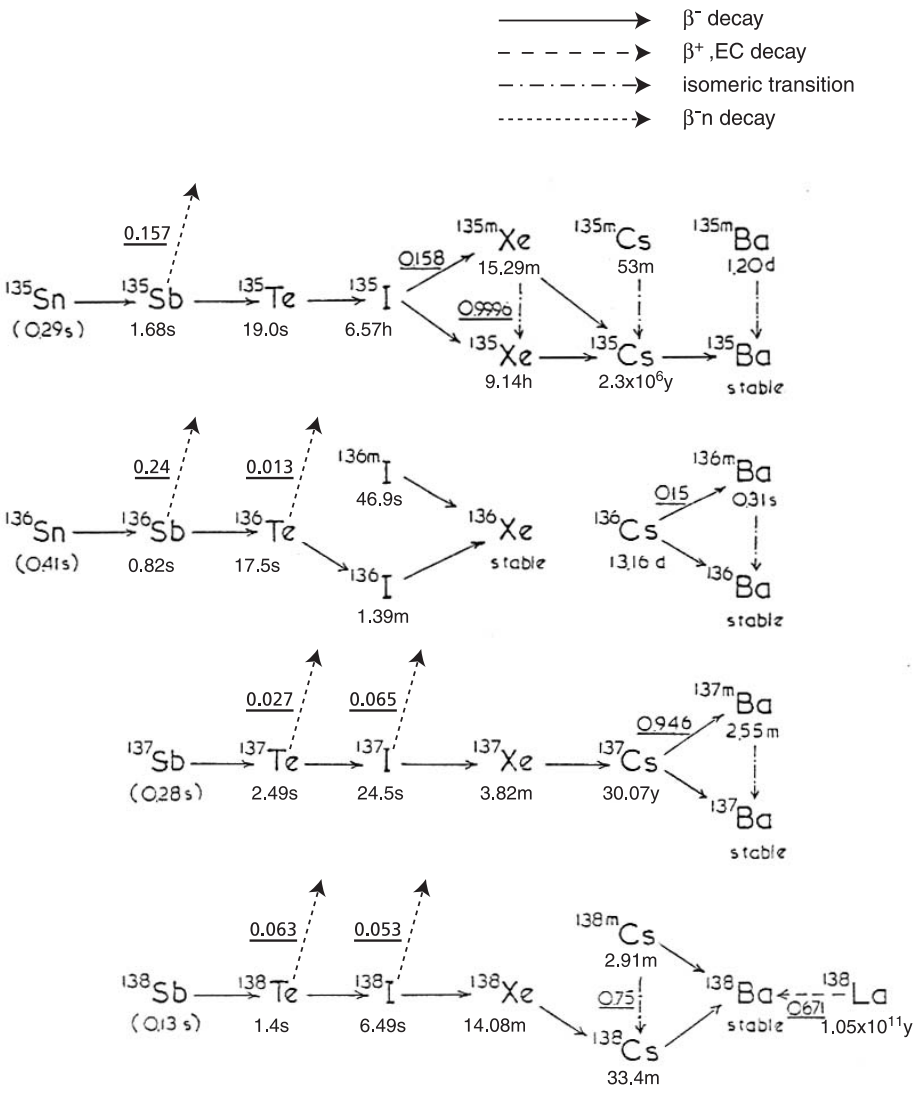

B.1.17 Fission products and decay chains

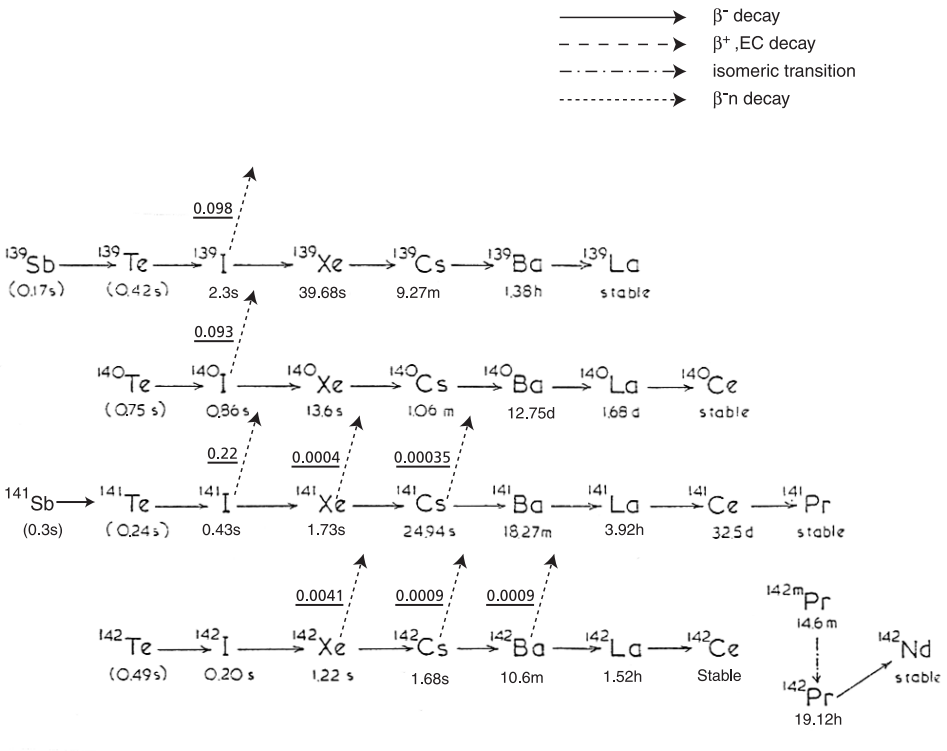

B.1.18 Fission products and decay chains

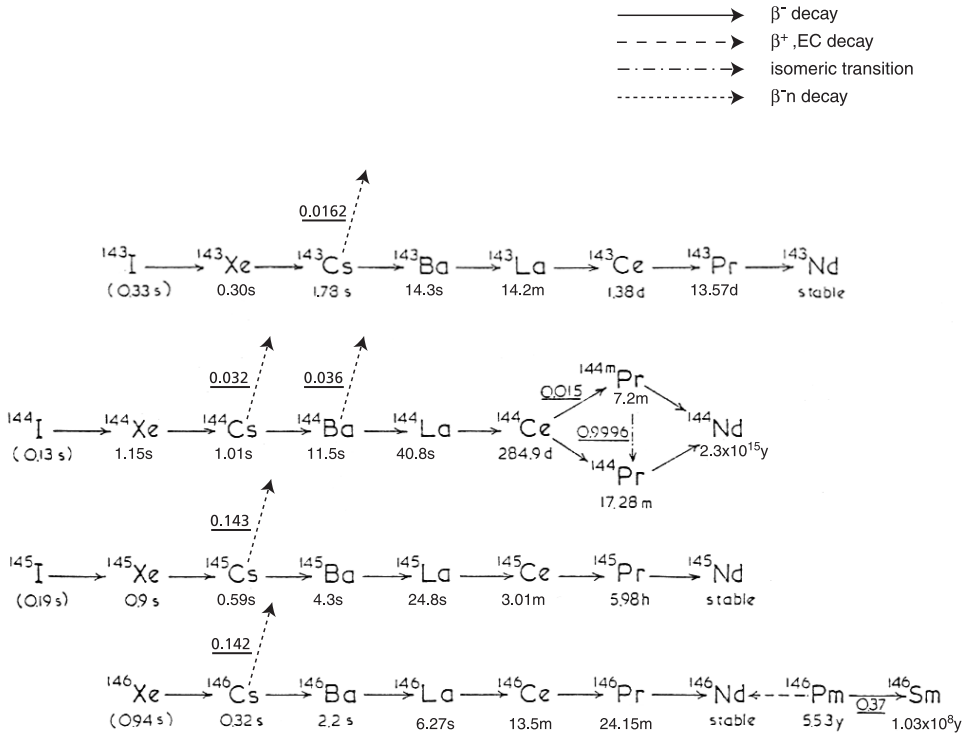

B.1.19 Fission products and decay chains

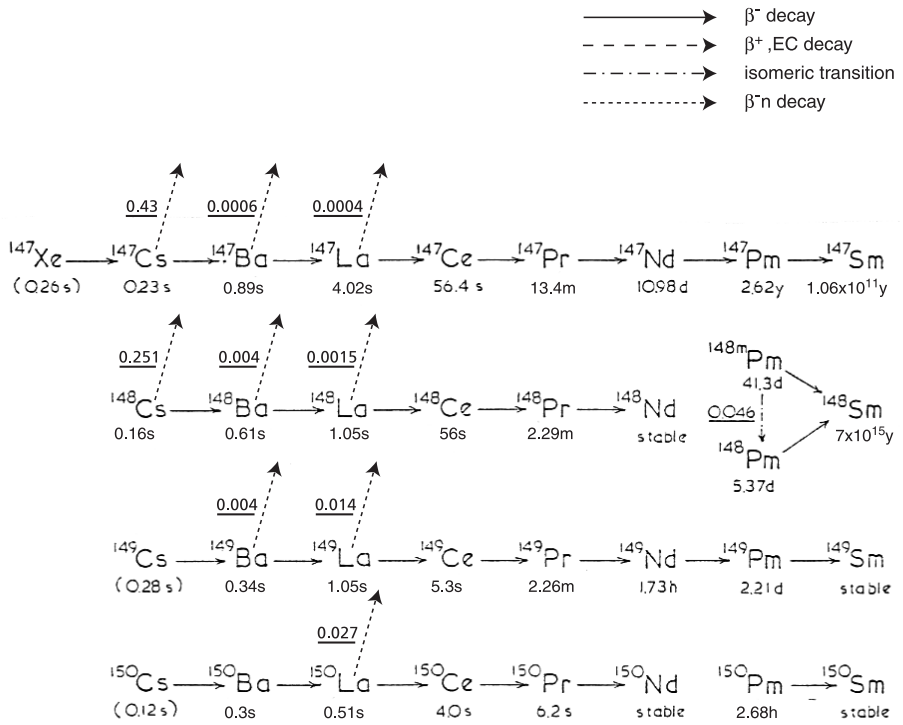

B.1.20 Fission products and decay chains

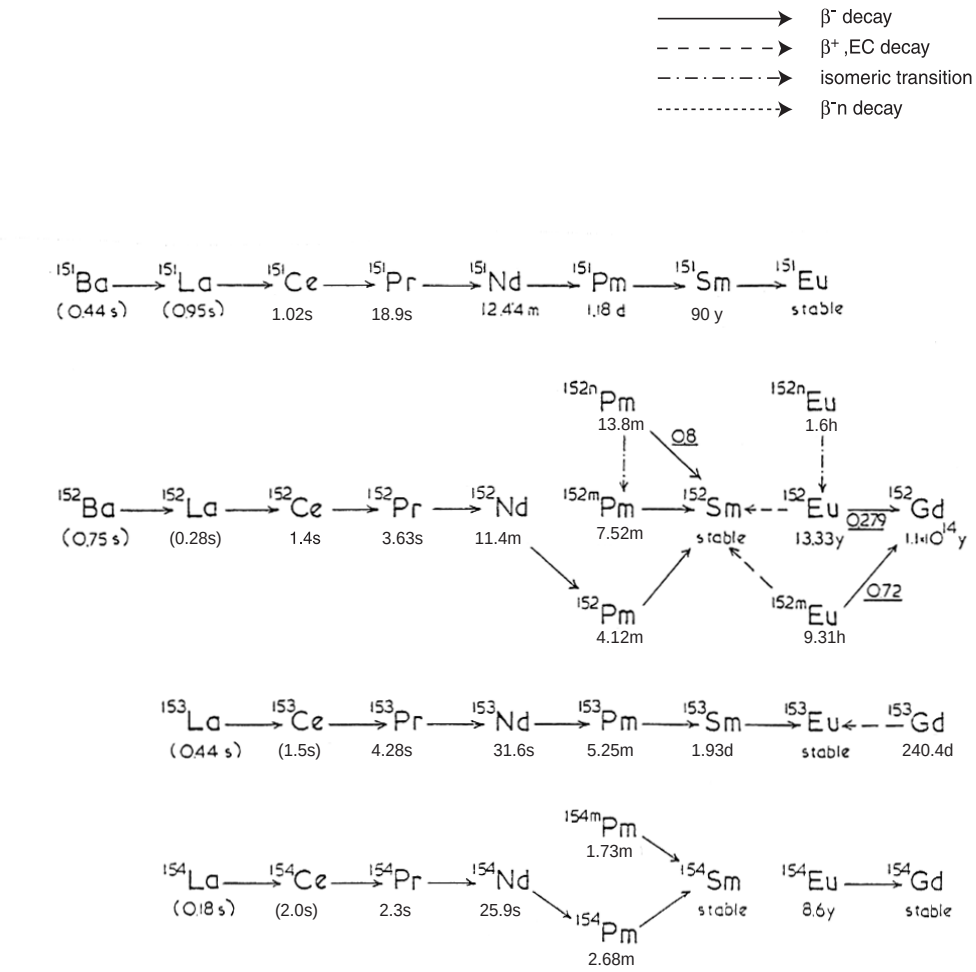

B.1.21 Fission products and decay chains

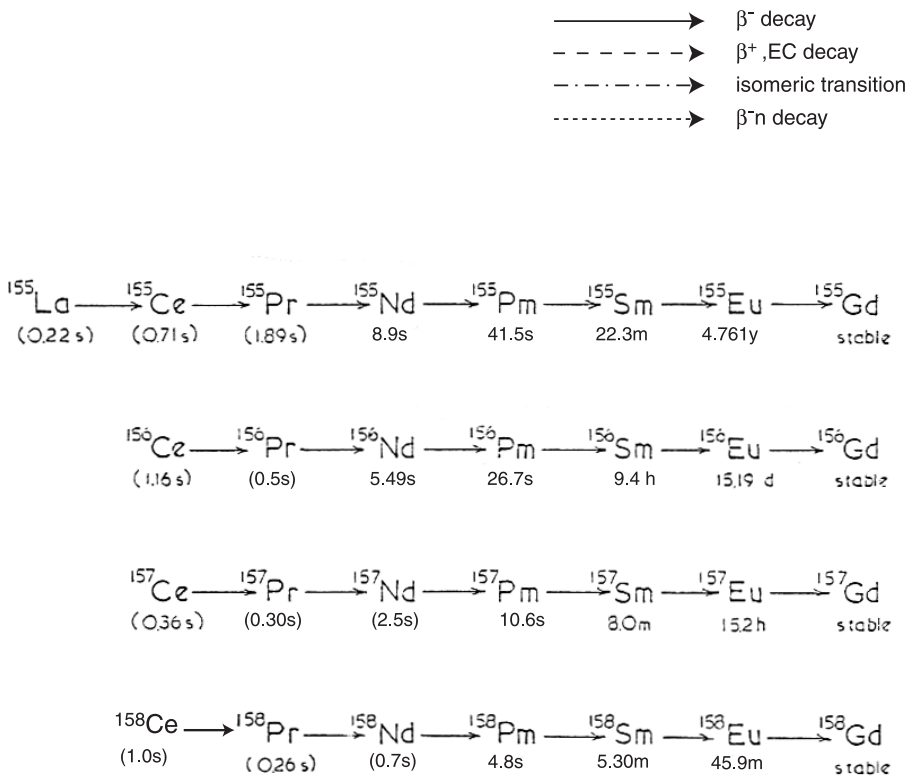

B.1.22 Fission products and decay chains

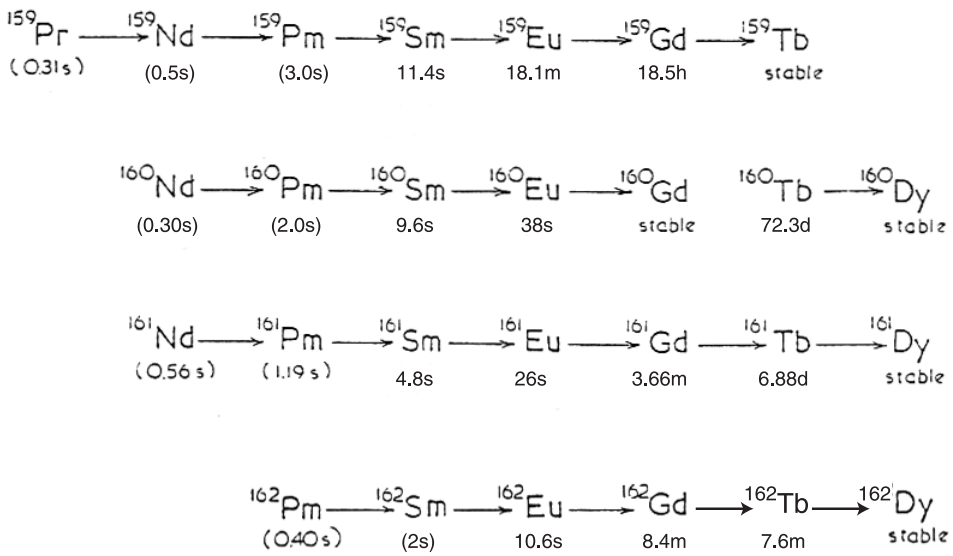

B.1.23 Fission products and decay chains

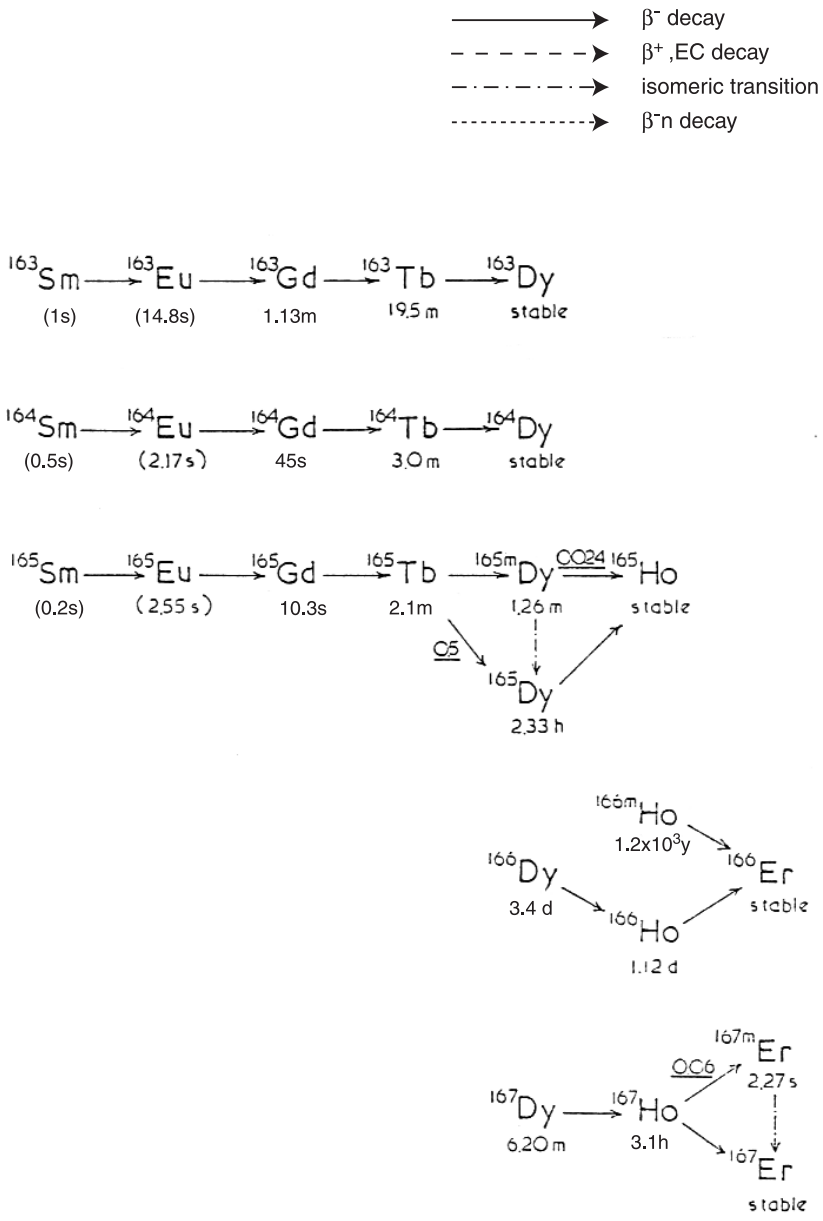

B.1.24 Fission products and decay chains

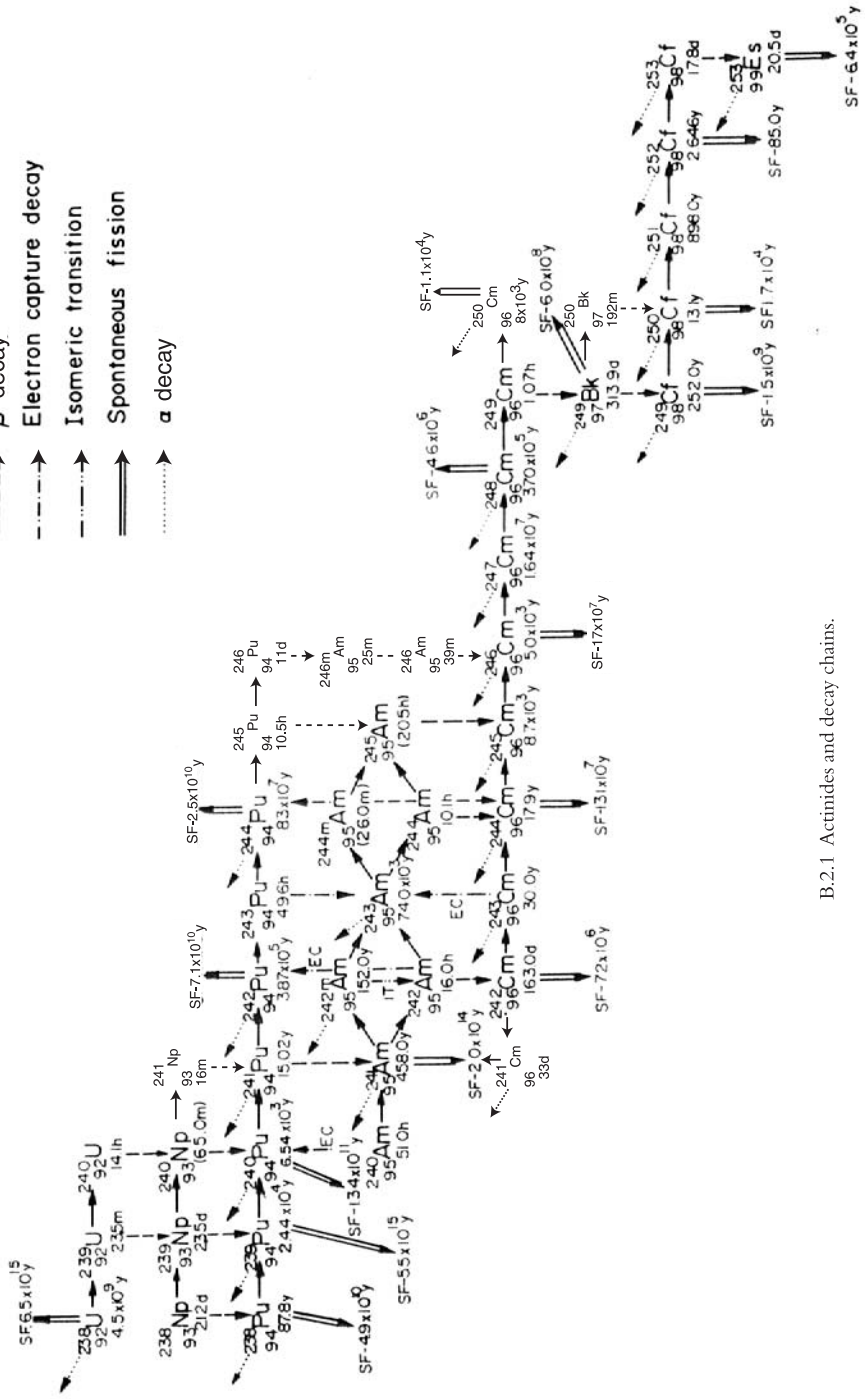

B.2.1 Actinides and decay chains.

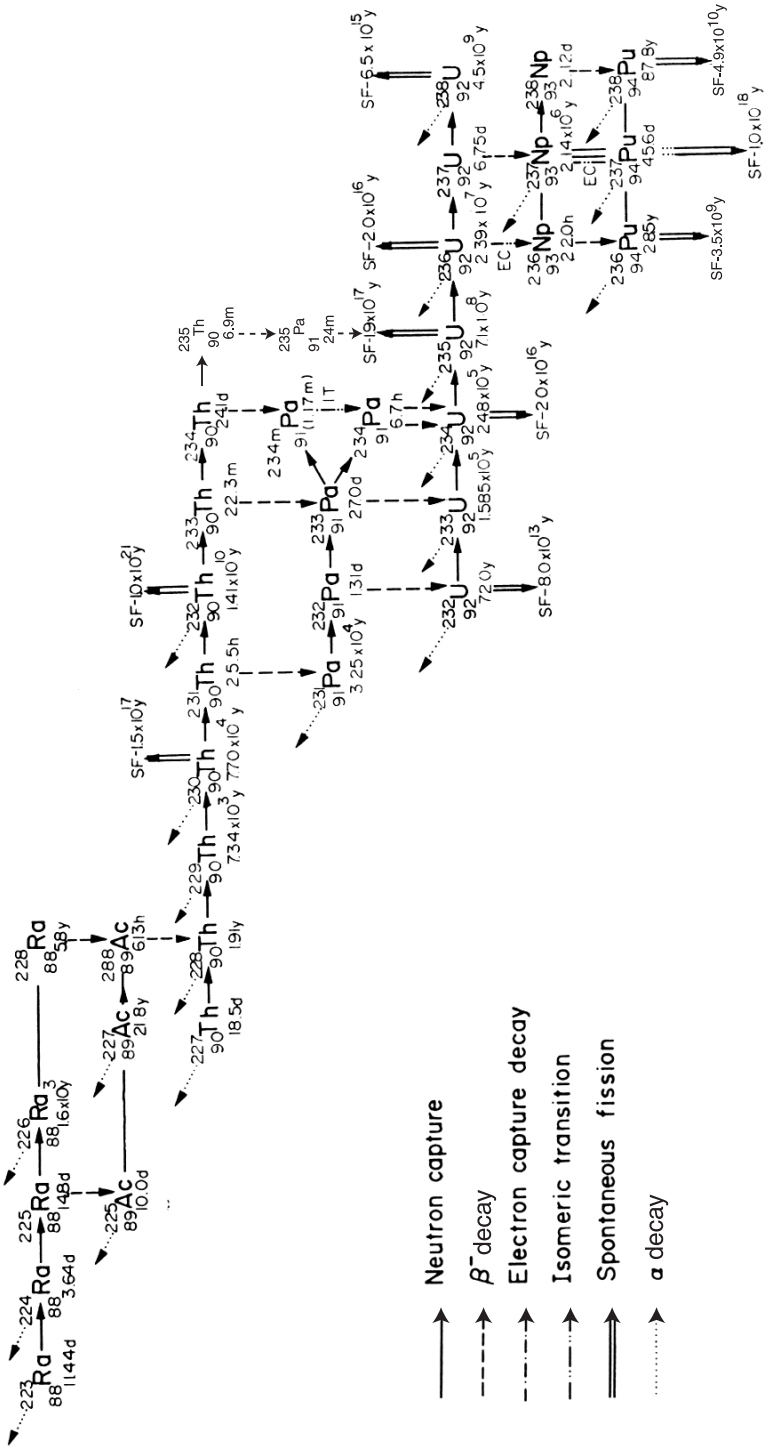

B.2.2 Actinides and decay chains.

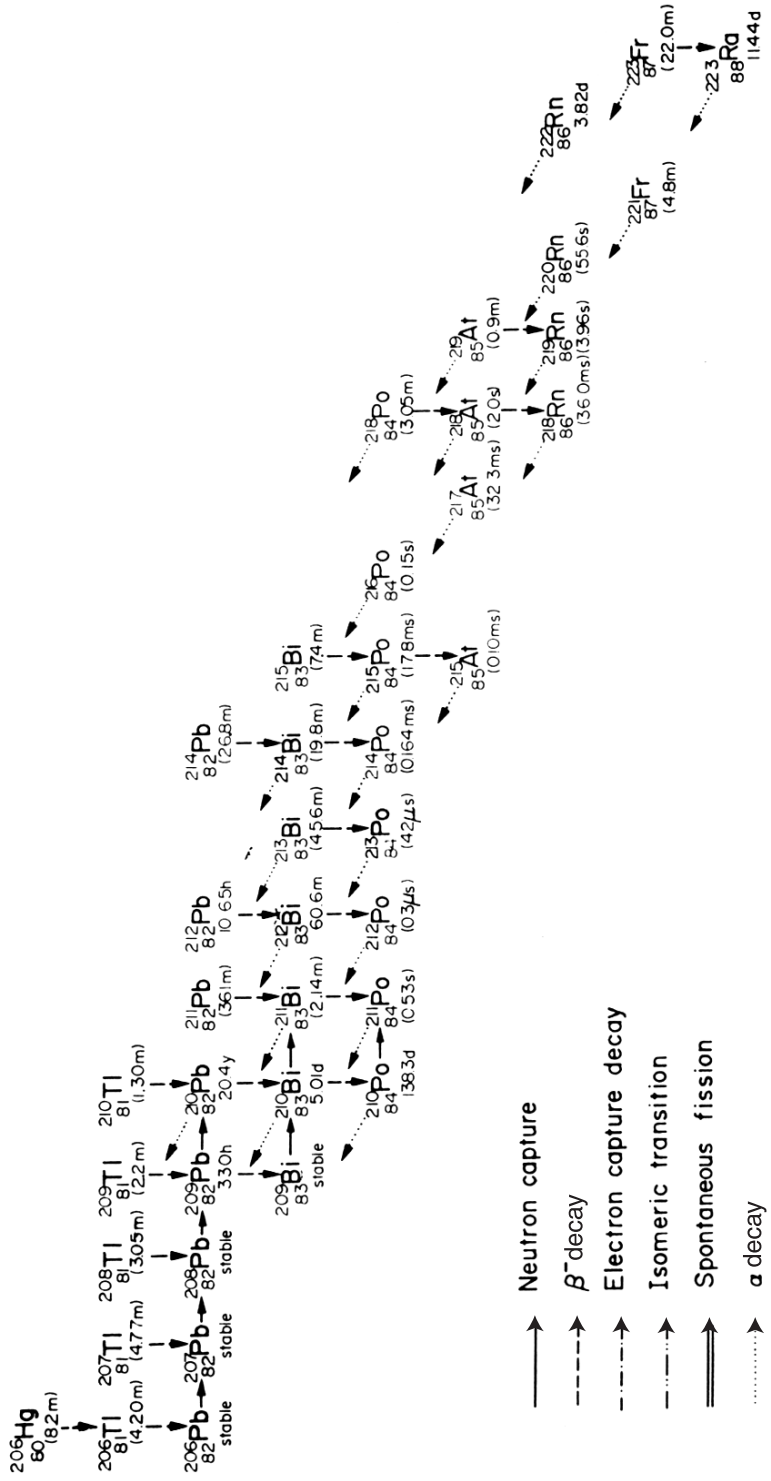

B.2.3 Actinides and decay chains.

Nuclear Power in the 21st Century: Status & Trends in Advanced Nuclear Technology Development

Debu Majumdar*

Nuclear Power Technology Development Section,
Division of Nuclear Power, Department of Nuclear Energy,
IAEA, Vienna, Austria

Lectures given at the
Workshop on Nuclear Reaction Data and
Nuclear Reactors: Physics, Design and Safety
Trieste, 25 February – 28 March 2002

LNS0520004

* D.Majumdar@iaea.org

Abstract

Global demand for energy is going to keep on increasing, especially in developing countries where per capita energy use is only a small fraction of that in industrialized countries. In this regard nuclear energy could play an important role, as it is an essentially unlimited source of energy. However, the nuclear option faces the challenges of increasingly demanding safety requirements, economic competitiveness and public acceptance. Worldwide, a significant amount of experience has been accumulated during development, licensing, construction, and operation of nuclear power reactors. This experience forms a sound basis for further improvements. Nuclear programs in many countries are addressing the development of advanced reactors, which are intended to have better economics, higher reliability, improved safety, and proliferation-resistant characteristics in order to overcome the current concerns about nuclear power. Advanced reactors, now being developed, could help to meet the demand for power in developed and developing countries, not only for electricity generation, but also for district heating, desalination and for process heat.

This paper reviews the status and trends in advanced nuclear power technology development around the world, discusses the challenges it faces, and summarizes the international approach and technical advances made with examples of new designs of reactors.

1. INTRODUCTION

An examination of the global energy use shows that fossil fuels account for nearly 80%, and nuclear power provides only 7%, of our current energy supply. Additionally, around 83% of nuclear power is produced only in a dozen industrialized countries out of 30 nuclear power producing countries. The demand for an increase of standard of living and population growth in developing countries are asking for a considerable increase of this energy supply. However, many factors come into play in specific countries in providing energy to the people - economics, infrastructure, and government policy being the most important factors. The effect on the environment is another crucial factor whose importance, however, has not yet received adequate attention in the energy mix.

The population of the earth, the prime reason for energy use, is increasing although the birth rate has decelerated since the early 1990s. Present trends suggest that total population may not exceed 8 billion people around 2050 and may start to decline shortly thereafter[1]. This is still a large increase from today's population of 6 billion, and energy for these people must be provided. It is important to note that virtually all of this growth will occur in developing countries. Industrialized country populations have peaked or will do so shortly. Moreover, the greater part of the population increase will be urban. The proportion of people living in rural areas has already peaked and will decline in future. An indication of urbanization is that today there are five mega cities of more than 15 million habitants (Tokyo, Mexico City, Mumbai, Sao Paulo and New York), but in 20 years there will be 15, mostly located in developing countries[1]. In energy terms, already we have nearly 2 billion people without access to a regular electricity supply. Even with lower population projections, the challenge to achieve access to energy for all is clearly substantial. An issue here is that concentration of people requires large sources of energy nearby; this needs to be solved in a way that does not create an environmental problem for the city dwellers.

The environmental issues have received prominence since the 1990s, particularly with respect to greenhouse gas emissions, climate change possibilities and their effect on our living conditions. The Third Assessment Report of the Inter-Governmental Panel on Climate Change (February 2001)[2] presented the strongest evidence yet that climate change is occurring (for example, temperatures have risen in the lowest 8 km of the atmosphere, snow and ice cover have decreased, and the sea level has risen between 0.1 and 0.2 meters in the last century). The report also finds that concentrations of atmospheric greenhouse gases have continued to increase as a result of human activities. However, the nations of the world have not unified in their response to this phenomenon.

Nuclear energy is one way to provide bulk electricity supply without greenhouse gas emissions; it is supported by ample uranium resources worldwide and can be made to last almost forever by using the breeder option. The nuclear industry accumulated 10,000 reactor years of operating experience. But nuclear is not without

its problems. The challenges facing nuclear power include (1) continuing to assure the highest level of safe operation of current plants, (2) implementing disposal of high level waste, (3) establishing and convincing the public of a sound basis for nuclear power for sustainable development, (4) achieving further technological advances to assure that future nuclear plants will be economically competitive with fossil alternatives, especially in deregulated and privatized electricity markets, and (5) developing economical and non-proliferating small and medium sized reactors to provide nuclear power to countries with small electricity grids and also for non-electric applications such as seawater desalination.

This paper will discuss the status and trends of advanced nuclear reactors, which could help in the solution of the energy problem of the world and, at the same time, address the issues raised by the nuclear critics.

2. CURRENT STATUS

There are only 30 nuclear electricity-generating countries. Table I below shows the total electricity generating capacity in various countries in the world. Note that only 8 countries have total capacity of more than 100 GWe, and of these two of the largest population countries, China and India, have only a few percentage of nuclear to share. However, China and India currently have solid programs for nuclear power. The important part of the table is that there are many dozens of countries with a total capacity of 2 GWe and less, who need the power most. Because of their grid size, these countries cannot add a large plant of the size of 1GWe; plants for these countries would have to be smaller and more cost-effective (and hence more innovative) than existing large plants.

The worldwide operating experience of power reactors is tremendous. Overall 438 reactors were in operation in 2002. The breakdown of these reactors by types and generating capacity are shown in Table II.

TABLE I. TOTAL ELECTRICITY GENERATING CAPACITY (2002)[3]

Total Capacity (GWe)	Countries	No. of Countries	Nuclear Share (%)
More than 100	USA, Japan, China, Russia, India, Canada, Germany, France	8	1 – 80
50 – 100	UK, Brazil, Spain, ROK, Ukraine, Mexico	6	2 - 39
50 – 100	Italy	1	None
10 – 50	S. Africa, Sweden, Argentina, Romania, Netherlands, Pakistan, Switzerland, Finland, Belgium, Czech Rep., Bulgaria	11	2 – 45
10 – 50	Australia, Austria, Denmark, Egypt, Greece, Iran, Indonesia, Poland, Turkey, Kazakhstan,…	23	None
2 – 9	Hungary, Slovakia, Lithuania, Armenia, Slovenia	5	31 – 65
2 – 9	New Zealand, Croatia†, Vietnam, Bangladesh, …	38	None
1 – 2	Algeria, Albania, Bolivia, Panama, Ghana, Zimbabwe, Myanmar, Iceland, …	18	None
Less than 1	Many small countries	~ 80	None

As shown in Figure 1, there are currently 32 nuclear power plants under construction in 12 countries; 8 in China, 4 each in Ukraine and Republic of Korea, 3 in Japan, 2 each in India, Slovakia, Russia, Iran, and Taiwan, China, and 1 each in Romania, Czech Republic and Argentina. China is building six PWRs in the range of 640 to 1000 MWe from Framatome, Russia and their own design, and two 730 MWe PHWRs from Canada. Two 500 MWe PHWRs are under construction in India. India has also announced that four more 220 MWe PHWRs and 2 1000 MWe WWERs and a 500 MWe prototype fast breeder reactor will be under construction soon. In Ukraine Khmelnitski Units 2, 3 and 4 and Rovno Unit 4, all 1000 MWe WWERs, are under construction since 1985 through 1987. Large advanced PWRs and BWRs are being built in Republic of Korea, Japan and Taiwan. Mohovce Units 3 and 4 in Slovakia, WWER 440 plants, are under construction since 1985 and are currently on hold. Atucha Unit 2 in Argentia, 700 MWe Siemens PHWR, is under construction since 1981 but currently on hold. Cernavoda Unit 2, CANDU 700 MWe PHWR, is under construction since 1983. Bushehr Units 1 and 2 in Iran, WWER 1000, are currently replacing the original reactor designs. Temelin Unit 2 in Czech Republic, WWER

† Croatia owns 50% of the Krsko 676 MWe Westinghouse PWR plant located in Slovenia.

1000 further modernized by Westinghouse, is currently under startup testing. Figure 2 gives their size breakdown. It is important to note that primarily large size reactors are being built: 22 in the range of 900 – 1350 MWe. Then there are 6 in 600 – 700 MWe range, and 4 between 300- 500 MWe. Thus it is apparent that the utilities will build power plants as large as the grid size will tolerate because that is most economical. However, there is a need for both small and large reactors for flexibility in power management, to suit the grid size and investment capitals, and for remote or special situations such as small localities in Siberia.

TABLE II. REACTOR TYPES AND GENERATING CAPACITY IN THE WORLD AS OF JUNE 2002

	PWR	BWR	HWR	LWGR	WWER	GCR	LMR	TOTAL
No of reactors in operation	208	92	35	17	51	32	3	438
No. of countries	17 Belgium Brazil China France Germany Japan, ROK Netherlands Pakistan S. Africa Slovenia Spain Sweden Switzerland Taiwan UK, USA.	10 Finland, Germany India Japan Mexico Spain Sweden Switzerland Taiwan USA	6 Argentina Canada India, ROK Pakistan Romania	2 Lithuania Russia	8 Armenia Bulgaria Czech R Finland Hungary Russia Slovakia Ukraine	1 UK	3 France Japan Russia	31
Generating capacity, Gwe	198	80	16	13	33	12	1	353
Operating experience of all reactors, Reactor-years	4351	2291	761	469	999	1460	151	10,482

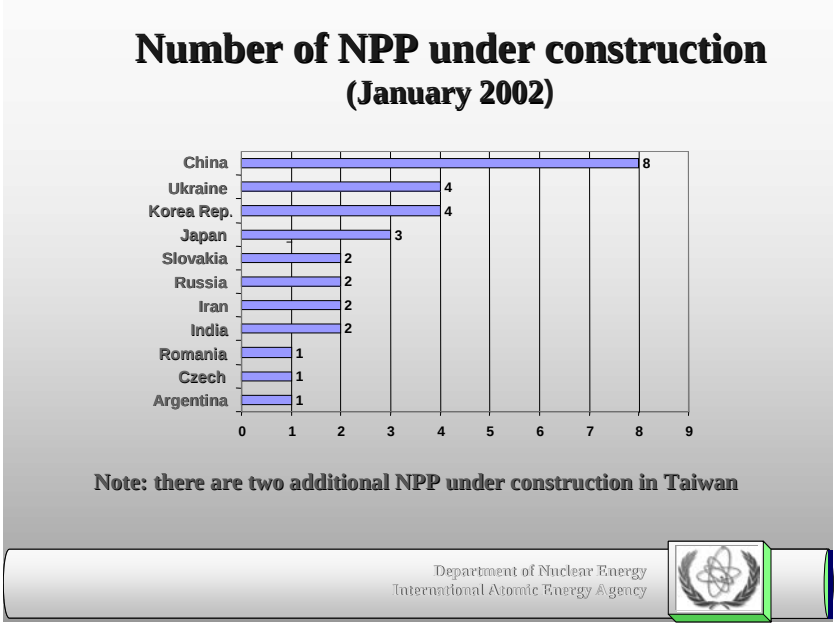

Fig. 1 Number of nuclear power plants under construction around the world[4]

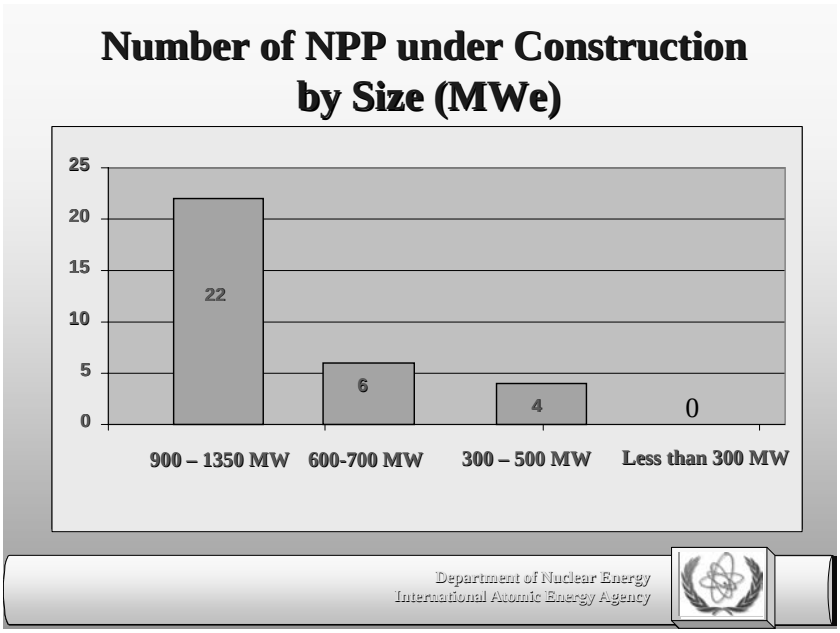

Fig. 2 Size breakdowns of nuclear power plants under construction around the world[4]

3. BASIC POWER NUCLEAR REACTOR DESIGNS

The main types of nuclear power reactors are shown in Table III. They are categorized by the material used to moderate the neutrons generated in nuclear fission and the coolants used for the transport of heat.

Pressurized Water Reactor (PWR): Primary water pressurized to about 160 bar act as both the moderator and the coolant. The fuel is up to 5% enriched uranium dioxide in Zircaloy tubes. The primary water heats water in a secondary circuit to produce steam. The reactor is housed in a containment building. The thermal efficiency is about 32%.

Boiling water Reactor (BWR): It is essentially a PWR without the steam generator and the secondary circuit. Water at a pressure of about 70 bar is pumped through the core and, since it is at a lower pressure compared to the PWR, steam is generated in the primary circuit. About 10% of the water is converted to steam and goes to the steam turbine. After condensing it is pressurized and returned to the coolant. The power density of a BWR is about half that of a PWR with lower temperature and pressure, but the efficiency is similar.

CANadian DeUterium Reactor (CANDU): Heavy water is used as both the moderator and the coolant with natural uranium oxide in Zircaloy tubes as the fuel. The fuel tubes pass through a tank of heavy water. Heavy water is pumped through the fuel tubes at about 90 bar pressure and then to a steam generator as in a PWR. The power density is about $1/10^{th}$ of that of a PWR.

High Temperature Gas-cooled Reactor (HTGR): These are graphite moderated, helium cooled reactors. The fuel is a coated particle to contain the fission products. Water has been used in the secondary circuit to generate steam. Recently a direct cycle (single loop) gas turbine concept has been developed.

Liquid Metal Fast Reactor (LMFR): Liquid metal transports heat very efficiently and only lightly moderates the neutrons from fission. LMFRs consequently need more fissile material to keep the chain reaction going. The core may also contain fertile material to produce new fuel. Since they can breed fuel, they are also known as breeder reactors. Sodium has been used as the most common form of liquid metal for these reactors. Enriched uranium and Plutonium dioxide and metals have been used as fuel. They operate at a much lower pressure compared to the common light water reactors.

TABLE III: CHARACTERISTICS OF NUCLEAR POWER REACTORS RELEVANT TODAY

Reactor type	Fuel	Moderator	Coolant and its pressure in bars (normal atmospheric pressure is about 1 bar)	Steam generation
PWR	uranium dioxide (~ 3.2% U-235)	ordinary water	pressurized ordinary water (160 bars)	separate circuit
CANDU	Natural uranium dioxide (0.7% U-235)	heavy water	Heavy water (90 bars)	separate circuit
BWR	uranium dioxide (2.6% U-235)	ordinary water	pressurized ordinary water which boils and produces steam directly (70 bars)	
HTGR	uranium dioxide in coated particle fuel (approx. 8-19%)	graphite	helium (~ 60 bars)	separate circuit (or direct helium cycle)
LMFR	uranium/plutonium oxide (~ 16-20%), high power density	none	liquid sodium at low pressure (~5 bar)	separate circuit

Other Reactor Types: There are two reactor types developed and built only in the UK, Magnox and AGR, which are still operating. Magnox is a carbon-dioxide cooled (at about 20 bar pressure), graphite moderated reactor. It has natural uranium fuel in a Magnesium alloy cladding. Overall thermal efficiency is about 30%. The AGR, Advanced Gas Cooled Reactor, is a gas-cooled reactor with graphite moderation and carbon-dioxide as the coolant at a pressure of about 40 bar. The fuel is 3% enriched uranium-dioxide and clad in Stainless Steel. Its thermal efficiency is about 40%. It is a unique UK design. Similarly, the Graphite Moderated Boiling Water Reactor (RBMK) is an older Russian design and built only in the former Soviet Union. The RBMK core is an assembly of graphite blocks through which runs the pressure tubes containing the fuel. Water is pumped through these tubes where it boils to steam. The fuel is 2% enriched uranium dioxide in Zircaloy tubes.

An older concept that is receiving new attention is the Molten Salt Reactor (**MSR**), which can generate energy and at the same time considerably burn the long-lived radioactive wastes. It is a circulating, molten salt homogeneous reactor. The fuel is a mixture of fluorides of Li-7, Be, Th, and U-233, U-235 or Pu-239 fissile material. Graphite is used as moderator although some moderation is achieved by the Li, Be

and F used in the fuel. Heat is transferred from the fuel leaving the core by an intermediate heat exchanger. Fuel processing is an integral part of the reactor operation. The fuel and the fuel composition can be changed without shutting down the reactor. One 8 MWt Molten Salt Reactor Experiment (MSRE) facility was operated for four years at Oak Ridge, USA, from 1965 – 69.

4. ADVANCED NUCLEAR POWER REACTORS

A lot of work has been done around the world to improve the existing reactor designs. The large base of experience with the current nuclear plants has been used to guide development of the new designs on the basis of User Requirements Documents (URDs) such as the Electric Power Research Institute URD[5] and the European Utility Requirements[6]. Common goals are simplification, larger margins to limit system challenges, longer grace periods for response to emergency situations, high availability, competitive economics and compliance with internationally recognized safety objectives. The new designs are also incorporating features to meet more stringent safety objectives by improving severe accident prevention and mitigation.

Several of these designs have reached a high degree of maturity, and some have been certified by nuclear regulatory authorities. Some are entering a design optimization phase to reduce capital cost. Many of the new design features have been tested to demonstrate technological readiness.

The full spectrum of these advanced nuclear power plants covers different types of reactors with different coolants. They are referred to as evolutionary or innovative designs. An evolutionary design is a design that achieves improvements over existing designs through small to moderate modifications with a strong emphasis on maintaining proven design features to minimize technological risks. It requires at most engineering and confirmatory testing. An innovative design is one, which incorporates radical conceptual changes in design approaches or system configuration in comparison with existing practices. They could have new types of coolant, moderator or fuel. Consequently, substantial R&D, and feasibility tests are required, and a prototype or demonstration plant may be necessary to bring the concept to commercial maturity. Figure 3 gives a relative standing of efforts and costs needed for development of advanced reactors[7].

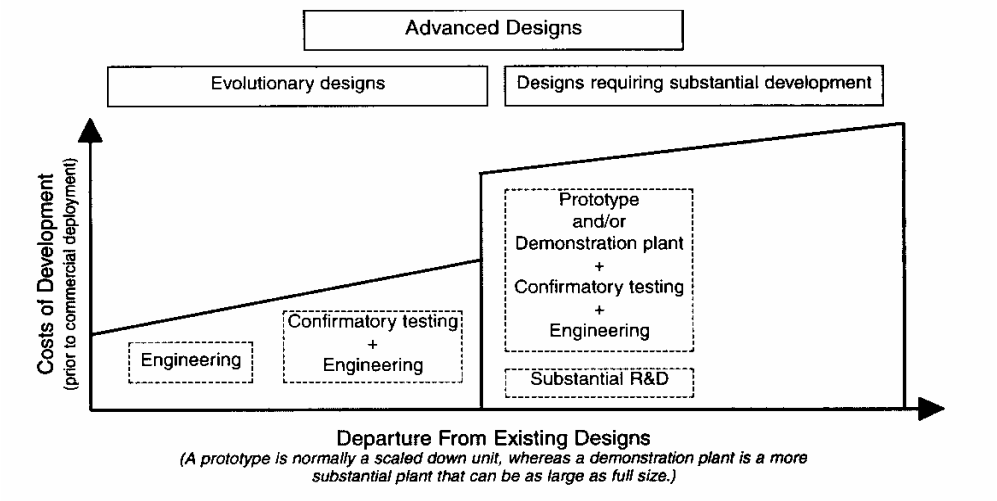

Fig.3 Relative indication of cost of development of advanced reactor designs

For new plants, the basis for achieving high performance is also being laid down during the design phase[8]. These include design for on-line maintenance and short outages. Many other aspects such as better man-machine interface using computers and improved information displays, and better operator qualification and simulator training, which have been applied at current plants, will contribute to high performance of future plants. The advanced designs also desire plant lifetimes of 60 years.

A new terminology is being used for the advanced reactors. Bill Magwood first introduced this from the US Department of Energy[9] and is shown in Table IV, which also describes the evolution of reactor designs. First generation reactors (Generation I) were those introduced early in the prototype stage of nuclear power. Generation II reactors were the commercial PWR, BWR, HWR, and WWER reactors built in the 70s and 80s. Generation III are the evolutionary advanced reactors. These could be divided into two categories: (1) those whose designs have been completed such as AP600/1000, SWR 1000, and the EPR, and (2) those which have been built such as ABWR, System 80+, KSNP. The next generation or Generation IV reactors are those designs that are beyond the current advanced designs and are "revolutionary" in nature. However, no Generation IV reactors have been built or even demonstrated, and so from a utility perspective, we may think of the next generation reactors as those just beyond the near term deployment designs. In other words, those are reactors that still need demonstration or some significant tests before commercial operation.

TABLE IV. EVOLUTION OF NUCLEAR POWER REACTORS

Evolution	Example
Generation I Early 1950s to late 1960s	Early Prototypes . Shippingport . Dresden, Fermi I . Magnox . VK-50, BiNPP
Generation II (1970 – 90)	Commercial power reactors . LWR – PWR & BWR . CANDU . RBMK/WWER
Generation III Improvements of designs started in late 1980s	Evolutionary and Advanced designs . ABWR . APWR . WWER 1000 . AP 600/1000 . GT-MHR, PBMR
Generation IV 21st century	Innovative designs .Molten salt reactors; supercritical water-cooled reactors; lead alloy, sodium and gas-cooled fast reactor systems; and very high temperature reactors.

4.1. Light Water-cooled Advanced Reactors

Worldwide, LWRs (PWRs, BWRs and WWERs) are the major types of nuclear power plants. They represent approximately 88% of today's global nuclear power capacity, and evolutionary designs, based on this experience base, are being developed in several countries. The major evolutionary LWR designs are shown in Table V.

TABLE V. MAJOR EVOLUTIONARY LWR DESIGNS

Reactor	Power (MWe)	Organization	Status/Significant Features
System 80+ PWR	1350	Westinghouse (formerly ABB Combustion Engineering)	Design certified by US NRC.
APWR	1530	Mitsubishi, Japan Westinghouse, USA	First unit planned at Tsuruga site in Japan.
AP 1000	1000	Westinghouse	Upgraded from AP-600; under licensing review
EPR	1545	Framatome ANP, France/Germany	Design complete; meets European Utility Requirements
WWER	1000 640	Gidropress & Atomenergoproject, Russia	Several planned in Russia, China, India and Iran. Design of WWER 640 with passive safety features is complete and 2 construction sites in Russia have been located.
KSNP	1000	Korea Electric Power Co., Republic of Korea (ROK)	Six operating in ROK and two under construction.
APR-1400	1400	KEPCO and Korean industry, Republic Of Korea	Based on System 80+ design; has received design certification and is expected to be built by 2010.
AC-600/1000	600/1000	NPIC, China	Similar to AP-600/1000 designs; expected in 2010.
ABWR	1360	General Electric, Hitachi-and Toshiba	2 operating and 10 planned in Japan; design based on well- proven active safety systems.
ABWR-II	1700	Japanese utilities and GE-Hitachi-Toshiba	Economy of scale design under consideration
ESBWR	1380	General Electric, USA	Incorporates economy of scale with passive safety, design based on earlier SBWR effort.
SWR-1000	1000	Framatome ANP, Germany	Design complete, based on German utility experience; active and passive safety systems.
BWR 90+	1500	Westinghouse Atom, Sweden	Evolutionary version of earlier ABB Atom designs.

The evolutionary LWR activities in different countries are briefly described in the following[10]:

In the USA, designs for a large sized advanced PWR (the Combustion Engineering System 80+) and a large sized BWR (General Electric's ABWR) were certified by the U.S. NRC in May 1997. Westinghouse's mid-size AP-600 design with passive safety systems was certified in December 1999. Efforts are currently underway by Westinghouse on a 1090 MWe plant called the "AP-1000," applying the passive safety technology developed for the AP-600 with the goal to reduce the capital costs through economies-of-scale. A certification application for the AP-1000 design has been made to the US NRC this year. General Electric is also designing a 1380 MWe ESBWR applying economies-of-scale together with modular passive safety systems. The design draws on technology features from General Electric's ABWR and from their earlier 670 MWe simplified BWR with passive systems.

In France and Germany, Framatome ANP completed the basic design for a 1545 MW(e) European Pressurized Water Reactor (EPR) in 1998, which meets European utility requirements. The EPR design includes the mitigation of core melt and vessel penetration accident scenarios ensuring the avoidance of evacuation of people in the vicinity of the plant. Accidents with molten core material outside the reactor pressure vessel are handled via a spreading concept in the basement of the containment. The EPR's higher power level relative to the latest series of PWRs operating in France (the N4 series) and Germany (the Konvoi series) has been selected to capture economies of scale. Framatome ANP's SWR 1000 is based on German BWR experience with added features to increase safety. It is an advanced BWR with active and passive safety features which allows for extended grace period for accident control and consequences of a core melt accident is limited to the immediate vicinity of the plant. This has been achieved by providing cooling of the reactor pressure vessel exterior. The essential elements of the SWR safety concepts are shown in figure 4.

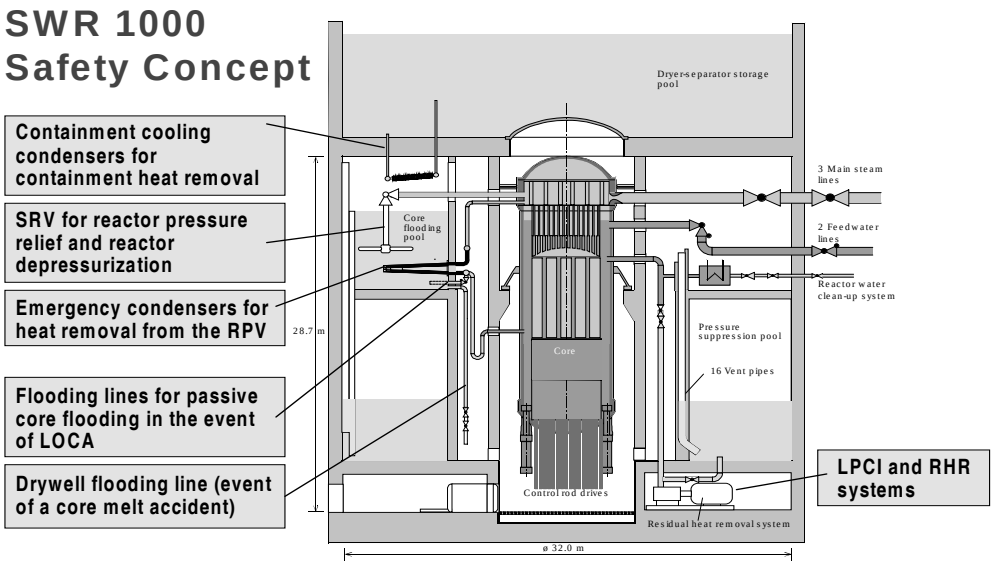

Fig. 4. A schematic drawing of SWR 1000 safety features

In Sweden, Westinghouse Atom is also developing the 1500 MWe BWR 90+, an advanced boiling water reactor with improved safety and operability. This is an upgraded version of the BWR operating in Sweden and Finland.

The first two ABWRs in Japan, the 1360 MWe Kashiwazaki-Kariwa 6 and 7 units, have been in commercial operation since 1996 and 1997, respectively. ABWR plants are under construction at Hamaoka Unit no. 5 and Shika Unit no. 2, and under licensing at Ohma Unit no. 1. Another eight ABWR plants are in the planning stage in Japan. The benefits of standardization and construction in series are being realized with the ABWR units. Expectations are that future ABWRs will achieve a significant reduction in generation cost due to standardization, design improvements and better project management. In addition, a development programme was started in 1991 for 1700 MWe ABWR-II, aiming to further improve and evolve the ABWR, with the goal of significant reduction in power generation cost. Commissioning of the first ABWR-II is foreseen in the late 2010s. Also in Japan, the basic design of a 1530 MWe advanced PWR has been completed by Mitsubishi Heavy Industries and Westinghouse for the Japan Atomic Power Company's Tsuruga-3 and –4 units.

In the Republic of Korea, the benefits of standardization and construction in series are also being realized with the 1000 MWe Korean Standard Nuclear Plant (KSNP). The first two KSNPs, Ulchin 3 and 4, have been in commercial operation

since 1998 and 1999, respectively, and four more units (Yonggwang 5 and 6 and Ulchin 5 and 6) were under construction in 2001, with Yonggwang 5 and 6 scheduled to begin commercial operation in 2002. In addition, ROK is developing the Korean Next Generation Reactor, now named the Advanced Power Reactor 1400 (APR-1400), which is focusing on improving availability and reducing costs. It has received design certification and is expected to be constructed by 2010.

In the Russian Federation, efforts continue on evolutionary versions of the currently operating WWER-1000 (V-320) plants. This includes the WWER-1000 (V-392) design, of which two units are planned at the Novovoronezh site, and WWER-1000 units are also planned in China, India and the Islamic Republic of Iran. Development of a WWER-1500 design has been initiated. Development is also ongoing on a mid-size WWER-640 with passive safety systems, and on an integral design with the steam generator system inside the reactor pressure vessel.

In China, the China National Nuclear Corporation (CNNC) is developing the CNP-1000 plant. China is pursuing self-reliance both in designing the plant to meet Chinese safety requirements, and in fostering local equipment manufacture with the objective of reducing construction and operation costs. Lessons learned from the design, construction and operation of the Qinshan and Daya Bay NPPs are being incorporated. Two ABWRs are under construction in Taiwan.

4.2. Heavy Water Advanced Reactors

Heavy water reactors (HWRs) at the beginning of 2001 represented about 8% by number and 4.7% by capacity of all operating power reactors. With many years of operating experience Canada has developed the 700 MWe CANDU-6, which has been built in several countries outside Canada. India has also built a series of 220 MWe HWRs. Work on evolutionary HWRs is ongoing in Canada, India and Russia and is briefly described below.

The new Canadian evolutionary Heavy Water Reactor[11] is the 935 MWe CANDU-9. Canada is also working on a 400 – 650 MWe Next Generation CANDU. The NG CANDU design features major improvements in economics, inherent safety characteristics and performance. It optimises the design by utilizing SEU fuel to reduce the reactor core size, which minimizes the amount of heavy water required for moderation, and allows light water to be used as the reactor coolant. It is expected that the potential for offsite releases of radioactive material in NG CANDU will be sufficiently low that a target of “no evacuation” can be achieved. In June 2002, Atomic Energy of Canada renamed the NG as Advanced Candu Reactor (ACR) and announced that the ACR-700 will be “market-ready” by 2005.

In India, a continuing process of evolution of HWR design has been carried out. In 2002 construction began on two 500 MWe units at Tarapur which incorporate feedback from several indigenously designed and built 220 MWe units. The Advanced HWR (AHWR), under development in India, is a 235 MW heavy water

moderated, boiling light water cooled, vertical pressure tube reactor with its design optimised for utilization of thorium for power generation. The conceptual design and the design feasibility studies for this reactor have been completed and the detailed design is in progress. The design incorporates a number of passive systems and the overall design philosophy includes achievement of simplification to the maximum extent.

A reactor design concept for an 'Ultimate Safe' reactor with 1000 MW output is being developed by the Russian Institute ITEP, in conjunction with other Russian organizations[12]. The prototype for this conceptual design is the KS150 reactor in Bohunice in the Slovak Republic. Low temperature heavy water is used as the moderator, and the design incorporates gaseous coolant, either CO_2 or a mixture of CO_2 and helium, and low fissile content fuel. The entire primary system, including main gas-circulators, steam generators and intermediate heat exchangers are contained within a multi-cavity, pre-stressed concrete pressure vessel. The design is said to be super safe, for example, accidental withdrawal of all control rods will add a relatively small amount of reactivity to the system compensated by the negative reactor power coefficient.

4.3. Gas-cooled Reactors

South Africa, Japan, China and a consortium of US, Russia, France and Japan are developing small gas-cooled reactor designs and technologies. Coated fuel particles are used in these reactors and they retain fission gases even under accident conditions. Modularization, inherent safety characteristics, direct cycle, and high temperature applications have generated renewed interest in High Temperature Gas-cooled Reactors (HTGR). Japan and China have made the most recent progress in the technology development as they have already constructed and are operating two research reactors; South Africa and the above-mentioned consortium are developing innovative power reactor designs with direct cycle gas turbine for power conversion.

China: The 10 MWe helium-cooled, pebble bed reactor (HTR-10) reached criticality in December 2000. It will initially have steam turbine for phase 1 and later helium turbine for phase 2. Preliminary design of the helium turbine is in progress. It will deliver He at 950 C for electricity generation and for heat applications for coal gasification/liquefaction.

Japan: A High Temperature Engineering Test Reactor (HTTR) with prismatic fuel elements has reached full power this year. This 30 MW_{th} reactor will be the first of its kind to be connected to a high temperature process heat utilization system with an outlet temperature of 850 C. The system will operate as a test and irradiation facility, and be utilized to establish the basic technology for advanced HTGR designs for nuclear process heat applications.

Russian Federation: MINATOM, General Atomics, Framatome and Fuji Electric have combined their efforts to develop the Gas Turbine Modular Helium

Reactor (GT-MHR). This plant features a 600 MW(th) helium cooled reactor as the energy source coupled to a closed cycle gas turbine power conversion system. This is under consideration for the purposes of burning weapon grade plutonium and for commercial deployment. The net efficiency of this advanced nuclear power concept is expected to be 47%. Substantial progress in the development of components such as magnetic bearings and fin-plate recuperators makes this type of HTGR plant a feasible alternative for commercial production of electricity.

South Africa: S. Africa is developing a Pebble Bed Modular Reactor (PBMR) based on technology developed in Germany. The design is a single loop direct gas cycle system that utilizes a helium cooled and graphite-moderated nuclear core as a heat source. The coolant gas transfers heat from the core directly to the power conversion system consisting of gas turbo-machinery, a generator, gas coolers and heat exchangers. The reactor has a thermal power of 268 MW with an electrical output of 110 MW. Improvements of the design are underway to increase the electrical output. The inlet and outlet Helium coolant temperatures are approximately 500 ºC and 900 ºC, respectively. The important design feature of PBMR is its tennis ball sized pebbles containing the silicon carbide coated HTGR fuel particles, which is expected to contain all fission products for the PBMR[13] during all accident conditions, and hence requires no separate containment building.

4.4. Liquid Metal-cooled Reactors

There has been renewed interest in recent years in liquid metal cooled reactors particularly for smaller sized designs and from a sustainable development point of view. They are significant because they can breed new fissile material and extend the potential of nuclear energy. Because of their fast neutron spectrum, which can be used as a burner or a breeder, they have also received recent attention for incinerating weapons plutonium, thorium utilization, partitioning and transmutation of actinides and burning nuclear waste. First used in Russian submarines, liquid lead and lead-bismuth have received worldwide attention in the last few years for power reactors and also for accelerator driven transmutation systems. Russia, India, and Japan have remained most active in recent years in liquid metal power reactor development[14]. The Republic of Korea is developing a pool-type sodium-cooled 150 MWe KALIMER plant with metal fuel and a passive safety decay heat removal system.

India: India's sodium-cooled Fast Breeder Test Reactor (FBTR), has been operating in Kalpakkam for several years. It has a unique mixed uranium carbide-plutonium carbide fuel. It was designed for 40 MWt but has only recently reached a power level of 17.4 MWt. It has achieved a fuel burnup of 90 GWd/t. Thorium blankets have been used in the breeder reactor in Kalpakkam. A 500 MWe sodium-cooled pool type Prototype Fast Breeder Reactor (PFBR) design is under development, also for the Kalpakkam site. It will use U-Pu MOX fuel. The Preliminary Safety Analysis Report for this reactor is nearing completion.

Japan: The two sodium-cooled fast reactors, the Experimental Fast Reactor "Joyo" and the prototype fast breeder reactor "Monju" are not operating at this time. Joyo will start operation in 2003 with a new high-flux core, and Monju is waiting for governmental approval for improvement work for sodium leaks, leading to its eventual startup in 3 more years. However, several small and medium size designs are being developed in Japan, the most prominent one being the 50 – 100 MWe sodium-cooled fast reactor design known as Super Safe, Small and Simple (4S)[15]. In this reactor, Burnup of the core is controlled by the annular reflector surrounding the core, and a long life is achieved by the long length of the core and upward movement of the reflector. The Modular Double Pool (MDP) is another concept of 325 MWe sodium-cooled fast reactor, which has steam generator and secondary pumps in the sodium filled annular space between the primary and the secondary vessel thereby reducing the secondary piping system. Metallic fuel is used for both of these two designs. MDP has been designed to reduce the construction cost and improve reliability by factory manufacture of most components, and 4S has been designed to obtain a long life core. A concept of Multipurpose Fast Reactor (MPFR) has also been proposed which has liquid plutonium-Uranium metallic fueled core. It has 300MW thermal power and does not require fuel reloading[16].

A Pb-Bi cooled Long-life, Safe, Simple, Small, Portable, proliferation-resistant reactor (LSPR)[17] has also been proposed. This is a 35 MWe (150 MWt) integral type design where the steam generators are installed within the reactor vessel. Nitride fuel is used. Natural or depleted Uranium fuel assemblies are placed at the center of the core and Pu fuel assemblies at the outside. In this composition, the burnup will progress from the outer core into the inner blanket region.

Russian Federation: Russia's experience in the construction and operation of sodium-cooled experimental and prototype fast reactors (the BR-10, BOR-60, BN-350 in Kazakhstan and BN-600 with hybrid core) has been very good. Efforts have been directed towards further improving safety and reliability, and making the Liquid Metal Fast Reactors (LMFRs) economically competitive to other energy sources. While these efforts would take some time, LMFRs are being considered to burn weapons plutonium and minor actinides. The current main efforts in sodium cooled fast reactors in Russia have been the lifetime extension for BOR-60 and BN-600, decommissioning of BR-10 and designing BN-800. By 2010, Russia wants to complete construction of the BN-800 fast reactor at Beloyarsk. Russia has also developed three small sodium-cooled reactor designs: MBRU-1.5, MBRU-12 and BMN-170 for production of 1.5, 12 and 170 MWe of electricity[18].

The design from Russia that has received the most recent attention is the BREST reactor, which uses lead coolant, uranium-plutonium mono-nitride fuel and indirect cycle for heat removal to a supercritical steam turbine. Owing to unique combination of the thermo-physical properties of the lead coolant and mono-nitride fuel, BREST can boast of a very high level of natural safety. Two conceptual designs have been developed for the 300 MWe and 1200 MWe BREST reactors. Figure 5

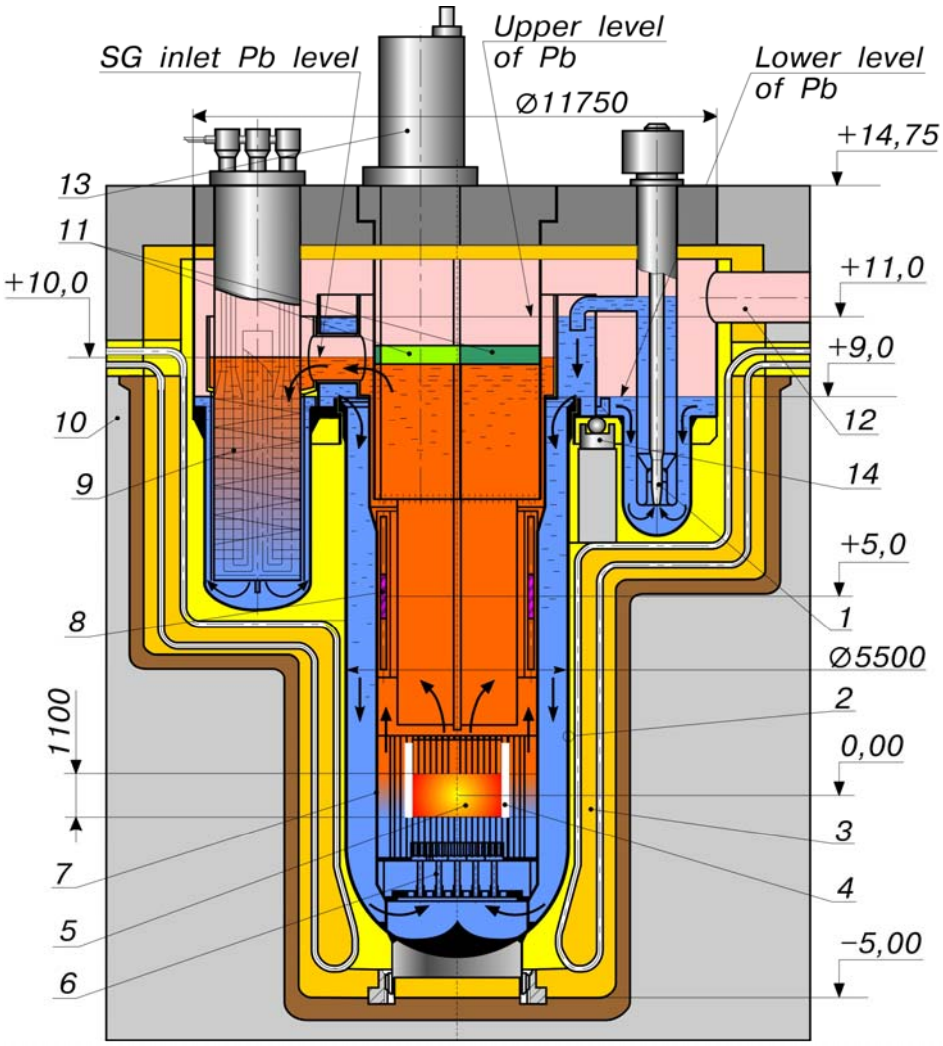

Fig. 5. BREST-300 reactor. Vertical section

gives the schematic details of the 300 MWe BREST design. Russian fast reactor R&D activities are concentrating on advanced concepts with enhanced safety features and designs with alternative coolants, as well as on the development of the basic design, and experimental confirmation, of the lead cooled BREST-300 demonstration reactor with on-site closed fuel cycle[19].

Studies of small fast spectrum reactor modules cooled by lead-bismuth eutectic are also being pursued. These designs, called SVBR-75/100, are based on the reactor operation experience with nuclear submarines. The designs could be used for electricity production, seawater desalination, or the utilization and transmutation of actinides. The SVBR-75 is a Pb-Bi cooled 75 MWe (268 MWt) fast reactor with two-circuits, the primary Pb-Bi circuit and the steam-water secondary loop[20]. Two other heat removal systems are provided for both scheduled and emergency cooling. The reactor operates for 8 years without refueling. Average fuel enrichment is 15.6%.

USA: Although the U.S. had a strong sodium cooled reactor program for many years, it has essentially halted. Recently, however, because of impetus in research for new generation of reactors, one innovative liquid metal cooled design called the Encapsulated Nuclear Heat Source (ENHS) has been proposed[21]. The ENHS is a Pb-Bi natural circulation cooled, 50 MWe (125 MWt), modular, fast reactor concept. It is designed that the fuel is installed sealed into the reactor module at the factory and transported to the site to be inserted into a secondary pool of Pb-Bi that contains the steam generators. Major components, such as the pool vessel and steam generators, are permanent and remain at the site while the reactor module is replaced every 15 or 20 years. The heat generated in the core is transferred through the primary coolant vessel wall to the secondary pool. The natural circulation avoids the need for active components but it requires a tall 19m primary vessel. A design with a lift pump reduces the height to 10m and reduces the coolant mass. The fuel considered is metallic Pu-U-Zr fuel with 11-12% of Pu. The peak fuel Burnup is approximately 105,000 MWD/t. The autonomous control and no fuel handling reduce the nuclear operations onsite to a minimum. Figure 6 gives a schematic description of ENHS.

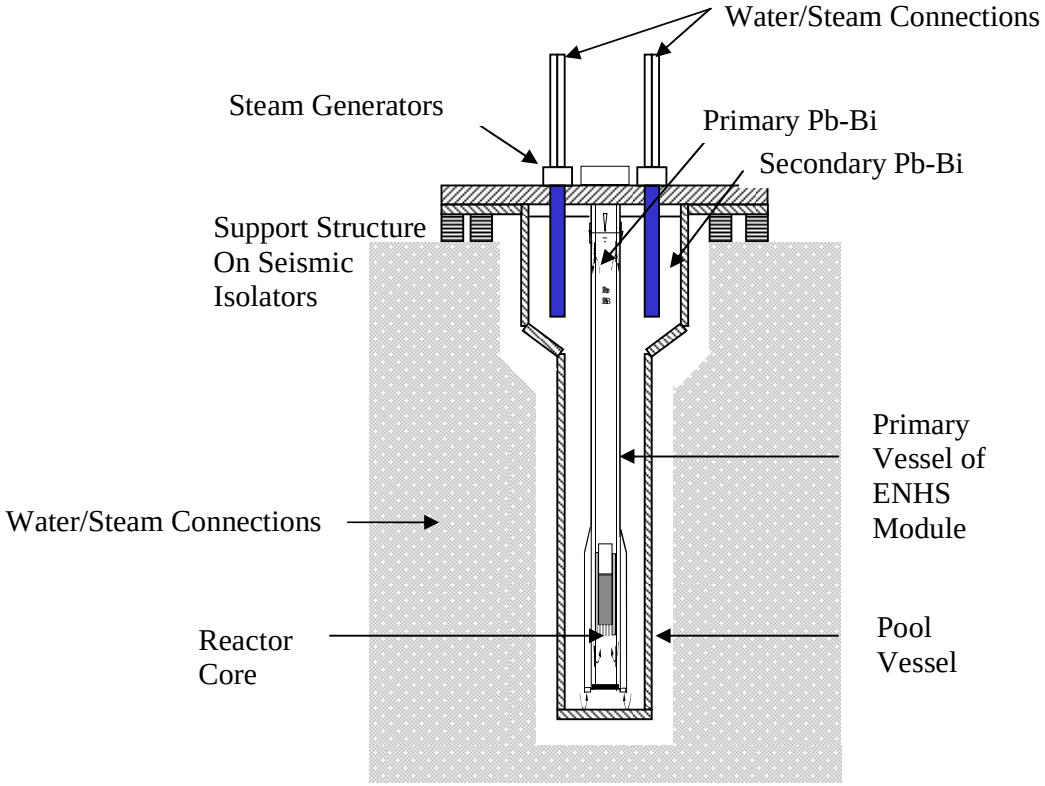

Fig. 6. A Schematic Vertical View of a Single ENHS (Not to Scale)

4.5. Molten Salt Reactors (MSR)

No molten salt reactor is operating now but a considerable interest has been generated among several investigators in the US, Japan and Russia for this concept. This is primarily due to the good operating record of the MSRE in Oak Ridge and to find innovative ways to (1) eliminate fissile material from dismantled nuclear weapons, (2) burn actinides and help in the solution of the nuclear high level waste problem, (3) utilize its inherent safety features, (4) flexibility of using any fissile fuel in continuous mode, (5) higher thermal efficiency from higher temperature operation, and (6) improve non-proliferation. Two types of designs are being pursued: one with fuel mixed with the molten salt coolant (Fig. 7) and the other where molten salt is used only as a coolant (Fig. 8). In the latter case prismatic or pebble bed type HTGR fuel has been advocated. Table VI describes[22] the list of currently known MSRs.

TABLE VI. SOME MSR DESIGNS

Country	Design	Power (MWt)	Primary circuit		Secondary Circuit	Status
			Coolant & Structure	Inlet/Outlet Temp C		
USA	Aircraft Reactor Experiment (ARE)	2.5	NaF ZrF_4UF_4 Inconel	655/800	Helium	Operated in 1954 at ~750 C
USA	Molten Salt Reactor Experiment (MSRE)	8.0	$LiFBeF_2$ ZrF_4UF_4 Hastalloy-NM	632/654	$LiFBeF_2$ Hastalloy-N	Operated during 1965-69
USA	Molten Salt Breeder Reactor (MSBR)	2250	$LiFBeF_2$ ThF_4UF_4 Hastalloy-NM	566/705	$NaFNaBF_4$ Hastalloy- NM	Th-233 U fuel cycle. Design effort discontinued in 1976
Japan	Fuji-II[23]	350	$LiFBeF_2$ ThF_4UF_4 Hastalloy-NM	566/705	$NaFNaBF_4$ Hastalloy- NM	Conceptual design
Russian Federation	High Temperature Molten Salt Reactor (MARS)	300	$LiFBeF_2$	600/750	Air	Conceptual Design
Russian Federation	Gas-cooled Molten Salt Reactor	2000	$LiFBeF_2$ ThF_4UF_4	600/750	$NaFNaBF_4$	Designed especially for industrial applications
France	CCDP	2000	$LiFBeF_2$ ThF_4UF_4	550/700	Plumbum	Conceptual Design
China	MSGR	2250	$NaFBeF_2$ Hastalloy-NM	566/705	$NaFNaBF_4$	Conceptual design

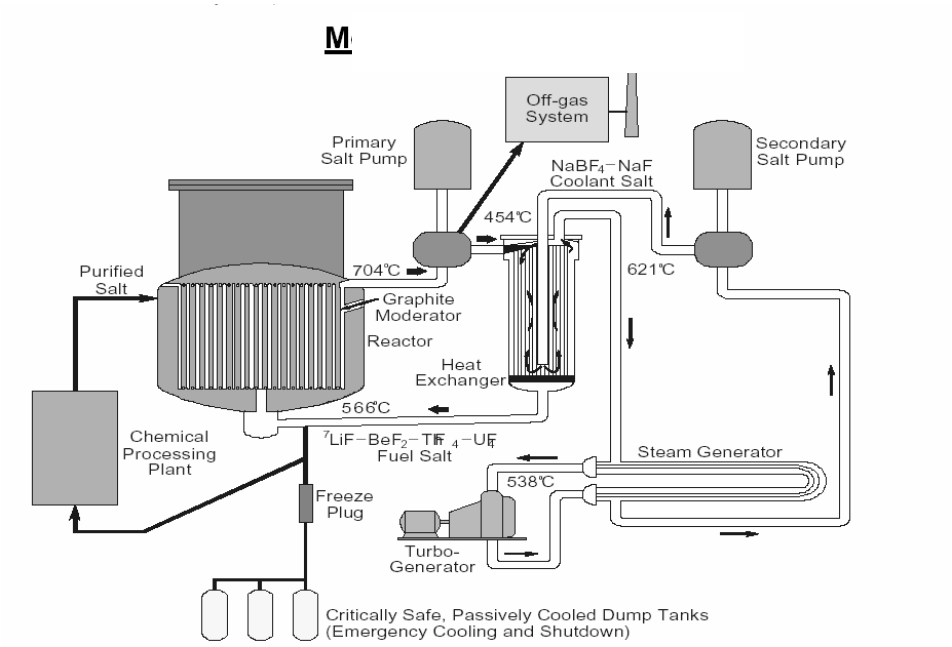

Fig. 7. Schematic diagram of a molten salt reactor such as the MSRE[21]

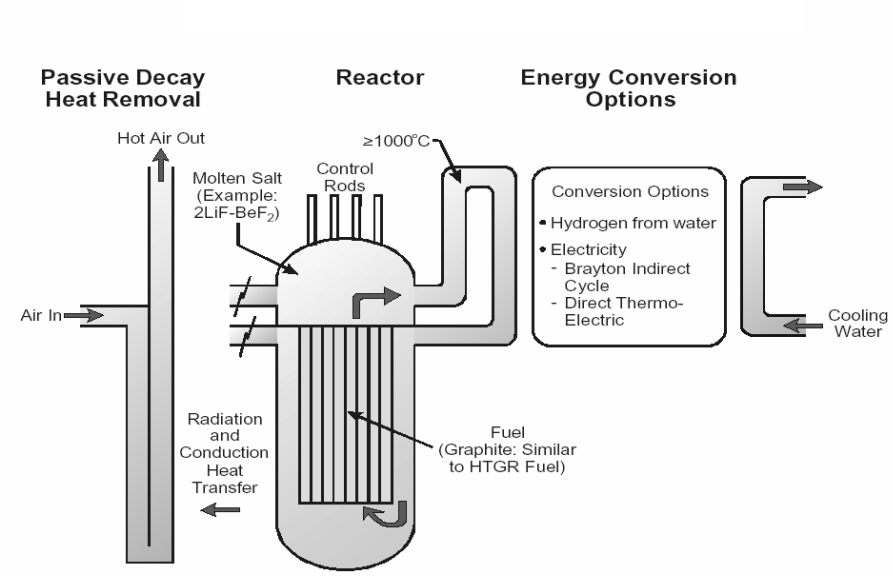

Fig. 8. Schematic diagram of a molten salt cooled reactor such as MARS[24]

4.6. Small and Medium Sized Reactors

Although a considerable progress has been made in the evolutionary designs of LWRs, these are large reactors and many believe[25] that development and demonstration of new, smaller, innovative designs with short construction and start-up times and low capital costs are necessary to usher a new era of nuclear power. Since the early 1990s, the interest of developing countries, mainly in Asia, has resulted in increased efforts on the design of small and medium sized power reactors. This is because in the next 50 years, electric demand is expected to be tripled, most of which will come from developing countries with small grid capacities. Also, in industrialized countries, electricity market deregulation is calling for power generation flexibility that smaller reactors may offer. Small and medium reactors (SMRs) are also of particular interest for non-electric applications such as seawater desalination and district heating, fuel synthesis, and, in the future, hydrogen production.

Small and medium sized reactors are, however, not new. We have currently 150 SMRs operational in the world, 41 of these with power levels less than 300 MWe and 109 having power levels between 300 and 700 MWe. The detailed breakdown show 32 gas cooled reactors in UK (AGR and GCR), 32 PWR, 24 BWR, 29 WWER and 27 HWRs.

Recent major drive for innovation in light water reactors has been toward integral reactors, where the core, pumps, pressurizers, and steam generators are contained inside a single reactor pressure vessel (RPV). They are of enhanced safety because there is no large break LOCA; they also endure less fluence on the reactor pressure vessel and employ passive safety systems. Three primary examples of these reactors are CAREM (Argentina), IRIS (USA), and SMART (Republic of Korea). Being small, they allow more shop-fabrication and hence improved quality. These are being designed primarily for sizes up to 700 MWe due to easy constructability of Reactor Pressure Vessels and to better match smaller electric grids.

SMR designs are also attempting to increase the fuel core life to enhance proliferation-resistant features and also to reduce the O&M costs. Eight to even 20 years of single core life has been envisioned. Another idea in this regard is to have refueling services provided by a central refueling organization, with crew dedicated to refueling, visiting each site as required. This would also improve efficiency. Similarly, barge mounted reactors could be returned to a central location for refueling.

Some designs have proposed to make extensive use of modularization, in which a significant portion of the plant is built as modules, which are fabricated outside of the principal buildings of the nuclear power plant. In some cases, the modules are fabricated off-site, to take advantage of existing fabrication facilities. Modularization serves to transfer a significant portion of the construction labor from

the nuclear power plant to more easily controlled manufacturing environment. This reduces the site construction infrastructure and shortens the construction schedule, and hence the capital cost.

In order to improve economics, small reactor designs strive to minimize the manpower costs associated with the operation of the reactors. The inherent reactor shutdown and passive decay heat removal capability of some designs, in combination with modern advanced communication systems, may even facilitate remote operation with fewer operators, or even unattended, for some applications.

New research is underway to utilize the unique thermo-physical properties of supercritical water to enhance nuclear plant thermal efficiency to 40 – 45% from the current 33 –34%. This will also lead to considerable plant simplification. Because there will be no change of phase in the core, the need for steam separators and dryers as well as for BWR-type recirculation pumps is eliminated, which will lead to smaller reactor vessels. In a direct cycle steam generators are not needed. However, to make this possible, advances are required in high temperature materials to improve corrosion, stress corrosion cracking, and wear resistance.

Major innovative reactors in the world[26] are tabulated in Table VII. Key features of SMRs include simplification and streamlining of designs as well as emphasis placed on safety features avoiding off-site impacts in case of accident. Such characteristics should facilitate their acceptability by local communities. However, none of these reactors have been built; only recently announcements have been made for beginning the preparatory phase for construction of KLT-40 in Severodvinsk in Russia and of a 65 MWt pilot version of SMART in KAERI, Republic of Korea. Two KLT-40 nuclear submarine reactors will be built on a floating barge with a displacement capacity of 20,000 tonnes. It is expected that the floating nuclear plant in Russia will produce power in 2006 and the pilot plant in Korea in 2008.

TABLE VII. MAJOR INNOVATIVE REACTOR DESIGNS UNDER DEVELOPMENT AROUND THE WORLD

Reactor	Power (MWe)	Country of origin	Status/imp. features
A. Light Water Reactors			
IRIS	100 – 300	USA-led multinational	Integral, 8-year core; under design.
Triga Power System	64	USA, General Atomic	Commercial design
CAREM-25	27	Argentina	Integral, self-pressurized; Regulatory approval received.
SMART	300 MWt	Republic of Korea	Integral. 65 MWt pilot plant to be built.
KLT-40	35	Russian Federation	Floating NPP, ready for construction
UNITHERM	15 MWt	Russian Federation	Based on marine reactor; 20 years core life, dual purpose.
RUTA-55	55 MWt	Russian Federation	Low-temp, Pool type at atm. pressure
VK-300	250	Russian Federation	Based 0n VK-50 BWR. Dual use possible.
ABV-6	6	Russian Federation	Compact, based on marine reactor; land or sea use.
ATU-2	40	Russian Federation	Water-graphite reactor.
MRX-based designs	Various	Japan	Integral; 8 year core life for PSRD. Some for heat only.
IMR	<300	Mitsubishi, Japan	Integral PWR
HABWR	600	Hitachi, Japan	Forced circulation BWR
HSBWR	300 – 600	Hitachi, Japan	Natural Circulation BWR
SSBWR	150	Hitachi, Japan	Small BWR with natural circulation
LSBWR	100 – 300	Toshiba, Japan	Long life core.
NHR-200	200 MWt	China	Upgrade from NHR-5; designed for non-electric.
B. Other Reactors			
PBMR	110	ESKOM, S. Africa	Pebble Bed Gas-cooled Reactor
GT-MHR	286	US, Japan, France, Russia	Gas-cooled prismatic reactor with direct gas turbine
4S	50 –100	Japan	Sodium-cooled fast reactor
Brest	300	Russian Federation	Lead-cooled, mono nitride fuel.
ENHS	50	USA	Lead-Bismuth-cooled, modular fast reactor.

5. UTILIZATION OF THORIUM FUEL

There has been a recent renewed interest in thorium fuel cycles. The reasons for this are to (1) burn excess weapons Pu without creating more, (2) generate less long-lived radioactive waste, (3) design reactors to operate in a safer mode, (4) reduce U-235 enrichment, (5) go to higher temperatures, and finally having large thorium deposits.

Thorium-232 is three times more abundant than uranium and available in India, Brazil, USA, Turkey and China. It is not a fissile material but it can produce U-233 in a reactor, which, from a neutronic standpoint, is an excellent nuclear fuel among the three nuclear fuels – U-235, Pu-239 and U-233. It also produces much less minor actinides from fission. Thorium dioxide is the only stable oxide of thorium, which accounts for its greater stability compared to uranium dioxide. It is also much more resistant to chemical interactions and has a high thermal conductivity. The melting point of thorium dioxide is 3050 degree centigrade. Thorium contains naturally up to about 100 ppm of Th-230; this and other neutron reactions of Th-232 and U-233 produces U-232, which decays with emission of hard gamma rays. Thorium fuel fabrication is similar to U-fuel but it requires remote operation because of the gamma emission from U-232 decay chains. In addition high chemical inertness of thorium dioxide makes it very difficult to be dissolved and reprocessed. Because of these drawbacks the thorium fuel cycle is considered a more proliferation-resistant fuel.

Thorium fuel cycles have been studied in the past in several countries on a smaller scale but its importance has increased in recent years as a non-proliferating fuel and also for reducing the inventory of Pu. Germany had used Thorium fuels for several years on the AVR, a pebble-bed high temperature research reactor, and on the THTR, Thorium High Temerature Reactor. Both in Germany and the US the fuel fabrication technology has been developed under high temperature reactor programs to a well proven, industrial process. The coated fuel particles for the HTGRs have shown excellent performance under irradiation and reactor operation. In Russia also tests of thorium-based fuels for WWER and LMFBRs have shown an excellent irradiation behavior.

The US has shown new interest in thorium fuel and has initiated four projects under the Nuclear Energy Research Initiative. Their primary motive is to develop an advanced proliferation-resistant, low cost uranium-thorium dioxide fuel. The Radkowski Thorium Reactor (RTR), being investigated in the US, Russia and Israel, revives the seed-blanket concept of the US Light Water Breeder Reactor design that operated in Shippingport in the late 50s. The concept assumes a once-through fuel cycle with no reprocessing; U-233 is bred and mostly burned in the reactor.

Most prominently, India has been pursuing a strong program on thorium fuel cycle activities. India has a closed fuel cycle strategy, which calls for using U-Pu fuel cycle for fast breeder reactors and a closed Th-U-233 fuel cycle in the next stage with

advanced heavy water reactors. The Advanced Heavy Water Reactor (AHWR), currently under design, plans to use thorium for 75% of the power. Utilization of thorium is their focal point for development. All aspects of the fuel cycle including the back end are being studied in India. Activities for Thorium fuel development in India include studying: (1) dissolution of irradiated thorium fuel, (2) effective utilization of recovered fissile and fertile material, and (3) thorium fuel fabrication.

6. PARTITIONING AND TRANSMUTATION OF RADIOACTIVE WASTE

A lot of attention has been given in recent years on the subject of partitioning and transmutation of the actinides and some long-lived fission products contained in the spent fuel as it has the potential of easing operational and safety requirements of a repository. Some would even like this to become an important alternative to direct disposal of spent fuel. Separation of the long-lived isotopes and transmutation of these into less hazardous materials have several advantages. It allows a reduction of the volume, toxicity, and fissile content of waste and supports a simpler repository. The issues related to long-term disposal of spent nuclear fuel is attributable to only ~1% of its content, namely plutonium, neptunium, americium, and curium (the transuranic elements) and long-lived isotopes of iodine and technetium. When transuranics are removed, the toxic nature of the spent fuel drops below that of natural uranium ore within a period of several hundred years. The removal of neptunium, technetium, and iodine also makes the waste safer for the biosphere. Removal of plutonium eliminates the relevance of the waste from the point of view of nuclear proliferation. Thus if the nuclear waste can be partitioned and transmuted economically to more benign materials, the waste can be disposed of in controlled environments having time scales of a few centuries rather than millenniums.

Partitioning and transmutation requires advanced reactor and fuel cycle technologies, including multiple recycle strategies. That is the spent fuel must be reprocessed. Partitioning of waste can be accomplished by both aqueous and non-aqueous methods. The Argonne National laboratory in the US has developed an electrometallurgical non-aqueous process that can separate fissile material from fission products. This process can be used for both metallic and oxide fuels. For transmutation, both accelerator driven systems (ADS) and fast reactors are being considered for actinide burning. The ADS has the potential of providing both plutonium and minor actinide utilization, and enhanced safety of sub-critical operation. It has been recognized that a pure accelerator driven system for transmutation of waste is too costly, and hence a dual concept of power production and transmutation is being envisioned. This option combines the accelerator and fission reactor technologies; neutrons are generated by directing a beam of high-energy protons from an accelerator against a heavy target such as lead or lead-bismuth eutectic and these neutrons are then used in a surrounding blanket to fission the actinides and transmute the long-lived fission products. Unlike a conventional reactor the blanket is sub-critical and cannot sustain a chain reaction without the

accelerator generated neutrons. Power is generated from this sub-critical facility while transmuting the waste.

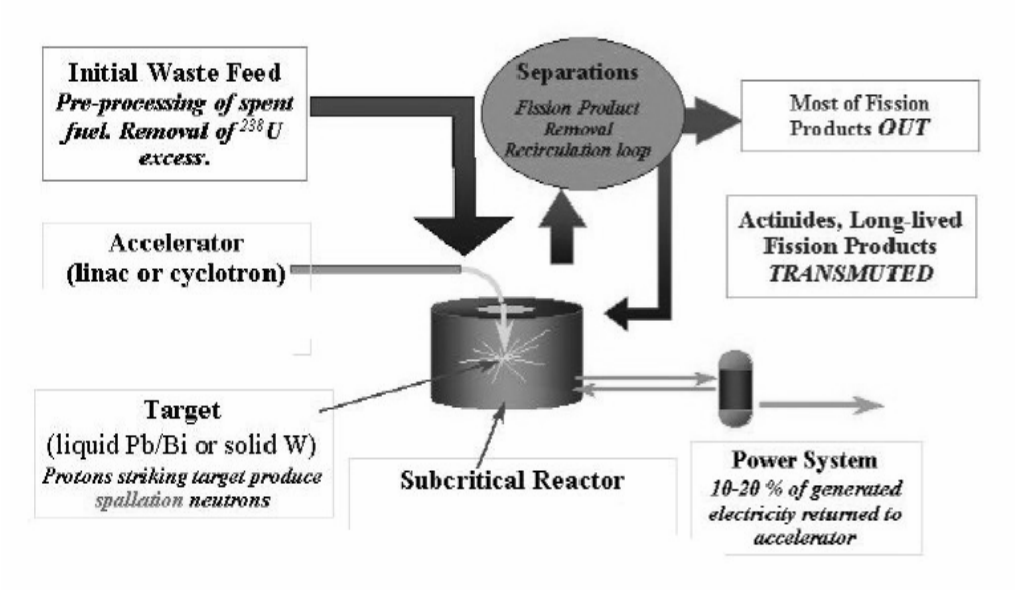

Fig. 9. A schematic diagram of an Accelerator Driven System to incinerate waste and produce electricity.[27]

Various ADS schemes are being studied in several countries: the OMEGA (Option Making Extra Gain from Actinides) project in Japan, Advanced Accelerator Applications (AAA) program in the US, HYPER (Hybrid Power Extraction Reactor) project in the Republic of Korea, European Industrial Partnership and other projects at CERN, and CEA, France, and China. Russia is also participating in international collaboration activities. Carlo Rubbia's "Energy Amplifier" is one ADS design that provided a strong, early impetus in developing a system to generate more energy than needed for the accelerator.

There are many technical problems to be solved; ADS is only at the beginning stage of investigation. It is very likely that the best results in terms of high level waste radio-toxicity reduction will be achieved by symbiotic systems, including critical fast reactors and hybrid systems (e.g., accelerator driven concepts).

7. CURRENT ISSUES

Although fuel diversity and energy security are important items for a country, economic competitiveness with alternate sources of electricity has been recognized as the critical element for the survival of nuclear power. Hence consorted efforts are being made with design, construction, operation and maintenance of new nuclear

power plants to reduce its capital and operation costs. Currently nuclear production costs (fuel and O&M) of existing plants are low, approaching 1 cent/KW-hr; hence the critical issue is capital cost for new plants. Also, investors expect a short-term payback of capital costs such as within 20 years of operation. It appears that capital costs in the range of $1000 – 1200 per KWe are needed for competition with natural gas. In this regard, construction of large nuclear power plants, if allowed by the infrastructure of a country, provides an advantage. At the same time, new generation of small, innovative plants are needed for specific markets and especially for developing countries.

Non-proliferation and physical protection have become more important for nuclear power plants since the September 11, 2001 terrorist event in New York. In spite of the demonstrated effectiveness of the international safeguards regime, the risk of proliferation of nuclear weapons remains a social and political concern. A significant deployment of nuclear power would lead to building a large number of reactors in many different countries and sites, and there may not be sufficient resources to safeguard all reactors. Therefore, gaining acceptance will require specific efforts of designers to enhance the proliferation resistance characteristics, particularly for the SMRs. It has also been argued that since no country has made nuclear weapons from the civilian nuclear power program and we surely have the international, scientific and regulatory mechanisms to handle the proliferation question, we should move forward as rapidly as possible to build nuclear power where it can meet human and environmental needs. In any case, the world must remain vigilant and the suppliers, verifiers, and buyers must assure safeguarding of nuclear materials.

The September 11, 2001 event has highlighted the importance of protecting nuclear facilities from sabotage and stealing of nuclear material by terrorist organizations. Even if the actual impact of a potential terrorist activity is very minimal, the occurrence of such an event will create havoc from the public perception point of view; hence nuclear facilities including spent fuel storage facilities must be secured. An issue here is how to achieve this in a cost-effective manner and how much security effort is good enough.

Disposition of spent fuel is a challenge and a roadblock for nuclear power. However, great progress has been made this year when the governments of Finland and USA have approved the construction of geologic repositories in Olkiluoto in Eurajoki, Finland and at Yucca Mountain, Utah, USA. Finland is now set to become the first country in the world to build a final repository for spent fuel from nuclear power plants. Sweden and the US are also well ahead with similar plans.

8. INTERNATIONAL EFFORTS

Several countries and groups are working on innovative reactor technology development. However, to develop a cost-effective innovative reactor design a large

amount of research is required, particularly for the design and testing of new fuel and other materials and the final demonstration. In the deregulated market no one company or even a country can afford to or willing to allocate the expenses necessary to bring a design to the market place. Hence international development and partnership may be required. From this perspective two efforts are already underway – the US-initiated Generation IV International Forum (GIF) and the IAEA-initiated International Project on Innovative Nuclear Reactors and Fuel Cycles (INPRO).

The time frame of interest to the GIF is two or three decades from now, and their goal is development of suitable technology for nuclear power (reliable and safe, sustainable, and economic). They also want to increase the assurance that the reactor system is a very unattractive and undesirable route for diversion or theft of weapons-usable materials. The US DOE has conducted wide-ranging discussions on the development of next-generation nuclear energy systems, engaging governments, industry and the research community of several countries. Ten countries have joined in this effort; they are Argentina, Brazil, Canada, France, Japan, Republic of Korea, South Africa, Switzerland, UK and the US. After long deliberations, the GIF has selected six areas for further research and collaboration among interested countries. These are gas-cooled fast reactor, molten salt reactor, liquid sodium metal-cooled reactor, lead alloy-cooled reactor, supercritical water-cooled reactor and very high temperature reactor systems.

The objective of INPRO is to support the safe, sustainable, economic and proliferation-resistant use of nuclear technology to meet the global energy needs of the 21st century. INPRO is mainly focusing on developing user's requirements for nuclear power for the long term – fifty years time frame. As of January 2002, there were 13 members in INPRO: Argentina, Brazil, Canada, China, Germany, India, Republic of Korea, Russian Federation, Spain, Switzerland, The Netherlands, Turkey and the European Commission. The INPRO is developing a report to identify global user requirements for economics, safety, spent fuel and waste, non-proliferation and the environment, and establishing the criteria and methodologies for examination of nuclear reactor and fuel cycle technologies. The INPRO developed criteria are expected to be used by individual countries to assess their situation with respect to nuclear power introduction or expansion.

Conclusion

The global energy market is rapidly increasing and is expected to triple in about 50 years. Nuclear energy is free from greenhouse gas emissions and is excellent from an environmental perspective. In a closed cycle mode of operation, nuclear energy is almost an infinite source of energy; it could help improve the standard of living of all countries in the world. So nuclear power should expand, especially in developing countries, and could contribute to sustainable energy development for the world. With this in mind, many evolutionary designs of nuclear power plants have been developed to meet the high performance and the safety goals. The efficiency and

economics of these new plants are excellent and are beginning to compete with other base load alternatives. These larger plants are currently being constructed in Japan, Republic of Korea and Taiwan, China. New small and medium sized designs are underway. They are of interest to many countries for many reasons. Due to population growth and demand for a higher standard of living, they are of primary importance to countries with a shortage of electric power and low grid capacity. Work is progressing on several innovative reactor and fuel cycle designs in several countries. However, these innovative, smaller reactor designs must be demonstrated in the near future because the time frame for the availability of commercial SMRs is very important as most developing countries can not wait for another two or three decades to increase their installed electricity generation capacities.

Many challenges remain for nuclear power to become an acceptable source of energy throughout the world. Notable among these are (1) implementing the disposal of high level waste, (2) making nuclear generated power economically competitive with fossil fuel alternatives in the deregulated market place, (3) continuing to assure non-proliferation and physical safety of nuclear plants, (4) developing economic reactors for small electricity grids and non-electric applications, and finally (5) continuing to assure the safety of nuclear reactors. The new evolutionary and innovative designs are responding to these challenges. Let us hope that the new surge of interest in nuclear power and the new activities that have been initiated in several countries will lead to a solution of the nuclear issues and provide adequate energy for all humanity.

References

[1] J. Murray "Global Energy Supply and Demand and the Potential Role of Nuclear Power," Proceedings of the International Seminar on Status and Prospects for Small and Medium Sized reactors, Cairo, 27 – 31 May 2001.

[2] IPCC Third Assessment Report: Climate Change 2001, Watson, R.T. and the Core Writing Team (Eds.), IPCC, Geneva, Switzerland.

[3] IAEA EEDB and PRIS data base, 2002.

[4] IAEA PRIS data base, Nuclear Power Reactors in the world, April 2002.

[5] *Advanced light water reactor utility requirements document*, Electric Power Research Institute.

[6] *European utility requirements for LWR nuclear power plants* (revision B), November, 1995.

[7] International Atomic Energy Agency, *Terms for Describing New, Advanced Nuclear Power Plants*, IAEA-TECDOC-936, IAEA, Vienna (1997). Also see *Projected costs of generating electricity - Update 1998*, OECD-NEA.

[8] J. Kupitz, "Status and trends in advanced nuclear power plants development and applications," presented in Workshop on Nuclear Reaction Data and Nuclear Reactors: Physics, Design and Safety, 13 March – 14 April 2000, Trieste, Italy.

[9] W. D. Magwood, "Looking Toward Generation Four: Considerations for a New Generation R&D Agenda," American Nuclear Society Proceedings, June 7, 1999.

[10] Nuclear Reactor technology Review 2001, IAEA report.

[11] International Atomic Energy Agency, 'Heavy Water Reactors: Status and Projected Development' TRS 407 IAEA 2002

[12] IAEA Technical report series no. 407, Heavy Water Reactors: Status and Projected Development, Vienna 2002.

[13] J.F.M. Slabber, "Non-proliferation aspects of the PBMR fuel cycle," Proceedings of the International Seminar on Status and Prospects for Small and Medium Sized reactors, Cairo, 27 – 31 May 2001.

[14] P.E. Juhn and Y.I. Kim, "Fast reactor technology development and IAEA's activities."

[15] I. Kinoshita and A. Minato, "Liquid metal cooled small reactors (MDP & 4S) in Criepi," Proceedings of the International Seminar on Status and Prospects for Small and Medium Sized reactors, Cairo, 27 – 31 May 2001.

[16] T. Swada, A. Netchaev, H. Endo, H.Ninokata, "Long life multipurpose small size fast reactor with liquid metallic-fuelled core," Proceedings of the International Seminar on Status and Prospects for Small and Medium Sized reactors, Cairo, 27 – 31 May 2001.

[17] H. Sekimoto, S. makino, K. Nakamura, Y. Kamishima, and T. Kawakita, "A long-life small reactor for developing countries, LSPR," Proceedings of the International Seminar on Status and Prospects for Small and Medium Sized reactors, Cairo, 27 – 31 May 2001.

[18] A. I. Kiryushin, B.A. Vasilev, V. Yu, Sedakov, and V. Polunichev, "Small power sodium cooled fast nuclear reactors," Proceedings of the International Seminar on Status and Prospects for Small and Medium Sized reactors, Cairo, 27 – 31 May 2001.

[19] E. Adamov, V. Orlov, et. al., "Conceptual Design of BREST-300 Lead-Cooled Fast Reactors", Proc. of ARS'94 International Topical Meeting on Advanced Reactor Safety, Volume 2, Pittsburgh, April, 1994.

[20] B. F. Gromov, O.G. Grigoriev, A.V. Dedoul, A.V. Zrodnikov, G.I. Toshinsky, et. Al., "Nuclear power complex based on SVBR-75 small reactors cooled by lead-bismuth liquid metal coolant, competitiveness, simplified life cycle, safety, non-proliferation," Proceedings of the International Seminar on Status and Prospects for Small and Medium Sized reactors, Cairo, 27 – 31 May 2001.

[21] D. Wade, J. Sienichi, N. Brown, Q. Hossain, M. Carelli, et. al., "The Encapsulated nuclear heat source reactor for low-waste proliferation-resistant nuclear energy," Proceedings of the International Seminar on Status and Prospects for Small and Medium Sized reactors, Cairo, 27 – 31 May 2001.

[22] P.N. Alekseev, I.A. Belov, N.N.Ponomarev-Stepnoy, S.A. Subbotin, Y.N. Udjansky, A.V. Chibinjaev, T.D. Schepetina, and P.A. Fomichenko, "Micro-particles fuel autonomous melted salt reactor (MARS)," Russian Research Centre, Kurchatov Institute, IAE-6216/4

[23] K. Furukawa, K.Mitachi, and Y. Kato, "Small molten-salt reactors with a rational thorium fuel cycle," Nucl. Eng. and Design 136, 157-165, 1992.

[24] Figure taken from GIF presentation at the Winter ANS meeting in Reno, Nevada, 2001.

[25] D. Majumdar, J. Kupitz, H. Rogner, T. Shea, F. Niehaus and F. Fukuda, "Development of Nuclear Reactors and Fuel Cycles: The need for innovation," IAEA Bulletin, Vol 42, No. 2, 2000.

[26] D. Majumdar and J. Kupitz, "A Global perspective on small and medium reactor designs," paper presented at the 4th International Conference on nuclear option in

countries with small and medium electricity grids, Dubrovnik, Croatia, June 16 – 20, 2002.

[27] H. Conde, “Introduction to ADS for waste incineration and energy production,” Uppsala University, Sweden.

Desalination and Other Non-electric Applications of Nuclear Energy

Debu Majumdar*

Nuclear Power Technology Development Section,
Division of Nuclear Power, Department of Nuclear Energy,
IAEA, Vienna, Austria

Lectures given at the
Workshop on Nuclear Reaction Data and
Nuclear Reactors: Physics, Design and Safety
Trieste, 25 February – 28 March 2002

LNS0520005

* D.Majumdar@iaea.org

Abstract

As the standard of living increases globally, the need for fresh water and industrial products is also increasing; they require energy for production and hence, the demand for energy – both electric and non-electric, is also increasing. Nuclear energy provides now only about 7% of global energy use; fossil fuels which degrade the environment provide the rest. Nuclear energy has the potential to provide an abundance of greenhouse-gas-free energy for mankind. Currently, nuclear energy is mainly used for electricity production. This paper discusses non-electric applications of nuclear energy, summarizing the global status and enumerating the areas where it could be used.

1. INTRODUCTION

Some of the first civilian reactors in the world were used to supply heat, e.g., Calder Hall in UK (1956) and Agesta in Sweden (1963). Calder Hall provided electricity to the grid and heat to a fuel reprocessing plant, and Agesta provided hot water for district heating of a suburb of Stockholm. The first nuclear power station in Russia (1954) was also a multi-purpose facility providing electricity and heat to the closed city of Obninsk in Kaluja region, near Moscow. Currently less than 1% of the heat generated in nuclear reactors is used for non-electric applications[1]. Direct use of heat energy is more desirable from an energy efficiency point of view and nuclear energy is an enormous source of greenhouse-gas-free energy. However, nuclear power has remained primarily a source for electricity generation. Presently about 30% of the world's primary energy is used for electricity production, and approximately 2/3 of this energy is thrown away as waste heat. Yet despite past and current use models, it is possible to optimise the use of nuclear heat for both electric and non-electric applications, thereby making more efficient use of nuclear energy. Experience in co-generation of nuclear electricity and heat has been gained in Bulgaria, Canada, China, Hungary, Kazakhstan, Russia, Slovakia and Ukraine[2]. This paper examines the scope of non-electric applications of nuclear energy[3] .

There are four areas where nuclear heat can be utilized: for desalination of salty and waste water, district heating of residence and commercial buildings in cold countries, industrial process heat supply, and fuel synthesis. Primary experience of non-electric applications of nuclear energy is in the first two categories. There are more than 150 reactor-years of operating experience with nuclear desalination, particularly in Japan and Kazakhstan. District heating systems from nuclear power plants have operated reliably in many countries, particularly in Eastern Europe. Fuel synthesis has evolved in recent years because nuclear energy can generate high temperature heat; this heat can be used for hydrogen production, coal gasification and production of other fuels. The heating requirements of different industrial processes vary. The temperature requirements for the principal applications are shown in Table I. They vary from low temperature applications for hot water to high temperature industrial processes.

TABLE I. TEMPERATURE NEEDS OF VARIOUS TYPES OF INDUSTRIAL PROCESSES

Industrial Process	Approximate Temperature Range (Centigrade)
Home and building heating	100 – 170
Desalination	100 – 130
Vinyl Chloride production	100 – 200
Urea synthesis	180 – 280
Process Steam	200 – 400
Paper and pulp production	200 – 400
Oil refining	200 – 600
Oil shale and oil sand processing	300 – 600
Crude oil desulphurisation	300 – 500
Petroleum refineries	450 –550
Production of synthetic gas and Hydrogen from natural gas or naphtha	400 – 800
Steel making via direct reduction	500 – 1000
Iron industry	600 – 1600
Production of styrene from ethyl-benzene	600 – 800
Production of ethylene from naphtha or ethane	700 – 900
Hydrogen production by thermo-chemical reaction	600 – 1000
Coal processing	400 – 1000
Coal gasification	800 –1000

Various types of reactors are designed with different ranges of inlet and outlet coolant temperatures, and hence will be useful for different applications. Table II shows the range of coolant temperatures for different reactor types. A nuclear plant can provide steam or process heat from about 100 C for district heating or desalination to about 1000 C for very high temperature industrial applications. Table III shows the characteristic parameters of steam that could be produced by various reactor types[4]. Water reactors can provide steam in the range of 250 to 300 C at about 5 to 7 Mpa pressure, while liquid metal and gas cooled reactors can generate steam at higher temperature and pressure. LMFBRs can provide steam at approximately 500 C and gas cooled reactors at somewhat higher temperatures.

TABLE II. TEMPERATURE CAPABILITIES OF REACTOR TYPES

Reactor Type	Typical Primary Coolant Inlet & Outlet Temperatures (Centigrade)
Pressurized Water Reactor (PWR)	280 – 320
Water Reactor (BWR)	278 – 288
Heavy Water Reactor (HWR)	250 – 295
Liquid Metal-cooled Reactor (LMCR)	390 – 540
High Temperature Gas-cooled Reactor (HTGR)	500 – 950

TABLE III. TYPICAL STEAM PRODUCTION BY DIFFERENT REACTOR TYPES

Nuclear Power Plant	Steam Parameters	
	Pressure (Mpa)	Temperature (C)
PWR (U-tube SG)	6.5	280
PWR (Once-through SG)	6.9	312
BWR	5.5	270
PHWR	5.6	271
CANDU PHWR	4.7	260
Phenix LMFBR	16.3	510
THTR-300	18.1	530
Fort St.Vrain HTGR	17.3	541

2. DESALINATION

Water is essential for living but over a billion people, approximately 20% of the world's population, lack safe drinking water, and three billion lack access to adequate sanitation[5] for lack of water. Unfortunately, 94% of the world's water is salt water and only 6% is fresh[6], and less than 1% of the fresh water is easily accessible (27% being in the glaciers and 72% underground). As the standard of living increases all over the globe, the demand for both energy and water is also increasing. In this regard, the development and use of water desalination technologies[7] are helping tremendously. Desalination of water requires energy but, as shown in Table I, it can be done at relatively low temperatures. Waste heat from power plants is sufficient for this purpose. Nuclear power can play a significant role, particularly in a dual capacity,

by providing water in addition to greenhouse-gas-free energy. Many years of successful operation have proved the technical feasibility and reliability of nuclear plants for producing fresh water[†].

Desalination technologies have evolved over the past 50 years to large-scale commercial processes. The major commercially available processes are of two kinds: (a) thermal processes, where heat is used to vaporize and distill fresh water from saline water; these are multi-stage flash distillation (MSF), multiple-effect distillation (MED), and vapor compression (VC), and (b) membrane processes where suitable membranes are used for the separation of salts such as the mechanism of reverse osmosis (RO). There are also other minor processes such as freezing and solar evaporation. Globally about 26 million m^3/d of fresh water is produced by desalination (including both brackish and seawater plants). The maximum is produced in Saudi Arabia, about 21%. The U.S. produces approximately 17%, 80% of which is achieved by membrane processes.

The possibility of using nuclear energy for desalination of seawater was realized as early as the 1960s. Experience with nuclear desalination now exceeds 150 reactor-years. Table IV gives a list of the nuclear plants, which have been used for desalination of water; it also provides information about the reactor types, desalination technologies employed and the fresh water capacity of the plant[8]. The Kazakhstan nuclear plant was shut down in 1999 and was the only power reactor in the world supplying heat for industrial-scale desalination[9]. It produced 80,000 m^3/d of potable water for municipal use. The Diablo Canyon Nuclear Power Plant in the U.S. also produces 4500 m^3/d of fresh water from the sea for in-plant use; they use RO membrane technology[10]. Table V gives details of operating experience of LWRs in Japan, a PHWR in Pakistan, and the LMR in Kazakhstan. It should particularly be noted that there was no incidence of radioactive contamination of the water produced.

[†] Nuclear desalination can be described as production of potable water from seawater or brackish water in a facility in which a nuclear reactor is used as the source of energy for the desalination process.

TABLE IV. EXPERIENCE IN NUCLEAR DESALINATION PLANTS

Plant Name	Reactor Type	Gross Power (MWe)	Desalination Process	Water Capacity M^3/d
Ikata-1,2 (Japan)	PWR	2x566	MSF	200
Ikata-3 (Japan)	PWR	890	RO	2000
Ohi-1,2 (Japan)	PWR	2x1175	MSF	3900
Ohi-3,4 (Japan)	PWR	2x1180	RO	2600
Genkai-4 (Japan)	PWR	1180	RO	1000
Genkai-3,4 (Japan)	PWR	2x1180	MED	1000
Takahama-3,4 (Japan)	PWR	2x870	MED	1000
Kashiwazaki (Japan)	BWR	1100	MSF	1000
KANUPP (Pakistan)	PHWR	137	RO	454
BN-350 (Kazakhstan)	LMR	150 (till 1999)	MSF & MED	80000

TABLE V. NUCLEAR DESALINATION OPERATING EXPERIENCE

	Japan	Kazakhstan	Pakistan
Starting Year	1978	1973	2000
Reactor Type	LWR	LMR	PHWR
Capacity (m^3/day)	100-3900	80,000 (design 120,000)	454
Average salinity of intake water (mg/l)	35,000	13,500	24,000
Average temperature (C)	17	2-24	
Radioactive leak	None	None	None
Water Production during NPP shutdown	Halted, no need for water. No backup source	Continued by a fossil boiler	None
Failures and types	Nothing reported	Corrosion and erosion of tubes and pump blades	Not reported
Availability	~50% Not operated once the storage tank is filled.	85%	
Product water use	In plant use for steam cycle	In plant & municipal use, including drinking water	In plant use

An example of how nuclear heat is used for desalination is shown in figure 1. In this example steam is produced in a secondary loop for generation of electricity and then another tertiary loop is used to heat the seawater for desalination. The salt water is in the 4th loop. This makes the production of fresh water far removed from the radioactive isotopes of the first, primary loop.

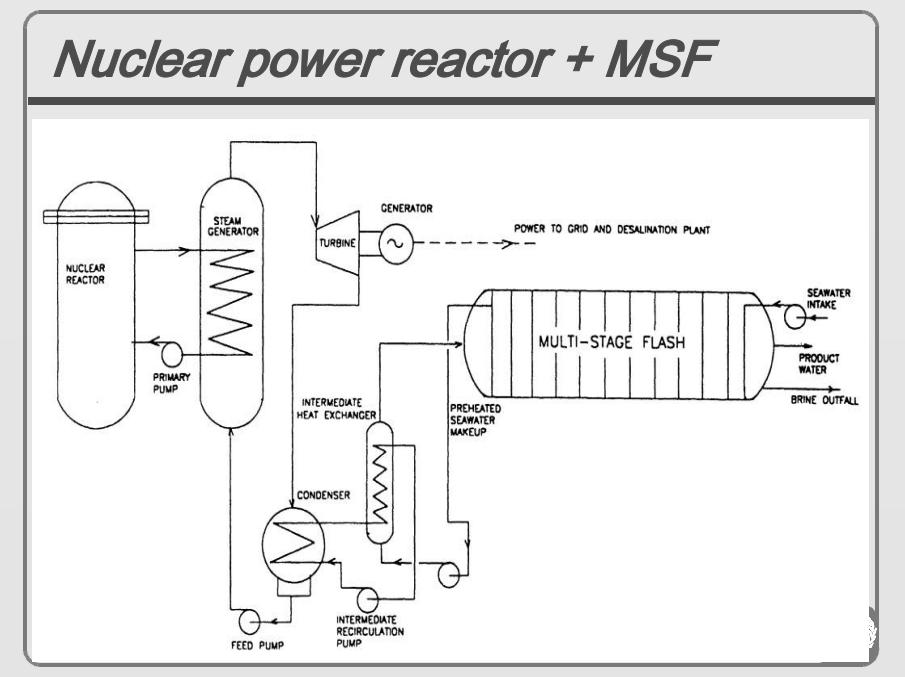

FIG. 1 Schematic presentation of nuclear desalination circuits

Economic studies performed at the IAEA indicate that nuclear energy can be competitive for desalination compared with fossil-fuelled energy sources[11]. The desalination costs range from $0.40 to $1.90 per m^3 of fresh water produced. It was generally found that (a) MSF processes cost higher than RO and MED processes, (b) RO and MED processes costs are in general comparable, (c) RO is economically more favourable for less stringent drinking standards, and (d) desalination costs are higher for smaller reactors.

Various research and construction project studies are being performed in several countries for nuclear desalination. Currently major activities are taking place in India, Pakistan, Russia, and China; Canada, Republic of Korea and France are also involved in nuclear desalination research. India[12] is constructing a 6300 m^3/d combined MSF-RO nuclear desalination demonstration plant connected to two 170 MWe PHWR units at Kalpakkam. Installation of the RO section has been completed

and the MSF section is expected to be done in 2003. Pakistan has initiated a feasibility study for coupling a 4500m^3/d desalination plant with the 137 MWe PHWR KANUPP. Russia has investigated various coupling schemes for 35 MWe KLT-40, 55 MWt RUTA, and 70 MWe NIKA reactors. Russia and Canada are working on a floating nuclear desalination plant with the KLT-40 reactor and an optimised Canadian desalination system involving reverse osmosis. The construction of the KLT-40 on a barge is expected to be completed in 2006. China is investigating a nuclear desalination project in Shandong peninsula with a 200 MWt nuclear heating reactor (NHR-200). Their plan is couple it to an MED process to produce 160,000 m^3/d of potable water. The study was finalized in 2001, and Tsinghua University is setting up a test system to verify the design performance of the MED process. Candesal Technologies in Canada is developing a unique approach to the design and operation of RO system to improve energy efficiency and reduce the life cycle cost of potable water. The Republic of Korea (ROK) is developing an integrated desalination plant with the SMART reactor for dual purpose application. They aim to provide 90 MWe and 40,000 m^3/d of fresh water. A 65 MWt pilot version of the SMART reactor is expected to be built in the ROK by 2008. ROK and Indonesia are also investigating the feasibility of nuclear desalination in Madura Island, Indonesia. France is working with Tunisia for a site-specific desalination study for La Skhira in Tunisia.

Nuclear desalination is thus a matured technology and can be installed in many nuclear plants to provide fresh water to solve regional water shortage problems. The desalination capacities of the world have been doubling each decade and hence there is a tremendous potential for nuclear desalination. Efforts are now primarily directed towards reducing production cost of desalinated water through innovations and technological enhancements.

3. DISTRICT HEATING

District heating is residential and commercial building heating. District heating systems use hot water or steam in the temperature range of 70 – 150 C with steam-water and water-water heat exchangers as needed. Usually steam is extracted from low pressure turbines in the nuclear power plant to provide the base heating load and steam from the high pressure turbine is used for the peak heat demand. Development of a heat distribution system is required but, due to heat losses in the heat distribution system, the source must be nearby, usually within a few kilometres at most. The longest known delivery distance is 24 km in Slovakia. Also, the demand for heat fluctuates with the season, being very high in cold winters and low in summer, and the source must be able to accommodate this fluctuation.

District heating has been used in some countries for decades. District heating networks exist in Bulgaria, Czech Republic, Hungary, Slovakia, Belarus, Russia and Ukraine. Denmark, Finland, Sweden, and Switzerland also have developed heating networks. The power capacity of heat networks is estimated to be about 600 – 1200

MWt in large cities and 10 –50 MWt in small communities[2]. At present nuclear district heating appears to be most promising in countries which already have heat distribution networks.

The concern of leakage of radioactivity into the heating network has been taken care of by intermediate heat transfer loops operating at higher pressures than the steam loop from the turbines, and by constant monitoring. The safe and reliable operation of several district heating networks (e.g., in Bulgaria, Hungary, Slovakia, Russia, Ukraine and Switzerland) has proved their effectiveness.

Table VI from IAEA Tecdoc 1056 (1998), as improved in ref 2, shows the world experience of nuclear reactors in commercial district heating. Out of these 46 reactors, only two in China and Russia were used for the sole purpose of district heating. Over twenty plants in Russia and the Bruce CANDU plants in Canada were used for electricity generation and to provide heat for both process heat and district heating. Steam from Bruce A plant was used for the heavy water production plant and for the nearby agricultural and industrial complex. One also notes that of the many existing and proposed designs of nuclear power systems for district heating, the majority are based on the use of water reactor technology.

TABLE VI. OPERATING NUCLEAR REACTORS WITH HEAT APPLICATIONS[‡]

Country	Plant type or name	Location	Application	Start of operation	Power (Mwe net)	Heat output (MWth)
Bulgaria	WWER-1000	Kozloduy 5 - 6	E, DH	1987,91	2x953	2x20
Canada	CANDU	Bruce Energy Centre[§], Ontario	E, P, DH	1977-87	750-860	79
China	NHR-5	Beijing	DH	1989	0	5
Hungary	WWER	Paks 2, 3, 4	E, DH	1984-87	3x433	3x30
Russia	Research reactor	Obninsk	DH	1954	0	10-20
Russia	RBMK	Bilibino 1 - 4	E, DH	1974-81	4x11	4x25
Russia	WWER	Novovoronezh – 3,4[**]	E, P, DH	1971, 72	2x385	2x32.5
Russia	WWER-1000	Novovoronezh – 5	E, P	1980	950	
Russia	WWER-1000	Balakovo 1-4	E, DH	1986-93	4x950	4x200
Russia	WWER-1000	Kalinin 1-2	E, P, DH	1984 –86	2x950	2x80
Russia	WWER-440	Kola 1 - 4	E, P, DH	1973-84	4x411	55
Russia	BN-600	Belojarsk-3	E, P, DH	1981	560	170
Russia	RBMK-1000	Leningrad 1 -4	E, P, DH	1974-81	4x925	4x25
Russia	RBMK-1000	Kursk 1- 4	E, P, DH	1977-86	4x925	127.5, 3x175
Russia	RBMK-1000	Smolensk	E, P, DH	1983-1990	3x925	3x173
Slovakia	WWER	Bohunice-3, 4	E, DH	1984 1985	2x408	2x240
Switzerland	PWR	Beznau 1, 2	E, DH	1969-71	2x365	2x80
Ukraine	WWER	Rovno 1, 2	E, DH	1980-81	381, 376	2x58
Ukraine	WWER	Rovno 3	E, DH	1987	950	233
Ukraine	WWER-1000	South Ukraine 1-3	E, DH	1983-89	3x950	2x151 1x232

[‡] E, P and DH stand for electricity, process heat and district heating.

[§] Bruce A reactors are currently laid up; it is expected to start up in 2003.

[**] Unit 1 was taken out of operation in 1988, unit 2 in 1990.

The market potential for district heating has been estimated[2] to be between 340GWt and 7600GWt. Table VI shows that nuclear power provides only about 4.4 GWt. Since there are various sources for heat such as oil, coal and natural gas, unless nuclear power is economical in the open market, it cannot make a big dent in commercialising nuclear district heating. The scaling effect is also important for nuclear district heating as it is more expensive at lower power. At 500 MWt and above the nuclear option shows good chances to be competitive even at higher discount rates[2]. Perhaps as nuclear power receives more acceptance from the public and nuclear electricity becomes competitive with other sources of electricity, nuclear district heating will also become more common.

4. INDUSTRIAL PROCESS HEAT APPLICATIONS

There are five primary areas of industrial heat applications: food processing, paper industry, chemical industry, petroleum and coal processing, and primary metal industries. Relative use of process heat in these industries is shown in Table VII for two developed countries, the U.S. (1994) and Germany (1989).

TABLE VII. INDUSTRIAL USE OF PROCESS HEAT IN THE U.S. AND GERMANY[2]

Industry	Percentage use of process heat in	
	Germany	USA
Food and products	19	5
Paper and products	18	12
Chemical	33	25
Petroleum and coal processing	8	33
Primary metal industries	10	12
Other	12	13

Industrial process heat is mainly used in the form of steam at appropriate temperature and pressure conditions. The demand is usually steady and there is no seasonal variation and hence quite suitable for supply by nuclear power. The only problem is that the source must be nearby as heat loss in transit is considerable.

There are three cases of commercial use of nuclear process heat in Canada, Germany and Switzerland. This is shown in Table VIII. The application to the heavy water production facility in Bruce, Canada was the largest use of nuclear process heat and it has operated very successfully for over 20 years. The six other industries the Bruce complex provided process heat were plastic film manufacturing, ethanol plant, apple juice concentration plant, alfalfa dehydration, cubing and pelletizing plant, a greenhouse, and an agricultural research facility.

TABLE VIII. NUCLEAR PLANTS PROVIDING COMMERCIAL PROCESS HEAT[1]

Country	Plant Name	Start of Operation		Power MWe	Heat Delivery MWt	Interface Temp C Feed/ Return	Distance to Industry Km	Application
		Reactor	Heat					
Switzerland	Goesgen PWR	1979	1979	970	25	220/100	1.75	Cardboard factory
Canada[a]	Bruce-A CANDU	1977-87	1981	4x848 4x860	5350		Nearby industrial complex	Heavy water production and 6 other industries
Germany	Stade PWR	1983		640	30	190/100	1.5	Salt refinery

[a] Unit 2 of Bruce A was taken out of service in 1995, units 1,3 and 4 were taken out of service in 1998. They are expected to start up in 2003.

The total potential market of industrial process heat is large and of the same order of magnitude as district heating. It is estimated to be between 240 GWt and 2900 GWt[2]. However, the demand in terms of size varies; some 50% of the users need less than 10 MWt, 40% need sizes from 10 to 50 MWt, and only 10% need sizes greater than 50 MWt[3]. Very few need a large amount of process heat as in the Bruce example in Canada. The market is also very competitive as small fossil fuel units can provide the needed steam.

5. HIGH TEMPERATURE APPLICATIONS: FUEL SYNTHESIS

As shown in Table II, liquid metal and gas-cooled reactors can generate very high temperatures, which could be used to create new synthetic fuels for energy. This will be an innovative application of nuclear energy and can considerably expand its use. This is because the transportation sector is responsible for about a quarter of the total energy use and almost 99% of this is currently supplied by organic fuel. Nuclear power can penetrate this large market through use of electric cars and production of synthetic fuels such as methanol, ethanol and their derivatives; nuclear power can also be used for coal gasification, oil extraction and hydrogen production. All of these are being seriously considered in the 21st century. However, the infrastructure for use of these fuels needs to be created first, particularly in the case of environmentally ideal hydrogen fuel.

Coal gasification (i.e., conversion of solid coal into a gaseous fuel like the natural gas) requires very high temperatures but could be practical because the infrastructure for use of natural gas already exists, and there are vast deposits of coal in the world and this conversion can remove environmental pollutants such as particulates like sulphur-dioxide and nitrogen oxides. The efficiency of coal fire plants will also be improved by coal gasification. The process of coal gasification is, however, quite energy intensive; one unit of gasified coal may require about 1.7 units of energy in solid coal[13]. High temperature gas-cooled reactors can play a role here.

Another possible use of nuclear energy is for oil extraction from tar and oil sands and for enhanced oil recovery operations, particularly from depleted oil deposits. Canada and Venezuela have large resources of oil and tar sands. Steam injection is used for these extraction applications and steam can also be used for processing the oil after the extraction.

The feasibility of nuclear application for production of more organic fuel really depends on the economics. So long as fossil fuel, particularly oil and gas, are available at low prices, nuclear will not be a preferable option. Only dual use, where nuclear electricity can compete in the market, could make these applications worthwhile.

Hydrogen economy has received renewed interest because of new developments in HTGR technologies. Several paths to hydrogen production are being considered: decomposition and gasification of fossil fuel such as steam reforming of methane and carbon dioxide reforming of methane; and decomposition of water, namely, low-temperature electrolysis, and combination of electricity and heat for high temperature electrolysis. These are briefly described below.

A. Steam Reforming of Methane

In this method Methane (CH_4), a main component of natural gas, and water react at temperatures of 600 – 800 C to produce hydrogen and carbon monoxide and dioxide. The steam reforming system can be easily coupled to a HTGR, which can provide the necessary heat and high temperature. Considerable R&D work has been carried out in Germany for the steam reforming of methane including performing experiments in a pilot plant, EVA-I and EVA-II. Currently work is in progress in JAERI for the HTTR[14], in China for the HTR-10[15] and in Russia.

B. CO_2 Reforming of Methane

The basic CH_4 and CO_2 reaction for this process (with no addition of steam) produces CO and hydrogen. The reforming process requires high temperature (800 – 900 C) and high energy input, both of which can be provided by HTGRs. The

generated CO and H_2 mixture (syngas) can be used directly as fuel for electricity generation (e.g., by fuel cells).

C. Thermo-chemical Water Splitting

One mechanism that is being considered seriously for hydrogen production is thermo-chemical water splitting by the Iodine-Sulfur (IS) process. The IS process was originally proposed by the General Atomic Company in early 1970's and is very promising because it involves only a few reaction steps. In this process Hydrogen-Iodide (HI) is produced by a cyclic chemical reaction chain utilizing Iodine, sulfur-dioxide and water; HI is then decomposed to produce hydrogen, releasing Iodine to the chemical reaction chain. Sulfuric acid, H_2SO_4, is generated in the process, which is vaporised and decomposed at a temperature of about 800 to 900 C to sulfur-dioxide, water and oxygen. The oxygen is released and sulfur-dioxide and water is returned to the reaction cycle. Laboratory scale experiments at Japan Atomic Energy Research Institute have demonstrated the feasibility of the IS process with continuous generation of hydrogen from water with recycling of the process material. An energy efficiency of 47% has been achieved in this process[16].

D. Electrolysis

Water electrolysis at ambient pressure and temperature of 70 – 90 C is a common method for production of high purity hydrogen. However, it has been found that the demand for electricity decreases with increase of temperature. That is the electric energy required is much reduced for the electrolysis of steam at higher temperatures (800 C and above). High temperature electrolysis is a reverse reaction of the Solid-oxide Fuel Cell, where water is decomposed in the solid polymer electrolyte to hydrogen and oxygen. This method is at an early stage of development[14].

Conclusion

There are several possibilities for direct utilization of heat from nuclear reactors. Nuclear desalination, district heating and industrial process heat are examples where this has been done, and these non-electric applications of nuclear power can be expanded in the future. It is also important to note that a wide range of temperatures, for low to high temperature applications, can be tailored for specific uses by different reactor types. Table IX shows the status of projects in several countries for non-electric applications of nuclear energy. The proposed applications are primarily for dual-purpose use but dedicated heating reactors are also being developed in China and Russia. Innovative applications are being explored with gas-cooled reactors because of their high temperatures. High temperature applications of nuclear energy, particularly for production of new fuel such as hydrogen, are in the laboratory stage now but have a great potential for the future[3].

Cost-effectiveness is in general a crucial issue for non-electric applications of nuclear power. As nuclear power captures a larger share of the electricity market, the non-electric applications will also flourish. Until now, the non-electric applications are only a very small part of power production. For some applications, however, close proximity of the power plant to a population centre is needed (to reduce energy and/or product transmission losses) and this requires further public acceptance. Some large applications also require the development of infrastructure - heat-distribution networks for district heating and water distribution systems (water pipes and pumps) for fresh water. Many countries are exploring these possibilities of nuclear power. As mentioned in the text, there is a large market for non-electric applications of nuclear energy and it is hoped that someday this potential will be realized.

TABLE IX. PROSPECTIVE NUCLEAR PROJECTS FOR NON-ELECTRIC APPLICATIONS

Country	Plant type or site	Location	Application[††]	Project status	Power, MW(e)	Heat output, MW(th)
Bulgaria	WWER	Belene	E, DH	Design	2x1000	400
China	NHR-200	Daqing City	DH	Dormant	0	200
China	HTR-10	Tsinghua University, Beijing	Electricity/ high temp. applications	Achieved criticality in Dec. 2000		10
Japan	HTTR	Oarai (JAERI)	High temp. process heat	Operating	0	30
Russia	RUTA	Apatity	DH / Air conditioning	Design	0	4x55
Russia	RUTA	Obninsk	DH	Design	0	55
Russia	ATEC-200	-	E, DH	Design	50-180	70-40
Russia	VGM ./ GT-MHR	-	P	Design	-	600
Russia	KLT-40	Floating	E, DH & Desalination	Regulatory process completed	35	150
Russia	AST-500	Voronez	DH	Construction suspended	0	500
Russia	AST-500	Seversk	DH	Completed feasibility study, approval of the project by State regulatory authority is nearing completion	0	500

[††] E: Electricity (Power), P: Steam supply for process heat, DH: Steam/Hot water supply for heating.

References

[1] IAEA-Tecdoc 1056, “Nuclear heat applications: design aspects and operating experience”, November 1998.

[2] B.J. Csik and J. Kupitz, “Nuclear power applications: supplying heat for home and industries”, IAEA Bulletin, Vol 39, No. 2, IAEA, Vienna, 1997.

[3] IAEA-TRS-410, “Market potential for non-electric applications of nuclear energy”, to be published.

[4] IAEA-Tecdoc-1085, “Hydrogen as an energy carrier and its production by nuclear power”, May 1999.

[5] World Water Vision Commission Report: A Water Secure World, World Water Forum, The Hague, Netherlands, 2000.

[6] O.K. Buros, “The ABCs of Desalting”, International Desalination Association, USA, February 2000.

[7] Introduction of nuclear desalination – a guidebook, IAEA Technical Reports Series No. 400, Vienna 2000.

[8] T. Konishi, R.S. Faibish, and M. Gasparini, “Application of nuclear energy for seawater desalination – design concepts of nuclear desalination plants”, Proc. of tenth Int. Conf. On nuclear engineering, April 14 – 18, 2002, Arlington, VA, USA.

[9] Y. Kupitz and T. Konishi, Encyclopedia of Desalination and Water Resources, EOSS publications, Oxford, 2000.

[10] Ted Prato et al., “Successful use of membranes at Diablo Canyon nuclear plant”, The International Desalination and Water Reuse Quarterly, 27, vol 10/4, Feb/March 2001.

[11] IAEA-Tecdoc-1186, “Examining the economics of seawater desalination using the DEEP code”, December 2000.

[12] P.K. Tewari and B.M. Misra, “Emerging trends in R&D on desalination in India”, Desalination and Water Reuse, 46,vol.12/1, 2001.

[13] Energy and nuclear power planning in developing countries, Technical Reports Series No. 245, IAEA, Vienna, 1985.

[14] S. Shiozawa, Y. Tachibana. O. Baba and M. Ogawa, “Present status and perspective of HTGR in Japan”, Proceedings of the International Seminar on Status and Prospects for Small and Medium Sized reactors, Cairo, 27 – 31 May 2001.

[15] Zongxin Wu and Yuliang Sun, "The technical design and safety features of the 10 MW HTGR test reactor", Proceedings of the International Seminar on Status and Prospects for Small and Medium Sized reactors, Cairo, 27 – 31 May 2001.

[16] IAEA-Tecdoc-1236, "Design and evaluation of heat utilization systems for the high temperature engineering test reactor", August 2001.

Experiences and Techniques in the Decommissioning of Old Nuclear Power Plants

Maurizio Cumo[1]

University of Rome "La Sapienza,"
Department of Nuclear Engineering and Energy Conversion, Rome, Italy

Lectures given at the
Workshop on Nuclear Reaction Data and
Nuclear Reactors: Physics, Design and Safety
Trieste, 25 February – 28 March 2002

LNS0520006

[1] maurizio.cumo@uniroma1.it

1. Introduction

Decommissioning of a nuclear power plant or other nuclear installations can be defined as the cessation of operations and the withdrawal of the facility from service, followed by its transformation into an out-of-service state and eventually, its complete removal, the so-called "green field" status, which, in principle, restores the site to the conditions existing before the construction of the plant. Alternative end conditions may include a situation in which the buildings, free of any radioactive contamination, are left for future conventional demolition, or situations in which these buildings, or the site itself, are used for other industrial purposes.

We will discuss the decommissioning activities starting from a situation in which spent fuel is not present any more on-site, or at least, in a completely independent storage facility. This removes from the plant more than 99,99% of the radioactivity present in the plant at the time of operation.

The main goal for the decommissioning activities is to place the facility in a condition that eliminate any risk for the health and safety of the general public and the environment, removing, in particular, from systems and structures any radioactivity that may have been accumulated during plant operations. Of course, all the decommissioning activities shall be carried out with great attention to assure the minimization of the risks to both the public and the workers involved in the process.

Decommissioning is a complex, long lasting and highly technological activity that presents smaller challenges, but similar to the plant construction activities. In some countries, in fact, it is called de-construction. Activities include use of technological tools, control of industrial safety, environmental impact minimization, licensing, safety analysis, structural analysis, etc. Other aspects very relevant are the activity planning, the calculation of related cash flow and anticipation of the funds needed to perform the activities. Aspects related to waste disposal and spent fuel strategy shall be covered as well.

2. Current decommissioning activities in the world

All power plants, coal, gas and nuclear, have a finite life beyond which it is no longer economical to operate them. Generally speaking, Nuclear Power Plants (NPP's) were designed for a life of about 30 years, though some have proved capable of continuing well beyond this term. Newer plants are designed for a 40 to 60 years operating life. To date, 70 commercial power reactors, over 250 research reactors and a number of fuel cycle facilities, have been retired from operation. Some of these have been fully dismantled. Assuming an average of about 25-years lifespan, almost 300 nuclear power plants would have to be decommissioned by the year 2010. By appropriate refurbishment, replacement or upgrading of some equipment, operations at many of these plants can probably be extended well beyond this conservative estimate.

However, ultimately it becomes either technically or economically advantageous to retire a facility from operation and, if necessary, replace it with a new plant.

Figure 1 – Location of Italian NPP's in decommissioning

In Italy 4 Nuclear Power Plants have been prematurely definitely shutdown and are now in different stages of decommissioning. They were operated by the National Electrical Utility ENEL, now partially privatized. In figure 1, the names and location of these plants are reported. The responsibility of carrying out the decommissioning projects and to manage the spent fuel has passed in the 1999 to SOGIN Company (which includes all nuclear competences of ENEL), which is now completely owned by the Italian Government (Ministry of Treasury). In Table 1 the main characteristics of these plants are summarized.

Table 1 - Italian NPP's main data

Plant	*Type*	*Designer*	*Mwe*	*Commercial operations*	*Plant shutdown*
Latina	Magnox	TNPG	200	1963	1986
Garigliano	BWR Dual cycle	General Electric	150	1964	1978
Trino	PWR	Westinghouse	260	1964	1987
Caorso	BWR	AMN - GETSCO	860	1978	1986

3. Possible decommissioning strategies

Possible approaches to decommissioning a Nuclear Power Plant may be widely varied and the optimal choice is made on the bases of a number of parameters which, in most cases, are site specific or, at least, country specific. Therefore there is no single optimal approach for all facilities. Decommissioning process could be subdivided, in somewhat schematic way, into stages. There is no official definition of the different stages, each country using its own definitions which vary slightly to suit each case. We could mention, as an example, the IAEA Technical Reports Series N° 375, ''Safe Enclosure of Shut Down Nuclear Installations'', 1995, which provides the following definitions:

"According to the definition of IAEA stages of decommissioning, the nuclear fuel or radioactive materials in the process systems as well as radioactive waters produced in normal operation is first removed by routine operation. Each of the three decommissioning stages of a nuclear plant can be defined by:

- *the physical state of the plant and its equipment ;*
- *the surveillance, inspections and tests necessitated by that state.*

Stage 1

a) The first contamination barrier is kept as it was during operation but the mechanical opening systems are permanently blocked and sealed (valves, plugs etc.). The containment building is kept in a state appropriate to the remaining hazard. The atmosphere inside the containment building is subject to appropriate control. Access to the inside of the containment building is subject to monitoring and surveillance procedures.

b) The unit is under surveillance and the equipment necessary for monitoring radioactivity both inside the plant and in the area around it is kept in good condition and used when necessary and in accordance with national legal requirements. Inspections are carried out to check that the plant remains in good condition. If necessary, checks are carried out to see that there are no leaks in the first contamination barrier and the containment building.

Stage 2

a) The first contamination barrier is reduced to a minimum size (all parts easily dismantled are removed). The sealing of that barrier is reinforced by physical means and the biological shield is extended if necessary so that it completely surrounds the barrier. After decontamination to acceptable levels, the containment building and the nuclear ventilation systems may be modified or removed if they no longer play a role in radiological safety and, depending on the extent to which other equipment is removed decontaminated, access to the former containment building, if it is left standing, can be permitted. The non-radioactive parts of the plant (buildings or equipment) may be converted for new purposes.

b) Surveillance around the barrier can be relaxed but is desirable for periodic spot checks to be continued, as well as surveillance of the environment. External inspections of the sealed parts should be performed. Checks for leaks are no longer necessary on any remaining containment buildings.

Stage 3

All materials, equipment and part of the plant, the activity of which remains significant despite decontamination procedures are removed. In all remaining parts contamination has been reduced to acceptable levels. The plant is decommissioned

(released) without restrictions. From the viewpoint of radiological protection, no further surveillance, inspection or tests are necessary.''

Other terms that are widely used to describe the strategy adopted for the decommissioning are those that have been introduced in USA by the Nuclear Regulatory Commission (US NRC):

DECON (or one step dismantling):
In this strategy, all components and structures that are radioactive are cleaned or dismantled, packaged and transported to a low-level waste disposal site (if available) or stored temporarily on site. Once this task is completed, the facility can be used for another power plant or other purposes, without restrictions.

SAFSTOR (or Safe Storage):
In SAFSTOR, the nuclear plant is kept intact and placed in protective storage for a very long time (up to 60 years[2]), and afterwards it is dismantled. This method, which involves locking that part of the plant containing radioactive materials and monitoring it with an on-site security force, uses time as a decontaminating agent—that is, the radioactive atoms "decay" by emitting their extra energy to become non-radioactive or stable atoms. [3]Once radioactivity has decayed to low levels, the activity is the same as the one described above as DECON. All building structures and systems which are necessary for workers and public safety shall be maintained in service during the safe storage period. A pre-condition to reach the safe storage condition is that the fuel has been removed from the plant and that radioactive liquids have been drained from systems and components and then processed.

ENTOMBMENT:
The radioactive inventory is enclosed in a monolithic structure, e.g. concrete, to secure the public safety. The monolithic structure should ensure integrity for about 100 years to derive benefit from the decay of the nuclides. After the entombment period, all enclosed components are very low radioactive and the assumption should be that dismantling at that time can be performed in a “conventional” way. During entombment the plant remains under a nuclear license.

The 3 categories presented above are a crude schematization of various situations. The DECON strategy for example may imply a really “quick” decommissioning and dismantling, or a longer process, that might optimize the use of plant personnel and reduce costs associated with engulfing activities on site.

[2] 60 years is a limitation existing in the USA. In other countries this condition may last longer up to 100 years and more
[3] If a plant is allowed to sit idle for 30 years, for example, only about 1/50th of its original radioactivity from cobalt-60 will remain; after 50 years, some 1/1,000th will remain.

On the other side, the SAFSTOR option may really imply a simple "close and seal the door", or a combination of immediate dismantling and safe store. In the latter case it may be considered the immediate dismantling of systems and buildings which are not, or only slightly, contaminated and a SAFSTOR strategy for the most radioactive portion of the plant. Also the safe storage period may range from 30 to more than 100 years, depending on a number of parameters and conditions that will be discussed later.

The third strategy (ENTOMBMENT) has never been applied yet to a NPP. There are several reasons for that. The first one is that the size of a NPP is too large to be simply entombed. A second reason is related to the fact that most power reactors will have radionuclides in concentrations exceeding the limits for unrestricted use even after 100 years and more and therefore this strategy cannot be successful. ENTOMBMENT is, however, a possible strategy for smaller reactors and for other small nuclear facilities.

4. Main decommissioning activities

The complete decommissioning process involves a number of stages (or activities) that shall be performed, even if the logical sequence may be changed according to the specific strategy.

Decommissioning Planning – The decommissioning planning is usually started while the plant is still operating. Some decision making process and some planning, associated with some cost evaluation shall be started well on time, since it is needed also for fund accumulation, that usually is performed during plant operation.

Post-Operation – It is the sum of the activities that are needed to maintain the safety of the plant even after the plant has been definitely shutdown. These activities are more relevant while the spent fuel is still present in the plant.

Characterization – The knowledge of the radioactive inventory in the systems, components and structures before start of decommissioning is a fundamental information to define strategy, costs, technologies and so on. Characterization is also an important process during plant dismantling in order to know exactly the content of the produced wastes. Finally, characterization is also an important, and complex activity to demonstrate that structures and systems, that have not been dismantled because no radioactive, are actually in this condition. In Table 2 a typical list of radioactive isotopes relevant to the decommissioning of NPP's is reported.

Decontamination – It is an activity that is oriented to remove radioactivity from systems and structures, in order to release components, to reduce doses to workers and to reduce the volume of wastes. It is applied to floors, walls, piping, etc. and may be performed essentially with mechanical or chemical means.

Dismantling – It is the real demolition activity. It may be a rather simple and quick activity, using conventional tools, but it may also be a very complex activity in the case of highly radioactive parts, using remote cutting and other sophisticated tools.

Safe Storage – It is the period in which the plant is left in dormancy, waiting for the radioactive decay. The plant is not left without controls, but a number of activities are still needed and, in some cases, some maintenance and even construction activities are necessary to maintain the safety for the workers and the public.

Table 2 – Major radionuclides identified in facility characterization

Isotope	Half-life (years)	Principal decay mode	Associated γ energy (MeV)	Materials where isotopes can be found
NEUTRON ACTIVATION PRODUCTS FOUND IN NUCLEAR REACTORS[4]				
H^{3} [5]	12,3	β^-	-	C,O,S[2]
C^{14}	5730	β^-	-	G, M, S
Na^{22} [2]	2,6	EC, β^+	0,51 - 1,28	O
Cl^{36}	$3{,}1\ 10^{8}$	β^-, EC	-	C
Ar^{39} [2]	269	β^-	-	C
Ca^{41}	$1\ 10^{5}$	EC	-	C
Ca^{45}	0,4	β^-	-	C
V^{49} [2]	0,9	EC	-	S[2]
Mn^{54}	0,9	EC, γ	0,83	A, M, S
Fe^{55} [2]	2,7	EC	-	C, M, O, S[2]
Co^{57} [2]	0,7	EC, γ	0,12 - 0,14	S[2]
Co^{60} [2]	5,3	β^-, γ	1,2 – 1,3	C, M, O, S, Z
Ni^{59}	$7{,}5\ 10^{4}$	EC	-	C, M, O, S, Z
Ni^{63} [2]	100	β^-	-	C, M, O, S[2]
Zn^{65}	0,7	β^+, γ, EC	0,51 – 1,12	A
Zr^{93}	$1{,}5\ 10^{6}$	β^-	-	O, Z
Nb^{94}	$2\ 10^{4}$	β^-, γ	0,70 – 0,87	M, O, S, Z
Mo^{93}	$3{,}5\ 10^{3}$	EC, γ	0,3	M
$Ag^{108}m$	130	EC, γ	0,4 – 0,6 – 0,7	M, O, S
$Ag^{110}m$	0,7	β^-, γ	0,6 – 0,9	M, O, S
Ba^{133} [2]	10,7	EC, γ	0,08 – 0,36	C
Sm^{151}	93	β^-, γ	0,02	C
Eu^{152}	13,4	β^-, γ. EC	0,1	C, G
Eu^{154}	8,2	β^-, γ	0,1 – 1,3	C, G

[4] Fission products are also often found in nuclear reactors as a result of defects in the fuel cladding

[5] Important in fusion devices also

5. Major factors relevant to the decommissioning strategy and planning

Optimization of a decommissioning strategy is a rather complex process. The parameters to be considered can be grouped in 3 categories: technical, economical, socio-political.

In the first group it is possible to list the following aspects:

- **Radioactive inventory** – Depending on the amount and characteristics of the radioactive inventory the strategy can change. For example, plants which experienced accidents with radioactive release or incidental spilling on the floors, or contamination of insulation, may require special attention. On the other side plants which have been prematurely shutdown may have a lower total inventory and a long Safe Storage period may not be justified.
- **Presence of other operating units on the same site or in the country** – This situation may imply the maintenance of a high level of nuclear technology that will be available for a longer time. To have them on the same site means also that the site cannot be released anyway and that work force can be easily re-employed. Therefore, generally, it is convenient to wait some time before dismantling.
- **Availability of a national waste repository** – Decommissioning and dismantling means essentially to cut in pieces a NPP and to concentrate and package the radioactivity. This is of little advantage if all the radioactive material shall remain on-site. In addition, if a repository does not exist, uncertainties are present on the specification of packaging that will be finally required by the repository, once it will made available.
- **Clearance levels and waste disposal costs**– Clearance levels are of fundamental importance to decide which strategy and which technologies shall be used. Since clearance levels can vary even by one order of magnitude and more, correspondingly the amount of radioactive wastes to be generated, classified as such, can vary by even more than one order of magnitude. This, in connection with the cost of waste final disposal, can force the decision in favor or against the preliminary decontamination of systems and structures.
- **Plant layout** – Difficulties in the dismantling process due to very compact layouts may lead to decisions about preliminary decontamination and different cutting strategies
- **Safety conditions of structures and systems** – Costs of maintaining the safe storage condition for decades shall be low to make the SAFSTOR strategy convenient. This means that structural conditions and corrosion conditions of all components shall be good and capable to withstand the expected conditions for several decades, without any need for major refurbishment.

- **Expectations about development of licensing rules and of technologies for decommissioning** – Licensing rules and available technologies change usually more quickly than expected. This is the experience of the last years. Extrapolations of the situation in 50 or 100 years are extremely difficult to be made and, more important, extremely uncertain. This means that in the case of the safe storage strategy it is wise to use contingencies in cost calculations and to leave open the introduction to new technologies.
- **Connections between conventional and nuclear safety** – In a NPP there are also some conventional safety issues and a production of conventional waste (such as asbestos). Complications may arise when the same waste is at the same time radioactive and toxic, such as in the case of contaminated asbestos. The extent of such situation may lead to the use of special techniques of dismantling and waste packaging.
- **Status of plant configuration documentation** - In the lack of a good documentation about plant design bases, plant modifications and plant conditions, the knowledge of the plant staff might lead to the decision to perform as many as possible activities, while the people are still available.

Worker doses are not included in the previous list, since it is assumed that with proper preparation and the use of proper tools, including remote operations and decontamination activities, the worker dose can always be reduced to acceptable levels. Also environment and public health impact levels have not been included in this list, since they are generally so low that do not present any serious concern. Of course also these elements have to be taken into account in a complete strategy evaluation.

In the second group, the following elements have to be considered:

- **Availability of funding** - Generally the fund accumulation during plant operation is based on a cost evaluation, which, in turn, is based on a specific strategy. Any change of the strategy would imply the identification of different fund sources.
- **Expectations about cost evolutions** - Calculated costs are affected by a certain level of uncertainties. Uncertainties grow with the extension of calculation extrapolation, because of the uncertainties in the evolution of technologies and the evolution in the safety rules and in the costs of waste disposal. The need to reduce uncertainties implies a reduction of decommissioning duration
- **Expectations in terms of inflation rate** - Funds tend to grow, because, with proper investments, they will produce a net interest. Assumptions about this net interest (that usually range from 2% to 5 %) are very sensitive for the definition of the convenience of different strategies
- **Assumptions in terms of contingencies** - Excessive contingencies intended as provisional funds to cover unexpected situations may tend to increase the needed

funds. In general, the amount of contingencies may be reduced, obviously, when the decommissioning time is shortened.

In the third group, the following aspects can be listed:

- **Work force policy** - In general at the time of final plant shutdown of one unit the work force is between 200 and 500 people. If the unit is isolated on the site and if the utility has no other nuclear operating plant, the social situation may become acute, also in areas industrially developed. Therefore the worker decrease curve shall be carefully studied and their useful employment in the decommissioning process shall be planned, even considering their requalification.
- **Pressures by central or local authorities** - Pressures may exist from local and central authorities to clean up the site as soon as possible to solve the occupational issue mentioned above, to improve the "image" of a certain area with touristic or agricultural objectives, and so on.

Detailed planning of the decommissioning activity is also a difficult task. Very few activities are routine activities and some last for years.

Dismantling can be approached in several ways, depending on the specific circumstances. For example the process can be followed “room by room”, dismantling everything present in a specific room of the plant, possibly starting from the most contaminated components to reduce the overall doses, or from the easiest components, in order to facilitate the remaining operations. Or it may proceed, system by system, keeping operating some support systems that may be still useful in the operations. In the general case the solution is a combination of the two strategies, to be decided on a case by case basis.

It is also necessary to mention that planning is also difficult because the plant configuration is different day by day. To keep under control the status of the plant and its configuration is an heavy task, addressed generally with complex and specific planning tools.

6. Waste management

Wastes related to plant decommissioning come only from the structures of the plant which have been either irradiated or contaminated with radioactive isotopes.

Criteria for waste classification are not standardized worldwide and therefore a consensus classification is not possible. Criteria may be related to the type of isotopes, to their concentration and/or to the total amount of radioactivity in a package. However, in general, 3 categories of wastes are identified:

1. Low level radwaste – these are waste that would not be radioactive (i.e. their radioactivity will be below the clearance level[6]) in a period that can last from few days to some decades. This type of waste is not the waste that concern most in the decommissioning. In the cases in which also concentration is important, then it becomes a very important issue for decommissioning. In fact, one of the isotopes that may influence the entire decommissioning process is Cobalt-60, which has an half-life of 5,3 years. Since it is present in significant quantities in all plants and since it is dangerous to workers, because it decays with a strong gamma, it may lead to very large quantities of waste. Therefore the need for concentration of radioactivity, the appropriate treatment and the waste form is strictly related to the country regulations, definitions and disposal costs for such a type of waste.

2. Intermediate level radwaste – this is the waste which needs up to some centuries to decay below the clearance threshold level

3. High level radwaste – All other radioactive waste, that do not fit in the 2 previous categories are classified as high level waste. This category may include activated materials, components contaminated with transuranic isotopes, Carbon-14 isotopes, such as graphite blocks of Magnox reactors, etc. Vitrified residues of reprocessing certainly fall into this category.

The need for proper processing indeed exists. However, in many cases the required technologies and the goals are the same as those for operational wastes. In particular, the goals to be achieved and optimized should be minimization of the quantities and volumes at the origin, stabilization, concentration, conditioning, sorting and packaging. Among the technologies used for waste conditioning we may recall: nitrification, bitumization, polymerization, cementation, super-compaction, incineration, vitrification, etc.

In fig.2 below a flow diagram is depicted to show the process of producing, treating, characterizing and packaging of decommissioning wastes.

[6] The clearance ‘’is the removal of material from a system of regulatory control provided that the radiological impact of these sources after removal from the system is sufficiently low as not to warrant any further control’’

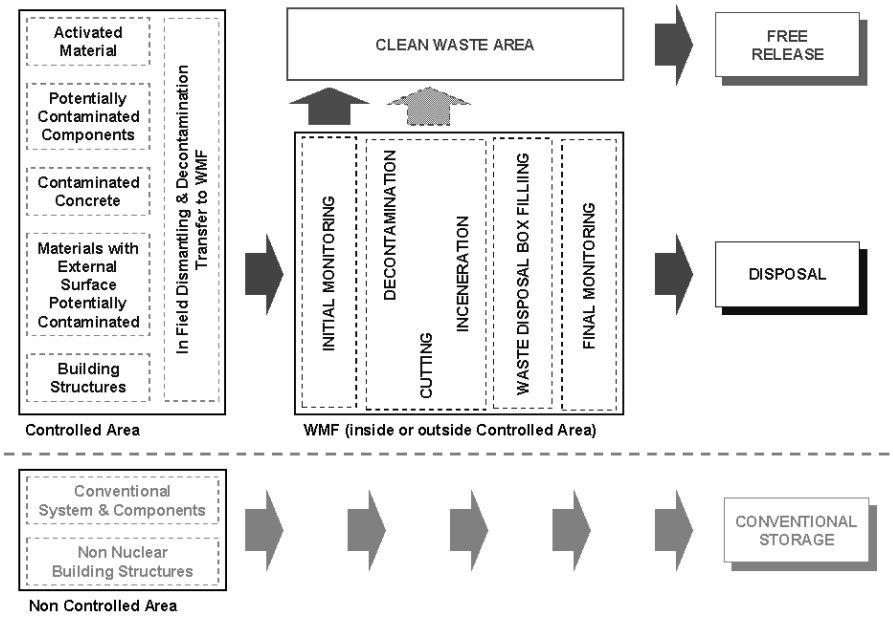

Figure 2 - Decommissioning waste processing

7. Decontamination technologies

The decontamination process is defined as the removal of contamination from the surfaces of installation structures and from internal and external surfaces of piping and equipment.

The major categories of techniques are washing, heating, chemical action, electrochemical action and mechanical action

The objectives of a decontamination process are:

- Reduce worker doses
- Reuse of materials and equipment
- Reduce the amount and volume of radioactive wastes to be disposed
- Remove radiological restraints in all or part of the plant
- Eliminate removable contamination and fix the other one
- Reduce the time after which a material can be freely released

Decontamination objectives can vary according to the specific strategy chosen and according to the specific phase of the decommissioning process. For example in the SAFSTOR strategy the decontamination can be reduced to eliminate the easy removable contamination and to minimize the doses to workers at the end of the safe store period.

In the definition of the most appropriate decontamination strategy considerations of cost-benefit must be applied. Decontamination itself causes doses to the operators and produces secondary wastes to be evaluated in terms of quantity and typology. This "cost" shall be compared with the corresponding savings expected as a consequence of the activity.

In the choice of a specific technology attention must be given to the specific geometry, surface characteristics and materials of the parts to be decontaminated.

Chemical techniques use diluted or concentrated solvents which come in contact with the radioactive substances to be dissolved. The dissolution may imply also the dissolution of part of the base material or simply of the radioactive deposit film on the surface. This last way is adopted when there is an interest in maintaining the integrity of the base metal such as in the case of operating plants, where the decontamination is applied only to reduce worker doses during maintenance activities. Chemical decontamination is applied by a continuous flushing in intact piping, creating a closed loop, and it is preferred for areas where access is difficult and for decontaminating the internal surfaces of piping. Chemical decontamination can be also successfully used for large areas such as floors and walls.

Mechanical decontamination (automatic or manual, locally or remotely controlled) is based on purely physical processes. It includes washing, flushing in closed loops, pipe swabbing, foaming agents and latex-peelable coatings. Most aggressive mechanical processes include wet or dry abrasive blasting, surface grinding, concrete spalling.

8. Dismantling technologies

The dismantling of a nuclear installation requires the cutting and segmenting of equipment and structures with varying sizes, dimensions, and materials. To assume a final decision it is necessary to take into account the acceptance specification of the national disposal site, where these wastes will be sent. In the USA, for example, some plants have disposed the entire reactor vessel, without any fine cutting. In other countries the vessel shall be segmented, generally with remote control techniques under water.

The conditions under which the cutting operations are carried out depend on the location and space of the working area, on the qualification and experiences of the

personnel, on the available tools and technologies as well as on the environmental conditions under which the operations will be performed: under water, in the air, under radioactive radiation, under contaminated atmosphere, etc.
There is a great diversity in existing cutting tools, which are useful and available under industrial conditions or in the R&D phase, each tool having its own performances, conditions and field of application.

The following techniques are presently available:

- thermal cutting
- hydraulic cutting
- laser cutting
- mechanical dismantling
- microwave spalling
- explosive cutting

When choosing cutting techniques the following factors should be taken into account:

- the technique (tool) should be used in practice, so that experience exists and a safety in furnish, spare parts and handling is available
- the technique (tool) should only generate a minimum of secondary waste, e.g. dust, particles, smokes, aerosols with controlled dispersion, liquid effluents
- low risk of contamination for personnel on site
- the technique (tool) has to be compatible to the working-environment.

In thermal cutting techniques, the solid material is melted and then blown away. Since molten states of material are present, the net amount of force needed is much smaller than for the techniques which use strain energy. Hence the contribution of mechanical force is only a minor part of thermal cutting processes.

It is possible to subdivide the thermal cutting techniques, according to the type of heat source, in:

- gas processes
- arc processes
- plasma arc processes
- a composition of the above processes

The energy density of the heat source increases from the gas flame over the arc and the plasma arc to the laser beam.

The abrasive water jet cutting technique is based on the application of plain water jets. Abrasive particles are accelerated by a high speed water jet and cause the removal of the material. Instead of an erosion process as in case of plain water jets, abrasive water jets cut by micro-chipping the material by the sharp-edged particles. When using the correct abrasive material, which has to be harder than the work piece material, any material can be cut - metals as well as ceramics, glass and concrete. With abrasive water jets, severance cutting as well as gouging, is possible. To generate abrasive water jets two different methods are currently available. The abrasive can be added to a plain water jet in a special mixing head (injection jet), or a premixed and pressurised abrasive water suspension can be released to the nozzle to form the abrasive jet (suspension jet). Sharp-edged mineral particles such as silicon sand, corundum or garnet sand are used as abrasives. The increasing number of cutting applications has helped the abrasive water suspension jet (AWSJ) to become more important despite the high consumption of water and abrasives.

The last groups of techniques are the mechanical cutting techniques. A limited list of such techniques is reported below as an example of the available alternatives to be optimized on a case by case basis:

- Grinder
- Hacksaw and Guillotine Saw
- Shears
- Milling Cutters and Orbital Cutters
- Knurl Tube Cutter (rotary disk knife or cutting wheel or plumber's pipe cutter)
- Diamond Saws and Cables

9. Health and safety aspects

The issue of health and safety aspects and the broader one of the environmental impact of the decommissioning process is far reaching and it may only be summarized.

It is convenient to distinguish at least three aspects:

1. Occupational safety, or safety of the workers directly involved in the decommissioning activities
2. Public safety, or the safety of the population surrounding the plant in decommissioning, excluding therefore those who may be affected by the waste disposal process
3. Environmental protection, including those aspects that are not directly related to human health

The first aspect is probably the most significant. Decommissioning is a very labour intensive activity and workers will be in contact with radioactive and other toxic wastes. However, all the means of the plant are still available to reduce the worker doses to the minimum and, while individual doses will always be below acceptable levels, an ALARA (As Low As Reasonably Achievable) analysis of single activities and process could reduce the cumulative occupational doses to values below a few years of plant operation for the entire decommissioning process (few hundreds of man-Sv).

Risks to the public are extremely low in comparison with those associated with plant operation. Radioactive inventory available for release to atmosphere or water bodies is a very small fraction of the previous ones. In general the most dangerous situations are associated with large fires in contaminated areas, breaks in tanks with large inventories of liquid radwaste, drop of contaminated loads. All these situations, however, in general would not even require the activation of an emergency plan.

The environmental issues, finally, are treated in a Environmental Impact Assessment (EIA), which is now required in Europe by a Directive of the European Union. Currently a lot of work is undergoing for a better harmonization of such assessments among the member countries. It is also needed to discuss the interaction between the EIA, presented generally to the Ministry of Environment, and the safety assessments that are presented to the Nuclear Regulatory Bodies. As in other EIA, the assessment would present an overall broad view on all interactions of the decommissioning with various environmental matrixes, and would include aspects not included in the Safety Report such as, for example, those related to site restoration, impact of material (radioactive and non radioactive) transports, disturbance to the local flora and fauna, etc.

10. Economic and financial aspects

Decommissioning is a costly activity. Therefore it is needed to calculate its cost well in advance and accumulate the funds during plant operation as an assurance for being able to close the existence cycle of the plant. Therefore both aspects of cost calculations and funding will be briefly addressed.

The total cost of decommissioning is dependent on the sequence and timing of the various stages of the program. Deferment of a stage tends to reduce its cost, due to decreasing radioactivity, but this may be offset by increased storage and surveillance costs.

Even allowing for uncertainties in cost estimates and applicable discount rates, decommissioning contributes less than 5% to total electricity generation costs. In USA many utilities have revised their cost projections downwards in the light of experience, and estimates now average 325 million dollars per reactor all-up.

The cost of decommissioning nuclear power plants is based on the following factors:

- The sequence of decommissioning stages chosen;
- The timing of each decommissioning stage;
- The decommissioning activities accomplished in each stage.

In addition, costs depend on such country- and site-specific factors as the type of reactor, waste management and disposal practices and labor rates. The importance of the last item is due to the fact that decommissioning is a labour intensive activity and, therefore, its cost is strongly connected with labour practices, working hours and, of course, labor rates.

Total decommissioning costs include all costs from the start of decommissioning until the site is released for unrestricted use.

The cost estimates are based on previous decommissioning and decontamination experience, on the cost of maintenance, surveillance and component replacements, and on the cost of similar non-nuclear work. Estimates for large NPPs. have been made by several European countries as well as Japan, Canada and the United States.

The results, which include a 25 per cent contingency factor, showed a range of costs for an immediate Stage 3 decommissioning of between 97 and 173 million U.S. dollars (1984). Costs for combining Stages 1 and 3 ranged from 117 to 181 million dollars. Only the United States estimated the costs of combining Stages 2 and 3, from 158 to 186 million dollars. While these figures cannot be absolutely precise, due to differences in the original contingency factors and definitions of decommissioning stages among countries, they nevertheless show what order of magnitude actual decommissioning costs are likely to be for large power plants.

Various methodologies are available for the calculation of decommissioning costs, which present different levels of reliability and precision and are used according to the different objectives of the evaluations. The major reasons that usually lead to the need of a cost evaluation are the following:

- To provide an input for the decommissioning funding during plant operational life
- To compare costs associated with different strategies for the decision making process
- To prepare long term budgeting and cash flow
- To provide a tool for project control

According to the above objectives, the methods include:

- Scaling up or down from similar plant evaluations or experiences according to plant power, or to the total plant activity or to the waste masses, or to other criteria
- Simple calculations based on unit costs for a number of overall parameters like mass of activated metals, mass of contaminated concrete, mass of contaminated metals. This method can be used also for a generic power plant (not site specific)
- Detailed site specific calculations based on a very detailed bottom-up approach, separating each elementary work package

In the last case a detailed database and a computer code treating a large number of information are needed.
For example, one of these computer codes (STILLKO) has been developed in Germany by NIS Company and has been extensively used not only in Germany, but also in many European countries, including Italy. The STILLKO Cost Breakdown Structure (CBS) includes all decommissioning activities that are necessary for the successful completion of the decommissioning project, beginning with the licensing procedure up to the green field status at the end. The CBS is organized into different levels in a hierarchical structure as described in fig. 3.

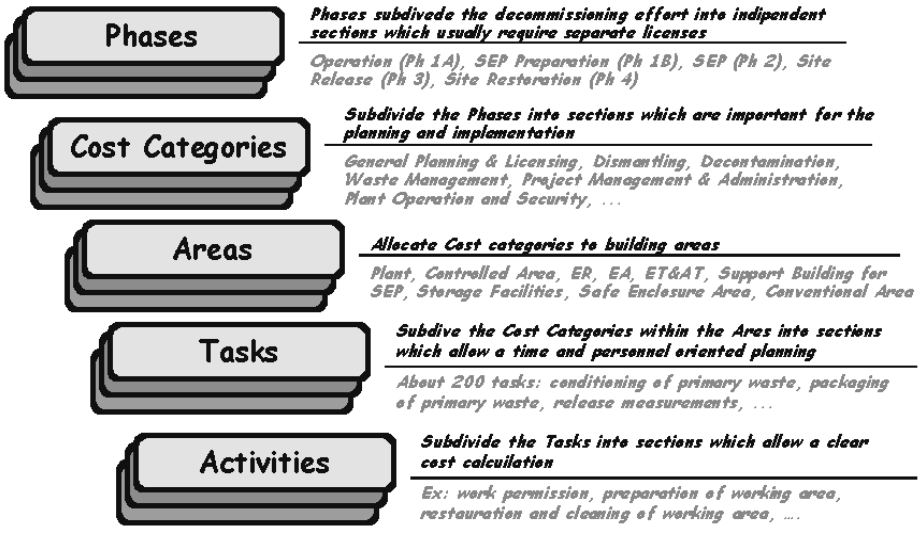

Figure 3 - Decommissioning Cost Breakdown Structure (CBS) Organization

On the first level the division of a decommissioning project is effected according to decommissioning phases which are separated according to time and obtained or necessary permits.

On the second level, the decommissioning phases are divided into the following cost categories:

- Project management and project administration
- Planning and licensing
- Plant operation and security
- Plant technical activities for Safe Enclosure
- Preparations for Dismantling
- Dismantling activated and contaminated components
- Decontamination
- Conventional dismantling
- Waste management
- Radiological and conventional worker protection

These cost categories have been created according to functional points of view and represent the volume of the decommissioning activities. The cost categories may occur in every decommissioning phase, with suitable contents of the cost categories regarding the respective phase.

The third level is used to allocate the decommissioning activities to the buildings and areas on site. Using this level in the cost structure it is possible to assign the work directly to the place where it arises but also to determine the sequence of the activities and their schedule in relation to the specific building.

On the fourth level, individual tasks are defined which allow a room by room or system by system planning, regarding to the situation on site. The execution of the tasks may be done parallel in different buildings, building levels or rooms.

On the fifth, the lowest level, the decommissioning tasks are divided into activities. These activities are formed in a way that each of them can be individually calculated.

It is useful to mention that a standardization of cost items has been developed in the framework of OECD and European Union and that it can be a useful reference for the future.

About financing methods, several alternatives can be used depending on the circumstances of each utility and the country in which it operates. In several countries, a fund of some type has been established, or proposed, to assure the availability of financing. This is usually done by an early estimation of the cost of decommissioning at the end of the normal plant lifetime and requiring payments, either annually or on a charge per kilowatt-hour basis, to ensure that this sum is in place. This estimate is updated regularly and the charge adjusted accordingly.

The drawback to this system is that the amount estimated would not be in place if the plant were to be shut down before the end of its normal lifetime. To avoid this, a fund could be established at the start of the plant's operation which would cover the cost of decommissioning whenever it became necessary. However, this represents a heavy burden for the utility at the moment when construction and start-up costs are already high, and thus, although it may be imposed by law, this solution is clearly not favoured by utilities.

Financing methods vary from country to country. Among the most common are:

- External sinking fund (Nuclear Power Levy): This is built up over the years from a percentage of the electricity rates charged to consumers. Proceeds are placed in a trust fund outside the utility's control. This is the main US system, where sufficient funds are set aside during the reactor's operating lifetime to cover the cost of decommissioning.
- Prepayment, where money is deposited in a separate account to cover decommissioning costs even before the plant begins operation. This may be done in a number of ways, but the funds cannot be withdrawn other than for decommissioning purposes.
- Surety fund, letter of credit, or insurance purchased by the utility to guarantee that decommissioning costs will be covered even if the utility defaults.

However, the uncertainties in cost calculations are among the issues in decommissioning that shall be further developed.

In Italy a fund has been established to enable the decommissioning of Italian NPPs and the closure of the nuclear fuel cycle. These special provisions are included in the Financial Statement of the SOGIN Company.

11. The need for R&D

From what has been seen, NPP's decommissioning appears to be a mature technology. However, while it is certainly true that we have today available all or most technologies needed to dismantle a NPP and return the site to essentially the initial, undisturbed condition, large margins exist for the process optimization in terms of efficiency, waste generation, occupational doses and especially costs. Specific areas that can be mentioned are:

- decontamination technologies : chemical, electrical, mechanical, ultrasonic …
- dismantling technologies;
- improvement of waste volume minimisation ;
- non-metallic material recycling ;
- control and measurement techniques ;
- remote operations.

In this field the role of the universities may be limited, since the matter is more related to an industrial development in many cases at competitive levels among suppliers, but it is anyway important, in the advanced and high technology fields (advanced chemical decontamination, waste treatment such as vitrification, robotization, waste stream characterization), as well as in computer codes for dose or environmental impact calculations.

12. The Italian experiences in decommissioning

First ENEL and then SOGIN have carried out a number of activities in the framework of the general decommissioning programs. They are both in-field activities and planning and designing activities. The current situation at the four NPP's is the following:

Garigliano

- Reactor defuelling and off-site shipment of spent fuel: 1985 - 1987
- Radiological characterisation of plant systems, components and structures: 1990
- Safe Enclosure of Reactor building: 1990 - 1998
- Safe Enclosure of Turbine building: 1994 - 1995
- Treatment of low-level waste and retrieval/conditioning of intermediate-level and high-level waste: 1988 - 1999
- Dismantling and safe enclosure of existing Radwaste system, demolition of Off-gas stack and Safe Enclosure condition to be reached within the year 2003

Latina

- Reactor defuelling and off-site shipment of spent fuel: 1988 - 1991
- Radiological characterisation of plant systems, components and structures: 1992
- Decontamination and dismantling of systems and components: 1992 - 1996
- Decontamination of the spent fuel pool: 1996 - 1999
- Treatment of radioactive waste, dismantling of primary circuit ducts and components and Safe Enclosure condition to be reached within the year 2006

Trino

- Radiological characterisation of plant systems, components and structures: 1992 - 1994
- Reactor defuelling: 1991
- Temporary dry storage of spent fuel at plant site within the year 2003
- Safe Enclosure condition to be reached in the year 2007

Caorso

- Radiological characterisation of plant systems, components and structures: 1992 - 1995

- Reactor defuelling: 1998
- Temporary dry storage of spent fuel at plant site within the year 2004
- Safe Enclosure condition to be reached in the year 2009

Most of the above mentioned decommissioning activities (in particular at Garigliano and Latina sites) were carried out using experience and skill gained by Company personnel during plant operation, in particular:

- headquarters personnel were involved in the design and licensing activities,
- plant personnel, who operated the plant, were involved in the activities for plant operation termination and decontamination/dismantling activities.

Engineering and R&D Departments of ENEL were also involved in the development and design of special equipments and tools, used for waste retrieval and decontamination of structures.

After plants shutdown the plant staff were significantly reduced; part of the personnel were transferred to fossil power plants, and retired personnel were not replaced.

13. Conclusions

Some broad conclusions can be drawn from the issues that have been briefly discussed.

The first point is that decommissioning is mainly a management challenge. It is a complex and multi-faceted problem, whose optimum solution requires a multidisciplinary approach. Nuclear experts, therefore, should be highly interested in being involved in it without living this experience as a kind of tedious and dirty job that somebody else has to do.

From a technical standpoint it is a substantially mature technology, which may have, however, important margins of improvement. Application of new advanced technologies may lead to reduced doses to workers and reduced amount of wastes to be disposed, with consequential important economic advantages. It is also clear that the sooner the decommissioning is prepared (even during plant operation) the better it is. We might also say that decommissioning is something that should be addressed as early as in the plant design process, as currently imposed by utility requirements as EUR (European Utility Requirements) for advanced NPP's. And it should be understood that the proof that decommissioning can be completed in reasonable time and economically **may be a prerequisite for building new NPP's.**

From the financial standpoint, decommissioning is also a challenge, because it is a cost intensive activity without any important direct investment return, if we exclude site reuse and returns in terms of image for the utility or the region. Therefore, a

correct funding scheme is very important to provide for all necessary funds at the end of the plant operating life.

International consensus and harmonization are needed in several areas. This need has been recognized only recently, in the last years, when a greater number of NPP's have terminated their service life.

A decision making process transparent both to the politicians and to the public, who deserve the information they want in an activity that is finally for their assurance, is undoubtedly useful.

Finally, let me introduce an example of design of a modular inherently safe reactor, called MARS, developed since 1983 at the University “La Sapienza” of Rome, in which the decommissioning aspects have been taken into account since the beginning.

This design has been aimed at strongly simplifying the plant layout, the components construction and assembling on the site in order to reduce construction times and costs.

This effort has produced, as a parallel significant result, a huge simplification of all decommissioning activities. In particular, the basic design choices of the MARS plant affecting decommissioning are shown in Table 3. These choices produce the results shown in Table 4.

A quick sequence of pictures (figs. 4 to 6) is self-explaining of the decommissioning phases for this reactor.

Table 3 - MARS main design choices affecting decommissioning

The selected plant characteristics (specific power, temperature, pressure, thermal inertia, etc.) have allowed to simplify all non safety-related auxiliary systems thanks to reduced performances.
The extensive use of passive systems to assure plant safety has allowed to eliminate some traditional safety-related auxiliary systems (e.g. injection systems) or to strongly simplify other ones, reducing the number of redundant components (e.g. boron emergency shutdown).
The selected plant power has allowed to reduce the size of main components, making them easily transportable.
The selected process parameters, even if reducing the plant global efficiency, guarantee a great retention of fission products inside the fuel matrix, that, together with low stressed fuel cladding, strongly reduce the amount of fission products dispersed within the primary coolant.
The selected structural materials (extensive use of stainless steel, elimination of cobalt alloys, etc.) have allowed to reduce the materials activation.
The adoption of metal structures to support components, to build the working floors and the biological screen, have allowed to limit the amount of concrete in the plant, simplifying and speeding the construction phase.
The adoption of flanged connections between components and piping (also for the primary loop) has allowed the easy mounting and dismounting of all components.
The adoption of an innovative design for all big components has allowed the possibility of their easy and fast construction, assembling and disassembling.

Table 4 - MARS decommissioning characteristics

The disassembling of flanged connections allows the easy and fast removal of all primary loop components (the biggest components may be also disassembled in transportable sub-components) with no needs for special equipment or complex activities to disassembly activated components inside the reactor building.
The general plant simplification allows a huge reduction, up to 50% in comparison with a same size traditional plant, of the number of contaminated or activated components (pumps, valves, tanks, etc.), with the correspondent reduction of the amount of radioactive materials.
The limited size, as well as the possibility of disassembling of components allows their easy transportability.
The use of a "clean" primary coolant and the reduced number of components allows the reduction of total and specific contamination of all materials facing the primary coolant.
The exclusive use of metallic structures allows the strong reduction, up to 50% in comparison with a same size traditional plant, of the volume of concrete buildings potentially contaminated.
The reduced number of components to be removed, their limited size and the presence of flanged connections make the decommissioning operations faster and faster than in traditional plants (usually characterized by a lot of big components welded to piping).
The short and easy decommissioning phase allows a strong reduction of doses to personnel.
The short and easy decommissioning phase allows a strong reduction of decommissioning cost.

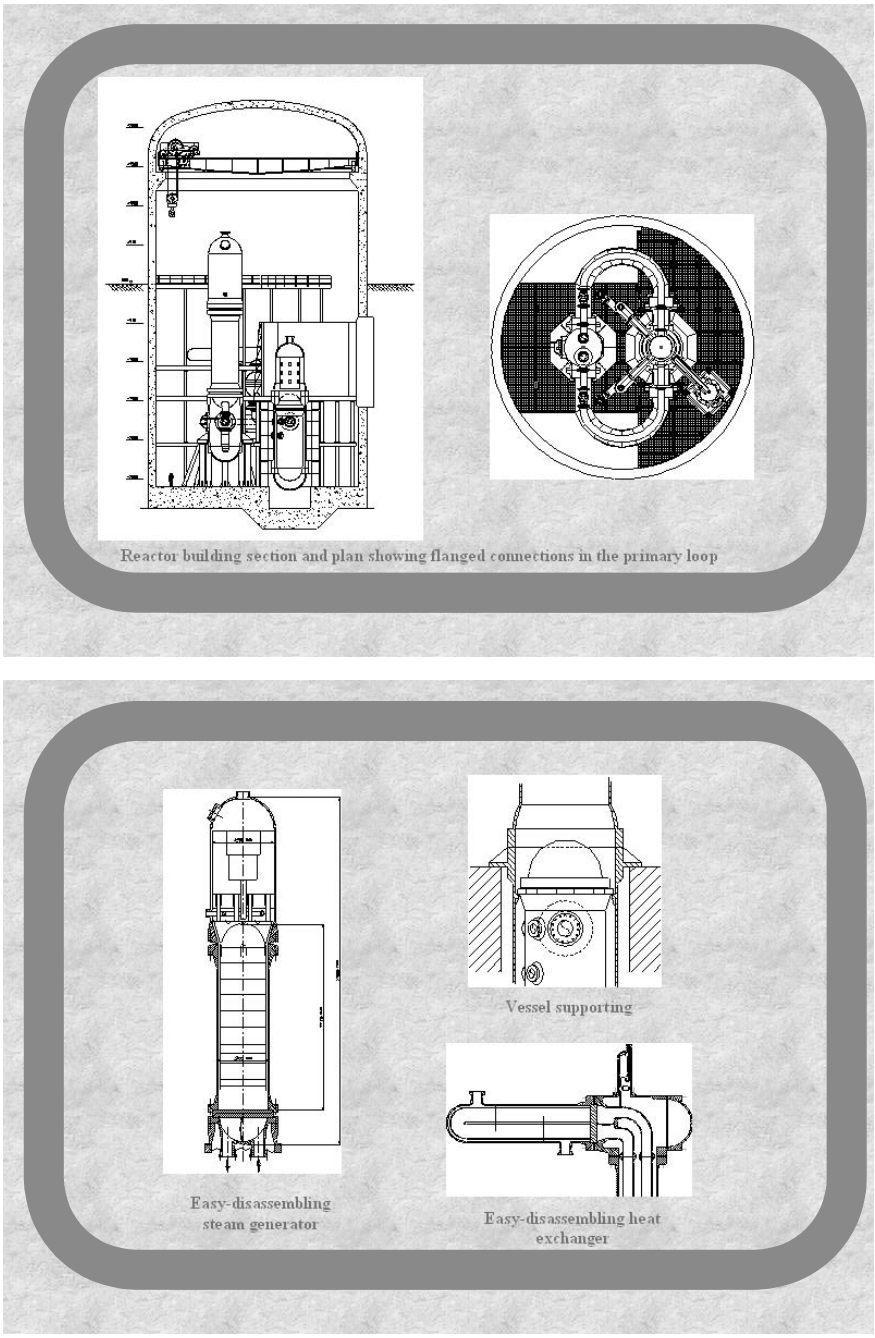

Figure 4 - MARS reactor design (Multipurpose Advanced Reactor inherently Safe)

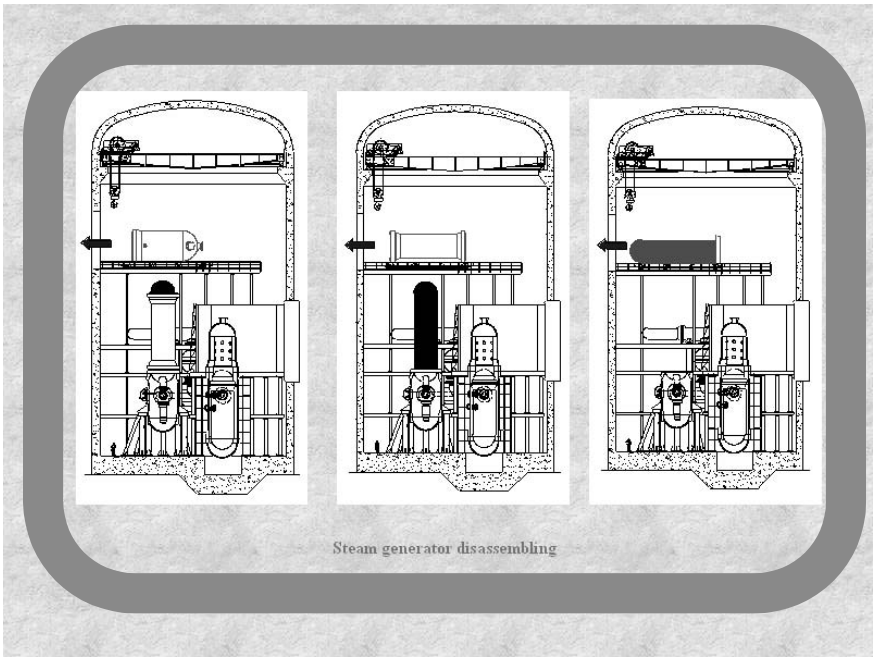

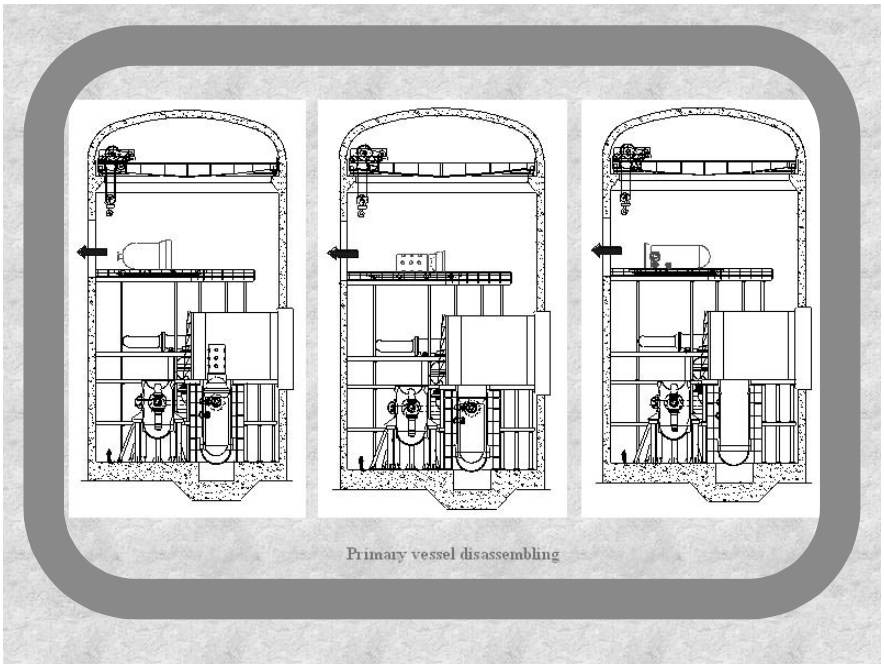

Figure 5 - Phases of decommisioning of MARS reactor

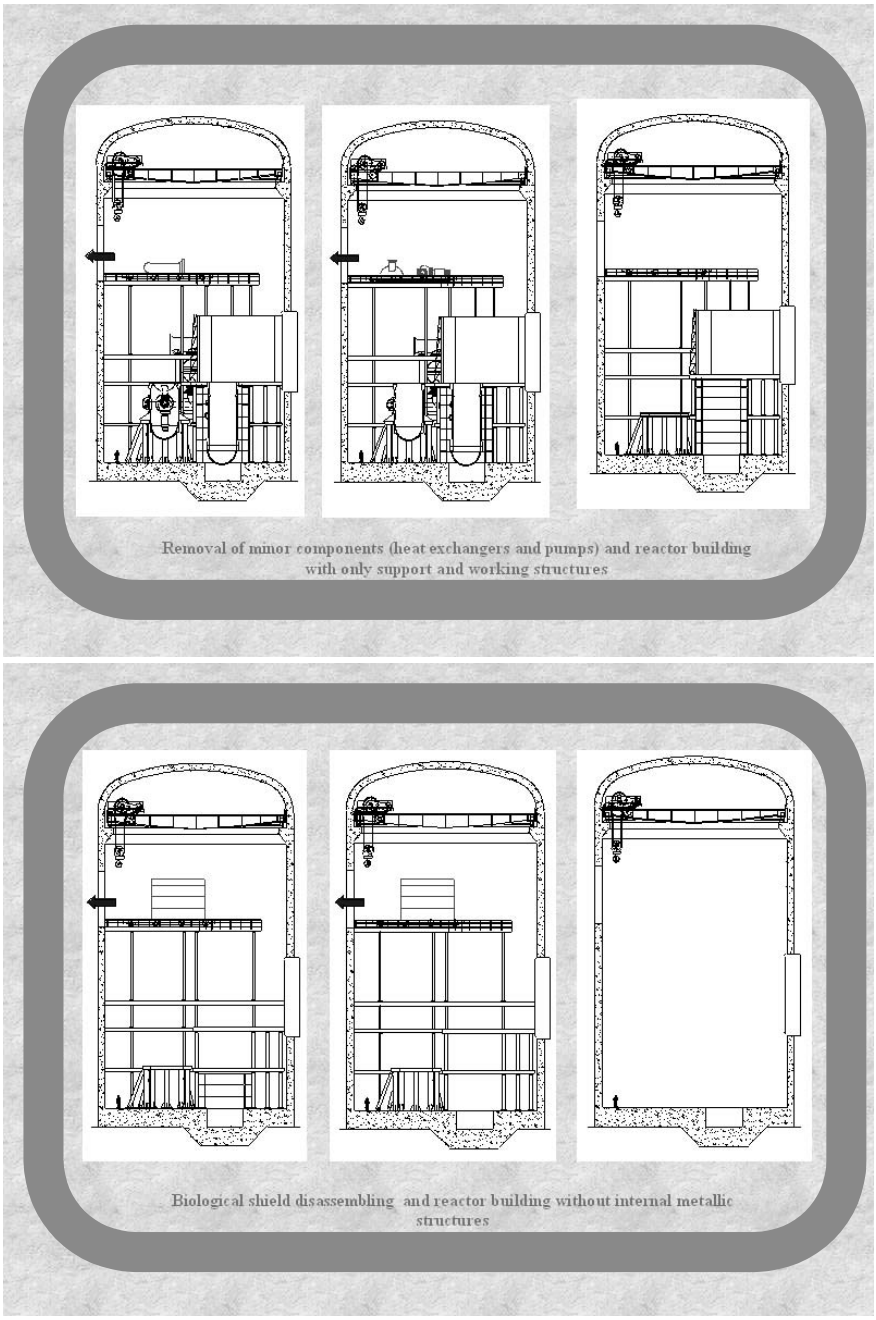

Figure 6 - Phases of decommisioning of MARS reactor